

UNIVERSITAT POLITÈCNICA DE VALÈNCIA

**INSTITUTO INTERUNIVERSITARIO DE INVESTIGACIÓN DE
RECONOCIMIENTO MOLECULAR Y DESARROLLO TECNOLÓGICO**



**Mesoporous silica and gold-based nanodevices:
new controlled delivery platforms for
biomedical applications**

PhD. THESIS

Submitted by

Gema Vivo Llorca

PhD. Supervisors:

**Prof. Ramón Martínez Máñez
Dra. María del Mar Orzáez Calatayud
Dr. José Ramón Murguía Ibáñez**

València, February 2021



UNIVERSITAT
POLITÈCNICA
DE VALÈNCIA

RAMÓN MARTÍNEZ MÁÑEZ, PhD in Chemistry and Professor at the *Universitat Politècnica de València*, MARÍA DEL MAR ORZÁEZ CALATAYUD, PhD in Biology at the *Universitat de València*, and JOSÉ RAMÓN MURGUÍA IBÁÑEZ, PhD in Biochemistry and Molecular Biology and associate professor at the *Universitat Politècnica de València*.

CERTIFY:

That the work “**Mesoporous silica and gold-based nanodevices: new controlled delivery platforms for biomedical applications**” has been developed by Gema Vivo Llorca under their supervision in the Instituto Interuniversitario de Investigación de Reconocimiento Molecular y Desarrollo Tecnológico (IDM) of the *Universitat Politècnica de València*, forming part of the Unidad Mixta UPV-CIPF de Investigación en Mecanismos de Enfermedades y Nanomedicina, as a Thesis Project in order to obtain the degree of PhD in Biotechnology at the *Universitat Politècnica de València*.

València, February 2021.

Prof. Ramón Martínez Máñez

Dra. Mar Orzáez Calatayud

Director

Directora

Dr. José Ramón Murguía Ibáñez

Director

A mi familia

Agradecimientos

Acknowledgements

En primer lugar, me gustaría dar las gracias a mis directores de tesis: el Prof. Ramón Martínez Máñez, la Dra. Mar Orzáez Calatayud y el Dr. José Ramón Murguía Ibáñez. A Ramón por darme la oportunidad de unirme a su grupo de investigación para realizar esta tesis doctoral. A Mar, muchas gracias por enseñarme el camino de la ciencia y transmitirme todos tus conocimientos e ideas, gracias a lo cual he podido llevar a cabo la tesis doctoral. Gracias por tu disposición, por tu ayuda, por tu apoyo y tus ánimos constantes. Poder formar parte de tu laboratorio ha sido una de las experiencias más enriquecedoras durante la tesis. A Joserra por darme a la oportunidad de conocer el que ha sido mi grupo durante estos años, y contribuir a mi desarrollo científico y personal.

Gracias al Prof. Félix Sancenón Galarza por tu dedicación, que ha hecho que los artículos que forman parte de este trabajo pudieran publicarse de una manera tan sencilla y eficiente. Gracias también a la Prof. María Dolores Marcos Martínez por tu orientación en la parte de caracterización química. Gracias a Eva Brun y a Arantxa por todos los trámites que facilitáis y por vuestra eficiencia. Gracias Tania por tu gran predisposición y por todos esos pedidos que has realizado en momentos intempestivos, para que pudiera tener todos los productos que necesitaba de la forma más rápida posible en la última etapa de mi tesis.

Muchas gracias a mis compañeras y compañeros del 2.6 con los que he tenido la oportunidad de coincidir en el laboratorio durante estos años: Carmen, Andrea Bernardos, Elena, Eva G., Andrea Escudero, Serena, Iris, Cris T, Lluís, Lorena, Andy, Toni, Adrián, Santi, Elisa, Bea, Juanfran, Luís Pla, Borja... y a los que me deje. Hemos sido tantos en el laboratorio que seguro que se me olvida más de uno. Pero en

Agradecimientos

general, gracias al 2.6. Ha sido un placer conocerlos y haber compartido momentos con vosotros.

Me gustaría dar las gracias de manera especial a Xente, María, Angy y Paula. A Xente, mi compañero de proyectos, por todo tu esfuerzo y persistencia para que esta tesis haya podido salir adelante; a pesar de todos los obstáculos que hemos ido encontrando por el camino (¡que no han sido pocos!). A María, mi referente en la parte química, por ser una guía en el laboratorio. Gracias por tu orientación y por toda tu dedicación a los proyectos que conforman esta tesis. Angy, compartir la última etapa de mi tesis contigo es una de las mejores cosas que me llevo no solo a nivel científico, sino también personal. Mil gracias por todos esos paseos entre la CPI y el CIPF para que las nanopartículas estuvieran listas a tiempo, y por dedicar todas las horas que tenías en el día a proyectos que forman parte de esta tesis (incluso en días festivos; gracias por acompañarme en el laboratorio). Paula, gracias por tu orientación; eres mi otra referente en la parte química. Gracias por transmitirme tu optimismo, tu buen humor y tu tranquilidad. Trabajar directamente con vosotras y vosotros ha sido un auténtico placer. ¡Gracias, porque habéis hecho que esta tesis sea posible!

También quiero dar las gracias a esas científicas con las que he colaborado de manera breve, pero intensa. Gracias Bea de Luis por tu dedicación durante el tiempo que trabajamos juntas. Gracias Ana Virginia Sánchez por tu tiempo, y por introducirme en el mundo de la experimentación con peces.

Gracias a mis compañeras de laboratorio del CIPF: Alba, Araceli, Alejandra, Irene, Amelia, Elena, Blanca, Mónica, Ally, Estefi, Mónica Sancho, Carmen, Danya, Paula y Paula Carrascosa. No podría haber caído en un mejor entorno de trabajo para hacer la tesis. Gracias por toda vuestra ayuda, las risas y los buenos momentos

dentro y fuera del laboratorio. Trabajar junto a vosotras es una de las mejores cosas que me llevo de esta etapa. Gracias a Mónica por tu orientación y todo el conocimiento que me has transmitido. Gracias Alba, que fuiste la primera persona con la que trabajé cuando me incorporé al grupo. Gracias por ser el nexo entre laboratorios, por tu disponibilidad en cualquier día y a cualquier hora, por tu orientación y tus consejos.

No puedo pasar por aquí sin expresar mi profundo agradecimiento a mi mentora en el CIPF. Gracias, Ally. Tuve la gran suerte ser tu patito en el laboratorio. Gracias por enseñarme tantísimas cosas, por tu disposición, tu apoyo y por tu persistencia para sacar el trabajo adelante. Eres una gran referente científica.

Muchas gracias a mis compañeras indispensables de viaje, a mi familia de laboratorio: Araceli, Estefanía y Alejandra. Todas las palabras que os pueda dedicar aquí se quedan cortas. Aun así, intentaré expresar lo agradecida que estoy a la vida por haberos puesto en mi camino. Gracias a las 3 por vuestro gran valor del compañerismo y vuestra ayuda constante, en el laboratorio y fuera de él. Siempre habéis estado ahí cuando os he necesitado, y habéis conseguido hacer que la tesis sea una experiencia muy enriquecedora a nivel personal. Gracias Araceli, porque te has convertido en un grandísimo apoyo para mí. Gracias por tu amistad incondicional, por todos los momentos que hemos compartido y tu optimismo que se contagia ahí donde estés. Gracias, también, por iluminarme más allá del laboratorio y ayudarme a poner las cosas en perspectiva. Gracias por leerme mi tesis entera y aportarme tu punto de vista crítico para hacerla mejor. Estefi, en primer lugar, gracias por todo el tiempo que has dedicado a la maquetación de mi tesis. La corrección insuperable y desinteresada del estilo; sin ti esta tesis estaría peor escrita. También muchísimas gracias por aportarme tu espíritu crítico, pragmático y detallista. Gracias por toda tu orientación en toda esta última etapa de tesis y,

Agradecimientos

sobre todo, por tu amistad. Alejandra, gracias por todos los momentos que hemos compartido durante estos años, por tu ayuda incondicional, y los planes improvisados en días de playa que acaban en lluvia. Gracias por aportar siempre tu visión inconformista y crítica de las cosas. ¡Solo terminar diciéndoos que vuestra amistad es lo más grande que me llevo de estos años!

Y por supuesto, muchas gracias a Alberto. Gracias por hacer las sesiones de confocal tan divertidas, por tu buen humor, por las risas y, sobre todo, por tus chistes malos.

Estefania, Alberto, Alejandra y Álvaro, también quiero agradecerlos el haberlos dejado, literalmente, la sangre en esta tesis. Gracias por las muestras de sangre proporcionadas para poder realizar los experimentos. No habría podido encontrar mejores voluntarios que vosotros.

También quiero dar las gracias a todas esas personas que conseguían romper mi rutina día tras día. Gracias a Mari Paz, Carmen, Angie, Ana, Pili, Carlos y Rubén, por hacer de los días más interesantes y mucho más divertidos.

No puedo pasar por aquí sin agradecer su ayuda a todas esas personas de fuera del laboratorio, que han contribuido de alguna manera u otra al desarrollo de esta tesis.

Gracias a todas mis amigas, que me han acompañado durante estos años (y durante prácticamente toda la vida algunas de vosotras): May, Elena, Teresa, Andrea, Clara, Inma. Gracias por estar ahí en los buenos momentos y en los peores. Vuestro apoyo y amistad han hecho mucho más fácil este recorrido, y muchos otros. Gracias a todas.

Gracias, Anna. En primer lugar, por el diseño de la portada de mi tesis; por todas las horas que has dedicado para que quede tan bonita, por tu paciencia para hacer mil retoques y por ser tan detallista y artista. Gracias por todos estos años de amistad desde que coincidimos en la carrera. Gracias por tu apoyo y tus consejos.

Gracias, Pau; porque me mejoras como persona. Gracias por ayudarme a salir de mi zona de confort y disfrutar conmigo de las pequeñas cosas de la vida. Gracias por tu apoyo, ayuda, comprensión, y por tu forma de ser.

Quiero dar mi mayor agradecimiento a las personas más importantes de mi vida, mi familia. A Mamá y Papá, gracias por vuestro apoyo incondicional y por estar ahí en los peores momentos de nervios, enfado y frustración. Gracias por interesaros siempre por la tesis, hasta el punto de querer entender los conceptos tan técnicos y específicos que forman el contenido de este trabajo, sólo por estar cerca de mí y para formar parte de mi mundo. Muchas gracias a mi hermano Martín. Gracias por ayudarme en todo el largo del camino; por tus consejos y aportarme tu forma de ver las cosas tan diferente a la mía, y tan enriquecedora. Gracias también por el año que hemos compartido en Valencia y, por supuesto, ¡por todos los túperes de comida que me preparabas con todo el amor y entusiasmo del mundo! Gracias a todos por vuestro apoyo, cuidado y comprensión. También gracias a mis abuelos y mi Tete; a los que faltan y a los que están. Gracias por vuestra alegría e ilusión cada vez que me veis aparecer por la puerta. Gracias por vuestro amor infinito. De no ser por todos vosotros, mi familia, nunca hubiera llegado tan lejos. ¡Gracias con todo mi corazón!

En definitiva, a todos y cada una de vosotras y vosotros:

Gracias por haber formado parte de este camino.

Resumen

La presente tesis doctoral titulada “Mesoporous silica and gold-based nanodevices: new controlled delivery platforms for biomedical applications” se centra en el diseño, síntesis, caracterización y evaluación de distintos nanodispositivos híbridos orgánico-inorgánicos. En concreto, se utilizan como soporte nanopartículas mesoporosas de sílice y nanopartículas de oro para su aplicación biomédica, en concreto en el campo del cáncer de mama.

En el primer capítulo se introduce el marco general en el que se engloban los estudios realizados. Se presentan los conceptos relacionados con nanotecnología y nanomedicina, así como la interacción de las nanopartículas a nivel biológico con el organismo y las células. Finalmente, se introducen conceptos básicos del cáncer de mama y la aplicación de nanomateriales como terapia.

A continuación, en el segundo capítulo, se exponen los objetivos de la presente tesis doctoral que son abordados en los siguientes capítulos experimentales.

En el tercer capítulo se describe el primer nanomaterial para la liberación controlada de dos inhibidores (navitoclax y S63845) de las proteínas anti- apoptóticas de la familia Bcl-2. Este sistema se ha diseñado con el objetivo de superar la resistencia a navitoclax en un modelo celular de cáncer de mama triple negativo. En concreto, se han preparado nanopartículas mesoporosas de sílice cargadas con navitoclax y S63845, y funcionalizadas con un aptámero dirigido a la proteína de superficie MUC1, que actúa como puerta molecular. En este trabajo hemos demostrado que las nanopartículas diseñadas son internalizadas preferentemente por células tumorales de cáncer de mama. También hemos demostrado la capacidad de las nanopartículas de revertir la resistencia a navitoclax

Resumen

en un modelo celular de cáncer de mama triple negativo. Además, ponemos de manifiesto la disminución del principal efecto adverso (trombocitopenia) asociado a la administración del navitoclax en su formulación libre, gracias a la encapsulación en las nanopartículas.

En el capítulo cuatro se presenta un sistema sensible a pH para la liberación controlada de un cargo fluorescente y la maquinaria de edición génica basada en el sistema CRISPR/Cas9, dirigido a la edición del gen codificante de la proteína fluorescente verde (GFP, del inglés *green fluorescent protein*). El nanodispositivo está constituido por nanopartículas mesoporosas de sílice cargadas con rodamina B, funcionalizadas con polietilenimina y revestidas con el plásmido codificante del sistema CRISPR/Cas9. En este trabajo se ha demostrado el escape lisosomal de las nanopartículas, mediado por el efecto esponja de protones de la PEI. Asimismo, mostramos un nanodispositivo pionero en su campo, basado en nanopartículas mesoporosas de sílice, capaz de realizar la doble función de llevar a cabo la edición del gen codificante de GFP y la liberación exitosa del cargo fluorescente.

En el quinto, y último, capítulo experimental se propone una nueva aproximación para realizar una terapia enzimática prodroga empleando nanopartículas de oro como transportadores enzimáticos. En este caso, se aborda la funcionalización de nanopartículas de oro con la enzima peroxidasa de rábano (HRP, del inglés *horseradish peroxidase*), capaz de transformar la prodroga inocua ácido indol-3-acético en especies radicales que resultan tóxicas para las células tumorales. En este capítulo se ha demostrado el efecto terapéutico del nanodispositivo en combinación con la prodroga en modelos celulares de cáncer de mama de los subtipos luminal A y triple negativo. Además, se ha confirmado la eficacia terapéutica del sistema en esferoides tumorales formados por células de cáncer de mama triple negativo.

Por último, se presentan en el capítulo seis las conclusiones extraídas del desarrollo de esta tesis doctoral. Los resultados obtenidos en este trabajo contribuirán al desarrollo de nuevos nanomateriales inteligentes con aplicación en diversas áreas de la nanomedicina.

Resum

La present tesi doctoral titulada “Mesoporous silica and gold-based nanodevices: new controlled delivery platforms for biomedical applications” se centra en el disseny, síntesi, caracterització i avaluació de diferents nanodispositius híbrids orgànic-inorgànics. En concret, s'utilitzen com a suport nanopartícules mesoporoses de sílice i nanopartícules d'or per a la seua aplicació biomèdica, en concret en el camp del càncer de mama.

En el primer capítol s'introdueix el marc general en el qual s'engloben els estudis realitzats. Es presenten els conceptes relacionats amb la nanotecnologia i nanomedicina, així com la interacció de les nanopartícules a nivell biològic amb l'organisme i les cèl·lules. Finalment, s'introdueixen conceptes bàsics del càncer de mama i l'aplicació de nanomaterials com a teràpia.

A continuació, en el segon capítol, s'exposen els objectius de la present tesi doctoral que són abordats en els següents capítols experimentals.

En el tercer capítol es descriu el primer nanomaterial utilitzat per a l'alliberament controlat de dos inhibidors (navitoclax i S63845) de les proteïnes anti-apoptòtiques de la família Bcl-2. Aquest sistema s'ha dissenyat amb l'objectiu de superar la resistència a navitoclax en un model cel·lular de càncer de mama triple negatiu. En concret, s'han preparat nanopartícules mesoporoses de sílice carregades amb navitoclax i S63845, i funcionalitzades amb un aptàmer dirigit a la proteïna de superfície MUC1, que actua com a porta molecular. En aquest treball hem demostrat que les nanopartícules dissenyades són internalitzades preferentment per cèl·lules tumorals de càncer de mama. També hem demostrat

Resum

la capacitat de les nanopartícules de revertir la resistència a navitoclax en un model cel·lular de càncer de mama triple negatiu. A més, posem de manifest la disminució del principal efecte advers (trombocitopènia) associat a l'administració del navitoclax en la seua formulació lliure, gràcies a l'encapsulació en les nanopartícules.

En el capítol quatre es presenta un sistema sensible a pH per a l'alliberament controlat d'una càrrega fluorescent i la maquinària d'edició gènica basada en el sistema CRISPR/Cas9, dirigit a l'edició gènica del gen codificant de la proteïna fluorescent verda (GFP, del anglés *green fluorescent protein*). El nanodispositiu està constituït per nanopartícules mesoporoses de sílice carregades amb rodamina B, funcionalitzades amb polietilenimina i revestides amb el plàsmid codificant del sistema CRISPR/Cas9. En aquest treball s'ha demostrat la fuga lisosomal de les nanopartícules, mediat per l'efecte esponja de protons de la PEI. Així mateix, vam mostrar un nanodispositiu pioner en el seu camp, basat en nanopartícules mesoporoses de sílice, capaç de realitzar la doble funció de dur a terme l'edició del gen codificant de la GFP i l'alliberament exitós de la càrrega fluorescent.

En el cinqué i últim capítol experimental es proposa una nova aproximació per a realitzar una teràpia enzimàtica prodroga emprant nanopartícules d'or com a transportadors enzimàtics. En aquest cas, s'aborda la funcionalització de nanopartícules d'or amb l'enzim peroxidasa de rave (HRP, del anglés *horseradish peroxidase*), capaç de transformar la prodroga innòcua àcid indol-3-acètic en espècies radicals que resulten tòxiques per a les cèl·lules tumorals. En aquest capítol s'ha demostrat l'efecte terapèutic del nanodispositiu en combinació amb la prodroga en models cel·lulars de càncer de mama dels subtipus luminal A i triple negatiu. A més, s'ha confirmat l'eficàcia terapèutica del sistema en esferoïdes tumorals formats per cèl·lules de càncer de mama triple negatiu.

Finalment, en el capítol sis es presenten les conclusions extretes del desenvolupament d'aquesta tesi doctoral. Els resultats obtinguts en aquesta tesi contribuiran al desenvolupament de nous nanomaterials intel·ligents amb aplicació en diverses àrees de la nanomedicina.

Abstract

This Ph.D. thesis entitled “Mesoporous silica and gold-based nanodevices: new controlled delivery platforms for biomedical applications” is focused on the design, synthesis, characterisation, and evaluation of several hybrid organic-inorganic nanomaterials. We have developed mesoporous silica nanoparticles and gold nanoparticles for biomedical applications, specifically in the breast cancer area.

The first chapter includes an overview of the concepts related to the research performed. Introductory notions about nanotechnology and biomedicine are presented, as well as the basis of the interactions of nanoparticles with biological systems. Finally, breast cancer disease and the application of nanomaterials as therapy are described.

Next, in the second chapter, the objectives addressed in the following experimental chapters are displayed.

In the third chapter, we present the first nanomaterial for the controlled delivery of two inhibitors (navitoclax and S63845) of the Bcl-2 anti-apoptotic proteins. This nanosystem has been designed to overcome navitoclax resistance in a triple-negative breast cancer cellular model. We have prepared mesoporous silica nanoparticles loaded with navitoclax and S63845 and functionalised with an aptamer targeting MUC1 surface protein as a molecular gate. In this work, the specific targeting of the nanodevice to breast cancer cells has been demonstrated. The ability to overcome navitoclax resistance has been shown in navitoclax-resistant triple-negative breast cancer cells. Furthermore, navitoclax encapsulation

Abstract

in the nanoparticles has proved to reduce the main adverse effect (thrombocytopenia) associated with free formulated drug administration.

In the fourth chapter, we describe a pH-responsive nanosystem for the controlled co-delivery of a fluorescent cargo and the genome-editing machinery based on CRISPR/Cas9, which targets the green fluorescent protein (GFP) coding gene. The nanodevice consists of mesoporous silica nanoparticles loaded with rhodamine B, functionalised with polyethyleneimine, and capped with the CRISPR/Cas9 plasmid. In the present work, we have shown the lysosomal escape capacity of the nanodevice enhanced by the proton sponge effect of PEI. We have also demonstrated a pioneering mesoporous silica-based nanodevice efficient in the simultaneous genome editing of the GFP gene (as a model gene) and the successful release of a fluorescent cargo (as a model drug).

In the fifth and last experimental chapter, we propose a new approximation to develop enzyme prodrug therapy using gold nanoparticles as enzyme carriers. In this case, we use gold nanoparticles functionalised with the enzyme horseradish peroxidase (HRP), which transforms the non-toxic prodrug indol-3-acetic acid into radical species toxic to tumour cells. In this chapter, the therapeutic effect of the nanodevice in combination with the prodrug has been demonstrated in two breast cancer cell subtypes (luminal A and triple-negative breast cancers). Also, the therapeutic effect of the material has been corroborated in multicellular tumour spheroid-like cultures formed by triple-negative breast cancer cells.

Finally, in the sixth chapter, the conclusions derived from the presented studies and the general conclusions of this Ph.D. thesis are released. The obtained results will promote the development of new smart nanomaterials with diverse biomedical applications.

Publications

Results of this Ph.D. thesis has resulted in the following scientific publications.

- **Gema Vivo-Llorca**, Vicente Candela-Noguera, María Alfonso, Alba García-Fernández, Mar Orzáez, Félix Sancenón, and Ramón Martínez-Máñez. MUC1 Aptamer-Capped Mesoporous Silica Nanoparticles for Navitoclax Resistance Overcoming in Triple-Negative Breast Cancer. *Chem. Eur. J.* **2020** Dec 9;26(69):16318-16327. doi: 10.1002/chem.202001579.
- Alba García-Fernández, **Gema Vivo-Llorca**, Mónica Sancho, Alicia García Jareño, José Ramón Murguía, Ramón Martínez-Máñez, Mar Orzáez, and Félix Sancenón. Nanodevices for the efficient co-delivery of CRISPR/Cas9 editing machinery and an entrapped cargo; submitted, **2020**.
- **Gema Vivo-Llorca**, Angela Morella-Aucejo, Alba García-Fernández, Paula Díez, Antoni Llopis-Lorente, Ramón Martínez Máñez, and Mar Orzáez. Horseradish peroxidase-functionalised gold nanoconjugates for breast cancer enzyme prodrug therapy; project in progress, **2021**.

Abbreviations and Acronyms

ABTS	2,2'-Azino-bis(3-ethylbenzothiazoline-6-sulfonic acid) diammonium salt
AMF	Alternating magnetic field
apMUC1	apMUC1 aptamer targeting
APTES	(3-Aminopropyl)triethoxysilane
AuNCs	Gold nanoconjugates
AuNPs	Gold nanoparticles
AuNRs	Gold nanorods
Bad	Bcl-2 antagonist of cell death
Bak	Bcl-2 associated killer protein
Bax	Bcl-2 associated X protein
β-CD	β-cyclodextrin
Bcl-2	B-cell lymphoma 2
Bcl-w	Bcl-2-like protein 2
Bcl-xL	B-cell lymphoma-extra large
BCs	Breast cancers
BET	Brunauer–Emmett–Teller
Bfl-1 (A1)	Bcl-2-related protein A1
BH	Bcl-2 homology
Bid	BH3 interacting-domain death agonist
Bim	Bcl-2-interacting mediator of cell death
BJH	Barret-Joyner-Halenda

Abbreviations and Acronyms

Cas9	CRISPR associated protein 9
CdSe	Cadmium selenide
CdTe	Cadmium telluride
CET	Cetuximab
C₃F₈	Perfluorocarbon octafluoropropane
CPPs	Cell-penetrating peptides
CRISPR	Clustered Regularly Interspaced Short Palindromic Repeats
CTAB	Cetyltrimethylammonium bromide
DEPT	Directed enzyme prodrug therapy
DFT	Density functional theory
DLS	Dynamic light scattering
DMEM	Dulbecco's Modified Eagle Medium
DNA	Deoxyribonucleic acid
DNase I	Deoxyribonuclease I
DPPC	1,2-dipalmitoyl-sn-glycero-3-phosphocholine
DPPE	1,2-dipalmitoyl-sn-glycero-3-phosphoethanolamine
DSPE	1,2-distearoyl-sn-glycero-3-phosphoethanolamine
EDC	N-(3-dimethylaminopropyl)-N'-ethylcarbodiimide
EDTA	Ethylenediaminetetraacetic acid
EGFR	Epidermal growth factor receptor
EGTA	Ethylene glycol-bis(β -aminoethyl ether)-N,N,N',N'-tetraacetic acid/egtazic acid
EPR	Enhanced and permeability retention

EPT	Enzyme prodrug therapy
ER	Estrogen receptor
ET	Endocrine therapy
FA	Folic acid
FBS	Foetal bovine serum
FDA	Food and Drug Administration
FITC	Fluorescein isothiocyanate
FR	Folate receptor
FTIR	Fourier-transform infrared spectroscopy
GFP	Green fluorescent protein
GRAS	Generally recognized as safe
gRNA	guide RNA
GSH	Glutathione
HER2	Human epidermal growth factor receptor 2
HAuCl₄	Chloroauric acid
HRP	Horseradish peroxidase
IAA	Indole-3-acetic acid
IFNα-2b	Interferon α -2b
IUPAC	International Union of Pure and Applied Chemistry
LCST	Low critical solution temperature
LSPS	Localised surface plasmon resonance
MA	Methacrylic acid
Mcl-1	Myeloid cell leukaemia 1
MCM	Mobile Composition of Matter

Abbreviations and Acronyms

MDA-MB-231-R	MDA-MB-231 resistant
MMP-2	Matrix metalloproteinase-2
MMPs	Matrix metalloproteinases
MOMP	Mitochondrial outer membrane permeabilisation
3-MPA	3-mercaptopropionic acid
MPS	Mononuclear phagocyte system
MRI	Magnetic resonance imaging
MSNs	Mesoporous silica nanoparticles
MUC1	Mucin 1
Na₃C₆H₅O₇	Sodium citrate
Nav	Navitoclax
NHS	N-hydroxysuccinimide
NIPAM	N-isopropylacrylamide
NIR	Near-infrared
NMR	Nuclear magnetic resonance
NOXA	Phorbol-12-myristate-13-acetate-induced protein 1
Opti-MEM	Opti-Minimal essential medium
PAGE	Polyacrylamide gel electrophoresis
PBS	Phosphate buffer saline
PEG	Poly(ethylene glycol)
PEI	Polyethyleneimine
PI3K	Phosphatidylinositol 3-kinase
PLK1	Polo-like kinase 1
PMSF	Phenylmethylsulfonyl fluoride

PR	Progesterone
PUMA	p53 upregulated modulator of apoptosis
PXRD	Powder X-ray diffraction
QDs	Quantum dots
RBIT	Rhodamine B isothiocyanate
RES	Reticuloendothelial system
RhB	Rhodamine B
rhTNF	Recombinant human tumour necrosis factor
RIPA	Radioimmunoprecipitation assay
RNA	Ribonucleic acid
ROS	Reactive oxygen species
SDS	Sodium dodecyl sulphate
SPIONs	Superparamagnetic iron oxide magnetic nanoparticles
TAT	Transactivator of transcription
TBOS	Tetrabutyl orthosilicate
TBS	Tris-hydroxymethyl-aminomethane
TEM	Transmission electron microscopy
TEM-EDX	Transmission electron microscopy coupled with energy-dispersive X-ray spectroscopy
TEOS	Tetraethyl orthosilicate
TKI	Tyrosine kinase inhibitor
TM	Transmembrane
TMOS	Tetramethyl orthosilicate
TN	Triple-negative

Abbreviations and Acronyms

TNBC	TN breast cancer
Tris	Tris-buffered saline
US	Ultrasounds
UV-Vis	Ultraviolet-visible
VEGF	Vascular endothelial growth factor
WST-1	Water soluble tetrazolium-1
ZnS	Zinc Sulphide

Table of contents

Chapter 1 General Introduction	1
1.1 Nanotechnology and nanomedicine.	3
1.2 Mesoporous silica materials in advanced applications.	5
1.2.1 Synthesis of mesoporous silica nanoparticles.....	7
1.2.2 Functionalisation of mesoporous silica materials.....	9
1.3 Stimuli-responsive gated materials.....	11
1.3.1 Endogenous stimuli-responsive materials.	13
1.3.2 Exogenous stimuli-responsive materials.....	21
1.3.3 Gated mesoporous silica nanoparticles as drug delivery systems in biomedical applications.	27
1.3.4 Clinical relevance of gated mesoporous silica nanoparticles.....	30
1.4 Gold nanoparticles.	31
1.4.1 Synthesis and functionalisation of gold nanoparticles.....	32
1.4.2 Clinical relevance of gold nanoparticles.....	36
1.5 Biocompatibility and biodistribution of nanoparticles.....	37
1.6 Breast cancer.....	45

Table of contents

1.6.1	Breast cancer intrinsic subtypes.	45
1.6.2	Current therapeutic approaches for breast cancer treatment.	47
1.6.3	Bcl-2 protein family and drug resistance in breast cancer.	49
1.6.4	Nanomedicine-based approach for breast cancer treatment.	55
1.7	References.	61
Chapter 2 Objectives.....		85
Chapter 3 Navitoclax resistance overcoming using mesoporous silica nanoparticles		89
3.1	Abstract.	95
3.2	Introduction.	95
3.3	Results and Discussion.....	97
3.3.1	Synthesis and characterisation of aptamer-capped nanoparticles...97	
3.3.2	Cargo controlled release and biocompatibility studies.....	102
3.3.3	Targeted cellular uptake studies.....	104
3.3.4	Navitoclax resistance overcoming in TNBC cells.	106
3.3.5	Platelets protection assay.	107
3.4	Conclusions.....	110

3.5	Experimental section.....	111
3.5.1	Synthesis of the mesoporous silica nanodevices.....	111
3.5.2	Synthesis of APTES-MSNs(RhB).....	111
3.5.3	Synthesis of apMUC1-MSNs(RhB).....	111
3.5.4	Synthesis of drug-loaded apMUC1-gated MSNs.....	112
3.5.5	Standard characterisation procedures of the prepared materials.	113
3.5.6	Cargo delivery studies.....	114
3.5.7	Cell culture conditions.....	114
3.5.8	Protein expression characterisation by western blot.....	114
3.5.9	Cytotoxicity cell studies with apMUC1-MSNs.....	115
3.5.10	Navitoclax resistance overcoming TNBC cells.....	116
3.5.11	Targeted cellular uptake studies.....	116
3.5.12	Platelets protection assay.....	117
3.6	References.....	118
3.7	Supporting information.....	121
	Chapter 4 CRISPR/Cas9 machinery and model drug co-delivery as one-shot treatment strategy	129

Table of contents

4.1	Abstract.	135
4.2	Introduction.....	135
4.3	Results and Discussion.....	137
4.3.1	Assembly and characterisation of CRISPR-MSNs.	137
4.3.2	Controlled release, biocompatibility, and internalisation studies. .	141
4.3.3	Gene editing of GFP and cargo delivery cellular studies.....	145
4.4	Conclusions.....	149
4.5	Materials and methods.	150
4.5.1	Materials.	150
4.5.2	General methods.	150
4.5.3	Synthesis of mesoporous silica nanoparticles (MSNs).	151
4.5.4	Synthesis of PEI-MSNs.....	152
4.5.5	Synthesis of CRISPR-MSNs.	152
4.5.6	Synthesis of PEI-RhB-MSNs.	152
4.5.7	Synthesis of CRISPR-RhB-MSNs.....	153
4.5.8	Synthesis of CRISPR-RhB*-MSNs.....	153
4.5.9	Preparation of the CRISPR/Cas9 vector.	153

4.5.10	Assembly and characterisation of CRISPR-RhB-MSNs.....	154
4.5.11	CRISPR-RhB-MSNs delivery studies.....	154
4.5.12	Stability studies of the CRISPR/Cas9 vector in MSNs complexes. ...	154
4.5.13	Toxicity studies with CRISPR-RhB-MSNs.	155
4.5.14	Cellular uptake studies with CRISPR-RhB*-MSNs.	155
4.5.15	Gene editing of GFP in U-2 OS-GFP cells with CRISPR-MSNs.	156
4.5.16	Gene editing of GFP in U-2 OS-GFP cells with CRISPR-RhB-MSNs. .	157
4.6	References.....	158
4.7	Supporting information.....	160

Chapter 5 | Enzyme prodrug therapy for breast cancer treatment 171

5.1	Abstract.....	177
5.2	Introduction.....	177
5.3	Results and Discussion.....	180
5.3.1	Synthesis and characterisation of HRP-AuNCs.....	180
5.3.2	Activity and stability of HRP-AuNCs.	183
5.3.3	Biocompatibility and cellular uptake of HRP-AuNCs.....	184
5.3.4	HRP-AuNCs for EPT in breast cancer cells.	187

Table of contents

5.3.5	HRP-AuNCs for EPT in breast cancer multicellular tumour spheroid-like cultures (MCTS).	188
5.4	Conclusions.....	190
5.5	Experimental section.....	192
5.5.1	Synthesis of gold nanoparticles (AuNPs).....	192
5.5.2	Synthesis of HRP-functionalised gold nanoconjugates (HRP- AuNCs).	192
5.5.3	Standard characterisation procedures of HRP-AuNCs.	193
5.5.4	HRP activity assay.....	193
5.5.5	Cell culture conditions.	195
5.5.6	Biocompatibility studies with HRP-AuNCs.	195
5.5.7	Cellular uptake studies.....	195
5.5.8	HRP-AuNCs for EPT in breast cancer cells.	196
5.5.9	HRP-AuNCs for EPT in triple-negative breast cancer MCTS.	196
5.6	References.....	198
5.7	Supporting information.....	204
Chapter 6 Conclusions and future perspectives		209

Chapter 1 | General Introduction

1.1 Nanotechnology and nanomedicine.

Nanotechnology is a multidisciplinary area of research in which the matter is manipulated at atomic and molecular scale leading to the construction of structures in the nanometre size range. It is a relatively new research field that resulted from the convergence of disciplines such as biology, chemistry, physics, material science, engineering, and electronics. At the nanoscale, dimensions are so small that they are difficult to understand from our everyday life human perspective. A nanometre (nm, 10^{-9} m) is one-millionth of a millimetre, i.e., approximately 100,000 times smaller than the diameter of a human hair (Figure 1).^[1] Ever since Richard Feynman introduced the concept in his famous lecture *There's plenty of room at the bottom* in 1959^[2] and Norio Taniguchi later in 1974 coined the term of the emerging area of nanotechnology,^[3] considerable advances in the nanotechnology area have been achieved.

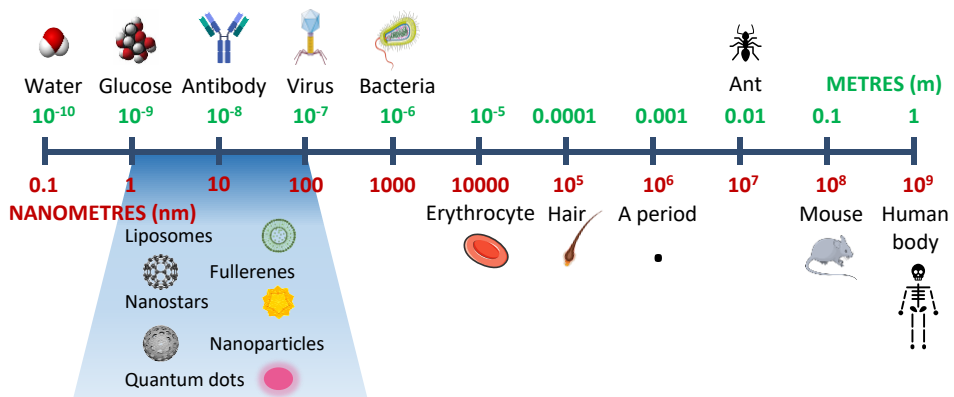


Figure 1. Scheme of nanomaterials scale compared to biomolecules, cells, and other items.

Materials behave differently when they present nanoscale dimensions, and they acquire superior properties compared to their bulk counterparts. These new properties of the nanomaterials are the basis of nanotechnology, which is based on

the principle that laws and behaviour change dramatically at the nanoscale because of two remarkable reasons: high surface-to-volume ratio and quantum effect. The main reason for the nanomaterials being special is the incredible increase of the surface-to-volume ratio at the nanoscale, which makes their properties dependent on their surface. Even some materials (e.g., fullerenes or single-walled nanotubes) are entirely surface. This phenomenon widens the applicability of nanomaterials, which can be applied in many industries and research fields, such as medicine, cosmetics, electronics, agriculture, energy storage, catalysis, food industry, etc. Another property of nanomaterials is the role of quantum effect, meaning they acquire new mechanical, electrical, or optical properties. For example, semiconductor nanomaterials change their optical properties as a function of their size.^[4] As [Figure 2](#) illustrates, a simple change in the size of semiconductor nanoparticles is translated into a shift in their emission band, while no interesting properties are shown by the same material at micro to macro dimensions.^[5]

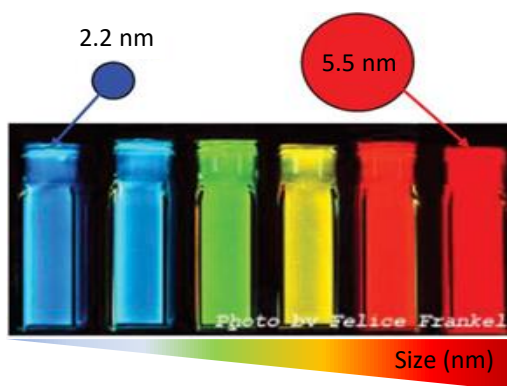


Figure 2. Illustration of quantum effect. Fluorescence emission of (CdSe)ZnS quantum dots of various sizes. Adapted from *J. Phys. Chem. B.* **1997**, 101, 46, 9463–9475. Copyright © 1997 American Chemical Society.

One of the most appealing fields of nanotechnology is nanomedicine. Nanomedicine emerges from the application of nanotechnology to the diagnosis

and treatment of diseases. Nanotechnology improves the performance of medical devices in three main areas of research, including imaging/diagnosis, drug delivery, and regenerative medicine.^[6] Among these three areas, perhaps the most widely expanded is the one dedicated to the design and development of novel drug delivery nanosystems. The need to overcome conventional drug downsides, i.e., non-specificity and poor biodistribution, rapid metabolism/excretion, or undesirable side effects, led to the rise of drug delivery nanocarriers. These nanodevices target specific organelles in individualized cells or specific cells within the diseased tissues.^[7] Within context, diverse nanoparticles and nanomaterials have been developed as drug delivery systems based on both organic supports (such as liposomes and polymers) and inorganic supports (iron oxide, quantum dots, gold, or silica based-nanomaterials among others).^[8] Despite remaining challenges to handle before nanoparticles are used in the clinical routine, nanomedicine is in constant growth and several advanced nanodevices anticipate the near future.

1.2 Mesoporous silica materials in advanced applications.

Over the past decade, the interest in porous materials has considerably increased because their physicochemical properties make them incredibly versatile for a wide range of applications, such as catalysis,^[9] adsorption of gases, and chemicals,^[10] sensing, and drug delivery.^[11] The International Union of Pure and Applied Chemistry (IUPAC) describes porous material according to the pore size as microporous (pore size < 2 nm), mesoporous (2-50 nm), and macroporous (>50 nm) materials.^[12,13]

Mesoporous silica materials have received great attention since in 1992 researchers from Mobil Oil Company reported the synthesis and characterisation

of these materials, known as the M41S phases.^[14] The family of M41S were encoded as Mobile Composition of Matter (MCM) and consists of a set of uniform pore, silicate-based, mesoporous molecular sieves, which include three main structure types: MCM-41 with a hexagonal arrangement of the mesopores (like honeycomb), MCM-48 with a cubic arrangement of mesopores and MCM-50 with a lamellar structure (Figure 3).^[15,16]

Among these, the MCM-41 phase has been the most investigated because of its properties, which confer improved features and advanced functionalities to the final nanomaterials. The unique properties that made mesoporous materials so attractive include:^[17]

- Large surface areas (500-1000 m²/g).
- Ordered and uniform pore system.
- Tuneable size (in a range of 7-300 nm range) and pore size (in a range of 2-10 nm).
- High pore volumes (in the order of 1 cm³/g) and loading capacity.
- High surface reactivity and easy surface functionalisation.
- Excellent stability (thermal, hydrothermal, chemical, mechanical, and biological).
- Biocompatibility.
- The synthesis requires inexpensive and safe chemicals.^[18]
- They can be synthesized produced on large scales.^[18]

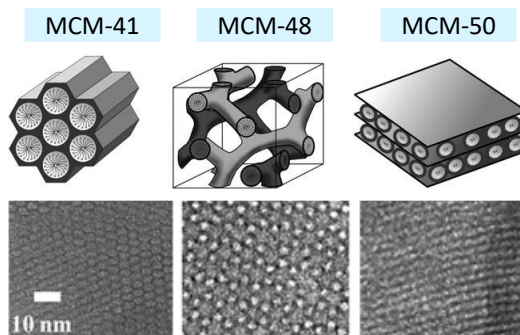


Figure 3. The M41S family of mesoporous silica nanomaterials. Schematic 3D structures on top and corresponding transmission electron microscopy (TEM) images of the pore network at the bottom. Adapted from *Angew. Chem. Int. Ed.* **2006**, 45, 20, 3216-51. Copyright © 2006 WILEY-VCH Verlag GmbH & Co. KGaA, Weinheim and from *Chem. Soc. Rev.* **2013**, 42, 3663-3670. Copyright © 2013 The Royal Society of Chemistry.

1.2.1 Synthesis of mesoporous silica nanoparticles.

In general, the synthetic procedure M41S materials imply the condensation of a silica precursor (tetraethyl orthosilicate (TEOS), tetramethyl orthosilicate (TMOS), tetrabutyl orthosilicate (TBOS)) around a cationic surfactant in basic conditions.^[19] It is considered a sol-gel process in which silica monomers in solution (sol) are integrated into a solid network (gel).^[20] The synthetic process is based on the Stöber method described in 1968^[21] but performed in the presence of cationic surfactants.^[22]

The standard M41S synthesis procedure consists of surfactant molecules self-aggregation to form micelles in a polar solvent. Individual micelles self-assemble themselves to yield a supermicellar structure, which acts as a structure-directing agent or template over which the silica precursor molecules condensate. After supermicelles formation, the silica precursor molecules are added to the reaction. In this step, the silica molecules are hydrolysed to form silanol groups (Si-OH),

which polymerise by condensation creating the final network of siloxane bonds (Si-O-Si) with the characteristic mesoporous structure. The supermicellar structure depends on the selected reaction conditions (such as temperature, pH, and ionic force, among others) and the surfactant concentration, which ultimately determines the porous framework in the final material (i.e., hexagonal, cubic, and laminar).^[23]

As mentioned above, the MCM-41 material is the most widely studied among M14S family. A typical synthesis involves the polymerisation of the silica precursor TEOS over cetyltrimethylammonium bromide (CTAB) supermicelles at 80 °C in basic conditions (Figure 4). The reaction mixture is stirred for 2 hours before the resulting white solid is collected by centrifugation or filtration. Finally, the surfactant template is removed by calcination at high temperatures or extraction in acidic media. Under these synthetic conditions, the final MCM-41 mesoporous scaffold presents a spherical shape of ca. (from latin *crīca*, meaning approximately) 80-100 nm of diameter with cylindrical unidirectional pores with a size of ca. 2.5 nm, arranged in a hexagonal distribution. The size and the pore volume of the final nanoparticles are easily tuneable by adjusting the synthesis parameters, such as the surfactant type and concentration,^[24–26] the silica precursor nature, the presence of additives,^[27–30] temperature,^[31] pH conditions^[32] and reaction time.^[33]

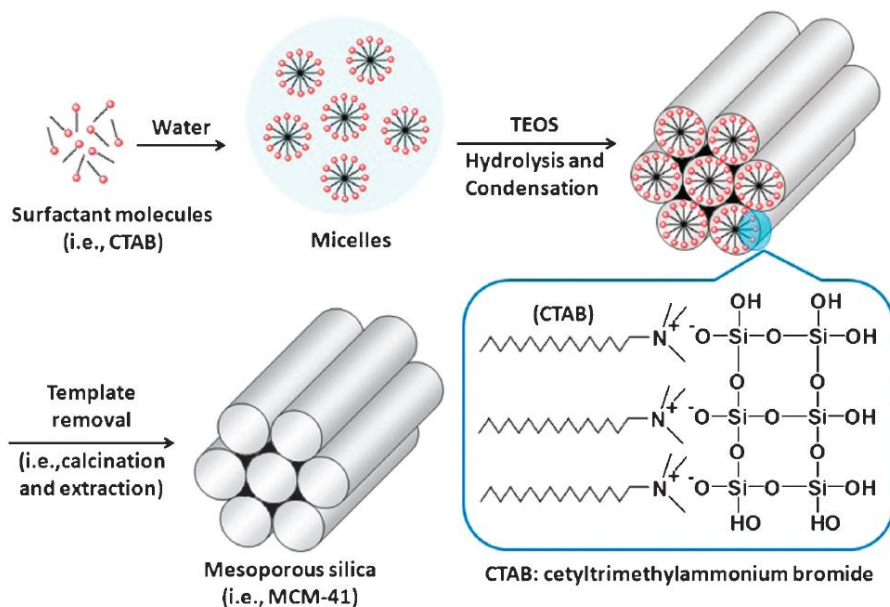


Figure 4. Schematic representation of the synthetic route of mesoporous silica MCM-41 type. Reprinted with permission from *Chem. Soc. Rev.* **2012**, 41, 9, 3679-98. Copyright © 2012 The Royal Society of Chemistry.

1.2.2 Functionalisation of mesoporous silica materials.

One of the most appealing properties of the MCM-41 phase is that its surface is easily modified with functional groups through a post-synthesis treatment, which introduces additional versatility to the nanoparticles. The term functionalisation refers to the incorporation of organic molecules onto the external or internal surface of the mesoporous silica scaffold. The functionalisation of inorganic materials leads to the synthesis of hybrid organic-inorganic materials. The symbiosis of the robustness of the mesoporous silica support together with the extensive functional versatility of the organic moieties is incredibly attractive for a wide range of applications, such as catalysis, adsorption, chromatography, and nanoelectronics. In general, two main strategies are used for porous hybrid materials functionalisation:

- i) **Grafting procedure:** the mesoporous silica material is functionalised in a post-synthetic step with selected organic groups. The surface of the silica materials can be easily modified because of the presence of silanol groups (Si-OH), which act as reactive points to covalently anchor organosilanes containing the desired organic group. Among organosilanes, trialkoxysilanes with $(R'O)_3\text{-Si-R}$ structures (R: organic group) are the most widely used. Using this method, the organic groups are preferentially placed on the external surface of the inorganic scaffold (Figure 5).^[34]

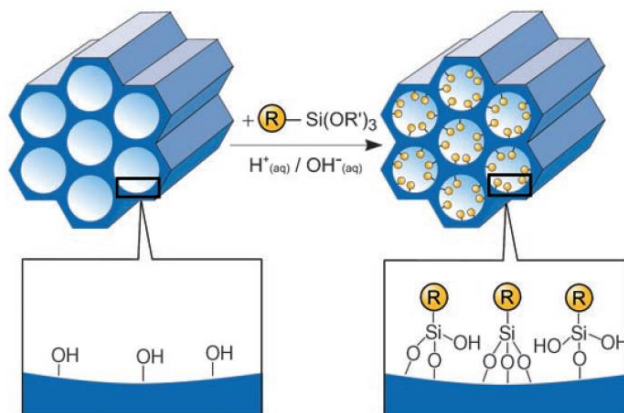


Figure 5. Schematic representation of the grafting procedure. The mesoporous silica material is functionalised in a post-synthetic step with organotrialkoxysilanes of the type $(R'O)_3\text{-Si-R}$, where R represents an organic functional group. Reprinted with permission from *Angew. Chem. Int. Ed.* **2006**, 45, 20, 3216-51. Copyright © 2006 Wiley-VCH.

- ii) **Co-condensation method (one-pot synthesis):** in this procedure, the selected organosilane is simultaneously incorporated with the silica precursor in the reaction mixture during the synthesis process and it condensates around the surfactant template. The resulting silica matrix contains the organosilane molecules, which are intercalated with the main silica skeleton on the external and the internal surface. The surfactant is

removed by extraction, otherwise, the organic functional groups would spoil due to high calcination temperatures (Figure 6).^[35]

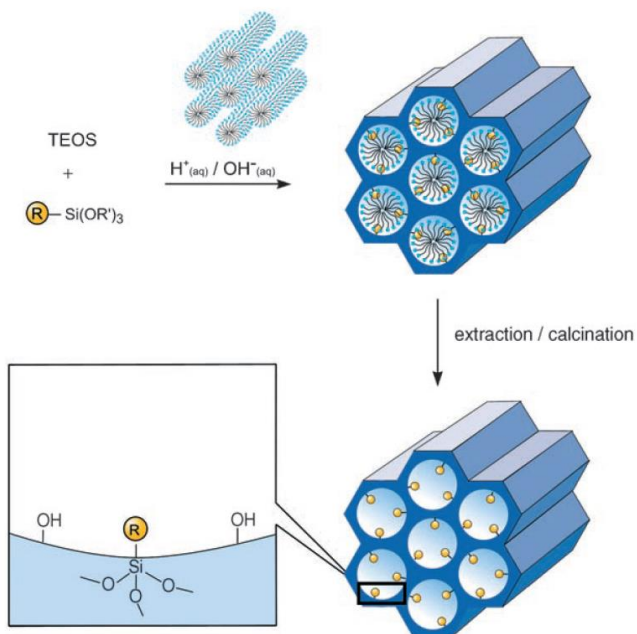


Figure 6. Schematic representation of the co-condensation procedure. The mesoporous silica material is functionalised with organic groups incorporated in the synthesis reaction mixture, where R is the organic functional group. Reprinted with permission from *Angew. Chem. Int. Ed.* **2006**, 45, 20, 3216-51. Copyright © 2006 Wiley-VCH.

1.3 Stimuli-responsive gated materials.

The functionalisation of inorganic materials with organic biomolecules leads to the development of hybrid organic-inorganic materials with novel advanced applications.^[36] Within functional nanodevices, the design of stimuli-responsive gated materials is an appealing approach for the preparation of smart nanoparticles with applications in several scientific areas (such as controlled delivery of chemical species and (bio)chemical sensors).^[37–39]

Gated materials are designed to finely deliver molecules from the porous support to a solution in response to a selected external stimulus. Gated nanodevices are generally composed of two subunits: (i) a porous inorganic scaffold, within the cargo is entrapped; and (ii) biomolecules or supramolecular entities (the so-called molecular gates, gatekeepers, or nanovalves) grafted onto the external surface, which confine the payload in the porous support. Several molecules have been used as gatekeepers (e.g., polymers,^[40–42] peptides/proteins,^[43–45] DNA,^[46–48] and enzymes^[49–51]). In presence of an external stimulus, the gatekeepers change their size/shape/conformation or they are displaced from the nanoparticle surface, allowing the cargo release to the external media in a controlled fashion (Figure 7).^[52] Several stimuli can be used to trigger the cargo delivery, such as light,^[53,54] temperature,^[55–57] magnetic fields,^[58–60] redox species,^[61–63] pH changes,^[64–66] and biomolecules.^[67–69]

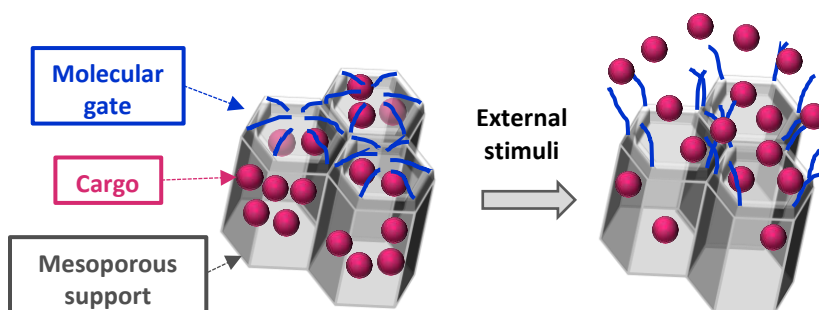


Figure 7. Scheme of the principal components and operation of a molecular gate.

Fujiwara and co-workers reported the first example of molecular gated material in 2003, which was a coumarin-modified mesoporous silica nanoparticle for the reversible release of guest molecules in response to light.^[70] Since then, numerous pioneering gated materials have been developed. Among inorganic porous materials, mesoporous silica nanoparticles (MSNs) have been perhaps the

most widely used because they gather unique features that make them ideal materials for controlled release applications in the biomedical field.

Extensive work about gated materials has been published in recent years. The next section shows some examples of gated MSNs classified according to the triggering stimulus, to give a comprehensive landscape of the work done so far.

1.3.1 Endogenous stimuli-responsive materials.

The vast majority of the reported gated nanocarriers for controlled drug delivery in *in vivo* models respond to endogenous cellular stimuli naturally present in the living organisms. The gated materials are designed to respond to intrinsic biological conditions as an autonomous mechanism for controlled delivery.

- **pH-driven drug delivery.**

Among different stimuli used to trigger cargo release in gated materials, pH might be the most employed. In these nanosystems, the abstraction or addition of protons induces a change in the gating ensemble that controls the open/close mechanism. Acidic pH in specific organs (gastrointestinal tract and vagina) or intracellular compartments (endosomes and lysosomes) have been exploited for the controlled delivery of drugs. Also, the acidic environment found in cancer or inflammation has been extensively used to trigger drug release.^[71-74] Different strategies exist to obtain pH-responsive gated materials. One common approach is to attach the gatekeeper molecules onto the nanomaterial through pH- hydrolysable linkages (such as imine, hydrazone, acetals, ketals, amides, and esters). The hydrolysis of such bonds induces the molecular gate detachment from the outer surface, with subsequent uncapping of the pores and cargo delivery.^[75,76] Another approach consists of coating the nanoparticles with ionisable polymers or

biomolecules by electrostatic interactions as assembly forces. In this case, protonation/deprotonation of the coating moieties leads to the disruption of the electrostatic interaction, coating detachment and payload delivery.^[77,78] Finally, a few examples are based on the conformational changes that protonation induces in the gating ensemble for cargo release.^[79]

For instance, Yang et al. prepared a pH-responsive core/shell nanosystem with cadmium telluride (CdTe) quantum dots (QDs) as the core and hollow mesoporous silica as the shell. The mesoporous silica was loaded with doxorubicin and capped with polyethylene glycol (PEG). Finally, the nanoparticles were equipped with an antibody targeting the endothelial growth factor (VEGF) for specific cancer detection and treatment.^[76] The nanoparticles were functionalised with amino groups and then succinimidyl carboxymethyl-PEG₅₀₀₀-maleimide was incorporated onto their external surface through amide bond formation. As a final step, the thiol-modified VEGF antibody was grafted to the nanoparticles through a Michael addition reaction (Figure 8). The pH-driven drug delivery was confirmed; doxorubicin release was triggered at acidic pH (pH 6.5 and pH 5.0), while at pH 7.4 no significant drug delivery was detected. The drug release is attributed to the hydrolysis of the amide bonds, which results in gatekeeper detachment and subsequent doxorubicin delivery. Targeting studies performed *in vitro* demonstrated preferential internalisation of the nanoparticles by VEGF-positive HeLa cervix tumour cells, when compared with VEGF-negative L929 fibroblast cells. *In vivo* studies performed in female nude mice bearing HeLa cell tumours corroborated the preferential accumulation in tumours due to the enhanced and

permeability retention (EPR) effect (see [section 1.4](#)) and the active targeting performed by VEGF antibody.

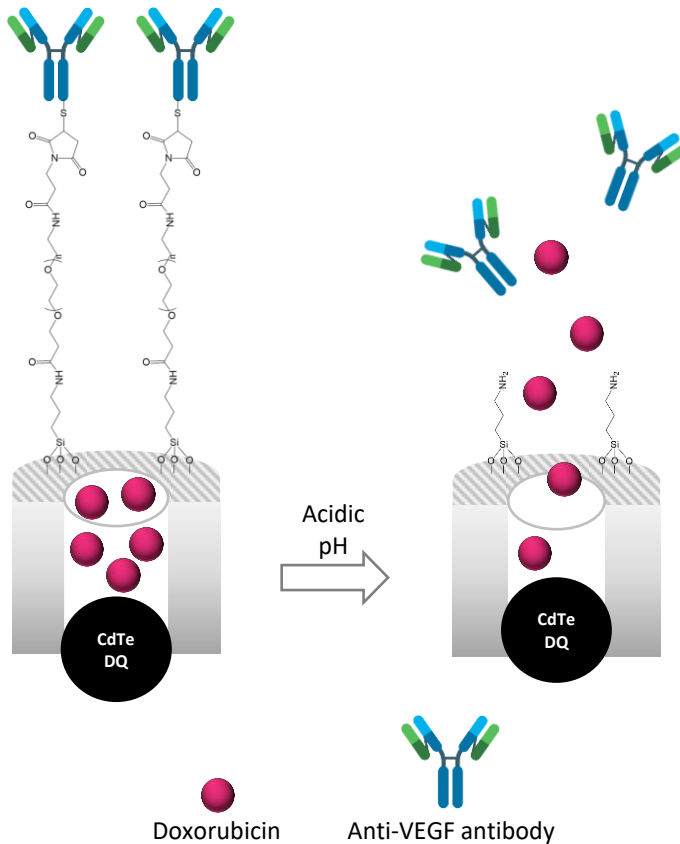


Figure 8. Schematic representation of pH-driven drug delivery. QDs integrated into hollow MSNs loaded with doxorubicin and capped with PEG functionalised with VEGF antibody. At acidic pH, the amide bond is hydrolysed, leading to doxorubicin release.

- **Redox-driven drug delivery.**

Oxidation and reduction reactions play an important role in the development of gated materials. Glutathione (GSH) is the main molecule used as a triggering stimulus. The intracellular concentration of GSH can be as high as 10 mM, while extracellular levels keep under 10 μM .^[80] In tumour cells, GSH concentration can be 4-fold higher than in healthy tissues.^[81] Those differences in the concentration of reducing agents can be exploited to efficiently release drugs from nanocarriers equipped with redox-sensitive supramolecular gating machinery in targeted cells.^[82] Most of the reported systems can be classified into two main categories: (i) capping ensembles attached to the nanoparticles through disulphide linkages,^[83] and (ii) capping ensembles based on molecules (rotaxanes) in which changes in the redox potential induce movement from close to open state.^[84]

For instance, Zhang and co-workers designed redox-responsive MSNs as a drug delivery carrier to overcome tyrosine kinase inhibitor (TKI) resistance in epidermal growth factor receptor (EGFR)-mutant lung cancer.^[85] For the preparation of the nanodevices, the surface of MSNs was functionalised with mercaptopropyl groups and then loaded with doxorubicin or with the TKI named gefitinib. Finally, the nanoparticles were capped with the anti-EGFR antibody (cetuximab) through the formation of redox-responsive disulphide bonds (Figure 9). Drug release from the pores was successfully controlled by GSH; in the absence of GSH small amount of doxorubicin was released, whereas in the presence of increasing concentrations of GSH drug delivery increased over time. The specific targeting mediated by cetuximab (CET) was confirmed in PC9 lung cancer cells overexpressing EGFR in comparison with epithelial Beas2B lung cells, which expressed low levels of EGFR. The nanoparticles loaded with gefitinib efficiently induced cell death in resistant PC9 cells. Additionally, *in vivo* experiments showed

a significant effect in targeting the tumour site with the subsequent growth inhibition of the gefitinib resistant tumour. The authors demonstrated an improved therapeutic effect of the nanoformulation with reduced side effects in comparison with the free drug.

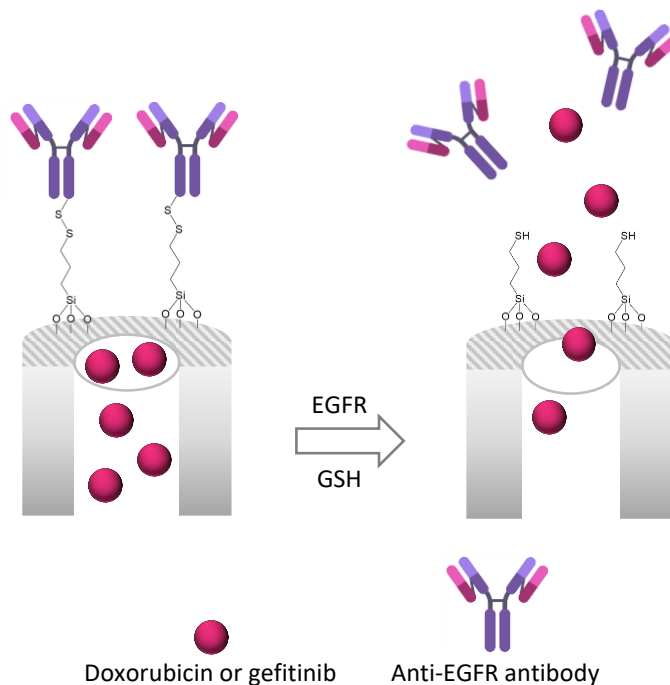


Figure 9. Schematic representation of redox-driven drug delivery. MSNs loaded with doxorubicin or with gefitinib and capped with CET, attached by disulfide bonds. In the presence of GSH, the disulfide bond is reduced, and CET is detached from the surface of the nanoparticles. Subsequently, cargo is delivered to the external media.

- **Enzyme-driven drug delivery.**

Enzyme-responsive gated materials have attracted great attention for drug delivery applications in recent years. In pathological conditions, such as cancer or inflammation disorders, some enzymes are overexpressed and can be used as triggering stimuli for drug delivery. Hyaluronidase and protease-responsive

materials are the most used materials in different pathological scenarios. Other employed enzymes include hydrolases, lipases, nucleases, phosphatases, glycosidases, oxidoreductases, and transferases.^[86]

Matrix metalloproteinases (MMPs) are a family of proteins extensively overexpressed in several tumours and have been widely used to design tailor-made enzyme-sensitive gated nanosystems. As an example, Yang and co-workers reported a multifunctional enzyme-responsive nanoparticle for anticancer drug delivery and real-time diagnosis by magnetic resonance imaging (MRI) in mouse models.^[87] For the preparation of the nanodevices, mesoporous silica-coated iron oxide (Fe_3O_4) nanoparticles were functionalised with mercaptopropyl moieties, and the thiol groups were reacted with 3-(maleimido)propionic acid *N*-hydroxysuccinimide ester through a Michael addition reaction. Afterward, the nanosystem was capped with a peptide substrate of the matrix metalloproteinase-2 (MMP-2) overexpressed in cancer cells, through the formation of amide bonds with the peptide *N*-terminus. At the final step, the nanodevice was loaded with doxorubicin (Figure 10). The authors demonstrated that only in the presence of MMP-2 the loaded doxorubicin was delivered, otherwise remained entrapped inside the pores. The antitumoural activity of the nanosystem was proven in fibrosarcoma cells. *In vivo* experiments demonstrated that the intravenously injected nanoparticles accumulated preferentially in tumour under magnet application and effectively reduce tumour burden in fibrosarcoma-bearing mice.

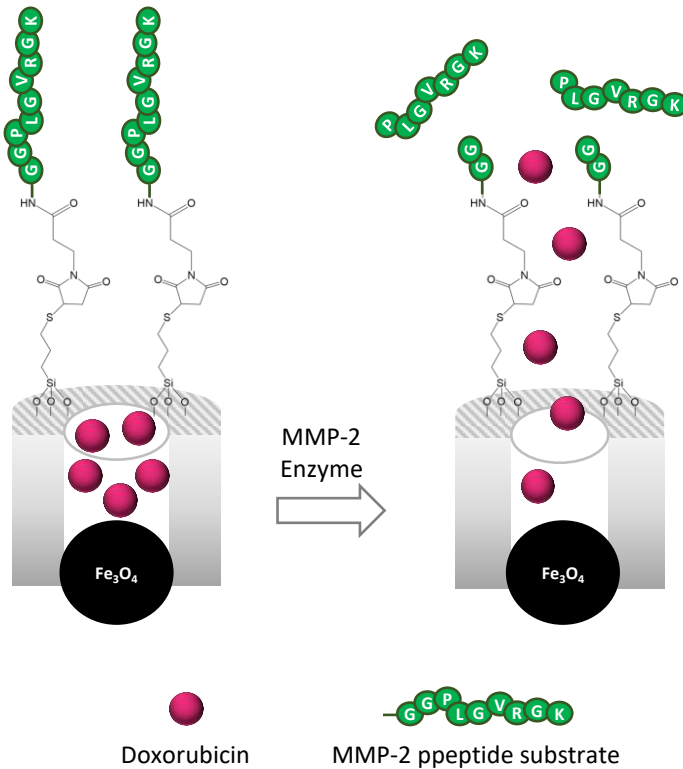


Figure 10. Schematic representation of enzyme-driven drug delivery. Fe_3O_4 nanoparticles coated with a mesoporous silica shell loaded with doxorubicin and capped with a peptide substrate of the MMP-2. In MMP-2 presence, the capping peptide is digested, and doxorubicin is delivered from the mesopores.

- **Temperature-driven drug delivery.**

Temperature can be considered either an endogenous or exogenous stimulus. Temperature-responsive nanodevices can be used to selectively deliver their content under temperature body changes. In this field, thermosensitive polymers have been widely exploited, as they change their properties (solubility, size, conformation, etc.) depending on temperature.^[88]

As an example, Wu and co-workers took advantage of polymer shrinkage to develop nanoparticles for the controlled co-delivery of two drugs used in Traditional Chinese medicine (i.e., evodiamine and berberine) to induce a synergistic antitumoural effect.^[89] The synthesized MSNs were first functionalised with 3-methacryloxypropyltrimethoxysilane. Then, the capping co-polymer named p(NIPAM-co-MA) was formed from *N*-isopropylacrylamide (NIPAM) and methacrylic acid (MA) through seed precipitation polymerisation. After that, the pores were loaded with berberine. Finally, evodiamine was modified with 1,2-distearoyl-*sn*-glycero-3-phosphoethanolamine-*N*-[methoxy(PEG₂₀₀₀)](DSPE-PEG₂₀₀₀) and absorbed onto the nanoparticle surface forming a lipid bilayer. The p(NIPAM-co-MA) presents a low critical solution temperature (LCST) of 39 °C. The solid showed a negligible drug release at pH 7.4 or 37 °C. Nevertheless, pH decrease (pH 5) and temperature rise to 41 °C led to sustained drug delivery. Below LCST, the polymer on the surface stretched to form a film that blocks nanoparticle pores. However, at 41 °C the polymer shrank, uncover the mesopores, and allows drug release. Additionally, when pH decreases, the polymer protonates, leading the materials to take a compact conformation that triggers drug release (Figure 11). The nanomaterial demonstrated good biocompatibility and safety in HepG2, HCT-8, and HeLa tumoural cell lines and the non-tumoural HUVEC cells. The nanoparticles presented great potential for effective antitumour therapy because they led to an important synergistic inhibition of tumour cell proliferation, as well as tumour cell migration and invasion. Also, the same nanoparticles were able to inhibit capillarity tube formation in HUVEC cells as a model of tumour angiogenesis. Finally, the nanoparticles were intravenously administered to female breast cancer-bearing mice. The nanosystem substantially decreased the tumour growth and the drug side effects when compared with the dual treatment with free drugs.

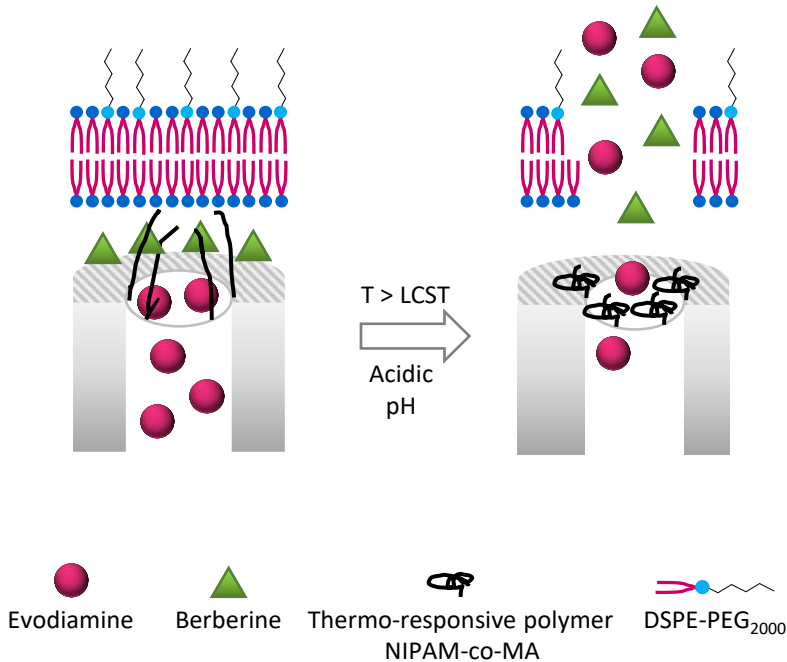


Figure 11. Schematic representation of temperature-driven drug delivery. MSNs loaded with berberine and evodiamine and capped with a thermosensitive p(NIPAM-co-MA) polymer and DSPE derivatized with PEG lipid bilayer. Above LCST or acidic pH, the payload is delivered.

1.3.2 Exogenous stimuli-responsive materials.

Gated materials responding to external stimuli represent a potential tool for on-command drug release in biomedical applications. These nanodevices provide more control of the premature release. Thus, the on-target effect of drugs is increased, and undesirable side effects are diminished. Examples reported of drug delivery from gated materials triggered by external stimuli are described below.

- **Light-driven drug delivery.**

Light can be used as a non-invasive triggering stimulus that offers remote finely spatiotemporal control of drug release from photosensitive systems. In the past years, a large number of light-driven on-command delivery nanoparticles have been engineered, which release their payloads in response to illumination of specific wavelengths in the ultraviolet, visible, or near-infrared (NIR) regions.^[80]

In this context, Xu and co-workers developed a multifunctional gated material to perform photodynamic therapy, drug release, gene therapy, and photoacoustic imaging.^[90] The authors prepared rattle-structured nanocapsules composed of hollow MSNs with core gold nanorods (AuNRs) for trimodal cancer therapy. The nanocapsules were functionalised with amino groups and then adamantanecarboxylic moieties were incorporated to the surface by an amidation reaction. After that, the nanoparticles were loaded with the antitumoural drug sorafenib. The pores were capped with a polycation designed with two-armed ethanolamine-functionalised poly(glycidylmethacrilate) units with one β -cyclodextrin (β -CD) core to carry genes for gene therapy; in this case the antioncogene p53 (Figure 12). The NIR-responsive behaviour of the nanocapsules was demonstrated; in absence of NIR, no sorafenib release was found, whereas when NIR laser was applied a massive drug release was recorded. This is due to the capping polycation detachment induced by the photothermal effect of gold nanorods. When the liver tumour cell line HepG2 was treated with the complete system, containing the p53 antioncogene and sorafenib, and irradiated with NIR laser light, the cell viability was dramatically reduced because of the combined effect of the gene, chemo and photothermal therapy. Finally, hepatoma-bearing nude mice were treated with the nanocapsules. The group of animals treated with the complete nanoparticles and irradiated experienced a highly suppressed tumour

growth and thus tumour size was notably reduced compared to control groups. Additionally, the nanoparticles were successfully employed for photoacoustic and computed tomography imaging due to the presence of the AuNRs core.

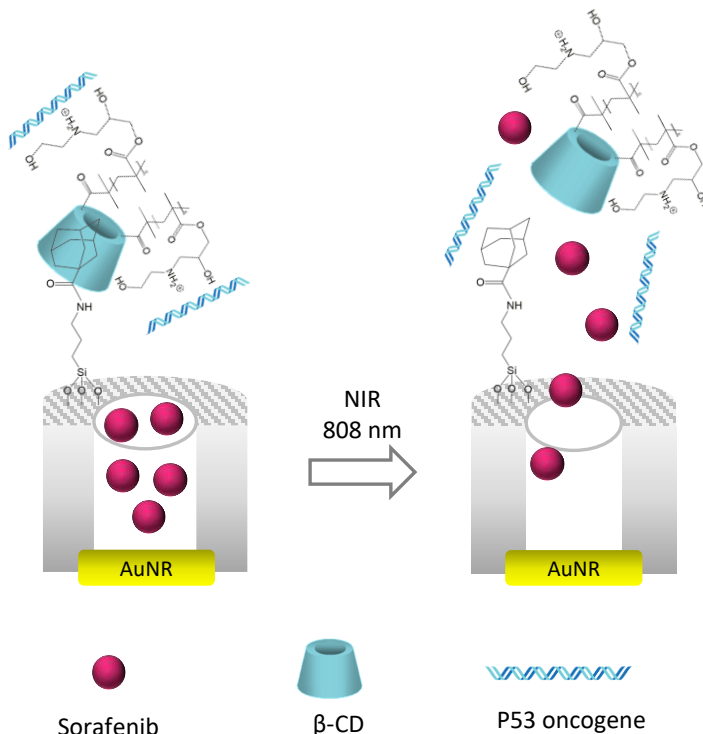


Figure 12. Schematic representation of light-driven drug delivery. AuNRs coated with mesoporous silica loaded with sorafenib, capped with a photosensitive inclusion complex with p53 antioncogene. Under NIR the polycation is detached from the nanoparticle surface and sorafenib is released.

- **Magnetically-driven drug delivery.**

Several systems are designed to allow drug delivery when exposed to a magnetic field as external stimuli to achieve completely spatiotemporal controlled delivery with minimal invasion. These systems are based on core-shell nanoparticles, usually having a Fe_2O_3 core surrounded by a mesoporous silica shell,

polymers, or liposomes.^[91] These systems allow magnetic guidance under a permanent magnetic field.^[92,93] Additionally, the application of an alternating magnetic field (AMF) leads to local heating of the nanoparticles. This phenomenon can be used to perform thermal therapy, to destroy malignant cells. Additionally, AMF-driven delivery systems combined with thermosensitive moieties (such as polymers) as molecular gates can trigger cargo release under the heat dissipated by the superparamagnetic core.^[94] Importantly, the incorporation of a magnetic core is appealing for biomedical application since it offers the possibility of performing magnetic resonance imaging, and thus to combine diagnostics and therapy within a single system (the so-called theragnostic approach).^[95,96]

As an illustrative example, Vallet-Regí and co-workers presented AMF-sensitive nanoparticles for *in vivo* tumour treatment.^[97] The system was built with superparamagnetic iron oxide magnetic nanoparticles (SPIONs) embedded in a mesoporous silica matrix. The MSN matrix was coated with a thermosensitive polymer shell as molecular gate. First, the external silica surface was functionalised with small PEG chains and [tris(trimethylsiloxy)silyl]propyl methacrylate. In the next step, radical polymerisation was performed using the monomers N-isopropylacrylamide, N-(hydroxymethyl)acrylamide, and N,N'-methylenebis(acrylamide) in the presence of ammonium persulfate as radical initiator (Figure 13). The polymer shell was designed to have a LCST of 42 °C. Below LCST, the unarranged polymer chains block the pore opening and keep the drug entrapped in the silica matrix. When the temperature rises to 42 °C, the polymer changes from hydrophilic to hydrophobic state and collapses. This event uncaps the pores in the structure and therefore allows the drug release. The authors validated their nanoparticles in melanoma-bearing mice using the final solid loaded with the anticancer drug doxorubicin. They found that the nanoparticles deeply penetrated

within the tumour. The study also revealed that doxorubicin-loaded nanoparticles under an AMF effectively reduce tumour growth, compared to single treatments with only doxorubicin or AFM. It can be explained because of the synergistic effect of heating and drug release.

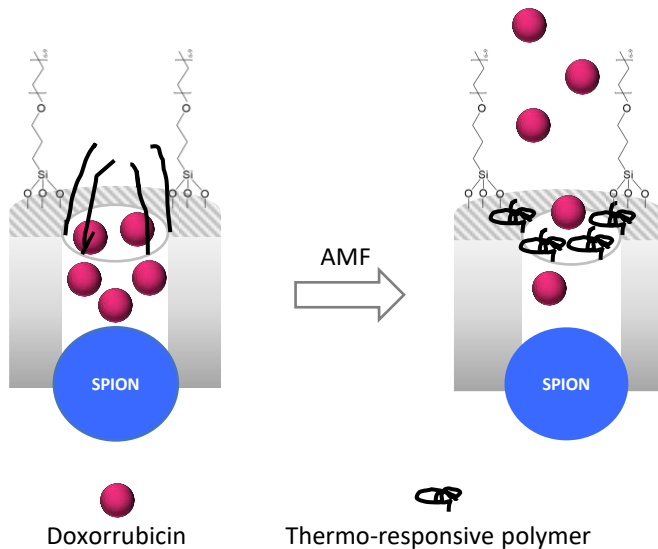


Figure 13. Schematic representation of magnetically-driven drug delivery. SPION coated with MSNs loaded with doxorubicin and functionalised with PEG. The thermosensitive polymer is used as molecular gate. The application of an AMF leads to a conformation change in the thermosensitive polymer and doxorubicin delivery.

- **Ultrasound-driven drug delivery.**

Ultrasounds (US) represent an effective exogenous stimulus for the spatiotemporal control of drug release, avoiding harmful side effects to healthy tissues and incrementing therapeutic effect in target cells. This type of irradiation is non-invasive and it is known to penetrate deep in tissues.^[98] US waves trigger drug release from the pore voids to the exterior by cavitation phenomena. Moreover, it has been described that physical forces associated with cavitation

transiently increase vessel permeability, leading to enhanced uptake of the therapeutic molecules.^[99] US can be also used as a safe visualisation technique by using microbubbles, usually made of perfluorocarbons, as contrast agents.^[100] During the last decade, microbubbles have been incorporated into nanocarriers for controlled delivery applications.^[101,102] All these features envision US-driven MSNs as excellent theragnostic systems for localised drug administration with superior imaging capability.

Zhang and co-workers developed a multifunctional drug delivery vehicle based on MSNs encapsulated into US-responsive microbubbles.^[103] MSNs were first functionalised with (3-Aminopropyl)triethoxysilane (APTES) and then *N*-hydroxysuccinimide-modified folic acid (FA) was incorporated in the nanoparticles by amide bond formation. Afterward, the nanoparticles were loaded with coumarin 6 or the apoptosis inducer tanshinone IIA. Finally, the nanoparticles were included in a microbubble formed by mixing 1,2-dipalmitoyl-sn-glycero-3-phosphocholine (DPPC) and 1,2-dipalmitoyl-sn-glycero-3-phosphoethanolamine (DPPE) lipids and injecting perfluorocarbon octafluoropropane (C₃F₈) during the microbubble formation process (Figure 14). In an initial step, the authors demonstrated the ultrasound imaging contrast enhancement capability of the final nanosystems *in vitro* and *in vivo*. In the next step, cytotoxicity evaluation in cervix tumour cells (HeLa) and lung tumour cells (A549) demonstrated that nanoparticles loaded with tanshinone IIA effectively induce apoptosis in a dose-dependent manner in both cell lines. Additionally, preferential internalisation of nanoparticles by HeLa cells overexpressing folate receptor (FR) was proven, compared with A549 cells expressing low levels of FR. Finally, tanshinone IIA-loaded final solid was injected in hepatocarcinoma-bearing mice. Mice injected with the nanoparticles and subsequently irradiated with ultrasounds exhibited excellent tumour growth

suppression. The efficacy of the treatment was associated with the combined action of membrane permeation and microbubble rupture, together with the FR active targeting of loaded MSNs and the controlled drug delivery upon US irradiation.

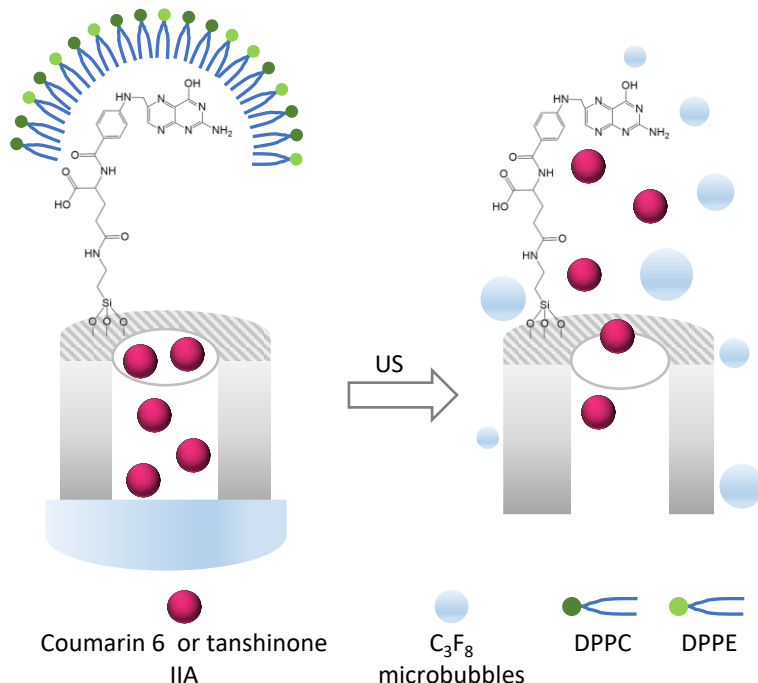


Figure 14. Schematic representation of US-driven drug delivery. FA-functionalised MSNs loaded with coumarin 6 or tanshinone IIA included into C_3F_8 and phospholipid microbubbles. Upon the application of US the microbubble is broken and coumarin 6/tanshinone IIA is released.

1.3.3 Gated mesoporous silica nanoparticles as drug delivery systems in biomedical applications.

In the last years, nanomedicine has emerged as an alternative to conventional therapeutic approaches, due to the superior performance of the therapeutic agents when nanocarriers are used as vehicles. The very first generation of nanoparticle-

based therapy included liposome nanoparticles, which are FDA-approved. Nowadays, there are on the market more than 50 nanosystems based on a great variety of materials, i.e., polymers, micelles, proteins, and metallic nanoparticles (Figure 15).^[104,105]

As an alternative to these traditional delivery systems, stimuli-responsive gated MSNs have been widely studied for the controlled release of therapeutic molecules with biomedical purposes (Figure 16).^[106] In 2001, a MCM-41-type mesoporous material was first reported as a drug delivery system by Vallet-Regí and co-workers.^[24] The authors prepared MSNs loaded with the anti-inflammatory drug ibuprofen and reported the successful controlled release in response to the presence of simulated human plasma. Nowadays, MSNs are widely investigated as a promising tool to enhance the performance of conventional therapeutic molecules, because of their several features that make them suitable candidates for human health care.

First, the mesoporous scaffold can entrap payloads from different natures (hydrophobic and hydrophilic)^[107] to improve drug solubility and pharmacokinetic profile. Also, nanoparticles accumulate preferentially in tumour areas through the so-called EPR effect (see [section 1.5](#)).^[108] Furthermore, the nanoparticle surface can be functionalised with specific targeting moieties to promote selectivity towards specific cell types. In order to achieve ligand-mediated targeting, also known as active targeting, specific molecules (i.e., antibodies,^[109–111] peptides,^[112–114] aptamers,^[115–117] etc.) are selected to bind surface molecules or receptors overexpressed in diseased organs, tissues, or cells (Figure 16). Together all these facts improve the therapeutic effect and minimize the off-target toxicity of the drug molecules encapsulated in the nanoparticles.

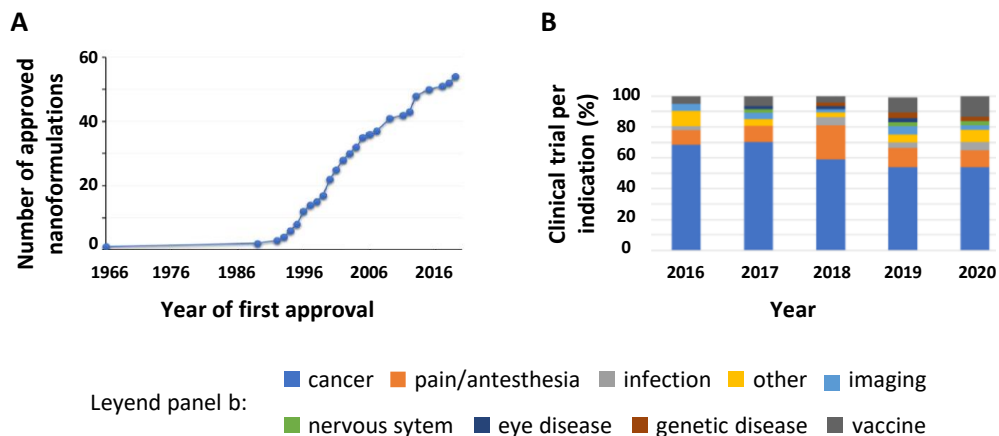


Figure 15. Date recompilation of the development of nanomedicines until 2020.

A) Evolution of the approved nanomedicine formulations (cumulative number/year). First year of approval reported for formulations approved by multiple agencies (e.g., EMA and FDA). **B)** Percentage nanoformulation in clinical trials per indication in the 2016-May 2020 period 333 trials). Adapted from *J. Control. Release.* **2020**, 326, 164–171.

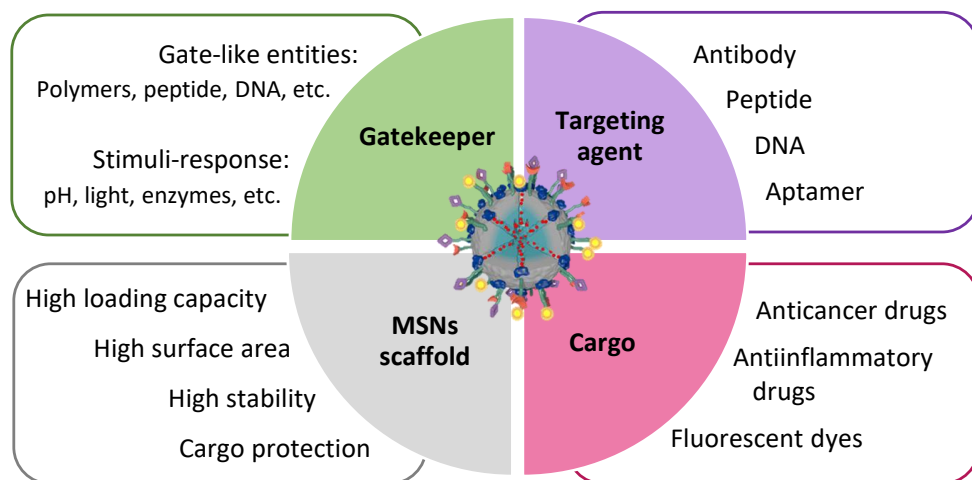


Figure 16. Schematic representation of multifunctional gated MSNs. The nanoparticle contains the necessary components for a stimuli-responsive controlled release of a loaded cargo into a targeted cell. Adapted from *Chem. Mater.* **2014**, 26, 1, 435-451. Copyright © 2013 American Chemical Society.

1.3.4 Clinical relevance of gated mesoporous silica nanoparticles.

As stated above, MSNs are promising vehicles for drug delivery to target locations in order to enhance the drug therapeutic index *in vitro* and *in vivo*. Nevertheless, clinical translation remains challenging nowadays. While FDA approved nanomaterials are mainly polymeric and liposomal-based nanoparticles (e.g., PEG-modified IFN α -2b protein and liposomal doxorubicin), there is an increasing interest in the development of novel nanomaterials: micelles, protein-based nanoparticles, and diversity of metallic and inorganic particles have already entered in clinical trials.^[118]

Silica is classified by the FDA as “generally recognized as safe” (GRAS).^[119] In recent years some clinical trials have been started using silica-based nanoparticles, but only one of them has been completed (NANOM-FIM) (ClinicalTrials.gov Identifier: NCT01270139). NANOM-FIM clinical trial purchased “Plasmonic Nanophotothermic Therapy of Atherosclerosis” based on nanotechnology. Researchers developed a bioengineered patch containing a silica-gold scaffold and stem cells for the treatment of coronary atherosclerosis. The patients treated with the scaffold demonstrated a great regression in atherosclerosis plaque volume, compared with the group treated only with stent implantation, without major complications.^[120,121]

There are some other promising studies in the early clinical phases focused on cancer diagnosis. For example, the trial referred to as “Targeted Silica Nanoparticles for Real-Time Image-Guided Intraoperative Mapping of Nodal Metastases” (ClinicalTrials.gov Identifier: NCT02106598). This work developed integrin-targeted core-shell silica nanoparticles functionalised with PEG and labelled with Cy5.5 as fluorescent dye and radioiodine for operative lymph node mapping for breast,

colorectal, and melanoma malignancies.^[122,123] Another study, referred to as Evaluation of “Nano-crystalline Hydroxyapatite Silica Gel in Management of Periodontal Intrabony Defects” (ClinicalTrials.gov Identifier: NCT02507596) is applying nano-crystalline hydroxyapatite silica gel for the management of periodontal defects.^[124,125]

In summary, the increasing progress in nanotechnology and nanomedicine fields has derived in the development of novel nanocarriers with some of them in clinical trials and even FDA-approved. Drug delivery nanosystems are suitable for the treatment of diverse ailments; while being cancer the most widely studied, there are also other diseases with high associated mortality (infections,^[126,127] inflammatory disorders,^[128,129] ageing-related diseases,^[130,131] etc.) that are attractive therapeutic targets, in which gated MSNs can play an essential role in the future medicine.

1.4 Gold nanoparticles.

Gold has been used for medical purposes since ancient times. Reports dating from the Middle Ages indicate the use of “soluble gold” for curative purposes.^[132] More recently, the use of colloidal gold nanoparticles (AuNPs) has greatly increased in various fields: catalysis, sensing, drug delivery, and theragnostic.^[133] AuNPs are the most stable metal nanoparticles and gather properties that make them excellent nanomaterials for biomedical applications, including: ^[134,135]

- Inertness and excellent biocompatibility.
- Large surface-to-volume ratio.
- Easily functionalisable surface.
- Size and shape-related optoelectronic properties.

- Efficient conversion of light into heat.
- Efficient absorption of X-ray radiation.

The most highlightable feature of AuNPs is perhaps their intrinsic optical properties. Due to the local surface plasmon resonance (LSPS), the optical properties of gold nanoparticles change dramatically depending on their size and shape (Figure 17). This trait is the principle of many gold-based nanodevices used in diagnosis, detection, or labelling applications, based on colorimetric techniques. Indeed, AuNPs are currently the standard technique of simple diagnostic assays, such as pregnancy tests.^[136]

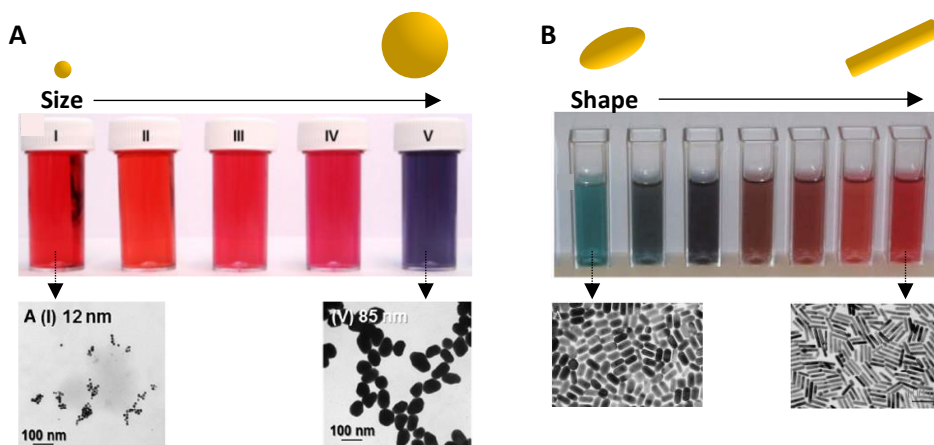


Figure 17. Local surface plasmon resonance of AuNPs. Tunable optical properties of AuNPs by changing **A)** the size of colloidal AuNPs and **B)** the aspect ratio. Adapted from *Nanomedicine*. **2017**, 13, 4, 1531-1542. Copyright © 2017 The Author(s). Published by Elsevier Inc. and *J. Adv. Res.* **2010**, 1, 1, 13–28. Copyright © 2009 University of Cairo

1.4.1 Synthesis and functionalisation of gold nanoparticles.

There are a large number of approaches to synthesize gold nanoparticles to finely control the size,^[137–139] shape,^[140] and surface functionality.^[141–144] Generally,

the procedures for the synthesis of gold nanoparticles can be divided into three categories: chemical, physical and biological methods.^[145]

Physical procedures include methods such as laser ablation,^[146] ultrasonic radiation^[147], and photochemical process,^[148] among others. In biological methods, nanoparticles are synthesized using plant-based extracts^[149] and microorganisms.^[150] On the other hand, chemical methods are performed in an aqueous medium by a reduction agent (for instance, hydrogen peroxide,^[151] borohydrides,^[152] hydroquinone,^[153] etc.).

Among chemical procedures, Turkevich-Frens method is one of the most well-known techniques. In 1951, Turkevich et al. developed a synthetic method based on citrate reduction of chloroauric acid (HAuCl_4) in boiling water, where sodium citrate ($\text{Na}_3\text{C}_6\text{H}_5\text{O}_7$) acts as a reducing and stabilizing agent.^[154] Frens et al. further improved this method to control the particle size by changing the gold-to-citrate ratio.^[155] Nowadays the Turkevich-Frens synthetic protocol is frequently employed because it is simple and highly reproducible. Moreover, the sodium citrate acts as a stabilizing capping agent, and possible modifications of the synthesis process depending on desired the final product are reported in the literature.^[156]

The Turkevich-Frens synthetic procedure is divided into three steps, namely, (i) precipitation of gold atoms, (ii) nucleation, and (iii) growth of the crystal nuclei (Figure 18). In the initial step, an aqueous solution of sodium citrate is quickly poured into a boiling aqueous solution of HAuCl_4 under mechanical stirring. The presence of the reducing agent (sodium citrate) leads to the precursor (HAuCl_4) reduction and the consequent increase in the concentration of gold atoms (stage i: precipitation of gold atoms). When the gold atoms concentration exceeds the critical supersaturation (stage ii: nucleation), the gold atoms start gathering to form

crystal nuclei. Gold atoms are gradually consumed and eventually the concentration of gold atoms declines below the critical supersaturation (stage iii: growth of crystal nuclei). Then, the number of crystal nuclei no longer increases, and the growth of nuclei dominates the reaction. When the concentration of gold atoms decreases to the saturation level, crystal nuclei stop growing and the process is completed.^[157]

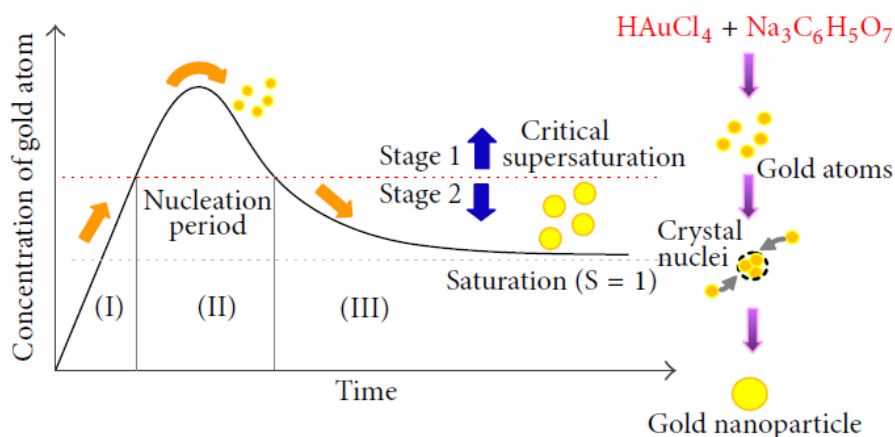


Figure 18. Schematic representation of the synthetic procedure of AuNPs. AuNPs formation is based on HAuCl_4 chemical reduction by sodium citrate. Reprinted with the *Adv. Mater. Sci. Eng.* **2015**, 160819. Copyright © 2015 Guojun Liu et al.

Sodium citrate as a reducing agent allows the preparation of monodisperse spherical AuNPs with diameters of 10 to 20 nm.^[158] Alternatively, methods with small variations in the synthesis protocol can be employed to finely control the nanoparticle size. For example, instead of using citrate as a reducing agent, hydroquinone^[159] or sodium borohydride^[160] have been used to obtain larger (50-500 nm) and smaller AuNPs (2-5 nm), respectively. Furthermore, several additives (e.g., CTAB or salicylic acid) can be added to the reaction to obtain AuNPs with various sizes and shapes (e.g., gold nanorods,^[161] triangular/hexagonal AuNPs, etc.).^[162]

Importantly, the use of nanoparticles for biomedical purposes requires surface modification with specific biomolecules (i.e., oligonucleotides,^[163–165] peptides,^[166–168] antibodies,^[169–171] drugs,^[172–174] etc.) that will introduce the required biofunctionalities. The ligand molecules can bind to the nanoparticle surface by either (i) electrostatic interaction, (ii) hydrophobic interaction, and (iii) chemisorption. Chemisorption, sometimes also noted as a covalent bond, is the term used to describe the interaction of thiol groups with noble metal surfaces, which is considered the one with the highest affinity; particularly to gold surfaces (approx. 200 kJ mol⁻¹).^[175] Mercaptocarboxylic acids are probably the most employed molecules to stabilize the nanoparticle surface, as they can be further exploited for the conjugation with additional biomolecules (Figure 19).^[176] For example, amide bond formation between free ends of the carboxylic acid and amino groups on biomolecules is the most widespread protocol and it has led to the preparation of numerous successful gold-based nanomaterials.^[177–181]

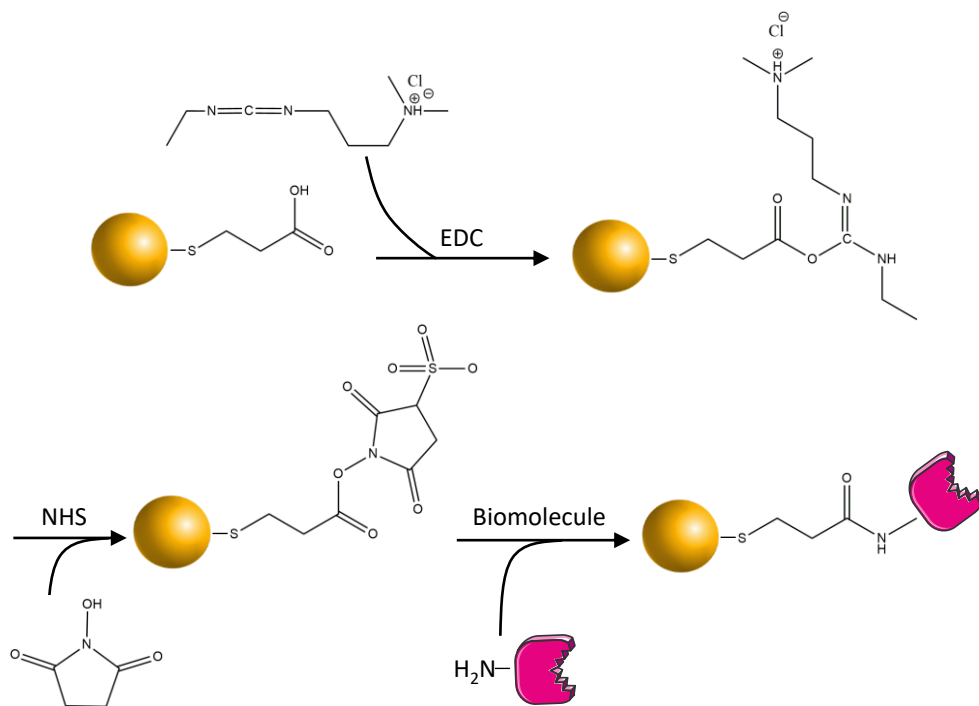


Figure 19. Schematic illustration of biomolecule conjugation reaction with AuNPs equipped with a terminal carboxylic acid function. The gold nanoparticles are firstly functionalised with mercaptocarboxylic acids by chemisorption. Afterward, the carbodiimide EDC forms an unstable intermediate, a so-called activated carboxylic group. This can react with a primary amino group present in a biomolecule through the formation of a stable amide bond. Optionally the activated carboxylic group can be reacted with NHS. The active ester has an extended half-life and reacts with primary amines in the biomolecules.

1.4.2 Clinical relevance of gold nanoparticles.

Gold nanoparticles are promising vehicles in a wide range of research fields due to their unique combination of optical/thermal properties and their tuneable size, shape, and surface chemistry.^[182–184] However, only a few examples of gold-based nanomaterials are actively investigated in clinical trials, and none has been approved to date for therapeutic applications by the FDA (see [Figure 15](#)).

The only clinical trial completed successfully was the previously mentioned NANOM-FIM study (ClinicalTrials.gov Identifier: NCT01270139) for atherosclerosis treatment with silica-gold nanoparticles.^[121] Another interesting clinical study is the trial referred to as “TNF-Bound Colloidal Gold in Treating Patients with Advanced Solid Tumors” (ClinicalTrials.gov Identifier: NCT00356980), focused on colloidal gold safety evaluation (Phase I).^[185] This work employed recombinant human tumour necrosis factor (rhTNF) bound to colloidal gold through PEG as a linker (CYT-6091). Researchers conducting this trial found that the maximum tolerated dose of rhTNF formulated as CYT-6091 was 3-fold higher than native rhTNF. Also, CYT-6091 accumulates in tumour tissues and preliminary data suggested partial responses in some cancer patients. These promising results led the authors to focus on future clinical studies combining CYT-6091 with chemotherapy for the systemic treatment of non-resectable cancers, yet any other results have been disclosed for far.

Together these trials anticipate the near future of next-generation therapy. The multifunctionality makes gold nanoparticles promising materials for their implementation in biomedical applications. To date, significant research advances have been done in cellular and animal models. However, the clinical translation is still challenging, and further investigation will assist the incorporation of AuNPs into the clinical daily routine.

1.5 Biocompatibility and biodistribution of nanoparticles.

The biological applicability of nanoparticles as drug delivery and diagnosis nanodevices has been reported in numerous studies. The fundamental requirement for a biomaterial to be applied in a living system is its biocompatibility, that is, the ability to perform the purchased medical therapy without eliciting

undesirable local or systemic effects in the recipient.^[186] Specifically, silica and gold-based nanoparticles are generally claimed as biocompatible materials,^[187–190] though in a few cases certain toxic effects have been observed, such as oxidative stress and cell damage.^[191–194]

The biological effects (such as biocompatibility, cellular uptake pathway, cellular fate, biodistribution, accumulation, retention, and clearance) of nanomaterials are complex as they rely on a range of nanoscale features (i.e., composition, size, shape, porosity, dosages, etc.).^[195–199] For example, in the case of MSNs, the increased porosity of the scaffold, as well as surface modification with amine groups, reduce the toxicity associated with nanoparticle treatment in mouse models.^[200] Clear evidence of the influence of size on the biodistribution is exemplified by spherical-shaped AuNPs. *In vivo* experiments showed that small AuNPs (<15 nm) were widely distributed in various organs, i.e., blood, liver, spleen, kidney, testis, thymus, heart, lung, and brain, whereas larger AuNPs were mainly detected in the liver and spleen.^[201]

Another key factor in nanoparticle safety is biodegradability. MSNs are constituted by -Si-O- bonds that are susceptible to hydrolytic breakdown of the siloxane (Si-O-Si) group, thus generating orthosilicic acid (Si(OH)₄).^[202,203] The degradation products are biocompatible and excreted in urine and faeces, depending on the nanoparticle size and the administration route.^[112,204–207] It has been determined that 50% of administered silica amount is removed from the organism 4-week after treatment and longer times are required to achieve the entire clearance of the particles. The long circulation time of silica-based materials has been claimed as another advantage to the development of stable nanocarriers for *in vivo* applications.^[188] In the case of AuNPs, the current dogma is that inertness prevents AuNPs from biodegradation, which could remain indefinitely in tissues.

Nevertheless, recent findings suggest that gold nanoparticles are progressively degraded inside de cells in a size-dependent manner.^[208,209] Alternatively, AuNPs can be also excreted in urine and faeces in a size and composition-dependent fashion.^[210–212] Besides, it has been reported that 50% of administered gold nanoparticles are cleared from the organism 8-week after treatment.^[213]

It has been established that nanoparticles circulate and accumulate in major target organs, which are the liver, spleen, and lungs, due to their high capacity to retain foreign substances.^[214] Moreover, nanomaterials can be designed for the passive and active targeting of diseased tissues. Nanoparticles display distinctive pharmacokinetic and biodistribution compared to small drug molecules, which results in the improvement of the efficacy profile with reduced toxic effects of the carried drug. The nanoparticle fate in a living organism can be divided into three major phases that represent complex biological barriers for nanodevices to overcome ([Figure 20](#)), namely: (i) systemic circulation and reticuloendothelial system (RES) interaction, (ii) extravasation and tumour penetration, and lastly, (iii) interaction with the target cells.

Properly formulated nanoparticles evade renal filtration cut-off size (i.e., the 5.5 nm)^[215] and exhibit prolonged blood circulation time for efficiently achieving the target tissue. Once in the blood circulation, nanoparticles interact with the mononuclear phagocyte system (MPS), which consists of a global system of macrophages resident in the liver, spleen, lungs, and lymph nodes, that rapidly sequester the nanoparticles.^[216,217] MPS recognizes and uptakes nanodevices-bearing opsonins (serum proteins), which are attached to the surface of the particles in blood circulation. There are several approximations to bypass the MPS, such as tailoring particle size and morphology or surface decoration with different biomolecules.^[218] The most common strategy may be functionalising the surface of

the nanoparticles with PEG (PEGylation), which results in a hydrating layer that hinders the protein adsorption (or protein “corona” effect) and the subsequent clearance by MPS.^[219–225]

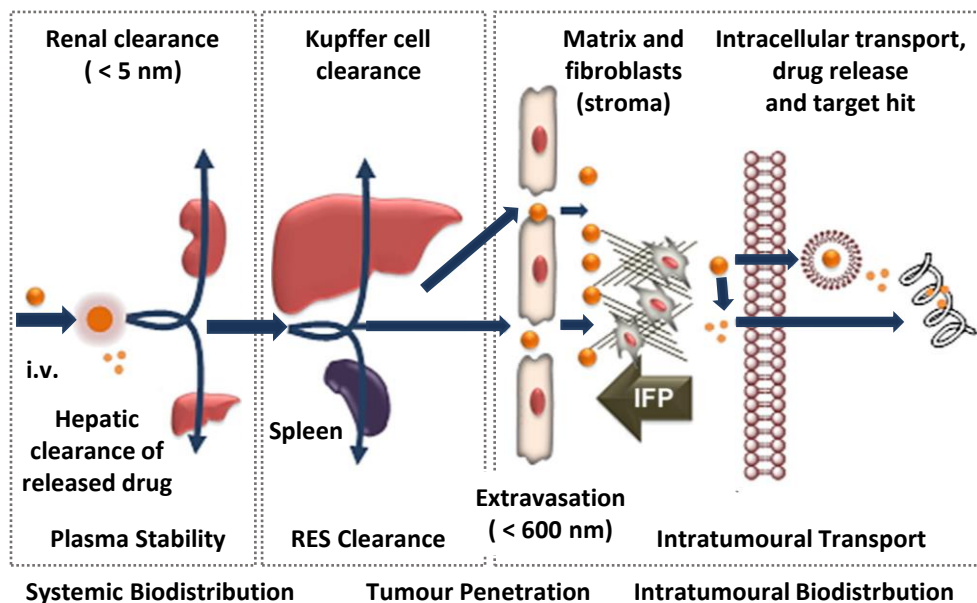


Figure 20. The three phases of controlled drug delivery by nanoparticles in the organism. Nanoparticles injected intravenously must (i) evade the renal filtration and RES system, (ii) remain stable in blood circulations, and (iii) penetrate in tumour tissues. Once the nanoparticles extravasate into the tumour, stimuli-responsive nanoparticles deliver the drug for performing the pharmacological effect. Reprinted with the permission of *J. Control. Rel.* **2013**, 172, 3, 782-94. Copyright © 2013 Elsevier B.V.

The nanoparticles exceeding the 5.5 nm renal filtration cut off size^[215] face a second size limit imposed by liver filtration. The liver presents vascular fenestrations that entrap nanoparticles smaller than 50 nm and larger than 200 nm.^[226] The upper limit of particle size is determined by two factors: splenic filtration and tumour permeability. It has been demonstrated that large particles are recruited by the spleen because they are retained into intercellular slits that

rarely exceed 200-500 nm in width.^[227,228] Other physicochemical properties than size (such as shape,^[229] superficial charge^[230,231] or surface functionalisation^[224,225]) are crucial parameters that impact circulation, accumulation in the target site, and clearance rate and route.

After successfully surviving in blood circulation and bypassing the RES, the second phase of drug delivery is nanoparticle extravasation from the bloodstream and retention in the tumour tissue, in which tumour permeability plays a critical role. It is well-known that solid tumours are characterised by a unique vasculature structure (i.e., dense, immature, chaotically branched, and dilated blood vessels) and impaired lymphatic drainage, which leads to the nanoparticle preferential and selective accumulation in tumour sites through the EPR effect ([Figure 21](#)). Tumours present vascular fenestrations from 400-600 nm to microns that allow the uptake of macromolecules and nanoparticles, which accumulate at higher concentrations and longer times than small drug molecules. In normal tissues (excepting RES), the continuous contact in the blood vessels prevents extravasation of nanoparticles.^[232–238] Generally, 100 nm in diameter tends to represent an optimal range to achieve the EPR effect and minimizing clearance.^[239] However, the optimal particle size is not necessarily equivalent for every type of nanomaterial, thus the biodistribution and pharmacokinetic profiles of each platform should be independently studied considering the set of physicochemical properties previously mentioned.

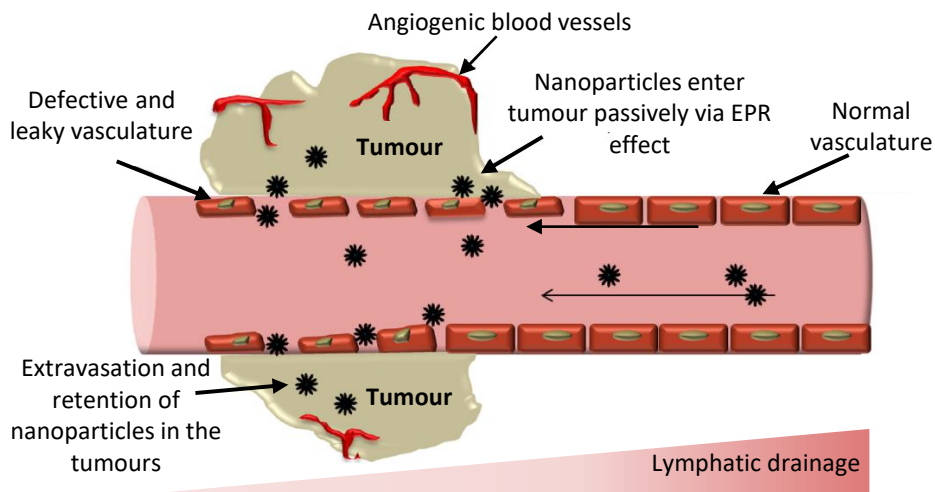


Figure 21. EPR effect and passive targeting. Nanocarriers can extravasate into the tumours through the gaps between endothelial cells and accumulate due to poor lymphatic drainage. Adapted from *Front. Pharmacol.* **2014**, 5, 77. Copyright © 2014 Jhaveri and Torchilin.

The third phase of drug delivery involves nanoparticle penetration in the tumour tissue and drug release. The nanoparticles that successfully extravasate into the tumour face additional barriers, such as high interstitial fluid pressure, dense stromal tissue, and fibroblasts, and macrophages associated with tumour cells. As nanomaterials extravasate into the tumour, there must be an internalisation and intracellular drug release to exert the pharmacological effect.^[218]

Multiple cellular routes are available for nanoparticles to cross the cellular membrane (Figure 22). Those are not well-understood yet; however, it is described that nanoparticles are mainly internalised by cells through pinocytosis. This is an energy-dependent and complex mechanism of endocytosis consisting of the internalisation of small particles upon the formation of a cell membrane invagination, which leads to the formation of a vesicle inside the cell containing the internalised material.^[240] Pinocytosis can be further divided into four distinct

pathways: (i) macropinocytosis, (ii) caveolae-mediated endocytosis, (iii) clathrin-mediated endocytosis, and (iv) clathrin/caveolin-independent endocytosis (see [Figure 22](#)).^[241] Several uptake mechanisms can be acting simultaneously, with different efficiencies, depending on the physicochemical features of the nanomaterial.^[242,243] Of all the four pathways, the clathrin-mediated endocytosis is the predominant for nanoparticles with a diameter smaller than 200 nm.^[244–246] Besides, the nanoparticles functionalised on their surface with active targeting molecules (such as antibodies, aptamers, proteins, peptides, etc.) promote the specific and active nanocarrier binding to certain receptors overexpressed on the target cell surface with the subsequent receptor-mediated cellular uptake.

The details of the exact endocytosis pathway are important because they determine the intracellular trafficking through various subcellular organelles. For example, nanoparticles internalised through clathrin-mediated endocytosis are destined for a lysosomal compartment, whereas those internalised through the caveolin-mediated pathway are trafficked to the endoplasmic reticulum and the Golgi apparatus.^[247] In some applications, such as gene delivery, it is mandatory to deliver the nanoparticles and their cargo into the cytoplasm. For this purpose, endosomal escape must occur before fusion with a lysosome to prevent degradation of the cargo under harsh lysosomal conditions.^[248,249] To achieve the escape from the endosomal compartments the most common strategy employed involves the functionalisation of the nanoparticles with cationic polymers, such as polyethyleneimine (PEI), which act as “proton sponges”. These polymers have a high buffering capacity in the endosomal pH range (pH 5-7); as consequence, they prevent the acidification of the endosomes and, simultaneously, swell when protonated, which facilitates the rupture of the endosomal membrane and the release of the nanoparticles.^[250,251] Alternatively, some strategies involve the use of

cell-penetrating peptides (CPPs), such as the transactivator of transcription (TAT) peptide, that allows the direct penetration of the nanoparticle into the cytoplasm through clathrin/caveolin-independent pathway.^[252,253]

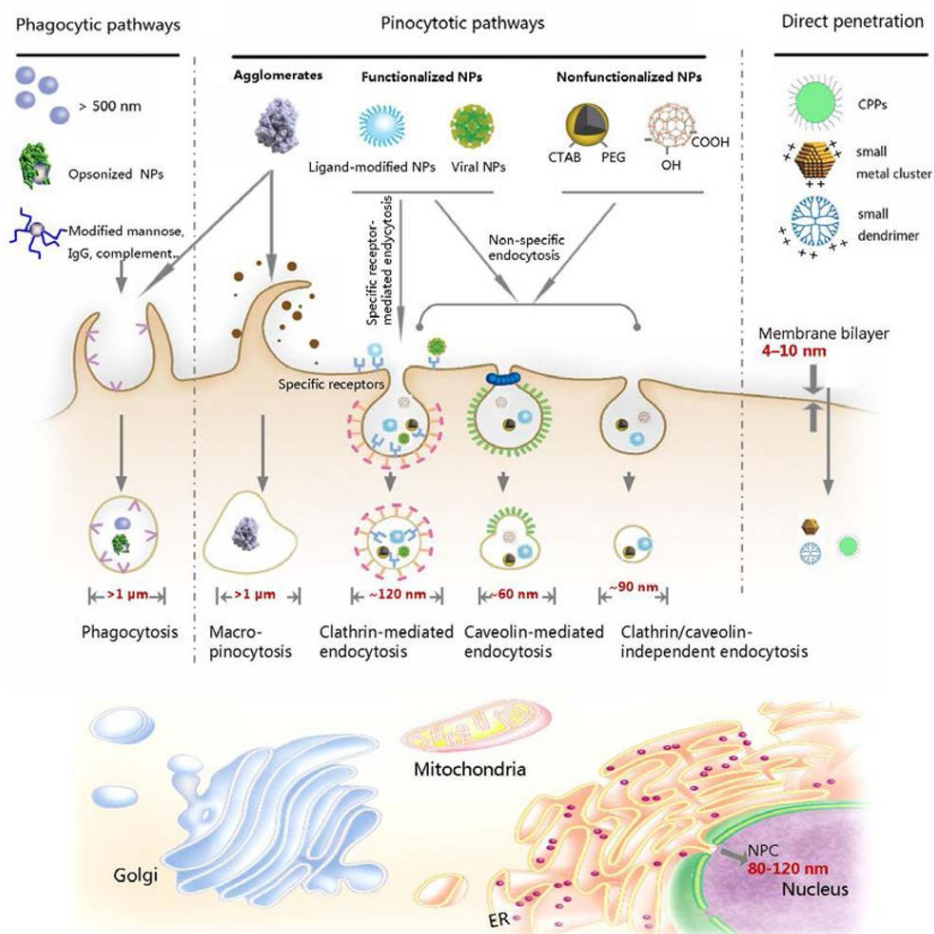


Figure 22. Schematic overview of the different internalisation pathways of nanomaterials. Reprinted with permission of *Acc. Chem. Res.* **2013**, 46, 3, 622-631. Copyright © 2012 American Chemical Society.

Considering all the presented variables influencing the nanoparticle fate in the living organism, only judicious tailoring of nanoscale features (i.e., composition,

size, shape, surface charge, surface functionalisation, etc.) would enable the precise control of the nanoparticles therapeutic effect. What is more, only the exhaustive control of the nanoparticle behaviour in the diseased organism would approach the use of the nanomaterials to the clinical routine as targetable and traceable drug delivery and diagnostic platforms.

1.6 Breast cancer.

Breast cancer is a group of diseases involving abnormal cell growth within the breast tissue, with the potential to invade or spread to other parts of the body. It is the second most common cancer worldwide and among women, it is the most commonly diagnosed, and the leading cause of death.^[254] Factor risks for breast cancer development include age, parity, alcohol use, body mass index, family history of breast cancer, contraceptives, and menopausal hormone therapy.^[255] The most frequent clinical signs of breast cancer are skin changes, such as redness or swelling, sudden change in breast or nipple size, form, or aspect, fluid exudate from the nipple, general breast pain, or appearance of different sized-lumps or nodes in the breast.^[256]

1.6.1 Breast cancer intrinsic subtypes.

Breast cancer has been traditionally classified according to clinicopathological variables: tumour size, tumour grade, and nodal involvement, together with the immunohistochemistry expression of three membrane proteins: estrogen (ER), progesterone (PR), EGFR (HER2) in biopsies.^[257]

The recent emergence of high-throughput technologies for gene expression analysis, such as microarrays, led to a deeper insight into breast cancer with a classification beyond PR/ER/HER2 expression status. This concept resulted in a new

paradigm in which breast cancer is a set of diseases affecting the same anatomical structures characterised by previously uncovered heterogeneity within patients in several features: clinical presentation, prognosis, outcome, and therapy responses. According to the molecular signature, breast cancer can be classified into six subtypes: i.e., luminal A, luminal B, HER2-enriched, basal-like (commonly referred to as triple-negative), claudin-low, and normal-like.^[258] Each breast cancer subtype presents a different prevalence (Figure 23A), as well as different survival rates (Figure 23B). Thus, gene expression profiling significantly contributed to patient stratification into subpopulations for prognosis and therapeutic decision-making.^[259]

As follows the two breast cancer subtype models employed in this thesis (luminal A and triple-negative breast cancer subtypes) are further described:

- **Luminal A** subtype is the most frequently diagnosed, accounting for 50-60% of the total breast cancers. It is characterised by the expression of ER and PR receptors and low expression levels of HER2 oncoprotein.^[257,260] Luminal A tumours present low proliferation rates, measured by Ki-67, and low histological grade.^[261] Patients with this subtype of cancer have a good prognosis, due to the high responsiveness to anti-hormone therapy. Also, luminal A patients present the longest median survival with distant metastasis (median of 2.2 years).^[262-264]
- **Triple-negative (TN)** tumours account for 10-20% of the newly diagnosed cases. The most relevant feature of this type of tumours is the absence of expression of the three key breast cancer receptors, i.e., ER, PR, and HER2.^[265] TN tumours constitute an extremely heterogenic and invasive group. Besides its aggressiveness and highly proliferative behaviour, this cancer presents lower detection rates compared with other subtypes.

Therefore, patients present large tumours in advanced stages when diagnosed. As a consequence, the TN group has the poorest prognosis and an increased risk of early recurrence with visceral metastasis (lungs and brain).^[266] Because of the lack of molecular targets, patients with TN breast cancer (TNBC) do not benefit from currently available targeted therapies. Fortunately, they exhibit higher sensitivity and response rates to chemotherapy when compared with non-TNBC patients, but despite initial responsiveness, they also show poorer outcomes, which is referred to as the TNBC paradox.^[267,268]

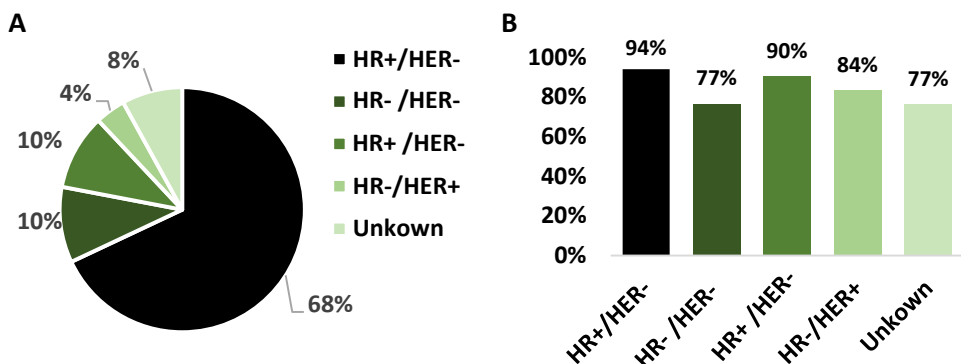


Figure 23. Female breast cancer statistics. A) Percent of female breast cases by cancer subtype (2013-2017). B) 5-year relative survival percent among female breast cases by cancer subtype (2010-2016). Data extracted from the *National Cancer Institute*. Cancer statistics: female breast cancer subtypes.

1.6.2 Current therapeutic approaches for breast cancer treatment.

Breast cancer is a complex pathology, and so is its treatment. The genomic signature and ER/PR/HER2 status help to determine the treatment choice, although suitable therapy is definitively established considering tumour burden/location and

biology, as well as the age, menopausal status, general health, and patient preferences.^[269]

Breast cancer treatment involves a combination of local modalities (i.e., surgery and radiotherapy), systemic cancer treatments (i.e., chemotherapy, endocrine therapy, and anti-HER2 therapy) (Figure 24), and supportive measures, administered in diverse sequences.^[269,270] TNBC patients are the most challenging subgroup to treat because they intrinsically lack druggable targets. Currently, the only available treatment for them is surgery combined with radiotherapy and (neo)adjuvant chemotherapy.^[271,272]

Chemotherapy and radiotherapy induce cell death triggering apoptosis (or programmed cell death).^[273–276] Those conventional therapies present a great impact on cancer treatment. However, due to their unspecific mechanism of action, chemotherapy and radiotherapy also damage highly proliferative but healthy cells (for instance, bone marrow or intestinal tissue) leading to well-known side-effects, such as loss of hair, pain, vomiting, constipation, fatigue, or a depressed immune system.^[277–284] Besides, despite initially effective, tumour cells can rapidly develop drug resistance mechanisms provoked by the selective pressure caused by anticancer treatments. Even some tumours present inherent resistance to apoptosis-inducing agents. This phenomenon avoids the complete elimination of the tumour mass and ultimately treatment failure.^[285–287]

To overcome treatment resistance, and the subsequent recurrence and mortal metastatic disease emergence, new strategies are being developed to activate apoptosis through alternative pathways.^[288–297] In this regard, increasing attention has been focused on targeting Bcl-2 anti-apoptotic proteins, as they play an important role in tumour development.^[298] In the following section, the

molecular mechanisms behind treatment resistance mediated by anti-apoptotic proteins overexpression and current strategies to bypass this resistance mechanism are further detailed, due to its significance in the development of the present thesis.

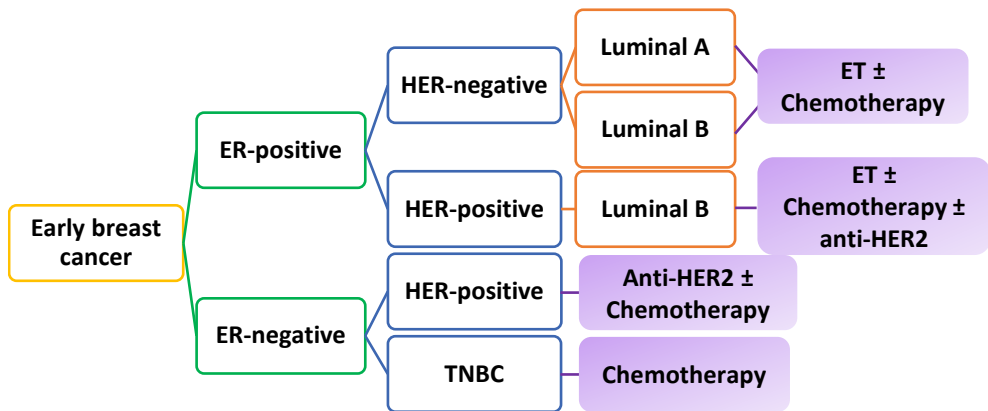


Figure 24. (Neo)adjuvant systemic treatment choice by marker expression and intrinsic phenotype. ER-positive tumours are treated with endocrine therapy (ET) (tamoxifen and aromatase inhibitors); luminal A tumours are not usually treated with chemotherapy, except those with high disease burden and high risk of recurrence.^[269] Luminal B tumours benefit from chemotherapy co-treatment.^[299] Tumours overexpressing HER2 are co-treated with anti-HER2 therapy (trastuzumab), which has proved to halve the recurrence and mortality risk.^[300–302] ER-negative tumours present the more pronounced benefit from chemotherapy (mainly taxanes and anthracyclines).^[303–306] Adapted from *Ann Oncol*, **2019**, 30, 8, 1194-1220 © Cardoso et al. 2019.

1.6.3 Bcl-2 protein family and drug resistance in breast cancer.

Apoptosis is a form of programmed cell death, which plays an essential role in organism development and tissue homeostasis. It is initiated by a variety of environmental perturbations such as growth factor withdrawal, infections, DNA damage, endoplasmic reticulum stress, reactive oxygen species overload,

replication stress, microtubular alterations, or mitotic defects.^[307] The proteins belonging to the Bcl-2 family act as master regulators of apoptosis. This family is divided into three subfamilies based on their primary function (Figure 25): (i) anti-apoptotic proteins, (ii) pro-apoptotic pore-formers, and (iii) pro-apoptotic BH3-only proteins. In general, the balance between these proteins determines cell survival or cell death, through the intrinsic or mitochondrial pathway. When activated, the intrinsic apoptotic pathway results in mitochondrial outer membrane permeabilization (MOMP), releasing cytochrome c into the cytosol and, ultimately, leading to cell death (Figure 26).^[308,309]

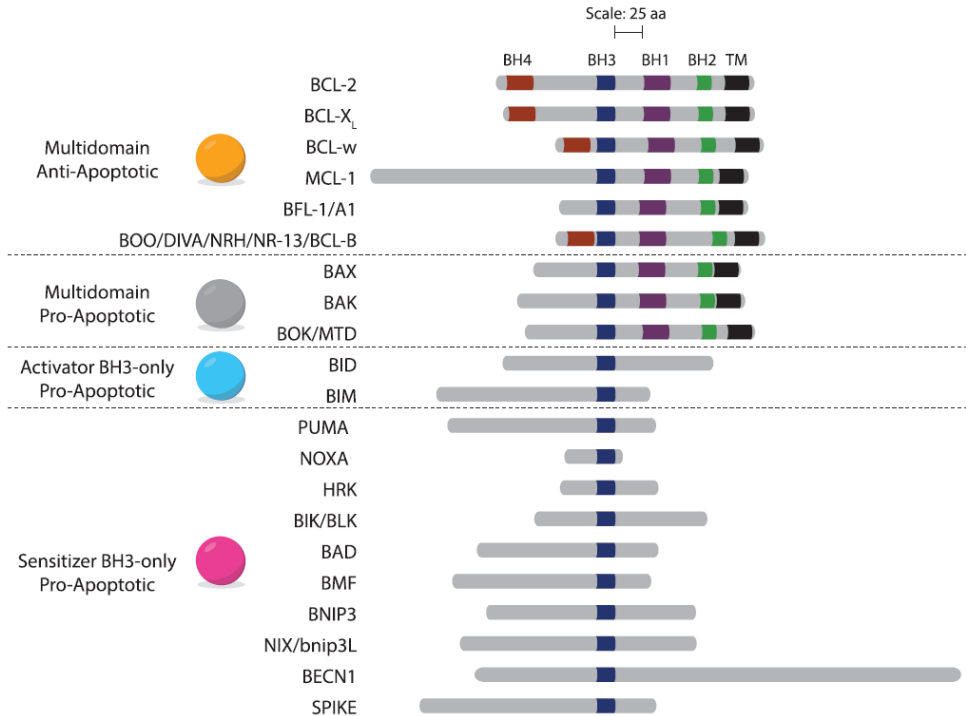


Figure 25. Classification of Bcl-2 family members. Bcl-2 proteins are grouped by their ability to inhibit or activate apoptosis. Shared, conserved Bcl-2 homology (BH) and transmembrane (TM) regions are depicted. Reprinted with permission from *Cell Death & Differ.* **2017**, 24, 8, 1348–1358. Copyright © 2017, Springer Nature.

Bcl-2 anti-apoptotic proteins are frequently overexpressed or hyperactivated in tumours, leading to evasion of apoptosis (which is a major hallmark of cancer).^[310] Several tumours have shown alterations in Bcl-2 proteins,^[311–314] including breast cancer.^[315,316] The inability to respond to apoptotic stimuli has been linked to breast cancer tumorigenesis,^[317–320] tumour progression,^[319,321–324] and treatment resistance.^[325–330] The involvement of Bcl-2 proteins in tumour pathology supports their pharmacological targeting for anticancer therapy. With this aim, a new class of small molecules, known as BH3 mimetics, has been recently developed (Figure 26). The first orally available BH3 mimetic was navitoclax (or ABT-263),

which binds to Bcl-2, Bcl-xL, and Bcl-w.^[331] Navitoclax presented efficacy in clinical trials against several malignancies as monotherapy or combined with other chemotherapeutic drugs.^[332–336] However, navitoclax clinical use has been impaired because it produces severe thrombocytopenia (platelet apoptosis) in patients mediated by Bcl-xL inhibition.^[337–339] As a consequence, venetoclax (or ABT-199) was developed, being 200- fold less active targeting Bcl-xL.^[340] The value of such a drug has been highlighted in the treatment of chronic lymphocytic leukaemia and acute myeloid leukaemia where venetoclax has received FDA approval.^[341–348]

Regarding breast cancer, several preclinical studies suggest that targeting anti-apoptotic Bcl-2 proteins in combination with conventional antitumour therapies would improve the treatment response.^[349–351] However, there are not completed clinical trials with results proving the antitumour efficacy in breast cancer patients yet. Encouragingly, several active clinical trials aim to determine the safety and efficacy of BH3 mimetics in combination with other chemotherapeutic agents to treat breast cancer patients (e.g., ClinicalTrials.gov Identifier: NCT03584009, NCT03900884, NCT04298918).

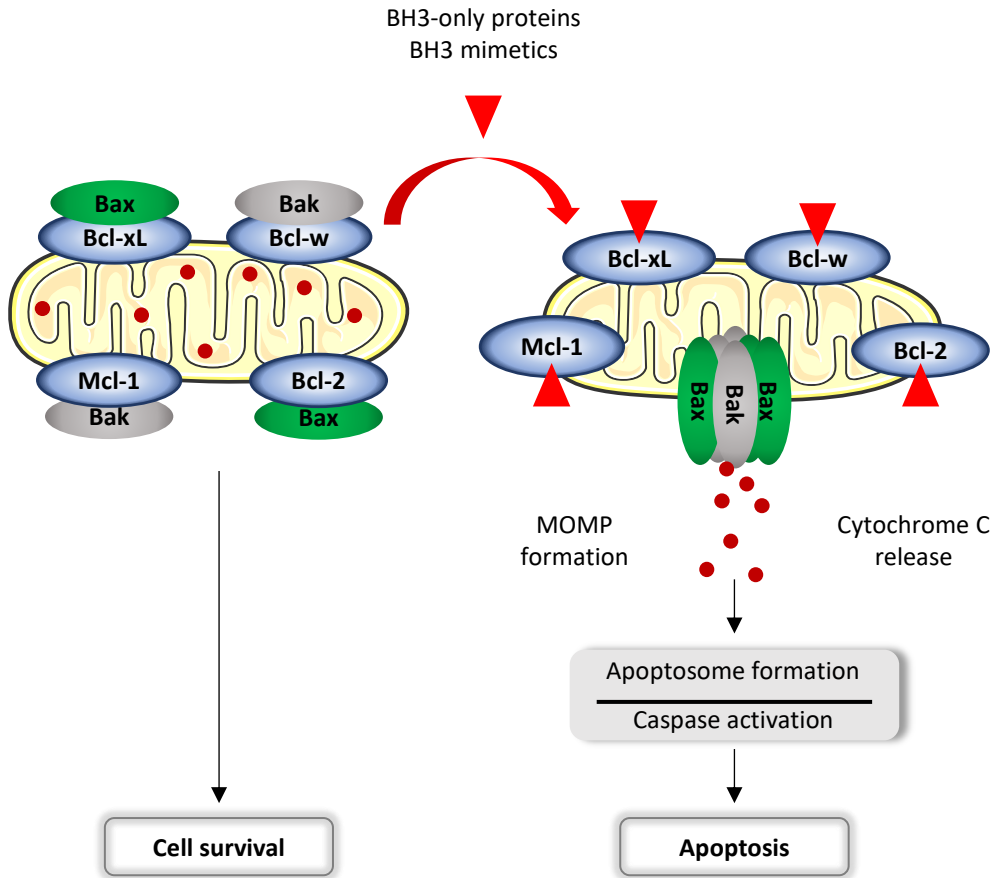


Figure 26. Representation of the intrinsic apoptosis pathway. The anti-apoptotic members (i.e., Bcl-2, Bcl-w, Bcl-xL, and Mcl-1) recruit and inactivate the pro-apoptotic proteins (i.e., Bax and Bak). When the BH3-only proteins are induced by stress signals or the cells are treated with BH3 mimetics, they trigger Bax and Bak activation. Bax and Bak oligomerize in the outer mitochondrial membrane resulting in MOMP and cytochrome c release into the cytosol, thereby committing the cell to apoptosis.

The very first generation of BH3 mimetic drugs bind with high affinity to Bcl-2, Bcl-xL, and Bcl-w, but fail to bind to Mcl-1. Because of the compensatory behaviour of the Bcl-2 family members, treatment with such BH3 mimetics leads to rapid drug resistance onset mediated by Mcl-1 overexpression.^[352–358] Therefore,

complementary treatments to overcome this resistance are urgently needed. In this context, the efforts focussed on developing Mcl-1 inhibitors. To date, there are seven selective and direct inhibitors of Mcl-1, four of them (AZD5991, AMG-176, AMG-397, and S64315/MIK665) being tested in clinical trials as monotherapy or combination with venetoclax for the treatment of acute myeloid leukaemia, multiple myeloma, non-Hodgkin lymphoma, and chronic lymphocytic leukaemia patients (ClinicalTrials.gov Identifier: NCT03218683, NCT02675452, NCT03797261, NCT03465540, NCT02979366, NCT02992483, and NCT03672695). Mcl-1 inhibitors have demonstrated preclinical efficacy in restoring sensitivity to BH3 mimetic drugs in breast cancer^[355] and other malignancies.^[359–361] Also, they have demonstrated synergistic activity with other anticancer treatments (i.e., docetaxel, trastuzumab, and lapatinib).^[362]

Based on the above, the two main clinical limitations derived from antitumoural agents, including the novel BH3 mimetic drugs, become apparent. The severe side effects, coupled with the rapid onset of drug resistances, call urgently for the development of new strategies that could succeed over current chemotherapy hurdles. As detailed in the following section, nanotechnology emerged as an attractive tool with the potential to improve tumour therapy outcomes. On one hand, the rational design of nanodevices for controlled drug delivery at specific diseased locations has released promising results regarding the reduction of drug-related adverse events and the increase of therapeutic benefits. On the other hand, the development of nanoparticles as carriers of smart drug combinations would boost the effective overcoming tumour drug resistance, such as the Bcl-2-mediated ones.

1.6.4 Nanomedicine-based approach for breast cancer treatment.

Nowadays, despite advances forward more targeted therapies (such as poly-ADP ribosepolymerase-1 inhibitors,^[288,289] PI3K/AKT pathway inhibitors,^[290,291] EGFR inhibitors,^[292,293] vascular growth factor inhibitors,^[294,295] immunotherapy,^[363] etc.), chemotherapy is still the most frequent approach to treat the majority of cancers.^[269] However, chemotherapy effectiveness is limited, and further research is needed to improve the clinical outcome of cancer patients. Several obstacles limit therapeutic success. Firstly, the therapeutic performance of cytotoxic drugs is markedly reduced by their poor solubility in aqueous media; low-soluble drugs preferentially accumulate in peripheral tissues, which translates into systemic toxicity and sub-optimal drug bioavailability in the tumour site.^[364] Moreover, the poor bioavailability problem is exacerbated by the development of multidrug resistance mechanisms, which leads to the failure of the chemotherapy.^[298,365,366] As a consequence of these unfavourable events, patients are treated with the maximum tolerated dose to achieve a therapeutic response.^[367] Therefore, the broad distribution of high drug concentrations in multiple cells causes well-known serious side effects and systemic toxicities.^[368]

According to these premises, nanomedicine has emerged as an alternative approach to overcome the limitations of conventional chemotherapy. Nanomedicine purchases the targeted and controlled drug delivery to specific diseased locations relying on passive and active targeting (see [section 1.2.7](#) and [section 1.4](#)). In this field, the design and application of novel targeted drug delivery systems for breast cancer treatment have arisen, and their efficacy have been widely proved in preclinical models.^[369] Nevertheless, nanomedicine clinical translation remains a challenge. To date, the limited number of FDA-approved nanoplatforms for breast cancer treatment are based on organic nanoparticles.^[370]

The most well-known are liposome-encapsulated doxorubicin (e.g., Doxil)^[371–377] and albumin-bounded paclitaxel nanoparticles (Abraxane or nab-paclitaxel),^[378–383] which have demonstrated greater permeation into the tumour site compared with the free drugs. Consequently, these nanomedicines significantly reduce adverse effects.

Despite the dramatically improved pharmacokinetics, biodistribution, efficacy, and safety profiles of nanomedicines in preclinical models, variable results regarding overall survival have been found in clinical trials.^[384] The inconsistency of clinical results suggests that patients have a significant variation in tumour pathophysiology, resulting in variable therapeutic outcomes that mask the real benefit of nanoformulated drugs. Particularly, the heterogeneous tumour vasculature is pointed as a crucial factor influencing tumour uptake and efficacy.^[384,385] Indeed, it is becoming widely accepted that only selected patients with highly permeable tumours can benefit from nanomedicine.^[386,387] Thus, biomarkers are urgently required to identify the receptive subpopulation and push the nanoparticle success beyond the bench-side.^[388]

On the other hand, inorganic nanoplatforms are less clinically represented, despite their enhanced versatility compared to organic nanodevices.^[105] In the case of MSNs and AuNPs, numerous preclinical studies have demonstrated that chemotherapeutic drugs and imaging agents carried by nanoparticles show superior performances when compared with their free counterparts (see [section 1.2.8](#) and [section 1.3.2](#)). Despite not being clinically implanted yet, strategies targeting tumour tissues using inorganic nanoparticles are a realistic alternative to increase the benefits of the systemic therapies currently used to treat cancer.

MSNs have already been applied in various cancer models, including different breast cancer subtypes. For example, Zeng and co-workers developed MSNs loaded with doxorubicin and capped with polydopamine (PDA) and PEG.^[389] PDA functions as an acidic pH-sensitive gatekeeper to control doxorubicin release from MSNs and PEG was further grafted on the surface of PDA to increase the stability and biocompatibility under physiological conditions. The therapeutic effect of the nanocarrier was confirmed in luminal A and TNBC cell lines and in nude mice bearing subcutaneous luminal A tumours. The nanoparticles significantly suppressed the tumour growth *in vivo*; the nanodevice demonstrated enhanced tumour inhibition ability compared with free doxorubicin. Besides, the nanodevices proved to be biocompatible and safe as neither systemic toxicity in major organs nor body weight loss in the mice was observed. Many other works show the potential of the MSNs for breast cancer treatment. In a recent work of our research group, Martínez-Máñez and co-workers encapsulated navitoclax in MSNs capped with a hexagalactooligosaccharide molecule.^[390] The work aimed to combine the senescence induction in tumour cells (i.e., cell cycle arrest that occurs in response to stressful stimuli) with their subsequent elimination (senolysis) as a strategy to inhibit tumour relapse *in vivo*. The drug-loaded nanoparticles were capped with the hexagalactooligosaccharide, which acts as a molecular gate and as a targeting agent. The hexagalactooligosaccharide is hydrolysed by the lysosomal enzyme β -galactosidase, only expressed in senescent cells. As a consequence, navitoclax is specifically delivered in senescent cells after the molecular gate opening upon enzymatic hydrolysis. The authors demonstrated the antitumour efficacy of the combination of senescence induction and targeted senolytic therapy in an immunocompetent orthotopic mouse model of TNBC subtype. Following palbociclib-induced senescence and nanoparticle treatment, they observed

inhibited tumour growth, reduced metastases, and a reduction in the systemic toxicity of navitoclax.

Regarding gold-based nanodevices, nanoparticles with an extremely wide variety of sizes and shapes have been successfully employed in the biomedical field, mostly in bioimaging and treatment applications. In this respect, AuNPs are still in very preliminary phases, as breast cancer investigations with AuNPs are performed in cell line models, and few examples in the bibliography step forward experiments in animal models. Both *in vitro* and *in vivo* studies led to promising results, showing the potential of gold-based nanomaterials for breast cancer treatment. For example, Kundu and co-workers aimed to augment the therapeutic effects and improve the clinical outcomes of curcumin in breast cancer therapy.^[172] With this objective, they explored FA conjugation and loading of curcumin into gold nanoconjugates functionalised with polyvinylpyrrolidone. The nanoparticles presented antitumour and antimetastatic activity against human and murine breast cancer cell lines. In contrast, the nanoparticles demonstrated low cytotoxicity when incubated with normal cells. Furthermore, the antitumour efficacy was evaluated in triple-negative breast tumour-bearing mice. The results demonstrated that tumour growth was significantly inhibited with nanoparticle treatment, whereas free curcumin and non-treated animals experienced any reduction in the tumour volume. The authors finally claim that the enhanced antitumour effect obtained with the gold nanoconjugates may be due to the increased water solubility, the specific targeting, and the slower clearance from the body of the nanoformulated curcumin. As another example of a promising work revealing the AuNPs potential for breast cancer therapy, Tang and co-workers presented a gold nanoparticle-mediated drug delivery nanoplatfrom for the co-delivery of doxorubicin and a siRNA targeted to polo-like kinase 1 (PLK1).^[173] PLK1 down-regulation has

demonstrated to inhibit cancer progression and to restore sensitivity to doxorubicin. Thus, the authors hypothesized that PLK1 protein suppression in combination with the anti-proliferative effect of doxorubicin would result in a synergistic therapeutic effect. With this purpose, they prepared gold nanoparticles functionalised with doxorubicin through pH-responsive thiol bonds. Besides, siRNA PLK1 was electrostatically bound to the gold core surface, which was previously functionalised with PEG/PEI co-polymer. The synergistic effect of the combinatorial treatment over chemotherapy and gene therapy alone has been demonstrated in a metastatic breast cancer cell line and spheroids. As a conclusion, the authors point to the designed nanomaterials as a versatile platform that can be adapted for further conjugation of other therapeutic drugs and clinically relevant genes.

Considering all these encouraging investigations, MSNs and AuNPs are potential candidates to be applied in the treatment and diagnosis of breast cancer. However, despite the numerous promising studies performed in cell and animal models, there is still a lack of inorganic nanoparticles available on the market. Even with their great potential to transform the current treatment strategies, their translation to the clinic remains a considerable challenge. Several reasons justify the absence of inorganic nanoparticle implementation in the daily routine of human health care. First, the extensive research on the topic evidences the huge variety of experimental designs among preclinical studies. The lack of homogeneous approximations and criteria for the evaluation of treatment effectiveness leads to not easily comparable experiment results. Specifically, there are controversial data about nanoparticle biocompatibility; MSNs and AuNPs are generally claimed as biocompatible materials, although some studies reported toxicity and immunological effects after nanoparticle administration in preclinical models.^[212,391–396] As previously detailed, the induction of toxicity is largely

dependent on the nanoparticle physicochemical properties (such as size, shape, porosity, and surface functionalisation, as well as exposure time and dose)(see [section 1.5](#)). Moreover, the lack of clinical translation is also attributed to the concern of nanoparticle persistence in organisms after the designed action, as currently, the long-term effects derived from the inevitable accumulation of the nanoparticles in major organs are largely unknown.^[397–401] For further development beyond preclinical stages, the long-term effects in the animal models need to be deeper addressed, and also standardized methods for assessing nanoparticle biocompatibility and persistence in the organism should be implemented.

1.7 References.

- [1] M. Jena, S. Mishra, S. Jena, S. S. Mishra, *Int. J. Basic Clin. Pharmacol. Rev. Artic.* **2013**, *2*, 353–359.
- [2] R. P. Feynman, *Eng. Sci.* **1960**, *23*, 22–36.
- [3] N. Taniguchi, *Japan Soc. Precis. Eng.* **1974**.
- [4] K. Narendra, K & Sunita, *Essentials in Nanoscience And Nanotechnology*, **2013**.
- [5] S. Eustis, M. A. El-sayed, M. Kasha, *Chem. Soc. Rev.* **2006**, *35*, 209–217.
- [6] B. Pelaz, C. Alexiou, R. A. Alvarez-Puebla, F. Alves, A. M. Andrews, S. Ashraf, L. P. Balogh, L. Ballerini, A. Bestetti, C. Brendel, S. Bosi, M. Carril, W. C. W. Chan, C. Chen, X. Chen, X. Chen, Z. Cheng, D. Cui, J. Du, C. Dullin, A. Escudero, N. Feliu, M. Gao, M. George, Y. Gogotsi, A. Grünweller, Z. Gu, N. J. Halas, N. Hampp, R. K. Hartmann, M. C. Hersam, P. Hunziker, J. Jian, X. Jiang, P. Jungebluth, P. Kadhiresan, K. Kataoka, A. Khademhosseini, J. Kopeček, N. A. Kotov, H. F. Krug, D. S. Lee, C.-M. Lehr, K. W. Leong, X.-J. Liang, M. Ling Lim, L. M. Liz-Marzán, X. Ma, P. Macchiarini, H. Meng, H. Möhwald, P. Mulvaney, A. E. Nel, S. Nie, P. Nordlander, T. Okano, J. Oliveira, T. H. Park, R. M. Penner, M. Prato, V. Puntès, V. M. Rotello, A. Samarakoon, R. E. Schaak, Y. Shen, S. Sjöqvist, A. G. Skirtach, M. G. Soliman, M. M. Stevens, H.-W. Sung, B. Z. Tang, R. Tietze, B. N. Udugama, J. S. VanEpps, T. Weil, P. S. Weiss, I. Willner, Y. Wu, L. Yang, Z. Yue, Q. Zhang, Q. Zhang, X.-E. Zhang, Y. Zhao, X. Zhou, W. J. Parak, *ACS Nano* **2017**, *11*, 2313–2381.
- [7] R. Bayford, T. Rademacher, I. Roitt, S. X. Wang, *Physiol. Meas.* **2017**, *38*, R183–R203.
- [8] D. Lombardo, M. A. Kiselev, M. T. Caccamo, *J. Nanomater.* **2019**, *2019*, 3702518.
- [9] C. Perego, R. Millini, *Chem. Soc. Rev.* **2013**, *42*, 3956–3976.
- [10] K. M. Thomas, *Catal. Today* **2007**, *120*, 389–398.
- [11] S. Jafari, H. Derakhshankhah, L. Alaei, A. Fattahi, B. S. Varnamkhasti, A. A. Saboury, *Biomed. Pharmacother.* **2019**, *109*, 1100–1111.
- [12] D. H. Everett, *Pure Appl. Chem* **1972**, *31*, 577–638.
- [13] X. S. Zhao, *J. Mater. Chem.* **2006**, *16*, 623–625.
- [14] J. S. Beck, J. C. Vartuli, W. J. Roth, M. E. Leonowicz, C. T. Kresge, K. D. Schmitt, C. T. W. Chu, D. H. Olson, E. W. Sheppard, S. B. McCullen, J. B. Higgins, J. L. Schlenker, *J. Am. Chem. Soc.* **1992**, *114*, 10834–10843.
- [15] J. C. Vartuli, K. D. Schmitt, C. T. Kresge, W. J. Roth, M. E. Leonowicz, S. B. McCullen, S. D. Hellring, J. S. Beck, J. L. Schlenker, D. H. Olson, E. W. Sheppard, *Chem. Mater.* **1994**, *6*, 2317–2326.
- [16] C. T. Kresge, W. J. Roth, *Chem. Soc. Rev.* **2013**, *42*, 3663–3670.

- [17] J. A. S. Costa, R. A. de Jesus, D. O. Santos, J. F. Mano, L. P. C. Romão, C. M. Paranhos, *Microporous Mesoporous Mater.* **2020**, *291*, 109698.
- [18] J. G. Croissant, Y. Fatieiev, A. Almalik, N. M. Khashab, *Adv. Healthc. Mater.* **2018**, *7*, 1700831.
- [19] S. Bhattacharyya, G. Lelong, M. L. Saboungi, *J. Exp. Nanosci.* **2006**, *1*, 375–395.
- [20] M. E. Morales, H. Castán, E. Ortega, M. A. Ruiz, *Pharm. Chem. J.* **2019**, *53*, 329–336.
- [21] W. Stöber, A. Fink, E. Bohn, *J. Colloid Interface Sci.* **1968**, *26*, 62–69.
- [22] Q. Cai, Z. S. Luo, W. Q. Pang, Y. W. Fan, X. H. Chen, F. Z. Cui, *Chem. Mater.* **2001**, *13*, 258–263.
- [23] N. K. Raman, M. T. Anderson, C. J. Brinker, *Chem. Mater.* **1996**, *8*, 1682–1701.
- [24] M. Vallet-Regi, A. Rámila, R. P. Del Real, J. Pérez-Pariente, *Chem. Mater.* **2001**, *13*, 308–311.
- [25] H. B. S. Chan, P. M. Budd, T. V. De Naylor, *J. Mater. Chem.* **2001**, *11*, 951–957.
- [26] K. Yano, Y. Fukushima, *J. Mater. Chem.* **2004**, *14*, 1579–1584.
- [27] K. Möller, J. Kobler, T. Bein, *Adv. Funct. Mater.* **2007**, *17*, 605–612.
- [28] H. Yamada, C. Urata, H. Ujiie, Y. Yamauchi, K. Kuroda, *Nanoscale* **2013**, *5*, 6145–6153.
- [29] K. Möller, T. Bein, *Chem. Mater.* **2017**, *29*, 371–388.
- [30] J. Kobler, K. Möller, T. Bein, *ACS Nano* **2008**, *2*, 791–799.
- [31] N. A. Zainala, S. R. A. Shukor, H. A. A. Wabb, K. Razakb, *Chem. Eng.* **2013**, *32*.
- [32] H. P. Lin, C. P. Tsai, *Chem. Lett.* **2003**, *32*, 1092–1093.
- [33] Y. D. Chiang, H. Y. Lian, S. Y. Leo, S. G. Wang, Y. Yamauchi, K. C. W. Wu, *J. Phys. Chem. C* **2011**, *115*, 13158–13165.
- [34] A. Stein, B. J. Melde, R. C. Schroden, *Adv. Mater.* **2000**, *12*, 1403–1419.
- [35] F. Hoffmann, M. Cornelius, J. Morell, M. Fröba, *Angew. Chemie - Int. Ed.* **2006**, *45*, 3216–3251.
- [36] M. Faustini, L. Nicole, E. Ruiz-Hitzky, C. Sanchez, *Adv. Funct. Mater.* **2018**, *28*, 1–30.
- [37] F. Sancenón, L. Pascual, M. Oroval, E. Aznar, R. Martínez-Máñez, *ChemistryOpen* **2015**, *4*, 418–437.
- [38] F. Sancenón, E. Yu, E. Aznar, M. D. Marcos, R. Martínez-Máñez, in *Drug Deliv. Syst.*, World Scientific, **2016**, pp. 113–183.
- [39] C. Coll, A. Bernardos, R. Martínez-Máñez, F. Sancenón, *Acc. Chem. Res.* **2013**, *46*, 339–349.
- [40] Q. Yan, X. Guo, X. Huang, X. Meng, F. Liu, P. Dai, Z. Wang, Y. Zhao, *ACS Appl. Mater. Interfaces* **2019**, *11*, 24377–24385.

- [41] S. Liu, B. Tian, S. Wu, Y. Wang, J. Huang, B. Gao, L. Jin, K. Li, Z. Wang, *Microporous Mesoporous Mater.* **2018**, *264*, 151–158.
- [42] A. Tukappa, A. Ultimo, C. De La Torre, T. Pardo, F. Sancenón, R. Martínez-Máñez, *Langmuir* **2016**, *32*, 8507–8515.
- [43] R. Bhat, À. Ribes, N. Mas, E. Aznar, F. Sancenón, M. D. Marcos, J. R. Murguía, A. Venkataraman, R. Martínez-Máñez, *Langmuir* **2016**, *32*, 1195–1200.
- [44] C. de la Torre, L. Domínguez-Berrocal, J. R. Murguía, M. D. Marcos, R. Martínez-Máñez, J. Bravo, F. Sancenón, *Chem. - A Eur. J.* **2018**, *24*, 1890–1897.
- [45] X. Chen, H. Sun, J. Hu, X. Han, H. Liu, Y. Hu, *Colloids Surfaces B Biointerfaces* **2017**, *152*, 77–84.
- [46] M. Ercan, V. C. Ozalp, B. G. Tuna, *Anal. Biochem.* **2017**, *537*, 78–83.
- [47] X. Liang, L. Wang, D. Wang, L. Zeng, Z. Fang, *Chem. Commun.* **2016**, *52*, 2192–2194.
- [48] S. Dehghani, N. M. Danesh, M. Ramezani, M. Alibolandi, P. Lavaee, M. Nejabat, K. Abnous, S. M. Taghdisi, *Anal. Chim. Acta* **2018**, *1030*, 142–147.
- [49] L. Pascual, S. El Sayed, M. D. Marcos, R. Martínez-Máñez, F. Sancenón, *Chem. - An Asian J.* **2017**, *12*, 775–784.
- [50] P. Díez, A. Sánchez, C. De La Torre, M. Gamella, P. Martínez-Ruíz, E. Aznar, R. Martínez-Máñez, J. M. Pingarrón, R. Villalonga, *ACS Appl. Mater. Interfaces* **2016**, *8*, 7657–7665.
- [51] X. Wang, P. Liu, Z. Chen, J. Shen, *RSC Adv.* **2016**, *6*, 25480–25484.
- [52] E. Aznar, M. Oroval, J. R. Murguía, R. Martínez-Máñez, F. Sancenón, *Chem. Rev.* **2016**, *116*, 561–718.
- [53] Q. Lin, Q. Huang, C. Li, C. Bao, Z. Liu, F. Li, L. Zhu, *J. Am. Chem. Soc.* **2010**, *132*, 10645–10647.
- [54] M. Wang, T. Wang, D. Wang, W. Jiang, J. Fu, *J. Mater. Sci.* **2019**, *54*, 6199–6211.
- [55] Y. Gao, Y. Xiao, K. Mao, X. Qin, Y. Zhang, D. Li, Y. Zhang, J. Li, H. Wan, S. He, *Chem. Eng. J.* **2020**, *383*, 123169.
- [56] P. Wang, L. Zhang, W. Zheng, L. Cong, Z. Guo, Y. Xie, L. Wang, R. Tang, Q. Feng, Y. Hamada, K. Gonda, Z. Hu, X. Wu, X. Jiang, *Angew. Chemie - Int. Ed.* **2018**, *57*, 1491–1496.
- [57] R. Jauregui, S. Srinivasan, L. N. Vojtech, H. S. Gammill, D. T. Chiu, F. Hladik, P. S. Stayton, J. J. Lai, *ACS Appl. Mater. Interfaces* **2018**, *10*, 33847–33856.
- [58] C. R. Thomas, D. P. Ferris, J. H. Lee, E. Choi, M. H. Cho, E. S. Kim, J. F. Stoddart, J. S. Shin, J. Cheon, J. I. Zink, *J. Am. Chem. Soc.* **2010**, *132*, 10623–10625.
- [59] E. Ruiz-Hernández, A. Baeza, M. Vallet-Regí, *ACS Nano* **2011**, *5*, 1259–1266.
- [60] E. Bringas, Ö. Köysüren, D. V. Quach, M. Mahmoudi, E. Aznar, J. D. Roehling, M. D. Marcos, R. Martínez-Máñez, P. Stroeve, *Chem. Commun.* **2012**, *48*,

- 5647–5649.
- [61] H. Kim, S. Kim, C. Park, H. Lee, H. J. Park, C. Kim, *Adv. Mater.* **2010**, *22*, 4280–4283.
- [62] H.-J. Liu, X. Luan, H.-Y. Feng, X. Dong, S.-C. Yang, Z.-J. Chen, Q.-Y. Cai, Q. Lu, Y. Zhang, P. Sun, M. Zhao, H.-Z. Chen, J. F. Lovell, C. Fang, *Adv. Funct. Mater.* **2018**, *28*, 1801118.
- [63] S. Zhao, M. Xu, C. Cao, Q. Yu, Y. Zhou, J. Liu, *J. Mater. Chem. B* **2017**, *5*, 6908–6919.
- [64] L. Dai, Q. Zhang, X. Shen, Q. Sun, C. Mu, H. Gu, K. Cai, *J. Mater. Chem. B* **2016**, *4*, 4594–4604.
- [65] C. Murugan, K. Rayappan, R. Thangam, R. Bhanumathi, K. Shanthi, R. Vivek, R. Thirumurugan, A. Bhattacharyya, S. Sivasubramanian, P. Gunasekaran, S. Kannan, *Sci. Rep.* **2016**, *6*, 34053.
- [66] W. Cheng, J. Nie, L. Xu, C. Liang, Y. Peng, G. Liu, T. Wang, L. Mei, L. Huang, X. Zeng, *ACS Appl. Mater. Interfaces* **2017**, *9*, 18462–18473.
- [67] S. Jimenez-Falcao, B. De Luis, A. García-Fernández, A. Llopis-Lorente, P. Diez, A. Sánchez, F. Sancenón, P. Martínez-Ruiz, R. Martínez-Mañez, R. Villalonga, *ACS Appl. Bio Mater.* **2019**, *2*, 3321–3328.
- [68] L. Hou, Y. Zheng, Y. Wang, Y. Hu, J. Shi, Q. Liu, H. Zhang, Z. Zhang, *ACS Appl. Mater. Interfaces* **2018**, *10*, 21927–21938.
- [69] K. Ren, J. Wu, Y. Zhang, F. Yan, H. Ju, *Anal. Chem.* **2014**, *86*, 7494–7499.
- [70] N. K. Mal, M. Fujiwara, Y. Tanaka, *Nature* **2003**, *421*, 350–353.
- [71] A. Asokan, M. J. Cho, *J. Pharm. Sci.* **2002**, *91*, 903–913.
- [72] M. Gisbert-Garzarán, M. Manzano, M. Vallet-Regí, *Bioengineering* **2017**, *4*, 3.
- [73] Y. Kato, S. Ozawa, C. Miyamoto, Y. Maehata, A. Suzuki, T. Maeda, Y. Baba, *Cancer Cell Int.* **2013**, *13*, 1–8.
- [74] F. G. Zampieri, J. A. Kellum, M. Park, O. T. Ranzani, H. V. Barbeiro, H. P. de Souza, L. M. da Cruz Neto, F. Pinheiro da Silva, *Crit. Care* **2014**, *18*, 1–8.
- [75] J. Liu, Z. Luo, J. Zhang, T. Luo, J. Zhou, X. Zhao, K. Cai, *Biomaterials* **2016**, *83*, 51–65.
- [76] D. Yang, N. Wang, H. Ji, S. Sun, J. Dong, Y. Zhong, C. Qian, H. Xu, *RSC Adv.* **2018**, *8*, 38987–38994.
- [77] C. Murugan, S. Venkatesan, S. Kannan, *ACS Omega* **2017**, *2*, 7959–7975.
- [78] Y. Li, Y. Duo, P. Zhai, L. He, K. Zhong, Y. Zhang, K. Huang, J. Luo, H. Zhang, X. Yu, *Nanomedicine* **2018**, *13*, 1753–1772.
- [79] J. Shen, H. Liu, C. Mu, J. Wolfram, W. Zhang, H.-C. Kim, G. Zhu, Z. Hu, L.-N. Ji, X. Liu, M. Ferrari, Z.-W. Mao, H. Shen, *Nanoscale* **2017**, *9*, 5329–5341.
- [80] S. Mura, J. Nicolas, P. Couvreur, *Nat. Mater.* **2013**, *12*, 991–1003.
- [81] M. P. Gamcsik, M. S. Kasibhatla, S. D. Teeter, O. M. Colvin, *Biomarkers*

- Biochem. Indic. Expo. response, susceptibility to Chem.* **2012**, *17*, 671–691.
- [82] X. Guo, Y. Cheng, X. Zhao, Y. Luo, J. Chen, W. E. Yuan, *J. Nanobiotechnology* **2018**, *16*, 1–10.
- [83] C.-Y. Lai, B. G. Trewyn, D. M. Jeftinija, K. Jeftinija, S. Xu, S. Jeftinija, V. S.-Y. Lin, *J. Am. Chem. Soc.* **2003**, *125*, 4451–4459.
- [84] T. D. Nguyen, H.-R. Tseng, P. C. Celestre, A. H. Flood, Y. Liu, J. F. Stoddart, J. I. Zink, *Proc. Natl. Acad. Sci. U. S. A.* **2005**, *102*, 10029–10034.
- [85] Y. Wang, H. Y. Huang, L. Yang, Z. Zhang, H. Ji, *Sci. Rep.* **2016**, *25468*, 1–10.
- [86] A. Llopis-Lorente, B. Lozano-Torres, A. Bernardos, R. Martínez-Mañez, F. Sancenón, *J. Mater. Chem. B* **2017**, *5*, 3069–3083.
- [87] E. Li, Y. Yang, G. Hao, X. Yi, S. Zhang, Y. Pan, B. Xing, M. Gao, *Nanotheranostics* **2018**, *2*, 233–242.
- [88] P. Zarrintaj, M. Jouyandeh, M. R. Ganjali, B. S. Hadavand, M. Mozafari, S. S. Sheiko, M. Vatankhah-Varnoosfaderani, T. J. Gutiérrez, M. R. Saeb, *Eur. Polym. J.* **2019**, *117*, 402–423.
- [89] Y. Feng, N.-X. Li, H.-L. Yin, T.-Y. Chen, Q. Yang, M. Wu, *Mol. Pharm.* **2019**, *16*, 422–436.
- [90] X. Chen, Q. Zhang, J. Li, M. Yang, N. Zhao, F. J. Xu, *ACS Nano* **2018**, *12*, 5646–5656.
- [91] K. E. Albinali, M. M. Zagho, Y. Deng, A. A. Elzatahry, *Int. J. Nanomedicine* **2019**, *14*, 1707–1723.
- [92] H. Yang, M. Hua, H. Liu, C. Huang, R. Tsai, Y. Lu, J. Chen, H. Tang, H. Hsien, Y. Chang, T. Yen, P. Chen, K. Wei, *Biomaterials* **2011**, *32*, 6523–6532.
- [93] B. Chertok, A. E. David, Y. Huang, V. C. Yang, *J. Control. Release* **2007**, *122*, 315–323.
- [94] A. Adamiano, M. Iafisco, A. Tampieri, in *Woodhead Publ. Ser. Biomater.* (Eds.: M.L. Focarete, A.B.T.-C.-S.N. for D.D. and T. Tampieri), Woodhead Publishing, **2018**, pp. 259–296.
- [95] O. Veisoh, J. W. Gunn, M. Zhang, *Adv. Drug Deliv. Rev.* **2010**, *62*, 284–304.
- [96] C. Zimmer, S. C. Wright, R. T. Engelhardt, G. A. Johnson, C. Kramm, X. O. Breakefield, R. Weissleder, *Exp. Neurol.* **1997**, *143*, 61–69.
- [97] E. Guisasola, L. Asín, L. Beola, J. M. de la Fuente, A. Baeza, M. Vallet-Regí, *ACS Appl. Mater. Interfaces* **2018**, *10*, 12518–12525.
- [98] V. Frenkel, *Adv. Drug Deliv. Rev.* **2008**, *60*, 1193–1208.
- [99] S. Mitragotri, *Nat. Rev. Drug Discov.* **2005**, *4*, 255–260.
- [100] N. Y. Rapoport, A. M. Kennedy, J. E. Shea, C. L. Scaife, K.-H. Nam, *J. Control. Release* **2009**, *138*, 268–276.
- [101] Z. Gao, A. M. Kennedy, D. A. Christensen, N. Y. Rapoport, *Ultrasonics* **2008**, *48*, 260–270.
- [102] N. Rapoport, Z. Gao, A. Kennedy, *J. Natl. Cancer Inst.* **2007**, *99*, 1095–1106.

- [103] Y. Lv, Y. Cao, P. Li, J. Liu, H. Chen, W. Hu, L. Zhang, *Adv. Healthc. Mater.* **2017**, *6*, 1–10.
- [104] A. C. Anselmo, S. Mitragotri, *Bioeng. Transl. Med.* **2019**, *4*, e10143–e10143.
- [105] D. Bobo, K. J. Robinson, J. Islam, K. J. Thurecht, S. R. Corrie, *Pharm. Res.* **2016**, *33*, 2373–2387.
- [106] Y. Wang, Q. Zhao, N. Han, L. Bai, J. Li, J. Liu, E. Che, L. Hu, Q. Zhang, T. Jiang, S. Wang, *Nanomedicine Nanotechnology, Biol. Med.* **2015**, *11*, 313–327.
- [107] Q. Liu, J. Zhang, W. Sun, Q. R. Xie, W. Xia, H. Gu, *Int. J. Nanomedicine* **2012**, *7*, 999–1013.
- [108] J. Fang, H. Nakamura, H. Maeda, *Adv. Drug Deliv. Rev.* **2011**, *63*, 136–151.
- [109] T. Mandal, M. Beck, N. Kirsten, M. Lindén, C. Buske, *Sci. Rep.* **2018**, *8*, 989.
- [110] M. Bouchoucha, É. Béliveau, F. Kleitz, F. Calon, M.-A. Fortin, *J. Mater. Chem. B* **2017**, *5*, 7721–7735.
- [111] W. Qu, B. Meng, Y. Yu, S. Wang, *Mater. Sci. Eng. C* **2017**, *76*, 646–651.
- [112] L. Pan, J. Liu, Q. He, J. Shi, *Adv. Mater.* **2014**, *26*, 6742–6748.
- [113] Y. Wei, L. Gao, L. Wang, L. Shi, E. Wei, B. Zhou, L. Zhou, B. Ge, *Drug Deliv.* **2017**, *24*, 681–691.
- [114] P. Tambe, P. Kumar, K. M. Paknikar, V. Gajbhiye, *Int. J. Nanomedicine* **2018**, *13*, 7669–7680.
- [115] X. Xie, F. Li, H. Zhang, Y. Lu, S. Lian, H. Lin, Y. Gao, L. Jia, *Eur. J. Pharm. Sci.* **2016**, *83*, 28–35.
- [116] Y. Li, Y. Duo, J. Bi, X. Zeng, L. Mei, S. Bao, L. He, A. Shan, Y. Zhang, X. Yu, *Int. J. Nanomedicine* **2018**, *13*, 1241–1256.
- [117] Y. Li, Y. Duo, S. Bao, L. He, K. Ling, J. Luo, Y. Zhang, H. Huang, H. Zhang, X. Yu, *Int. J. Nanomedicine* **2017**, *12*, 6239–6257.
- [118] T. Tagami, T. Ozeki, *J. Pharm. Sci.* **2017**, *106*, 2219–2226.
- [119] “US Food and Drug Administration GRAS Substances (SCOGS) Database—Select Committee on GRAS Substances (SCOGS) Opinion: Silicates,” **2020**.
- [120] A. N. Kharlamov, J. A. Feinstein, J. A. Cramer, J. A. Boothroyd, E. V. Shishkina, V. Shur, *Future Cardiol.* **2017**, *13*, 345–363.
- [121] A. N. Kharlamov, A. E. Tyurnina, V. S. Veselova, O. P. Kovtun, V. Y. Shur, J. L. Gabinsky, *Nanoscale* **2015**, *7*, 8003–8015.
- [122] M. S. Bradbury, E. Phillips, P. H. Montero, S. M. Cheal, H. Stambuk, J. C. Durack, C. T. Sofocleous, R. J. C. Meester, U. Wiesner, S. Patel, *Integr. Biol. (Camb)*. **2013**, *5*, 74–86.
- [123] F. Chen, K. Ma, M. Benezra, L. Zhang, S. M. Cheal, E. Phillips, B. Yoo, M. Pauliah, M. Overholtzer, P. Zanzonico, S. Sequeira, M. Gonen, T. Quinn, U. Wiesner, M. S. Bradbury, *Chem. Mater.* **2017**, *29*, 8766–8779.
- [124] A. Kasaj, B. Röhrig, G.-G. Zafiroopoulos, B. Willershausen, *J. Periodontol.* **2008**, *79*, 394–400.

- [125] B. Heinz, A. Kasaj, M. Teich, S. Jepsen, *Clin. Oral Investig.* **2010**, *14*, 525–531.
- [126] D. Pedraza, J. Díez, I. I. Barba, M. Colilla, M. Vallet-Regí, *Biomed. Glas.* **2018**, *4*, 1–12.
- [127] S. Kanugala, S. Jinka, N. Puvvada, R. Banerjee, C. G. Kumar, *Sci. Rep.* **2019**, *9*, 1–16.
- [128] J. Xie, D. Xiao, J. Zhao, N. Hu, Q. Bao, L. Jiang, L. Yu, *Adv. Healthc. Mater.* **2016**, *5*, 1213–1221.
- [129] A. H. Teruel, É. Pérez-Esteve, I. González-Álvarez, M. González-Álvarez, A. M. Costero, D. Ferri, M. Parra, P. Gaviña, V. Merino, R. Martínez-Mañez, F. Sancenón, *J. Control. Release* **2018**, *281*, 58–69.
- [130] D. H. Han, H. K. Na, W. H. Choi, J. H. Lee, Y. K. Kim, C. Won, S. H. Lee, K. P. Kim, J. Kuret, D. H. Min, M. J. Lee, *Nat. Commun.* **2014**, *5*, 5633.
- [131] N. Biswas, *Eur. J. Pharm. Sci.* **2017**, *99*, 152–160.
- [132] L. A. Dykman, N. G. Khlebtsov, *Russ. Chem. Rev.* **2019**, *88*, 229–247.
- [133] E. Boisselier, D. Astruc, *Chem. Soc. Rev.* **2009**, *38*, 1759–1782.
- [134] A. F. Versiani, L. M. Andrade, E. M. N. Martins, S. Scalzo, J. M. Geraldo, C. R. Chaves, D. C. Ferreira, M. Ladeira, S. Guatimosim, L. O. Ladeira, F. G. Da Fonseca, *Future Virol.* **2016**, *11*, 293–309.
- [135] E. C. Dreaden, M. A. Mackey, X. Huang, B. Kang, M. A. El-Sayed, *Chem. Soc. Rev.* **2011**, *40*, 3391–3404.
- [136] E. C. Dreaden, A. M. Alkilany, X. Huang, C. J. Murphy, M. A. El-sayed, *Chem. Soc. Rev.* **2012**, *41*, 2740–2779.
- [137] R. Sardar, J. S. Shumaker-Parry, *J. Am. Chem. Soc.* **2011**, *133*, 8179–8190.
- [138] I. Hussain, S. Graham, Z. Wang, B. Tan, D. C. Sherrington, S. P. Rannard, A. I. Cooper, M. Brust, *J. Am. Chem. Soc.* **2005**, *127*, 16398–16399.
- [139] N. R. Jana, L. Gearheart, C. J. Murphy, *Langmuir* **2001**, *17*, 6782–6786.
- [140] M. Grzelczak, J. Pérez-Juste, P. Mulvaney, L. M. Liz-Marzán, *Chem. Soc. Rev.* **2008**, *37*, 1783–1791.
- [141] J. D. E. T. Wilton-Ely, *Dalt. Trans.* **2008**, 25–29.
- [142] N. Garg, S. Bera, A. Ballal, *Spectrochim. Acta - Part A Mol. Biomol. Spectrosc.* **2020**, *228*, 117701.
- [143] D. A. Gonzalez-Carter, Z. Y. Ong, C. M. McGilvery, I. E. Dunlop, D. T. Dexter, A. E. Porter, *Nanomedicine Nanotechnology, Biol. Med.* **2019**, *15*, 1–11.
- [144] Y. Ou, X. Jin, J. Liu, Y. Tian, N. Zhou, *Anal. Biochem.* **2019**, *587*, 113432.
- [145] N. Elahi, M. Kamali, M. H. Baghersad, *Talanta* **2018**, *184*, 537–556.
- [146] R. Herizchi, E. Abbasi, M. Milani, A. Akbarzadeh, *Artif. Cells, Nanomedicine, Biotechnol.* **2016**, *44*, 596–602.
- [147] J. A. Fuentes-García, J. Santoyo-Salzar, E. Rangel-Cortes, G. F. Goya, V. Cardozo-Mata, J. A. Pescador-Rojas, *Ultrason. Sonochem.* **2021**, *70*, 105274.
- [148] K. L. McGilvray, M. R. Decan, D. Wang, J. C. Scaiano, *J. Am. Chem. Soc.* **2006**,

- 128, 15980–15981.
- [149] I. Kumar, M. Mondal, V. Meyappan, N. Sakthivel, *Mater. Res. Bull.* **2019**, *117*, 18–27.
- [150] U. Munawer, V. B. Raghavendra, S. Ningaraju, K. L. Krishna, A. R. Ghosh, G. Melappa, A. Pugazhendhi, *Int. J. Pharm.* **2020**, *588*, 119729.
- [151] Q. Li, B. Lu, L. Zhang, C. Lu, *J. Mater. Chem.* **2012**, *22*, 13564–13570.
- [152] J. P. Oliveira, A. R. Prado, W. J. Keijok, M. R. N. Ribeiro, M. J. Pontes, B. V Nogueira, M. C. C. Guimarães, *Arab. J. Chem.* **2020**, *13*, 216–226.
- [153] D. Kumar, I. Mutreja, P. Sykes, *Nanotechnology* **2016**, *27*, 355601.
- [154] J. Turkevich, P. C. Stevenson, J. Hillier, *Discuss. Faraday Soc.* **1951**, *11*, 55–75.
- [155] G. Frens, *Nat. Phys. Sci.* **1973**, *241*, 20–22.
- [156] J. R. Nicol, D. Dixon, J. A. Coulter, *Nanomedicine* **2015**, *10*, 1315–1326.
- [157] G. Liu, X. Yang, Y. Li, Z. Yang, W. Hong, J. Liu, *Adv. Mater. Sci. Eng.* **2015**, *2015*, 160819.
- [158] Y.-C. Yeh, B. Creran, V. M. Rotello, *Nanoscale* **2012**, *4*, 1871–1880.
- [159] S. D. Perrault, W. C. W. Chan, *J. Am. Chem. Soc.* **2009**, *131*, 17042–17043.
- [160] M. Brust, M. Walker, D. Bethell, D. J. Schiffrin, R. Whyman, *J. Chem. Soc. Chem. Commun.* **1994**, 801–802.
- [161] N. R. Jana, L. Gearheart, C. J. Murphy, *Adv. Mater.* **2001**, *13*, 1389–1393.
- [162] N. Malikova, I. Pastoriza-Santos, M. Schierhorn, N. A. Kotov, L. M. Liz-Marzán, *Langmuir* **2002**, *18*, 3694–3697.
- [163] C.-S. Lee, H. Kim, J. Yu, S. H. Yu, S. Ban, S. Oh, D. Jeong, J. Im, M. J. Baek, T. H. Kim, *Eur. J. Med. Chem.* **2017**, *142*, 416–423.
- [164] L. Hong, M. Lu, M.-P. Dinel, P. Blain, W. Peng, H. Gu, J.-F. Masson, *Biosens. Bioelectron.* **2018**, *109*, 230–236.
- [165] M. A. Zaimy, A. Jebali, B. Bazrafshan, S. Mehrtashfar, S. Shabani, A. Tavakoli, S. H. Hekmatimoghaddam, A. Sarli, H. Azizi, P. Izadi, B. Kazemi, A. Shojaei, A. Abdalaian, J. Tavakkoly-Bazzaz, *Cancer Gene Ther.* **2016**, *23*, 315–320.
- [166] L. Zhao, Y. Li, J. Zhu, N. Sun, N. Song, Y. Xing, H. Huang, J. Zhao, *J. Nanobiotechnology* **2019**, *17*, 30.
- [167] R. A. Morshed, M. E. Muroski, Q. Dai, M. L. Wegscheid, B. Auffinger, D. Yu, Y. Han, L. Zhang, M. Wu, Y. Cheng, M. S. Lesniak, *Mol. Pharm.* **2016**, *13*, 1843–1854.
- [168] B. Albertini, V. Mathieu, N. Iraci, M. Van Woensel, A. Schoubben, A. Donnadio, S. M. L. Greco, M. Ricci, A. Temperini, P. Blasi, N. Wauthoz, *Mol. Pharm.* **2019**, *16*, 2430–2444.
- [169] P. Singh, Bharti, R. Kumar, V. Bhalla, *Anal. Chim. Acta* **2019**, *1078*, 151–160.
- [170] F. Emami, A. Banstola, A. Vatanara, S. Lee, J. O. Kim, J.-H. Jeong, S. Yook, *Mol. Pharm.* **2019**, *16*, 1184–1199.

- [171] Y.-S. S. Yang, K. D. Moynihan, A. Bekdemir, T. M. Dichwalkar, M. M. Noh, N. Watson, M. Melo, J. Ingram, H. Suh, H. Ploegh, F. R. Stellacci, D. J. Irvine, *Biomater. Sci.* **2019**, *7*, 113–124.
- [172] S. Mahalunkar, A. S. Yadav, M. Gorain, V. Pawar, R. Braathen, S. Weiss, B. Bogen, S. W. Gosavi, G. C. Kundu, *Int. J. Nanomedicine* **2019**, *14*, 8285–8302.
- [173] B. Shrestha, L. Wang, H. Zhang, C. Y. Hung, L. Tang, *Int. J. Nanomedicine* **2020**, *15*, 8109–8119.
- [174] N. S. Elbialy, M. M. Fathy, R. AL-Wafi, R. Darwesh, U. A. Abdel-dayem, M. Aldhahri, A. Noorwali, A. A. AL-ghamdi, *Int. J. Pharm.* **2019**, *554*, 256–263.
- [175] J. C. Love, L. A. Estroff, J. K. Kriebel, R. G. Nuzzo, G. M. Whitesides, *Chem. Rev.* **2005**, *105*, 1103–1170.
- [176] S.-Y. Lin, Y.-T. Tsai, C.-C. Chen, C.-M. Lin, C. Chen, *J. Phys. Chem. B* **2004**, *108*, 2134–2139.
- [177] M. T. Azar, N. Saglam, M. Turk, *J. Nano Res.* **2019**, *58*, 1–9.
- [178] M. Fazel-Ghaziyani, D. Shahbazi-Gahrouei, M. Pourhassan-Moghaddam, B. Baradaran, M. Ghavami, *J. Nanomedicine* **2018**, *5*, 172–179.
- [179] Q. ZHANG, R.-X. LI, X. CHEN, X.-X. HE, A.-L. HAN, G.-Z. FANG, J.-F. LIU, S. WANG, *Chinese J. Anal. Chem.* **2017**, *45*, 662–667.
- [180] C. Arib, Q. Liu, N. Djaker, W. Fu, M. Lamy de la Chapelle, J. Spadavecchia, *Plasmonics* **2019**, *14*, 1029–1038.
- [181] M. H. Jazayeri, H. Amani, A. A. Pourfatollah, A. Avan, G. A. Ferns, H. Pazoki-Toroudi, *Cancer Gene Ther.* **2016**, *23*, 365–369.
- [182] W. Q. Lim, Z. Gao, *Nano Today* **2016**, *11*, 168–188.
- [183] F. Y. Kong, J. W. Zhang, R. F. Li, Z. X. Wang, W. J. Wang, W. Wang, *Molecules* **2017**, *22*, 1445.
- [184] Y. Liu, B. M. Crawford, T. Vo-Dinh, *Immunotherapy* **2018**, *10*, 1175–1188.
- [185] S. K. Libutti, G. F. Paciotti, A. A. Byrnes, H. R. Alexander Jr, W. E. Gannon, M. Walker, G. D. Seidel, N. Yuldasheva, L. Tamarkin, *Clin. Cancer Res.* **2010**, *16*, 6139–6149.
- [186] D. F. Williams, *Biomaterials* **2008**, *29*, 2941–2953.
- [187] D. Bhavsar, V. Patel, K. Sawant, *Microporous Mesoporous Mater.* **2019**, *284*, 343–352.
- [188] T. Liu, L. Li, X. Teng, X. Huang, H. Liu, D. Chen, J. Ren, J. He, F. Tang, *Biomaterials* **2011**, *32*, 1657–1668.
- [189] V. Raji, J. Kumar, C. S. Rejiya, M. Vibin, A. John, A. Abraham, *J. Exp. Nanosci.* **2012**, *7*, 174–188.
- [190] A. L. Bailly, F. Correard, A. Popov, G. Tselikov, F. Chaspoul, R. Appay, A. Al-Kattan, A. V. Kabashin, D. Braguer, M. A. Esteve, *Sci. Rep.* **2019**, *9*, 1–12.
- [191] L. Li, T. Liu, C. Fu, L. Tan, X. Meng, H. Liu, *Nanomedicine Nanotechnology, Biol. Med.* **2015**, *11*, 1915–1924.

- [192] Y. S. Chen, Y. C. Hung, I. Liau, G. S. Huang, *Nanoscale Res. Lett.* **2009**, *4*, 858–864.
- [193] M. Rathore, I. R. Mohanty, U. Maheswari, N. Dayal, R. Suman, D. S. Joshi, *J. Nanoparticle Res.* **2014**, *16*, 1–12.
- [194] H. Jaganathan, B. Godin, *Adv. Drug Deliv. Rev.* **2012**, *64*, 1800–1819.
- [195] T. Wu, M. Tang, *J. Appl. Toxicol.* **2018**, *38*, 25–40.
- [196] T. Yu, D. Hubbard, A. Ray, H. Ghandehari, *J. Control. Release* **2012**, *163*, 46–54.
- [197] P. Dogra, N. L. Adolphi, Z. Wang, Y. S. Lin, K. S. Butler, P. N. Durfee, J. G. Croissant, A. Nouredine, E. N. Coker, E. L. Bearer, V. Cristini, C. J. Brinker, *Nat. Commun.* **2018**, *9*, 1–14.
- [198] W. S. Cho, M. Cho, J. Jeong, M. Choi, H. Y. Cho, B. S. Han, S. H. Kim, H. O. Kim, Y. T. Lim, B. H. Chung, J. Jeong, *Toxicol. Appl. Pharmacol.* **2009**, *236*, 16–24.
- [199] X. D. Zhang, D. Wu, X. Shen, P. X. Liu, N. Yang, B. Zhao, H. Zhang, Y. M. Sun, L. A. Zhang, F. Y. Fan, *Int. J. Nanomedicine* **2011**, *6*, 2071–2081.
- [200] T. Yu, K. Greish, L. D. McGill, A. Ray, H. Ghandehari, *ACS Nano* **2012**, *6*, 2289–2301.
- [201] W. H. De Jong, W. I. Hagens, P. Krystek, M. C. Burger, A. J. A. M. Sips, R. E. Geertsma, *Biomaterials* **2008**, *29*, 1912–1919.
- [202] B. C. Bunker, *J. Non. Cryst. Solids* **1994**, *179*, 300–308.
- [203] N. Hao, H. Liu, L. Li, D. Chen, L. Li, F. Tang, *J. Nanosci. Nanotechnonology* **2012**, *12*, 6346–6354.
- [204] Q. He, Z. Zhang, F. Gao, Y. Li, J. Shi, *Small* **2011**, *7*, 271–280.
- [205] J. A. Lee, M. K. Kim, H. J. Paek, Y. R. Kim, M. K. Kim, J. K. Lee, J. Jeong, S. J. Choi, *Int. J. Nanomedicine* **2014**, *9*, 251–260.
- [206] J. Lu, M. Liong, Z. Li, J. I. Zink, F. Tamanoi, *Small* **2010**, *6*, 1794–1805.
- [207] J. F. Popplewell, S. J. King, J. P. Day, P. Ackrill, L. K. Fifield, R. G. Cresswell, M. L. Di Tada, K. Liu, *J. Inorg. Biochem.* **1998**, *69*, 177–180.
- [208] J. Kolosnjaj-Tabi, Y. Javed, L. Lartigue, J. Volatron, D. Elgrabli, I. Marangon, G. Pugliese, B. Caron, A. Figuerola, N. Luciani, T. Pellegrino, D. Alloyeau, F. Gazeau, *ACS Nano* **2015**, *9*, 7925–7939.
- [209] A. Balfourier, N. Luciani, G. Wang, G. Lelong, O. Ersen, A. Khelfa, D. Alloyeau, F. Gazeau, F. Carn, *Proc. Natl. Acad. Sci. U. S. A.* **2020**, *117*, 103–113.
- [210] M. Semmler-Behnke, W. G. Kreyling, J. Lipka, S. Fertsch, A. Wenk, S. Takenaka, G. Schmid, W. Brandau, *Small* **2008**, *4*, 2108–2111.
- [211] J. Lipka, M. Semmler-Behnke, R. A. Sperling, A. Wenk, S. Takenaka, C. Schleh, T. Kissel, W. J. Parak, W. G. Kreyling, *Biomaterials* **2010**, *31*, 6574–6581.
- [212] S. K. Balasubramanian, J. Jittiwat, J. Manikandan, C. N. Ong, L. E. Yu, W. Y. Ong, *Biomaterials* **2010**, *31*, 2034–2042.

- [213] R. Goel, N. Shah, R. Visaria, G. F. Paciotti, J. C. Bischof, *Nanomedicine (Lond)*. **2009**, *4*, 401–410.
- [214] D. Cassano, S. Pocióví-Martínez, V. Voliani, *Bioconjug. Chem.* **2018**, *29*, 4–16.
- [215] H. S. Choi, W. Liu, P. Misra, E. Tanaka, J. P. Zimmer, B. Itty Ipe, M. G. Bawendi, J. V. Frangioni, *Nat. Biotechnol.* **2007**, *25*, 1165–1170.
- [216] S. M. Moghimi, H. M. Patel, *Adv. Drug Deliv. Rev.* **1998**, *32*, 45–60.
- [217] R. Furth, Z. A. Cohn, J. Hirsch, J. Humphrey, W. Spector, H. Langevoort, *Bull. World Health Organ.* **1972**, *46*, 845–852.
- [218] M. J. Ernsting, M. Murakami, A. Roy, S. D. Li, *J. Control. Release* **2013**, *172*, 782–794.
- [219] J. M. Harris, R. B. Chess, *Nat. Rev. Drug Discov.* **2003**, *2*, 214–221.
- [220] A. M. Clemments, C. Muniesa, C. C. Landry, P. Botella, *RSC Adv.* **2014**, *4*, 29134–29138.
- [221] X. He, H. Nie, K. Wang, W. Tan, X. Wu, P. Zhang, *Anal. Chem.* **2008**, *80*, 9597–9603.
- [222] Q. He, J. Zhang, J. Shi, Z. Zhu, L. Zhang, W. Bu, L. Guo, Y. Chen, *Biomaterials* **2010**, *31*, 1085–1092.
- [223] G. F. Paciotti, L. Myer, D. Weinreich, D. Goia, N. Pavel, R. E. McLaughlin, L. Tamarkin, *Drug Deliv. J. Deliv. Target. Ther. Agents* **2004**, *11*, 169–183.
- [224] T. Niidome, M. Yamagata, Y. Okamoto, Y. Akiyama, *J. Control. Release* **2006**, *114*, 343–347.
- [225] S. D. Perrault, C. Walkey, T. Jennings, H. C. Fischer, W. C. W. Chan, *Nano Lett.* **2009**, *9*, 1909–1915.
- [226] B. Zapotoczny, K. Szafranska, K. Owczarczyk, E. Kus, S. Chlopicki, M. Szymonski, *Sci. Rep.* **2017**, *7*, 1–6.
- [227] L.-T. Chen, L. Weiss, *Blood* **1973**, *41*, 529–537.
- [228] S. M. Moghimi, C. J. H. Porter, I. S. Muir, L. Illum, S. S. Davis, *Biochem. Biophys. Res. Commun.* **1991**, *177*, 861–866.
- [229] X. Huang, L. Li, T. Liu, N. Hao, H. Liu, D. Chen, F. Tang, *ACS Nano* **2011**, *5*, 5390–5399.
- [230] J. S. Souris, C. Lee, S. Cheng, C. Chen, C. Yang, J. A. Ho, C. Mou, L. Lo, *Biomaterials* **2010**, *31*, 5564–5574.
- [231] C. H. Lee, S. H. Cheng, Y. J. Wang, Y. C. Chen, N. T. Chen, J. Souris, C. T. Chen, C. Y. Mou, C. S. Yang, L. W. Lo, *Adv. Funct. Mater.* **2009**, *19*, 215–222.
- [232] H. Maeda, J. Wu, T. Sawa, Y. Matsumura, K. Hori, *J. Control. Release* **2000**, *65*, 271–284.
- [233] Y. Matsumura, H. Maeda, *Cancer Res.* **1986**, *46*, 6387–6392.
- [234] H. Maeda, *J. Control. Release* **1992**, *19*, 315–324.
- [235] F. Yuan, M. Dellian, D. Fukumura, M. Leunig, D. A. Berk, R. K. Jain, V. P. Torchilin, *Cancer Res.* **1995**, *55*, 3752–3756.

- [236] T. Konno, H. Maeda, K. Iwai, S. Maki, S. Tashiro, M. Uchida, Y. Miyauchi, *Cancer* **1984**, *54*, 2367–2374.
- [237] Y. Noguchi, J. Wu, R. Duncan, J. Strohalm, K. Ulbrich, T. Akaike, H. Maeda, *Japanese J. Cancer Res.* **1998**, *89*, 307–314.
- [238] F. Alexis, E. Pridgen, L. K. Molnar, O. C. Farokhzad, *Mol. Pharm.* **2008**, *5*, 505–515.
- [239] S. D. Li, L. Huang, *Mol. Pharm.* **2008**, *5*, 496–504.
- [240] S. D. Conner, S. L. Schmid, *Nature* **2003**, *422*, 37–44.
- [241] F. Zhao, Y. Zhao, Y. Liu, X. Chang, C. Chen, Y. Zhao, *Small* **2011**, *7*, 1322–1337.
- [242] F. Lu, S. Wu, Y. Hung, C. Mou, *Small* **2009**, *5*, 1408–1413.
- [243] A. Verma, F. Stellacci, *Small* **2010**, *6*, 12–21.
- [244] J. Rejman, V. Oberle, I. S. Zuhorn, D. Hoekstra, *Biochem. J.* **2004**, *377*, 159–169.
- [245] B. D. Chithrani, W. C. W. Chan, *Nano Lett.* **2007**, *7*, 1542–1550.
- [246] T. H. Chung, S. H. Wu, M. Yao, C. W. Lu, Y. S. Lin, Y. Hung, C. Y. Mou, Y. C. Chen, D. M. Huang, *Biomaterials* **2007**, *28*, 2959–2966.
- [247] B. Yameen, W. Il Choi, C. Vilos, A. Swami, J. Shi, O. C. Farokhzad, *J. Control. Release* **2014**, *190*, 485–499.
- [248] I. Nakase, S. Kobayashi, S. Futaki, *Biopolymers* **2010**, *94*, 763–770.
- [249] A. K. Varkouhi, M. Scholte, G. Storm, H. J. Haisma, *J. Control. Release* **2011**, *151*, 220–228.
- [250] X. Wang, D. Niu, C. Hu, P. Li, *Curr. Pharm. Des.* **2015**, *21*, 6140–6156.
- [251] R. A. Jones, C. Y. Cheung, F. E. Black, J. K. Zia, P. S. Stayton, A. S. Hoffman, M. R. Wilson, *Biochem. J.* **2003**, *372*, 65–75.
- [252] J. P. Richard, K. Melikov, E. Vives, C. Ramos, B. Verbeure, M. J. Gait, L. V. Chernomordik, B. Lebleu, *J. Biol. Chem.* **2003**, *278*, 585–590.
- [253] E. Vivès, J.-P. Richard, C. Rispal, B. Lebleu, *Curr. Protein Pept. Sci.* **2003**, *4*, 125–132.
- [254] F. Bray, J. Ferlay, I. Soerjomataram, R. L. Siegel, L. A. Torre, A. Jemal, *CA. Cancer J. Clin.* **2018**, *68*, 394–424.
- [255] American Cancer Society, *Am. Cancer Soc.* **2019**, 1–44.
- [256] National Cancer Institute (NCI), *Natl. Institutes Heal.* **2014**, 1–105.
- [257] C. Vallejos, H. Gómez, W. Cruz, J. Pinto, R. Dyer, R. Velarde, J. Suazo, S. Neciosup, M. León, M. De La Cruz, C. Vigil, *Clin. Breast Cancer* **2010**, *10*, 294–300.
- [258] C. M. Perou, T. Sørile, M. B. Eisen, M. Van De Rijn, S. S. Jeffrey, C. A. Rens, J. R. Pollack, D. T. Ross, H. Johnsen, L. A. Akslen, Ø. Fluge, A. Pergammenschlkov, C. Williams, S. X. Zhu, P. E. Lønning, A. L. Børresen-Dale, P. O. Brown, D. Botstein, *Nature* **2000**, *406*, 747–752.
- [259] J. S. Reis-Filho, L. Pusztai, *Lancet* **2011**, *378*, 1812–1823.

- [260] K. M. O'Brien, S. R. Cole, C. K. Tse, C. M. Perou, L. A. Carey, W. D. Foulkes, L. G. Dressler, J. Geradts, R. C. Millikan, *Clin. Cancer Res.* **2010**, *16*, 6100–6110.
- [261] M. C. U. Cheang, S. K. Chia, D. Voduc, D. Gao, S. Leung, J. Snider, M. Watson, S. Davies, P. S. Bernard, J. S. Parker, C. M. Perou, M. J. Ellis, T. O. Nielsen, *J. Natl. Cancer Inst.* **2009**, *101*, 736–750.
- [262] T. Sørli, C. M. Perou, R. Tibshirani, T. Aas, S. Geisler, H. Johnsen, T. Hastie, M. B. Eisen, M. Van De Rijn, S. S. Jeffrey, T. Thorsen, H. Quist, J. C. Matese, P. O. Brown, D. Botstein, P. E. Lønning, A. L. Børresen-Dale, *Proc. Natl. Acad. Sci. U. S. A.* **2001**, *98*, 10869–10874.
- [263] S. Paik, S. Shak, G. Tang, C. Kim, J. Baker, M. Cronin, D. Watson, J. Bryant, J. Costantino, N. Wolmark, *J. Clin. Oncol.* **2005**, *23*, 510.
- [264] H. Kennecke, R. Yerushalmi, R. Woods, M. C. U. Cheang, D. Voduc, C. H. Speers, T. O. Nielsen, K. Gelmon, *J. Clin. Oncol.* **2010**, *28*, 3271–3277.
- [265] A. Bosch, P. Eroles, R. Zaragoza, J. R. Viña, A. Lluch, *Cancer Treat. Rev.* **2010**, *36*, 206–215.
- [266] E. A. Rakha, S. Chan, *Clin. Oncol.* **2011**, *23*, 587–600.
- [267] R. Rouzier, C. M. Perou, W. F. Symmans, N. Ibrahim, M. Cristofanilli, K. Anderson, K. R. Hess, J. Stec, M. Ayers, P. Wagner, P. Morandi, C. Fan, I. Rabiul, J. S. Ross, G. N. Hortobagyi, L. Pusztai, *Clin. Cancer Res.* **2005**, *11*, 5678–5685.
- [268] M. De Laurentiis, D. Cianniello, R. Caputo, B. Stanzione, G. Arpino, S. Cinieri, V. Lorusso, S. De Placido, *Cancer Treat. Rev.* **2010**, *36*, S80–S86.
- [269] F. Cardoso, S. Kyriakides, S. Ohno, F. Penault-Llorca, P. Poortmans, I. T. Rubio, S. Zackrisson, E. Senkus, *Ann. Oncol.* **2019**, *30*, 1194–1220.
- [270] F. Cardoso, S. Paluch-Shimon, E. Senkus, G. Curigliano, M. S. Aapro, F. André, C. H. Barrios, J. Bergh, G. S. Bhattacharyya, L. Biganzoli, F. Boyle, M.-J. Cardoso, L. A. Carey, J. Cortés, N. S. El Saghir, M. Elzayat, A. Eniu, L. Fallowfield, P. A. Francis, K. Gelmon, J. Gligorov, R. Haidinger, N. Harbeck, X. Hu, B. Kaufman, R. Kaur, B. E. Kiely, S.-B. Kim, N. U. Lin, S. A. Mertz, S. Neciosup, B. V Offersen, S. Ohno, O. Pagani, A. Prat, F. Penault-Llorca, H. S. Rugo, G. W. Sledge, C. Thomssen, D. A. Vorobiof, T. Wiseman, B. Xu, L. Norton, A. Costa, E. P. Winer, *Ann. Oncol.* **2020**.
- [271] J. Furlanetto, S. Loibl, *Breast Care (Basel)*. **2020**, *15*, 217–226.
- [272] C. H. Li, V. Karantz, G. Aktan, M. Lala, *Breast Cancer Res.* **2019**, *21*, 143.
- [273] P. A. Ellis, I. E. Smith, K. McCarthy, S. Detre, J. Salter, M. Dowsett, *Lancet* **1997**, *349*, 849.
- [274] D. Guimarães Tiezzi, J. Moreira De Andrade, F. José Cândido Dos Reis, H. Ricardo Cosiski Marana, A. Ribeiro-Silva, M. Guimarães Tiezzi, A. Plácido Pereira, *Pathology* **2006**, *38*, 21–27.
- [275] B. A. Rupnow, S. J. Knox, *Apoptosis* **1999**, *4*, 115–143.

- [276] L. A. Henríquez-Hernández, R. Carmona-Vigo, B. Pinar, E. Bordón, M. Lloret, M. I. Núñez, C. Rodríguez-Gallego, P. C. Lara, *Radiat. Oncol.* **2011**, *6*, 60.
- [277] A. E. Kayl, C. A. Meyers, *Curr. Opin. Obstet. Gynecol.* **2006**, *18*, 24–28.
- [278] R. Maguire, J. Cowie, C. Leadbetter, K. McCall, K. Swingler, L. McCann, N. Kearney, *J. Res. Nurs.* **2009**, *14*, 27–40.
- [279] A. Pearce, M. Haas, R. Viney, S.-A. Pearson, P. Haywood, C. Brown, R. Ward, *PLoS One* **2017**, *12*, e0184360.
- [280] D.-H. Kang, M. T. Weaver, N.-J. Park, B. Smith, T. McArdle, J. Carpenter, *Nurs. Res.* **2009**, *58*, 105–114.
- [281] V. Dilalla, G. Chaput, T. Williams, K. Sultanem, *Curr. Oncol.* **2020**, *27*, 107–112.
- [282] W. D. Newhauser, A. Berrington de Gonzalez, R. Schulte, C. Lee, *Front. Oncol.* **2016**, *6*, 13.
- [283] J. Jeba, R. Isiah, J. Subhashini, S. Backianathan, B. Thangakunam, D. J. Christopher, *J. Clin. Diagn. Res.* **2015**, *9*, XC01–XC05.
- [284] B. Ozturk, I. Egehan, S. Atavci, M. Kitapci, *Int. J. Radiat. Oncol.* **2004**, *58*, 213–219.
- [285] Y. Tang, Y. Wang, M. F. Kiani, B. Wang, *Clin. Breast Cancer* **2016**, *16*, 335–343.
- [286] M. Nikolaou, A. Pavlopoulou, A. G. Georgakilas, E. Kyrodimos, *Clin. Exp. Metastasis* **2018**, *35*, 309–318.
- [287] M. García-Aranda, E. Pérez-Ruiz, M. Redondo, *Int. J. Mol. Sci.* **2018**, *19*, 3950.
- [288] M. E. Robson, N. Tung, P. Conte, S.-A. Im, E. Senkus, B. Xu, N. Masuda, S. Delaloge, W. Li, A. Armstrong, W. Wu, C. Goessl, S. Runswick, S. M. Domchek, *Ann. Oncol. Off. J. Eur. Soc. Med. Oncol.* **2019**, *30*, 558–566.
- [289] J. K. Litton, H. S. Rugo, J. Ettl, S. A. Hurvitz, A. Gonçalves, K.-H. Lee, L. Fehrenbacher, R. Yerushalmi, L. A. Mina, M. Martin, H. Roché, Y.-H. Im, R. G. W. Quek, D. Markova, I. C. Tudor, A. L. Hannah, W. Eiermann, J. L. Blum, *N. Engl. J. Med.* **2018**, *379*, 753–763.
- [290] S.-B. Kim, R. Dent, S.-A. Im, M. Espié, S. Blau, A. R. Tan, S. J. Isakoff, M. Oliveira, C. Saura, M. J. Wongchenko, A. V Kapp, W. Y. Chan, S. M. Singel, D. J. Maslyar, J. Baselga, S.-B. Kim, K. S. Lee, S.-A. Im, M. Espié, H.-C. Wang, S. Blau, R. Dent, A. Tan, J. H. Sohn, M. De Laurentiis, L. G. Estevez, C.-S. Huang, G. Romieu, M. Velez, R. Villanueva, P. F. Conte, S. Dakhil, M. Debled, A. G. Martin, S. Hurvitz, J. H. Kim, C. Levy, M. Oliveira, P. S. Rovira, J. H. Seo, V. Valero, G. Vidal, A. Wong, M. A. K. Allison, R. Figlin, D. Chan, S.-C. Chen, Y.-H. Chen, M. Cobleigh, F. De Braud, L. Dirix, V. Hansen, A. H. Bessard, N. Iannotti, S. Isakoff, W. Lawler, A. Montañó, M. Salkini, L. Seigel, *Lancet Oncol.* **2017**, *18*, 1360–1372.
- [291] P. Schmid, J. Abraham, S. Chan, D. Wheatley, A. M. Brunt, G. Nemsadze, R.

- D. Baird, Y. H. Park, P. S. Hall, T. Perren, R. C. Stein, L. Mangel, J.-M. Ferrero, M. Phillips, J. Conibear, J. Cortes, A. Foxley, E. C. de Bruin, R. McEwen, D. Stetson, B. Dougherty, S.-J. Sarker, A. Prendergast, M. McLaughlin-Callan, M. Burgess, C. Lawrence, H. Cartwright, K. Mousa, N. C. Turner, *J. Clin. Oncol.* **2019**, *38*, 423–433.
- [292] L. A. Carey, H. S. Rugo, P. K. Marcom, E. L. Mayer, F. J. Esteva, C. X. Ma, M. C. Liu, A. M. Storniolo, M. F. Rimawi, A. Forero-Torres, A. C. Wolff, T. J. Hobday, A. Ivanova, W.-K. Chiu, M. Ferraro, E. Burrows, P. S. Bernard, K. A. Hoadley, C. M. Perou, E. P. Winer, *J. Clin. Oncol.* **2012**, *30*, 2615–2623.
- [293] J. Baselga, P. Gómez, R. Greil, S. Braga, M. A. Climent, A. M. Wardley, B. Kaufman, S. M. Stemmer, A. Pêgo, A. Chan, J.-C. Goeminne, M.-P. Graas, M. J. Kennedy, E. M. Ciruelos Gil, A. Schneeweiss, A. Zubel, J. Groos, H. Melezínková, A. Awada, *J. Clin. Oncol.* **2013**, *31*, 2586–2592.
- [294] P. A. Fasching, S. Loibl, C. Hu, S. N. Hart, H. Shimelis, R. Moore, C. Schem, H. Tesch, M. Untch, J. Hilfrich, M. Rezai, B. Gerber, S. D. Costa, J.-U. Blohmer, T. Fehm, J. Huober, C. Liedtke, R. M. Weinshilboum, L. Wang, J. N. Ingle, V. Müller, V. Nekljudova, K. E. Weber, B. Rack, M. Rübner, G. von Minckwitz, F. J. Couch, *J. Clin. Oncol.* **2018**, *36*, 2281–2287.
- [295] W. M. Sikov, D. A. Berry, C. M. Perou, B. Singh, C. T. Cirrincione, S. M. Tolaney, C. S. Kuzma, T. J. Pluard, G. Somlo, E. R. Port, M. Golshan, J. R. Bellon, D. Collyar, O. M. Hahn, L. A. Carey, C. A. Hudis, E. P. Winer, *J. Clin. Oncol.* **2015**, *33*, 13–21.
- [296] A. Gucalp, S. Tolaney, S. J. Isakoff, J. N. Ingle, M. C. Liu, L. A. Carey, K. Blackwell, H. Rugo, L. Nabell, A. Forero, V. Stearns, A. S. Doane, M. Danso, M. E. Moynahan, L. F. Momen, J. M. Gonzalez, A. Akhtar, D. D. Giri, S. Patil, K. N. Feigin, C. A. Hudis, T. A. Traina, T. B. C. R. C. (TBCRC 011), *Clin. Cancer Res.* **2013**, *19*, 5505–5512.
- [297] T. A. Traina, K. Miller, D. A. Yardley, J. Eakle, L. S. Schwartzberg, J. O’Shaughnessy, W. Gradishar, P. Schmid, E. Winer, C. Kelly, R. Nanda, A. Gucalp, A. Awada, L. Garcia-Estevez, M. E. Trudeau, J. Steinberg, H. Uppal, I. C. Tudor, A. Peterson, J. Cortes, *J. Clin. Oncol. Off. J. Am. Soc. Clin. Oncol.* **2018**, *36*, 884–890.
- [298] M. M. Williams, R. S. Cook, *Oncotarget* **2015**, *6*, 3519–3530.
- [299] J. S. Parker, J. S. Parker, A. Prat, M. Cheang, M. E. Lenburg, S. Paik, C. M. Perou, C. Hill, *Cancer Res.* **2009**, *69*, Abstract nr 2019.
- [300] D. Slamon, W. Eiermann, N. Robert, T. Pienkowski, M. Martin, M. Press, J. Mackey, J. Glaspy, A. Chan, M. Pawlicki, T. Pinter, V. Valero, M.-C. Liu, G. Sauter, G. von Minckwitz, F. Visco, V. Bee, M. Buyse, B. Bendahmane, I. Tabah-Fisch, M.-A. Lindsay, A. Riva, J. Crown, B. C. I. R. Group, *N. Engl. J. Med.* **2011**, *365*, 1273–1283.

- [301] E. A. Perez, E. H. Romond, V. J. Suman, J. H. Jeong, G. Sledge, C. E. Geyer, S. Martino, P. Rastogi, J. Gralow, S. M. Swain, E. P. Winer, G. Colon-Otero, N. E. Davidson, E. Mamounas, J. A. Zujewski, N. Wolmark, *J. Clin. Oncol.* **2014**, *32*, 3744–3752.
- [302] D. Cameron, M. J. Piccart-Gebhart, R. D. Gelber, M. Procter, A. Goldhirsch, E. de Azambuja, G. J. Castro, M. Untch, I. Smith, L. Gianni, J. Baselga, N. Al-Sakaff, S. Lauer, E. McFadden, B. Leyland-Jones, R. Bell, M. Dowsett, C. Jackisch, *Lancet (London, England)* **2017**, *389*, 1195–1205.
- [303] C. Liedtke, C. Mazouni, K. R. Hess, F. André, A. Tordai, J. A. Mejia, W. F. Symmans, A. M. Gonzalez-Angulo, B. Hennessy, M. Green, M. Cristofanilli, G. N. Hortobagyi, L. Pusztai, *J. Clin. Oncol.* **2008**, *26*, 1275–1281.
- [304] L. A. Carey, E. C. Dees, L. Sawyer, L. Gatti, D. T. Moore, F. Collichio, D. W. Ollila, C. I. Sartor, M. L. Graham, C. M. Perou, *Clin. cancer Res. an Off. J. Am. Assoc. Cancer Res.* **2007**, *13*, 2329–2334.
- [305] A. Wardley, *Adv. Breast Cancer* **2006**, *3*, 45.
- [306] Early Breast Cancer Trialists' Collaborative Group (EBCTCG), *Lancet* **2008**, *371*, 29–40.
- [307] L. Galluzzi, I. Vitale, S. A. Aaronson, J. M. Abrams, D. Adam, P. Agostinis, E. S. Alnemri, L. Altucci, I. Amelio, D. W. Andrews, M. Annicchiarico-Petruzzelli, A. V Antonov, E. Arama, E. H. Baehrecke, N. A. Barlev, N. G. Bazan, F. Bernassola, M. J. M. Bertrand, K. Bianchi, M. V Blagosklonny, K. Blomgren, C. Borner, P. Boya, C. Brenner, M. Campanella, E. Candi, D. Carmona-Gutierrez, F. Cecconi, F. K.-M. Chan, N. S. Chandel, E. H. Cheng, J. E. Chipuk, J. A. Cidlowski, A. Ciechanover, G. M. Cohen, M. Conrad, J. R. Cubillos-Ruiz, P. E. Czabotar, V. D'Angiolella, T. M. Dawson, V. L. Dawson, V. De Laurenzi, R. De Maria, K.-M. Debatin, R. J. DeBerardinis, M. Deshmukh, N. Di Daniele, F. Di Virgilio, V. M. Dixit, S. J. Dixon, C. S. Duckett, B. D. Dynlacht, W. S. El-Deiry, J. W. Elrod, G. M. Fimia, S. Fulda, A. J. García-Sáez, A. D. Garg, C. Garrido, E. Gavathiotis, P. Golstein, E. Gottlieb, D. R. Green, L. A. Greene, H. Gronemeyer, A. Gross, G. Hajnoczky, J. M. Hardwick, I. S. Harris, M. O. Hengartner, C. Hetz, H. Ichijo, M. Jäättelä, B. Joseph, P. J. Jost, P. P. Juin, W. J. Kaiser, M. Karin, T. Kaufmann, O. Kepp, A. Kimchi, R. N. Kitsis, D. J. Klionsky, R. A. Knight, S. Kumar, S. W. Lee, J. J. Lemasters, B. Levine, A. Linkermann, S. A. Lipton, R. A. Lockshin, C. López-Otín, S. W. Lowe, T. Luedde, E. Lugli, M. MacFarlane, F. Madeo, M. Malewicz, W. Malorni, G. Manic, J.-C. Marine, S. J. Martin, J.-C. Martinou, J. P. Medema, P. Mehlen, P. Meier, S. Melino, E. A. Miao, J. D. Molkenin, U. M. Moll, C. Muñoz-Pinedo, S. Nagata, G. Nuñez, A. Oberst, M. Oren, M. Overholtzer, M. Pagano, T. Panaretakis, M. Pasparakis, J. M. Penninger, D. M. Pereira, S. Pervaiz, M. E. Peter, M. Piacentini, P. Pinton, J. H. M. Prehn, H. Puthalakath, G. A. Rabinovich, M. Rehm, R. Rizzuto,

- C. M. P. Rodrigues, D. C. Rubinsztein, T. Rudel, K. M. Ryan, E. Sayan, L. Scorrano, F. Shao, Y. Shi, J. Silke, H.-U. Simon, A. Sistigu, B. R. Stockwell, A. Strasser, G. Szabadkai, S. W. G. Tait, D. Tang, N. Tavernarakis, A. Thorburn, Y. Tsujimoto, B. Turk, T. Vanden Berghe, P. Vandenabeele, M. G. Vander Heiden, A. Villunger, H. W. Virgin, K. H. Vousden, D. Vucic, E. F. Wagner, H. Walczak, D. Wallach, Y. Wang, J. A. Wells, W. Wood, J. Yuan, Z. Zakeri, B. Zhivotovsky, L. Zitvogel, G. Melino, G. Kroemer, *Cell Death Differ.* **2018**, *25*, 486–541.
- [308] R. J. Youle, A. Strasser, *Nat. Rev. Mol. Cell Biol.* **2008**, *9*, 47–59.
- [309] H.-C. Chen, M. Kanai, A. Inoue-Yamauchi, H.-C. Tu, Y. Huang, D. Ren, H. Kim, S. Takeda, D. E. Reyna, P. M. Chan, Y. T. Ganesan, C.-P. Liao, E. Gavathiotis, J. J. Hsieh, E. H. Cheng, *Nat. Cell Biol.* **2015**, *17*, 1270–1281.
- [310] D. Hanahan, R. A. Weinberg, *Cell* **2000**, *100*, 57–70.
- [311] D. L. Vaux, S. Cory, J. M. Adams, *Nature* **1988**, *335*, 440–442.
- [312] J. Watanabe, F. Kushihata, K. Honda, K. Mominoki, S. Matsuda, N. Kobayashi, *Int. J. Oncol.* **2002**, *21*, 515–519.
- [313] C. Castilla, B. Congregado, D. Chinchón, F. J. Torrubia, M. A. Japón, C. Sáez, *Endocrinology* **2006**, *147*, 4960–4967.
- [314] E. T. Olejniczak, C. Van Sant, M. G. Anderson, G. Wang, S. K. Tahir, G. Sauter, R. Lesniewski, D. Semizarov, *Mol. Cancer Res.* **2007**, *5*, 331–339.
- [315] A. F. Schott, I. J. Apel, G. Nuñez, M. F. Clarke, *Oncogene* **1995**, *11*, 1389–1394.
- [316] D. Del Bufalo, A. Biroccio, C. Leonetti, G. Zupi, *FASEB J. Off. Publ. Fed. Am. Soc. Exp. Biol.* **1997**, *11*, 947–953.
- [317] R. Jäger, U. Herzer, J. Schenkel, H. Weiher, *Oncogene* **1997**, *15*, 1787–1795.
- [318] Q. Ding, X. He, W. Xia, J.-M. Hsu, C.-T. Chen, L.-Y. Li, D.-F. Lee, J.-Y. Yang, X. Xie, J.-C. Liu, M.-C. Hung, *Cancer Res.* **2007**, *67*, 4564–4571.
- [319] L. Zhao, X.-Y. Zheng, *Onco. Targets. Ther.* **2016**, *9*, 4505–4516.
- [320] K. J. Campbell, S. Dhayade, N. Ferrari, A. H. Sims, E. Johnson, S. M. Mason, A. Dickson, K. M. Ryan, G. Kalna, J. Edwards, S. G. W. Tait, K. Blyth, *Cell Death Dis.* **2018**, *9*, DOI 10.1038/s41419-017-0035-2.
- [321] M. A. Shibata, M. L. Liu, M. C. Knudson, E. Shibata, K. Yoshidome, T. Bandey, S. J. Korsmeyer, J. E. Green, *EMBO J.* **1999**, *18*, 2692–2701.
- [322] M. D. Planas-Silva, R. D. Bruggeman, R. T. Grenko, J. S. Smith, *Exp. Mol. Pathol.* **2007**, *82*, 85–90.
- [323] A. Sierra, X. Castellsagué, A. Escobedo, B. Lloveras, M. García-Ramirez, A. Moreno, A. Fabra, *Int. J. Cancer* **2000**, *89*, 142–147.
- [324] J. Chang, G. M. Clark, D. C. Allred, S. Mohsin, G. Chamness, R. M. Elledge, *Cancer* **2003**, *97*, 545–553.
- [325] P. A. Ellis, I. E. Smith, S. Detre, S. A. Burton, J. Salter, R. A'Hern, G. Walsh, S.

- R. Johnston, M. Dowsett, *Breast Cancer Res. Treat.* **1998**, *48*, 107–116.
- [326] P. J. Real, A. Sierra, A. De Juan, J. C. Segovia, J. M. Lopez-Vega, J. L. Fernandez-Luna, *Oncogene* **2002**, *21*, 7611–7618.
- [327] C. Teixeira, J. C. Reed, M. A. Pratt, *Cancer Res.* **1995**, *55*, 3902–3907.
- [328] J. M. Balko, J. M. Giltane, K. Wang, L. J. Schwarz, C. D. Young, R. S. Cook, P. Owens, M. E. Sanders, M. G. Kuba, V. Sánchez, R. Kurupi, P. D. Moore, J. A. Pinto, F. D. Doimi, H. Gómez, D. Horiuchi, A. Goga, B. D. Lehmann, J. A. Bauer, J. A. Pietenpol, J. S. Ross, G. A. Palmer, R. Yelensky, M. Cronin, V. A. Miller, P. J. Stephens, C. L. Arteaga, *Cancer Discov.* **2014**, *4*, 232–245.
- [329] A. Crawford, R. Nahta, *Curr. Pharmacogenomics Person. Med.* **2011**, *9*, 184–190.
- [330] P. Raha, S. Thomas, K. T. Thurn, J. Park, P. N. Munster, *Breast Cancer Res.* **2015**, *17*, 26.
- [331] C. Tse, A. R. Shoemaker, J. Adickes, M. G. Anderson, J. Chen, S. Jin, E. F. Johnson, K. C. Marsh, M. J. Mitten, P. Nimmer, L. Roberts, S. K. Tahir, Y. Xiao, X. Yang, H. Zhang, S. Fesik, S. H. Rosenberg, S. W. Elmore, *Cancer Res.* **2008**, *68*, 3421–3428.
- [332] W. H. Wilson, O. A. O’Connor, M. S. Czuczman, A. S. LaCasce, J. F. Gerecitano, J. P. Leonard, A. Tulpule, K. Dunleavy, H. Xiong, Y.-L. Chiu, Y. Cui, T. Busman, S. W. Elmore, S. H. Rosenberg, A. P. Krivoshik, S. H. Enschede, R. A. Humerickhouse, *Lancet. Oncol.* **2010**, *11*, 1149–1159.
- [333] L. Gandhi, D. R. Camidge, M. R. De Oliveira, P. Bonomi, D. Gandara, D. Khaira, C. L. Hann, E. M. McKeegan, E. Litvinovich, P. M. Hemken, C. Dive, S. H. Enschede, C. Nolan, Y. L. Chiu, T. Busman, H. Xiong, A. P. Krivoshik, R. Humerickhouse, G. I. Shapiro, C. M. Rudin, *J. Clin. Oncol.* **2011**, *29*, 909–916.
- [334] A. W. Tolcher, P. LoRusso, J. Arzt, T. A. Busman, G. Lian, N. S. Rudersdorf, C. A. Vanderwal, J. F. Waring, J. Yang, K. D. Holen, L. S. Rosen, *Cancer Chemother. Pharmacol.* **2015**, *76*, 1041–1049.
- [335] A. W. Tolcher, P. LoRusso, J. Arzt, T. A. Busman, G. Lian, N. S. Rudersdorf, C. A. Vanderwal, W. Kirschbrown, K. D. Holen, L. S. Rosen, *Cancer Chemother. Pharmacol.* **2015**, *76*, 1025–1032.
- [336] A. W. Roberts, R. H. Advani, B. S. Kahl, D. Persky, J. W. Sweetenham, D. A. Carney, J. Yang, T. B. Busman, S. H. Enschede, R. A. Humerickhouse, J. F. Seymour, *Br. J. Haematol.* **2015**, *170*, 669–678.
- [337] W. H. Wilson, O. A. O. Connor, M. S. Czuczman, S. Lacasce, J. F. Gerecitano, J. P. Leonard, A. Tulpule, K. Dunleavy, H. Xiong, D. Ph, Y. Chiu, D. Ph, Y. Cui, D. Ph, S. H. Enschede, R. A. Humerickhouse, *Lancet Oncol.* **2010**, *11*, 1149–1159.
- [338] S. M. Schoenwaelder, K. E. Jarman, E. E. Gardiner, M. Hua, J. Qiao, M. J. White, E. C. Josefsson, I. Alwis, A. Ono, A. Willcox, R. K. Andrews, K. D.

- Mason, H. H. Salem, D. C. S. Huang, B. T. Kile, A. W. Roberts, S. P. Jackson, *Blood* **2011**, *118*, 1663–1674.
- [339] A. Kaefer, J. Yang, P. Noertersheuser, S. Mensing, R. Humerickhouse, W. Awni, H. Xiong, *Cancer Chemother. Pharmacol.* **2014**, *74*, 593–602.
- [340] A. J. Souers, J. D. Levenson, E. R. Boghaert, S. L. Ackler, N. D. Catron, J. Chen, B. D. Dayton, H. Ding, S. H. Enschede, W. J. Fairbrother, D. C. S. Huang, S. G. Hymowitz, S. Jin, S. L. Khaw, P. J. Kovar, L. T. Lam, J. Lee, H. L. Maecker, K. C. Marsh, K. D. Mason, M. J. Mitten, P. M. Nimmer, A. Oleksijew, C. H. Park, C.-M. Park, D. C. Phillips, A. W. Roberts, D. Sampath, J. F. Seymour, M. L. Smith, G. M. Sullivan, S. K. Tahir, C. Tse, M. D. Wendt, Y. Xiao, J. C. Xue, H. Zhang, R. A. Humerickhouse, S. H. Rosenberg, S. W. Elmore, *Nat. Med.* **2013**, *19*, 202–208.
- [341] A. W. Roberts, M. S. Davids, J. M. Pagel, B. S. Kahl, S. D. Puvvada, J. F. Gerecitano, T. J. Kipps, M. A. Anderson, J. R. Brown, L. Gressick, S. Wong, M. Dunbar, M. Zhu, M. B. Desai, E. Cerri, S. Heitner Enschede, R. A. Humerickhouse, W. G. Wierda, J. F. Seymour, *N. Engl. J. Med.* **2016**, *374*, 311–322.
- [342] A. W. Roberts, S. Ma, T. J. Kipps, S. E. Coutre, M. S. Davids, B. Eichhorst, M. Hallek, J. C. Byrd, K. Humphrey, L. Zhou, B. Chyla, J. Nielsen, J. Potluri, S. Y. Kim, M. Verdugo, S. Stilgenbauer, W. G. Wierda, J. F. Seymour, *Blood* **2019**, *134*, 111–122.
- [343] O. Al-Sawaf, C. Zhang, M. Tandon, A. Sinha, A.-M. Fink, S. Robrecht, O. Samoylova, A. M. Liberati, J. Pinilla-Ibarz, S. Opat, L. Sivcheva, K. Le Dû, L. M. Fogliatto, C. U. Niemann, R. Weinkove, S. Robinson, T. J. Kipps, E. Tausch, W. Schary, M. Ritgen, C.-M. Wendtner, K.-A. Kreuzer, B. Eichhorst, S. Stilgenbauer, M. Hallek, K. Fischer, *Lancet. Oncol.* **2020**, *21*, 1188–1200.
- [344] K. Fischer, O. Al-Sawaf, J. Bahlo, A.-M. Fink, M. Tandon, M. Dixon, S. Robrecht, S. Warburton, K. Humphrey, O. Samoylova, A. M. Liberati, J. Pinilla-Ibarz, S. Opat, L. Sivcheva, K. Le Dû, L. M. Fogliatto, C. U. Niemann, R. Weinkove, S. Robinson, T. J. Kipps, S. Boettcher, E. Tausch, R. Humerickhouse, B. Eichhorst, C.-M. Wendtner, A. W. Langerak, K.-A. Kreuzer, M. Ritgen, V. Goede, S. Stilgenbauer, M. Mobasher, M. Hallek, *N. Engl. J. Med.* **2019**, *380*, 2225–2236.
- [345] J. F. Seymour, T. J. Kipps, B. Eichhorst, P. Hillmen, J. D’Rozario, S. Assouline, C. Owen, J. Gerecitano, T. Robak, J. De la Serna, U. Jaeger, G. Cartron, M. Montillo, R. Humerickhouse, E. A. Punnoose, Y. Li, M. Boyer, K. Humphrey, M. Mobasher, A. P. Kater, *N. Engl. J. Med.* **2018**, *378*, 1107–1120.
- [346] C. D. DiNardo, K. Pratz, V. Pullarkat, B. A. Jonas, M. Arellano, P. S. Becker, O. Frankfurt, M. Konopleva, A. H. Wei, H. M. Kantarjian, T. Xu, W.-J. Hong, B. Chyla, J. Potluri, D. A. Pollyea, A. Letai, *Blood* **2019**, *133*, 7–17.

- [347] C. D. DiNardo, B. A. Jonas, V. Pullarkat, M. J. Thirman, J. S. Garcia, A. H. Wei, M. Konopleva, H. Döhner, A. Letai, P. Fenaux, E. Koller, V. Havelange, B. Leber, J. Esteve, J. Wang, V. Pejisa, R. Hájek, K. Porkka, Á. Illés, D. Lavie, R. M. Lemoli, K. Yamamoto, S.-S. Yoon, J.-H. Jang, S.-P. Yeh, M. Turgut, W.-J. Hong, Y. Zhou, J. Potluri, K. W. Pratz, *N. Engl. J. Med.* **2020**, *383*, 617–629.
- [348] A. H. Wei, P. Montesinos, V. Ivanov, C. D. DiNardo, J. Novak, K. Laribi, I. Kim, D. A. Stevens, W. Fiedler, M. Pagoni, O. Samoiloova, Y. Hu, A. Anagnostopoulos, J. Bergeron, J.-Z. Hou, V. Murthy, T. Yamauchi, A. McDonald, B. Chyla, S. Gopalakrishnan, Q. Jiang, W. Mendes, J. Hayslip, P. Panayiotidis, *Blood* **2020**, *135*, 2137–2145.
- [349] F. Vaillant, D. Merino, L. Lee, K. Breslin, B. Pal, M. E. Ritchie, G. K. Smyth, M. Christie, L. J. Phillipson, C. J. Burns, G. B. Mann, J. E. Visvader, G. J. Lindeman, *Cancer Cell* **2013**, *24*, 120–129.
- [350] S. R. Oakes, F. Vaillant, E. Lim, L. Lee, K. Breslin, F. Feleppa, S. Deb, M. E. Ritchie, E. Takano, T. Ward, S. B. Fox, D. Generali, G. K. Smyth, A. Strasser, D. C. S. Huang, J. E. Visvader, G. J. Lindeman, *Proc. Natl. Acad. Sci. U. S. A.* **2012**, *109*, 2766–2771.
- [351] J.-Y. Li, Y.-Y. Li, W. Jin, Q. Yang, Z.-M. Shao, X.-S. Tian, *J. Exp. Clin. Cancer Res.* **2012**, *31*, 102.
- [352] D. Yecies, N. E. Carlson, J. Deng, A. Letai, *Blood* **2010**, *115*, 3304–3313.
- [353] M. F. van Delft, A. H. Wei, K. D. Mason, C. J. Vandenberg, L. Chen, P. E. Czabotar, S. N. Willis, C. L. Scott, C. L. Day, S. Cory, J. M. Adams, A. W. Roberts, D. C. S. Huang, *Cancer Cell* **2006**, *10*, 389–399.
- [354] M. Konopleva, R. Contractor, T. Tsao, I. Samudio, P. P. Ruvolo, S. Kitada, X. Deng, D. Zhai, Y. X. Shi, T. Sneed, M. Verhaegen, M. Soengas, V. R. Ruvolo, T. McQueen, W. D. Schober, J. C. Watt, T. Jiffar, X. Ling, F. C. Marini, D. Harris, M. Dietrich, Z. Estrov, J. McCubrey, W. S. May, J. C. Reed, M. Andreeff, *Cancer Cell* **2006**, *10*, 375–388.
- [355] M. M. Williams, D. L. Elion, B. Rahman, D. J. Hicks, V. Sanchez, R. S. Cook, *Oncotarget* **2019**, *10*, 5389–5402.
- [356] M. M. Williams, L. Lee, D. J. Hicks, M. M. Joly, D. Elion, B. Rahman, C. McKernan, V. Sanchez, J. M. Balko, T. Stricker, M. V. Estrada, R. S. Cook, *Mol. Cancer Res.* **2017**, *15*, 259–268.
- [357] G. S. Choudhary, S. Al-Harbi, S. Mazumder, B. T. Hill, M. R. Smith, J. Bodo, E. D. Hsi, A. Almasan, *Cell Death Dis.* **2015**, *6*, e1593-12.
- [358] M. Marczyk, G. A. Patwardhan, J. Zhao, R. Qu, X. Li, V. B. Wali, A. K. Gupta, M. M. Pillai, Y. Kluger, Q. Yan, C. Hatzis, L. Pusztai, V. Gunasekharan, *Cancers (Basel)*. **2020**, *12*, 2551.
- [359] Z. Li, S. He, A. T. Look, *Leukemia* **2019**, *33*, 262–266.
- [360] K. Y. Wong, C. S. Chim, *J. Pharm. Pharmacol.* **2020**, *72*, 728–737.

- [361] M. Hormi, R. Birsén, M. Belhadj, T. Huynh, L. Cantero Aguilar, E. Grignano, L. Haddaoui, F. Guillonneau, P. Mayeux, M. Hunault, J. Tamburini, O. Kosmider, M. Fontenay, D. Bouscary, N. Chapuis, *Eur. J. Haematol.* **2020**, *105*, 588–596.
- [362] D. Merino, J. R. Whittle, F. Vaillant, A. Serrano, J. N. Gong, G. Giner, A. L. Maragno, M. Chanrion, E. Schneider, B. Pal, X. Li, G. Dewson, J. Gräsel, K. Liu, N. Lalaoui, D. Segal, M. J. Herold, D. C. S. Huang, G. K. Smyth, O. Geneste, G. Lessene, J. E. Visvader, G. J. Lindeman, *Sci. Transl. Med.* **2017**, *9*, eaam7049.
- [363] S. Adams, V. Diéras, C. H. Barrios, E. P. Winer, A. Schneeweiss, H. Iwata, S. Loi, S. Patel, V. Henschel, S. Y. Chui, H. S. Rugo, L. A. Emens, P. Schmid, *Ann. Oncol.* **2020**, *31*, 582–589.
- [364] M. Narvekar, H. Y. Xue, J. Y. Eoh, H. L. Wong, *AAPS PharmSciTech* **2014**, *15*, 822–833.
- [365] M. Nedeljković, A. Damjanović, *Cells* **2019**, *8*, 957.
- [366] M. R. Lackner, T. R. Wilson, J. Settleman, *Future Oncol.* **2012**, *8*, 999–1014.
- [367] Y. Lu, K. Park, *Int. J. Pharm.* **2013**, *453*, 198–214.
- [368] J. J. Tao, K. Visvanathan, A. C. Wolff, *Breast* **2015**, *24*, S149–S153.
- [369] P. Falagan-Lotsch, E. M. Grzincic, C. J. Murphy, *Bioconjug. Chem.* **2017**, *28*, 135–152.
- [370] D. Wu, M. Si, H. Y. Xue, H. L. Wong, *Int. J. Nanomedicine* **2017**, *12*, 5879–5892.
- [371] R. Torrisi, E. Montagna, E. Scarano, S. Dellapasqua, G. Canello, M. Iorfida, A. Luini, P. Veronesi, G. Viale, A. Goldhirsch, M. Colleoni, *Breast* **2011**, *20*, 34–38.
- [372] Y. Barenholz, *J. Control. Release* **2012**, *160*, 117–134.
- [373] E. Tahover, Y. P. Patil, A. A. Gabizon, *Anticancer. Drugs* **2015**, *26*, 241–258.
- [374] M. J. Gil-Gil, M. Bellet, S. Morales, B. Ojeda, L. Manso, C. Mesia, E. Garcia-Martínez, N. Martínez-Jáñez, M. Melé, A. Llombart, S. Pernas, P. Villagrasa, C. Blasco, J. Baselga, *Breast Cancer Res. Treat.* **2015**, *151*, 597–606.
- [375] R. Torrisi, A. Cardillo, G. Canello, S. Dellapasqua, A. Balduzzi, R. Ghisini, A. Luini, P. Veronesi, G. Viale, A. Goldhirsch, M. Colleoni, *Clin. Breast Cancer* **2010**, *10*, 483–488.
- [376] K. M. Rau, Y. C. Lin, Y. Y. Chen, J. S. Chen, K. Der Lee, C. H. Wang, H. K. Chang, *BMC Cancer* **2015**, *15*, 1–8.
- [377] M. E. R. O’Brien, N. Wigler, M. Inbar, R. Rosso, E. Grischke, A. Santoro, R. Catane, D. G. Kieback, P. Tomczak, S. P. Ackland, F. Orlandi, L. Mellars, L. Alland, C. Tendler, *Ann. Oncol.* **2004**, *15*, 440–449.
- [378] Y. Li, N. Chen, M. Palmisano, S. Zhou, *Mol. Pharm.* **2015**, *12*, 1308–1317.
- [379] N. Desai, V. Trieu, Z. Yao, L. Louie, S. Ci, A. Yang, C. Tao, T. De, B. Beals, D. Dykes, P. Noker, R. Yao, E. Labao, M. Hawkins, P. Soon-Shiong, *Clin. Cancer Res.* **2006**, *12*, 1317–1324.

- [380] N. Chen, Y. Li, Y. Ye, M. Palmisano, R. Chopra, S. Zhou, *J. Clin. Pharmacol.* **2014**, *54*, 1097–1107.
- [381] E. R. Gardner, W. L. Dahut, C. D. Scripture, J. Jones, J. B. Aragon-Ching, N. Desai, M. J. Hawkins, A. Sparreboom, W. D. Figg, *Clin. Cancer Res.* **2008**, *14*, 4200–4205.
- [382] M. Untch, C. Jackisch, A. Schneeweiss, B. Conrad, B. Aktas, C. Denkert, H. Eidtmann, H. Wiebringhaus, S. Kümmel, J. Hilfrich, M. Warm, S. Paepke, M. Just, C. Hanusch, J. Hackmann, J. U. Blohmer, M. Clemens, S. Darb-Esfahani, W. D. Schmitt, S. Dan Costa, B. Gerber, K. Engels, V. Nekljudova, S. Loibl, G. von Minckwitz, *Lancet Oncol.* **2016**, *17*, 345–356.
- [383] W. J. Gradishar, S. Tjulandin, N. Davidson, H. Shaw, N. Desai, P. Bhar, M. Hawkins, J. O’Shaughnessy, *J. Clin. Oncol.* **2005**, *23*, 7794–7803.
- [384] R. K. Jain, T. Stylianopoulos, *Nat. Rev. Clin. Oncol.* **2010**, *7*, 653–664.
- [385] M. J. Ernsting, W. D. Foltz, E. Undzys, T. Tagami, S. Li, *Biomaterials* **2012**, *33*, 3931–3941.
- [386] T. Lammers, F. Kiessling, W. E. Hennink, G. Storm, *J. Control. Release* **2012**, *161*, 175–187.
- [387] U. Prabhakar, H. Maeda, R. K. Jain, E. M. Sevick-Muraca, W. Zamboni, O. C. Farokhzad, S. T. Barry, A. Gabizon, P. Grodzinski, D. C. Blakey, *Cancer Res.* **2013**, *73*, 2412–2417.
- [388] R. Jain, J. Gutierrez, J. Narang, L. Scarpace, L. R. Schultz, N. Lemke, S. C. Patel, T. Mikkelsen, J. P. Rock, *Am. J. Neuroradiol.* **2011**, *32*, 388–394.
- [389] Y. Duo, Y. Li, C. Chen, B. Liu, X. Wang, X. Zeng, H. Chen, *RSC Adv.* **2017**, *7*, 39641–39650.
- [390] I. Galiana, B. Lozano-Torres, M. Sancho, M. Alfonso, A. Bernardos, V. Bisbal, M. Serrano, R. Martínez-Máñez, M. Orzáez, *J. Control. release* **2020**, *323*, 624–634.
- [391] S. Lee, M. S. Kim, D. Lee, T. K. Kwon, D. Khang, H. S. Yun, S. H. Kim, *Int. J. Nanomedicine* **2013**, *8*, 147–158.
- [392] M. Cho, W. S. Cho, M. Choi, S. J. Kim, B. S. Han, S. H. Kim, H. O. Kim, Y. Y. Sheen, J. Jeong, *Toxicol. Lett.* **2009**, *189*, 177–183.
- [393] J.-H. Kim, C.-S. Kim, R. M. C. Ignacio, D.-H. Kim, M. E. J. Sajo, E. H. Maeng, X.-F. Qi, S.-E. Park, Y.-R. Kim, M.-K. Kim, K.-J. Lee, S.-K. Kim, *Int. J. Nanomedicine* **2014**, *9 Suppl 2*, 183–193.
- [394] A. Nemmar, S. Albarwani, S. Beegam, P. Yuvaraju, J. Yasin, S. Attoub, B. H. Ali, *Int. J. Nanomedicine* **2014**, *9*, 2779–2789.
- [395] H. Chen, A. Dorrigan, S. Saad, D. J. Hare, M. B. Cortie, S. M. Valenzuela, *PLoS One* **2013**, *8*, e58208.
- [396] X. D. Zhang, H. Y. Wu, D. Wu, Y. Y. Wang, J. H. Chang, Z. Bin Zhai, A. M. Meng, P. X. Liu, L. A. Zhang, F. Y. Fan, *Int. J. Nanomedicine* **2010**, *5*, 771–781.

- [397] C. Fu, T. Liu, L. Li, H. Liu, D. Chen, F. Tang, *Biomaterials* **2013**, *34*, 2565–2575.
- [398] R. Mohammadpour, M. Yazdimamaghani, D. L. Cheney, J. Jedrzkiewicz, H. Ghandehari, *J. Control. Release* **2019**, *304*, 216–232.
- [399] L. Yang, H. Kuang, W. Zhang, Z. P. Aguilar, H. Wei, H. Xu, *Sci. Rep.* **2017**, *7*, 3303.
- [400] E. Sadauskas, G. Danscher, M. Stoltenberg, U. Vogel, A. Larsen, H. Wallin, *Nanomedicine Nanotechnology, Biol. Med.* **2009**, *5*, 162–169.
- [401] P. Falagan-Lotsch, E. M. Grzincic, C. J. Murphy, *Proc. Natl. Acad. Sci.* **2016**, *113*, 13318 LP – 13323.

Chapter 2 | Objectives

Given the growing interest in smart nanodevices with biomedical applications, the main objective of this Ph.D. thesis is the design and development of biomolecule-functionalised nanoparticles for breast cancer treatment. This strategy will generate novel therapies, which could improve treatment effectiveness and safety, while diminishing the side effects of the drugs.

This global aim frames the following specific objectives:

- To develop and evaluate a targeted-breast cancer system based on gated mesoporous silica nanoparticles for navitoclax resistance overcoming in triple-negative breast cancer.
- To synthesize and evaluate the efficacy of a mesoporous silica-based nanodevice for the co-delivery of the DNA editing machinery CRISPR/Cas9 and an entrapped cargo.
- To design and evaluate an enzyme delivery system based on gold nanoparticles for breast cancer treatment through nanogold-directed enzyme prodrug therapy.

**Chapter 3 | Navitoclax resistance
overcoming using mesoporous silica
nanoparticles**

MUC1 Aptamer-Capped Mesoporous Silica Nanoparticles for Navitoclax Resistance Overcoming in Triple-Negative Breast Cancer

Gema Vivo-Llorca,^{[a],[b],[e]} Vicente Candela-Noguera,^{[a],[b]} María Alfonso,^{[a],[b]} Alba García-Fernández,^{[a],[b],[c],[e]} Mar Orzáez,^{[e],[f]}* Félix Sancenón,^{[a],[b],[c],[d],[e]}* and Ramón Martínez-Máñez^{[a],[b],[c],[d],[e]}*

^[a] Instituto Interuniversitario de Investigación de Reconocimiento Molecular y Desarrollo Tecnológico (IDM) Universitat Politècnica de València, Universitat de València, Spain. E-mail: rmaez@qim.es

^[b] Departamento de Química Universitat Politècnica de València, Camino de Vera s/n, 46022 València, Spain.

^[c] CIBER de Bioingeniería, Biomateriales y Nanomedicina (CIBER-BBN).

^[d] Unidad Mixta de Investigación en Nanomedicina y Sensores. Universitat Politècnica de València, IIS La Fe, Valencia, Spain

^[e] Unidad Mixta UPV-CIPF de Investigación en Mecanismos de Enfermedades y Nanomedicina Universitat Politècnica de València y Centro de Investigación Príncipe Felipe, València, Spain.

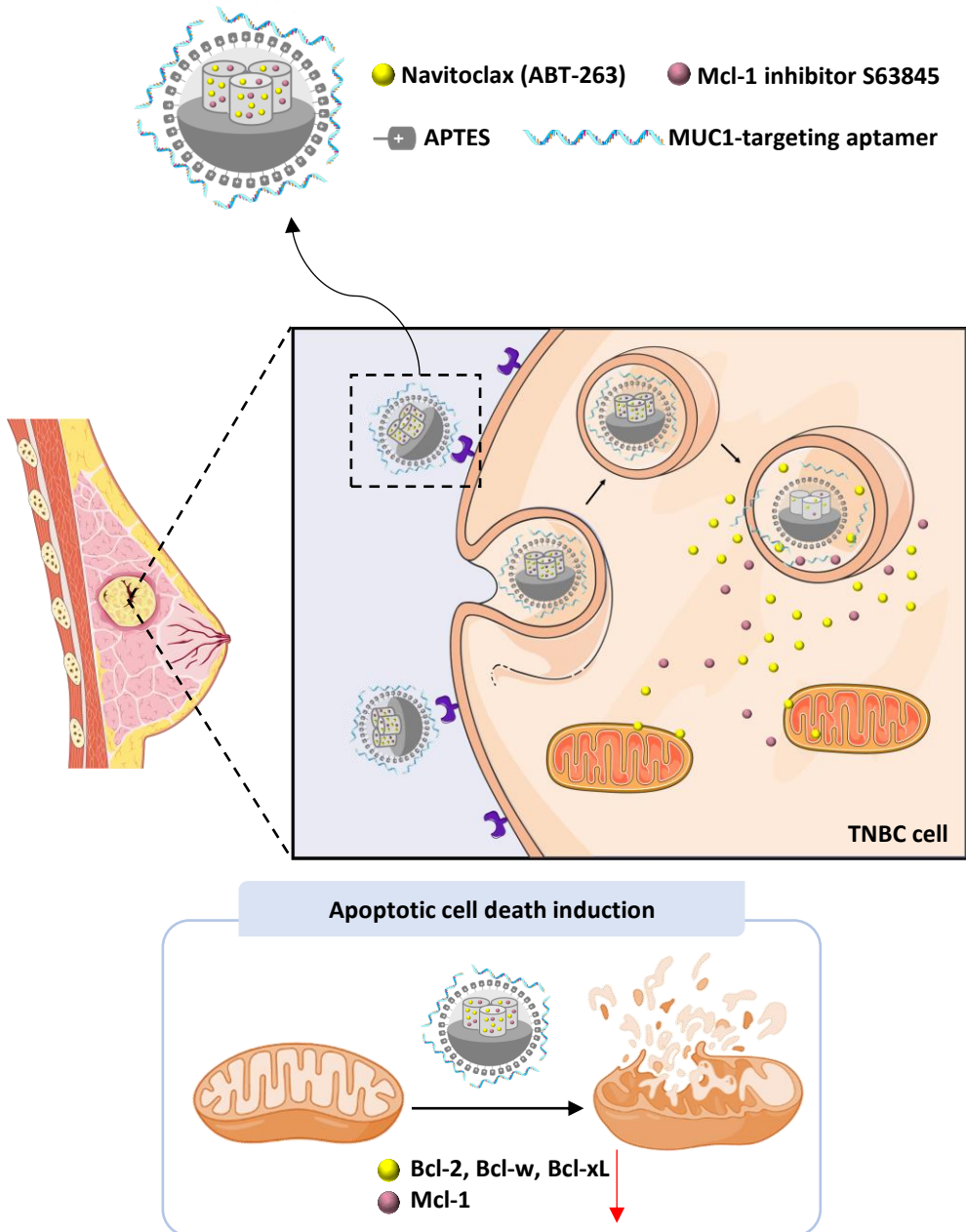
^[f] Centro de Investigación Príncipe Felipe, Eduardo Primo Yúfera, 3. València 46012, Spain. E-mail: morzaez@cipf.es

Published online: July 31, 2020

(Reprinted with permission from *Chem. Eur. J.* **2020**, *26*, 16318

© Wiley-VCH GmbH).

▪ Graphical abstract.



3.1 Abstract.

Triple-negative breast cancer (TNBC) is the most aggressive breast cancer subtype. In the last years, navitoclax has emerged as a possible treatment for TNBC. Nevertheless, rapid navitoclax resistance onset has been observed thorough Mcl-1 overexpression. As a strategy to overcome Mcl-1-mediated resistance, herein we present a controlled drug co-delivery system based on mesoporous silica nanoparticles (MSNs) targeted to TNBC cells. The nanocarrier is loaded with navitoclax and the Mcl-1 inhibitor S63845 and capped with a MUC1-targeting aptamer (**apMUC1-MSNs(Nav/S63845)**). The apMUC1-capped nanoparticles effectively target TNBC cell lines and successfully induce apoptosis, overcoming navitoclax resistance. Moreover, navitoclax encapsulation protects platelets against apoptosis. These results point apMUC1-gated MSNs as suitable BH3 mimetics nanocarriers in the targeted treatment of MUC1-expressing TNBC.

3.2 Introduction.

As briefly explained in the introduction (see [section 1.6](#)), breast cancer is the most frequently diagnosed and the leading cause of cancer death in women worldwide.^[1,2] Among breast cancers, TNBC accounts for approximately 15-20% of breast carcinomas.^[3] Moreover, TNBC shows the poorest outcome due to its aggressiveness, chemotherapy resistance, early recurrence, and high risk of metastasis.^[4] Triple-negative breast cancer is defined by the lack of the three main breast cancer biomarkers, i.e., estrogen, progesterone, and HER2 receptors.^[5] Due to the loss of such receptors, TNBC patients do not respond to targeted treatments (endocrine or anti-HER2 therapy), and first-line treatment of TNBC patients is chemotherapy combined with surgery and/or radiotherapy. This scenario warrants the need for the development of new strategies to treat TNBC.^[6,7]

Evasion of apoptosis is a hallmark of cancer.^[8] The proteins from Bcl-2 family are the key mediators of this type of cell death. They are divided into three subfamilies: the pro-apoptotic BH3-only ligands (Bid, Bad, Bim, Puma, Noxa, etc.), the pro-apoptotic multi-BH domain effector proteins (Bax and Bak), and the anti-apoptotic proteins (Bcl-2, Bcl-xL, Bcl-w, Mcl-1, and Bfl-1).^[9-11] The balance between pro-apoptotic and anti-apoptotic members determines cell survival or death. In the case of tumours, this equilibrium often leans towards survival, leading to sustained tumour expansion and chemotherapy resistance.^[12] To overcome this tumour survival mechanism, several inhibitors of Bcl-2 anti-apoptotic proteins, also called BH3 mimetic drugs, such as ABT-263 (known as navitoclax) have been developed.^[13] Navitoclax is currently involved in several clinical trials on different solid and liquid tumours (NCT01989585, NCT02520778, NCT03181126, NCT03366103, NCT03222609, and NCT02079740).^[14]

From these clinical trials, it became apparent that there are two main limitations to the use of navitoclax. First, some side effects on patients, from which the most relevant is thrombocytopenia, as a consequence of platelets dependence on Bcl-xL for survival.^[15] A second drawback is that navitoclax targets only three anti-apoptotic members of the Bcl-2 protein family (i.e., Bcl-w, Bcl-2, and Bcl-xL), but it does not target the anti-apoptotic protein Mcl-1. This leads to the rapid development of treatment resistance in cancer cells through Mcl-1 overexpression.^[13,16] Mcl-1 overexpression has been associated with a bad prognosis in breast cancer patients.^[16,17] Recently, a highly specific Mcl-1 inhibitor, named S63845, has been developed and its antiproliferative activity has been demonstrated in several malignancies *in vitro* and *in vivo*.^[18] In this scenario, the synergistic action of the Mcl-1 inhibitor S63845 and BH3 mimetic drugs against breast cancer and other malignancies has been reported.^[19,20]

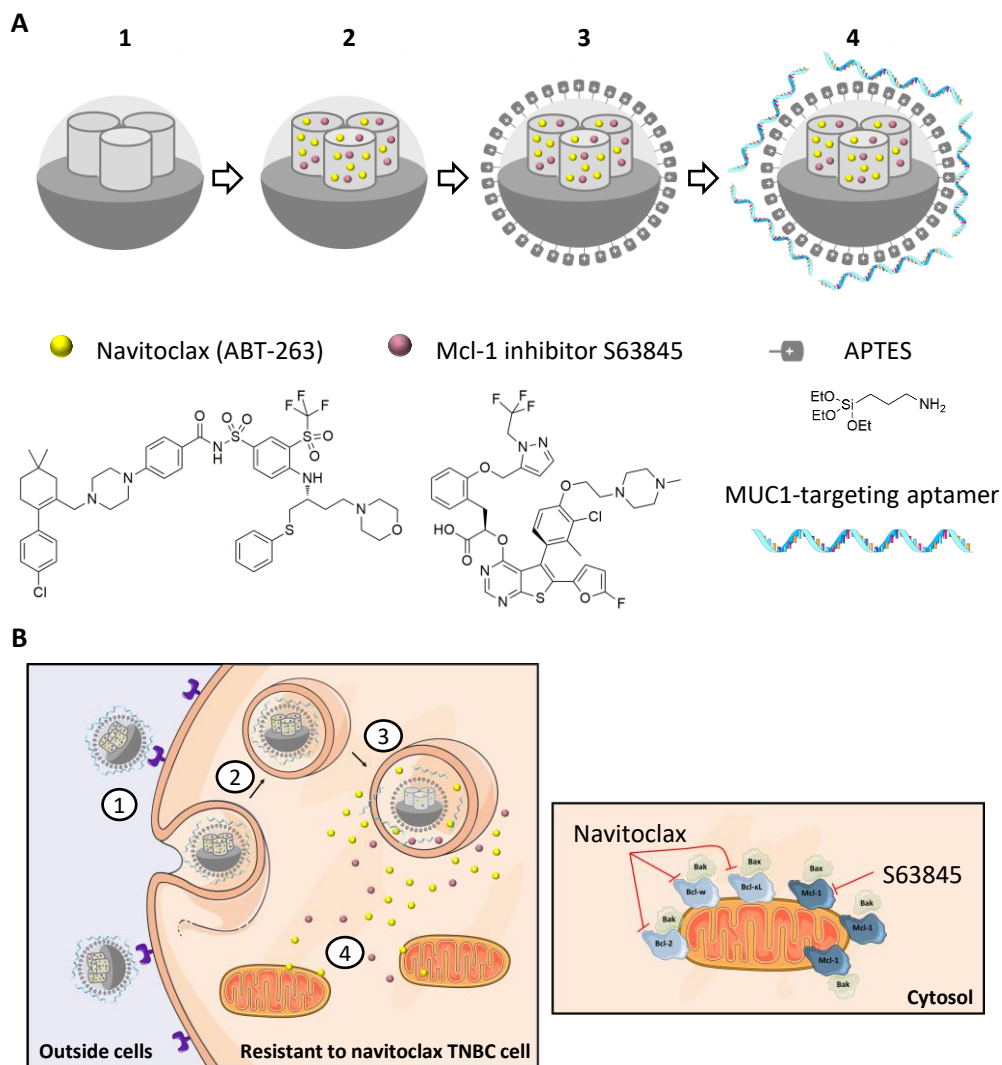
Based on the above-mentioned facts, we were interested in designing nanoparticles for their potential enhanced use in the treatment of breast cancer. Specifically, we focused our attention on the preparation of nanoparticles that could overcome the two limiting properties of navitoclax as a drug: i.e., platelet toxicity and resistances through Mcl-1 overexpression. With this aim, we prepare herein MSNs loaded with navitoclax and the Mcl-1 inhibitor S63845, and capped with an aptamer (apMUC1) targeting the MUC1 surface protein overexpressed in TNBC cells (**apMUC1-MSNs(Nav/S63845)**). Aptamers are short single-strand DNA or RNA oligonucleotides that fold into 3D structures that bind and target molecules with high affinity and specificity. To develop active nanocarriers with targeting abilities, a common approach is to target surface receptors overexpressed in selected cells.^[21–24] In this scenario and concerning breast cancer, MUC1 is a transmembrane glycoprotein belonging to the mucin family, which is aberrantly overexpressed in 70% of breast cancer and it has been recognized as an important molecular target in cancer.^[25–27]

3.3 Results and Discussion.

3.3.1 Synthesis and characterisation of aptamer-capped nanoparticles.

For the synthesis of apMUC1-gated nanodevices, we used MSNs and loaded them with different cargos (*vide infra* and [Table S1](#)). After the loading process, the nanoparticles were functionalised with (3-aminopropyl)triethoxysilane (APTES). This gave nanoparticles externally functionalised with amino groups. Amino groups are partially protonated at neutral pH and are known to give strong electrostatic and hydrogen bonding interactions with aptamers such as the MUC1 aptamer (i.e 5-GCA GTT GAT CCT TTG GAT ACC CTG G-3'), which was used to cap the pores. This procedure yielded the nanoparticles **apMUC1-MSNs(RhB)**,

apMUC1- MSNs(Nav), **apMUC1-MSNs(S63845)**, in which the apMUC1-capped MSNs are loaded with the fluorescent rhodamine B dye, navitoclax, and the Mcl-1 inhibitor S63845, respectively. Moreover, apMUC1-capped MSNs were also simultaneously loaded with navitoclax and S63845 using two different molar ratios to give the nanoparticles **apMUC1-MSNs(Nav/S63845, 10:1)** and **MSNs(Nav/S63845, 2:1)**, respectively ([Scheme 1A](#)). For the biocompatibility study, empty MSNs were functionalised with APTES and capped with apMUC1 (**apMUC1- MSNs**). Additionally, control nanoparticles loaded with rhodamine B, functionalised with APTES, and capped with a random aptamer were also synthesized (**apRandom-MSNs(RhB)**). The designed nanodevices are expected to be endocytosed after interaction between the MUC1 aptamer and the overexpressed MUC1 receptor in the membrane of TNBC cells, resulting in nanoparticle internalisation and cargo delivery inside cells. Delivery of navitoclax and the Mcl-1 inhibitor S63845 is expected to neutralize Bcl-2 anti-apoptotic proteins, leading to tumour cell death by apoptosis ([Scheme 1B](#)).



Scheme 1. Illustration of the apMUC1-MSNs(Nav/S63845) nanodevices. A) Scheme of MSNs (1) loaded with navitoclax and the Mcl-1 inhibitor S63845 (2), functionalised with APTES (3) and capped with the MUC1-targeting aptamer (4). **B)** Scheme of the mechanism of action of apMUC1-MSNs(Nav/S63845). After the interaction of the MUC1-targeting aptamer with the MUC1 surface protein (1), MSNs endocytosis takes place (2) and nanoparticles reach the lysosome (3). Drugs are released from the nanoparticles and they reach their target proteins in the mitochondria (4): i.e., navitoclax targets Bcl-2, Bcl-w, and

Bcl-xL, and S63845 targets Mcl-1. The inhibition of Bcl-2 anti-apoptotic set of proteins triggers apoptosis by Bax/Bak oligomerization in the mitochondria membrane.

The prepared nanoparticles were characterised using powder X-ray diffraction (PXRD), N₂ adsorption-desorption isotherms, Fourier-transform infrared spectroscopy (FTIR), transmission electron microscopy (TEM), transmission electron microscopy coupled with energy-dispersive X-ray spectroscopy (TEM-EDX) and ζ potential. The PXRD pattern of calcined MSNs is typical for mesoporous silica materials with low-angle peaks characteristic of a hexagonal-ordered pore array. The preservation of the (100) reflection demonstrated that loading and functionalisation processes with APTES did not damage the mesoporous structure in the nanoparticles (see for instance the PXRD pattern of **APTES-MSNs(RhB)** in [Figure S1A](#)). The FTIR spectrum of **APTES-MSNs(RhB)** showed symmetric and asymmetric stretching N-H and C-H bands from APTES within the 3100-2840 cm⁻¹ range, whereas nanoparticle capped with the MUC1 aptamer, additionally, showed vibrations of the nucleobases (C=O, C=N, C=C, and C-C bonds) in the 1750-1550 cm⁻¹ range ([Figure S1B](#)).^[28,29] The N₂ adsorption-desorption isotherms of the starting MSNs ([Figure S1C](#)) showed the typical type IV isotherm with a specific surface area of 1088 m²g⁻¹, by applying the Brunauer–Emmett–Teller (BET) model, and a pore volume and pore diameter of 0.732 cm³g⁻¹ and 3.31 nm, respectively, by using the density functional theory (DFT) method on the adsorption branch of the isotherm. In contrast, N₂ adsorption-desorption isotherm of **APTES-MSNs(RhB)** was typical of mesoporous systems with partially filled mesoporous, with a reduced specific surface area (203 m²g⁻¹) and pore volume (0.125 cm³g⁻¹). We also monitored the different steps of the preparation of the final nanocarriers by hydrodynamic diameter using dynamic light scattering (DLS) and ζ potential ([Table S2](#)). The hydrodynamic diameter increased after each preparation step. The starting calcined nanoparticles presented a hydrodynamic diameter of 173 ± 1.3 nm. The

functionalisation of the drug-loaded nanoparticles with APTES increased the hydrodynamic size (to ca. 200 nm) and the subsequent capping with apMUC1 yield nanoparticles with a hydrodynamic diameter of ca. 500 nm. We also monitored the different steps of the preparation of the final nanocarriers by ζ potential. In this respect, calcined MCM-41 nanoparticles presented a ζ potential of -27 ± 2 mV (due to the presence of silanolate moieties onto its external surface) which changed to positive values after loading and functionalisation with APTES (due to the ionisable amino groups). After capping with the MUC1 aptamer, ζ potential shifted back to negative, indicating the successful incorporation of the DNA into the final nanodevices (Table S2).

TEM images of the starting MSNs showed spherical nanoparticles (average size of ca. 100 nm) and the presence of alternated black and white stripes, typical of mesoporous systems (Figure S2A). The same morphology and similar size were observed for the intermediate (APTES-functionalised nanoparticles) (Figure S2B) and the final apMUC1-capped solids (Figure S2C), confirming the preservation of the mesoporous structure during the functionalisation process. Furthermore, TEM-EDX mapping studies were also performed. As an example, Figure 1A shows TEM-EDX images of **apMUC1-MSNs(Nav/S63845, 10:1)**, that clearly demonstrated the presence of Si and O (from the silica scaffold), F and S (from the cargoes), N (from APTES and apMUC1) and P (from apMUC1), which indicates the correct loading with the drugs (i.e., navitoclax and S63845), the presence of APTES and the capping apMUC1 aptamer.

Moreover, drug loading and the aminopropyl and apMUC1 contents in the nanoparticles were determined by thermogravimetric studies, elemental analyses, and ^1H MNR upon forced cargo delivery in ethanol. The amount of navitoclax and S63845 in **apMUC1-MSNs(Nav)** and **apMUC1-MSNs(S63845)** was quantified as

97.5 $\mu\text{mol g}^{-1}$ and 102.0 $\mu\text{mol g}^{-1}$, respectively. Using a similar procedure, the amount of drugs in **apMUC1-MSNs(Nav/S63845, 10:1)** was determined as 106.9 $\mu\text{mol g}^{-1}$ of navitoclax and 11.9 $\mu\text{mol g}^{-1}$ of S63845, and in **apMUC1-MSNs(Nav/S63845, 2:1)** as 60.3 $\mu\text{mol g}^{-1}$ of navitoclax and 31.9 $\mu\text{mol g}^{-1}$ of S63845 per mg of MSNs, which is consistent with the navitoclax/S63845 ratio used when loading the nanoparticles. The APTES and apMUC1 content were determined as ca. 2588,1 $\mu\text{mol g}^{-1}$ and apMUC1 ca. 7.96 $\mu\text{mol g}^{-1}$, respectively. The specific values for each solid are gathered in [Table S3](#).

3.3.2 Cargo controlled release and biocompatibility studies.

To study the gating capacity of the MUC1 aptamer, we performed studies of rhodamine B delivery from **apMUC1-MSNs(RhB)** in the presence of a deoxyribonuclease I (DNase I). Uncapping, due to hydrolysis of the capping apMUC1 aptamer by DNase I, and subsequent payload delivery from **apMUC1-MSNs(RhB)** was monitored by following the fluorescence emission of rhodamine B at 572 nm ($\lambda_{\text{exc}}=555\text{ nm}$) in the solution at scheduled times ([Figure 1B](#)). There was low cargo release from **apMUC1-MSNs(RhB)** in the absence of DNase I (less than 20% of the total delivery observed after 60 min), which demonstrates the correct blockage of the pores. However, a marked cargo release was detected in the presence of DNase I. Hence, apMUC1 efficiently prevents premature delivery of the cargo from the capped nanoparticles.

To study the biocompatibility of the apMUC1-capped MSNs, the TNBC cell line MDA-MB-231, and the corresponding navitoclax resistant cell line, MDA-MB-231-R (*vide infra*), were incubated with different concentrations of **apMUC1-MSNs** (0-200

$\mu\text{g/mL}$) for 72 h. Cell viability was kept around 80%, even at concentrations up to 200 $\mu\text{g/mL}$ (Figure 1C). These results demonstrated that MUC1-gated MSNs are not toxic in TNBC cell lines.^[26,27]

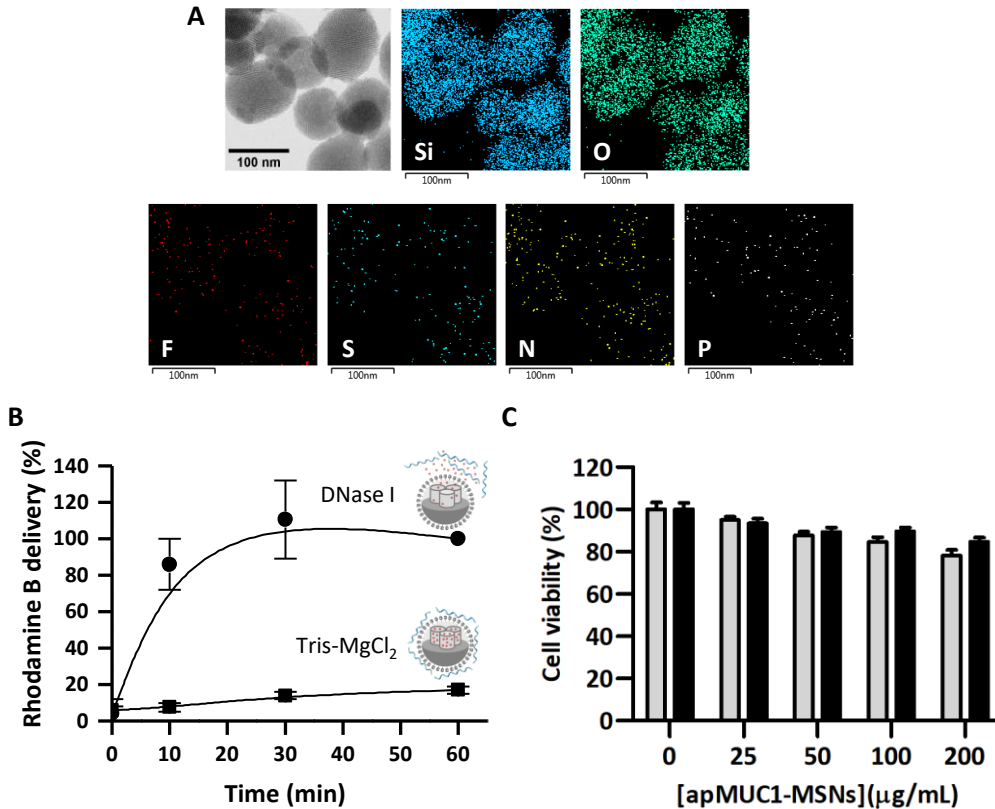


Figure 1. Characterisation and biocompatibility of apMUC1-MSNs. **A)** TEM-EDX map for apMUC1-MSNs(Nav/S63845, 10:1) showing the presence of Si and O (from the silica scaffold), F and S (from the cargoes), N (from APTES and apMUC1), and P (from apMUC1). **B)** Release profile of rhodamine B from apMUC1-MSNs(RhB) in the absence (bottom) and presence (top) of DNase I. **C)** Cytotoxicity profile of apMUC1-MSNs in MDA-MB-231 (grey bars) and MDA-MB-231-R (black bars). Cell viability study by WST-1 at 72 h in presence of different nanoparticle dosages. Data represent means \pm SEM (n = 3).

3.3.3 Targeted cellular uptake studies.

As previously stated, the nanoparticles are capped with an aptamer designed to target the MUC1 surface protein, which has been reported to be overexpressed in breast cancer cell lines.^[30,31] To carry out targeting studies, we first created a TNBC cell line model resistant to navitoclax (MDA-MB-231-R) by treating MDA-MB-231 cells with a constant concentration of navitoclax for two months. Then, we demonstrated that MUC1 expression is found in both MDA-MB-231 and MDA-MB-231-R cell lines (Figure 2A). In a second step, the targeting ability of **apMUC1-MSNs(RhB)** was studied via cell internalisation studies of this solid and nanoparticles capped with a random aptamer (**apRandom-MSNs(RhB)**) in MDA-MB-231 and MDA-MB-231-R cells by flow cytometry and confocal microscopy. Both cell lines showed a clear increase of RhB fluorescence signal inside the cells over time when treated with **apMUC1-MSNs(RhB)**, whereas a remarkable weaker fluorescence intensity was observed in cells when treated with **apRandom-MSNs(RhB)** (Figure 2B).

The role played by the apMUC1 aptamer in the preferential internalisation of **apMUC1-MSNs(RhB)** was also assessed by confocal microscopy. A larger emission signal of rhodamine B was detected in cells treated with **apMUC1-MSNs(RhB)** when compared with those incubated with **apRandom-MSNs(RhB)** (Figure 2C). These results demonstrate the targeting ability of **apMUC1-MSNs(RhB)** to TNBC cell lines, as a consequence of the selective interaction between the capping apMUC1 aptamer and the MUC1 receptor in the cell membrane.

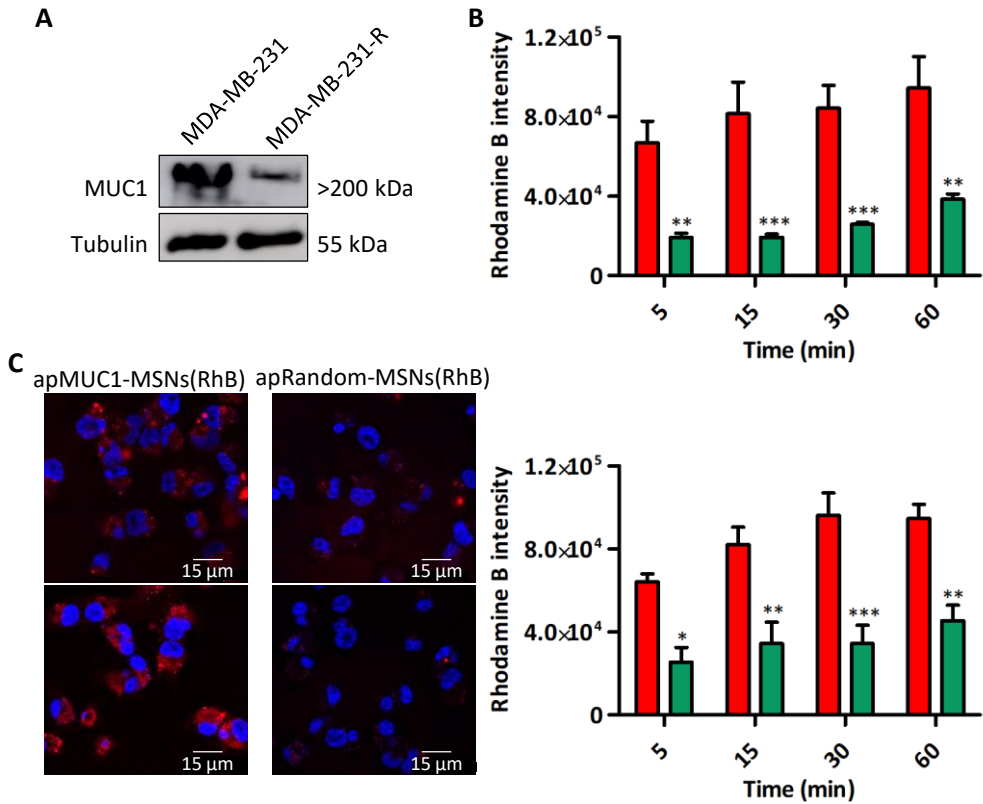


Figure 2. Specific targeting of apMUC1-MSNs(RhB) to TNBC cell lines. **A)** Western blot analysis of MUC1 expression in MDA-MB-231 and MDA-MB-231-R. **B)** Fluorescence intensity kinetic of MDA-MB-231 cells (top graph) and MDA-MB-231-R (bottom graph) analysed by flow cytometry after treatment with **apMUC1-MSNs(RhB)** (red bars) or **apRandom-MSNs(RhB)** (green bars). Data represent the means \pm SEM of at least three independent experiments. Statistical significance was determined by one-way ANOVA and Bonferroni post-test (* $p < 0.05$, ** $p < 0.025$, *** $p < 0.001$). **C)** Confocal images of nanoparticles uptake by MDA-MB-231 (top panel) and MDA-MB-231-R (bottom panel) in presence of **apMUC1-MSNs(RhB)** (left) or **apRandom-MSNs(RhB)** (right) after 3 h of treatment with the nanoparticles.

3.3.4 Navitoclax resistance overcoming in TNBC cells.

As stated above we aimed to develop nanoparticles able to overcome navitoclax resistance in TNBC cells by using apMUC1-capped nanoparticles loaded with both navitoclax and the highly selective Mcl-1 inhibitor S63845. To carry out this study we created, as stated above, a TNBC cell line model resistant to navitoclax (MDA-MB-231-R) by treating MDA-MB-231 cells with navitoclax for two months. Protein characterisation confirmed that treatment with navitoclax produced Mcl-1 overexpression in MDA-MB-231-R (Figure 3A). Resistance to navitoclax was confirmed in dose-response assays, which demonstrated that navitoclax IC₅₀ increased from 2 µM in MDA-MB-231 to 17 µM in MDA-MB-231-R (Figure 3B). Then, MDA-MB-231 cells were treated with **apMUC1-MSNs**, **apMUC1-MSNs(S63845)**, **apMUC1-MSNs(Nav)**, **apMUC1-MSNs(Nav/S63845, 10:1)** and **apMUC1-MSNs(Nav/S63845, 2:1)** (25 µg/mL) and cell viability was determined by WST-1 assay (Figure 4A, left). A statistically significant cell viability reduction was observed in MDA-MB-231 cell line for all the nanoparticles containing navitoclax (i.e., **apMUC1-MSNs(Nav)**, **apMUC1-MSNs(Nav/S63845, 10:1)** and **apMUC1-MSNs(Nav/S63845, 2:1)**), as the MDA-MB-231 cell line is sensitive to navitoclax. In contrast, the treatment of the navitoclax-resistant MDA-MB-231-R cell line with **apMUC1-MSNs(Nav)** resulted in no change in viability (Figure 4A, right) compared with the control (untreated cells). Viability of the cell line MDA-MB-231-R was neither affected upon treatment with the nanoparticles only containing the Mcl-1 inhibitor S63845 (i.e., **apMUC1-MSNs(S63845)**). As a clear contrast, a remarkable cell viability reduction to 30%, when compared with the untreated control (see also Figure 4A, right), was found for MDA-MB-231-R cells treated with the nanocarriers loaded with both navitoclax and S63845 drugs (i.e., **apMUC1-MSNs(Nav/S63845, 10:1)** and **apMUC1-MSNs(Nav/S63845, 2:1)**). The

results obtained clearly indicate that apMUC1-gated nanocarriers can be used not only for TNBC cell apoptosis induction by releasing BH3 mimetic drugs (i.e., navitoclax), but also for killing navitoclax-resistant TNBC cells when navitoclax is combined in the same nanoparticle with the Mcl-1 inhibitor S63845. This result, together with the targeting ability of the nanoparticles to the membrane protein MUC1 overexpressed in TNBC cells (*vide ante*), makes these nanodevices functional potential candidates to treat TNBC.

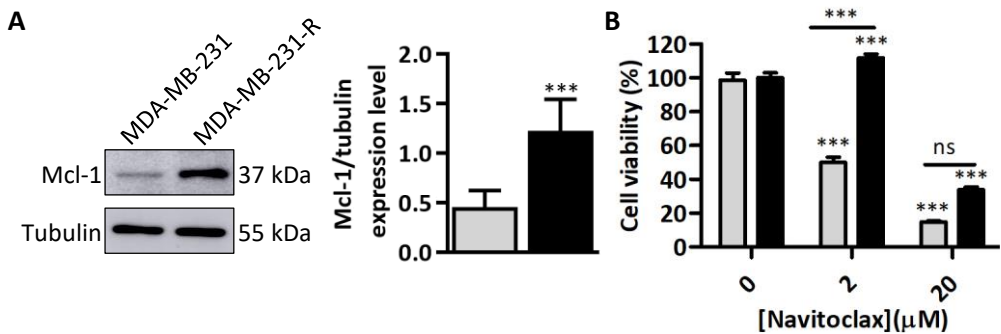


Figure 3. Characterisation of Mcl-1 expression and navitoclax dose-response analysis in TNBC cell lines. A) Western blot assay and Mcl-1 expression level quantification in MDA- MB-231 (grey bar) and MDA- MB-231-R (black bar). Data represent means \pm SEM (n = 6). Statistical significance was determined by the t Student test (***) p < 0.001. **B)** Navitoclax cytotoxicity evaluation in MDA-MB-231 (grey bars) and MDA-MB-231-R (black bars). Data represent means \pm SEM (n=3). Statistical significance was determined by one-way ANOVA and Tukey post-test (***) p < 0.001).

3.3.5 Platelets protection assay.

Preclinical and clinical studies have shown that navitoclax exhibits a therapeutic effect against different malignancies. Nevertheless, thrombocytopenia is the major adverse effect of this drug and the main reason why navitoclax clinical use has not been approved.^[32–34] Severe thrombocytopenia in preclinical animal

models and patients is caused by Bcl-xL inhibition in platelets, which dramatically reduces platelet lifespan.^[32,33,35,36] In order to study platelet protection from thrombocytopenia due to navitoclax encapsulation, human complete blood cell extract was treated with **apMUC1-MSNs(Nav)** and the free drug at equivalent doses. Also, blood samples were treated with **apMUC1-MSNs** as a non-toxicity control. As expected, **apMUC1-MSNs** scaffold did not induce apoptosis in platelets (**Figure S3**). Moreover, we found that navitoclax encapsulation in **apMUC1-MSNs(Nav)** protected platelets from apoptosis since annexin V levels were significantly lower when platelets were treated with the encapsulated drug, in comparison to the free drug (**Figure 4B**). These results demonstrate that MSNs navitoclax encapsulation protects platelets from apoptosis induced by Bcl-xL inhibition. This suggests that the encapsulation of navitoclax can be a suitable potential strategy to widen the therapeutic window of navitoclax and other drugs, whose clinical applications have been limited because of secondary effects.^[37-40]

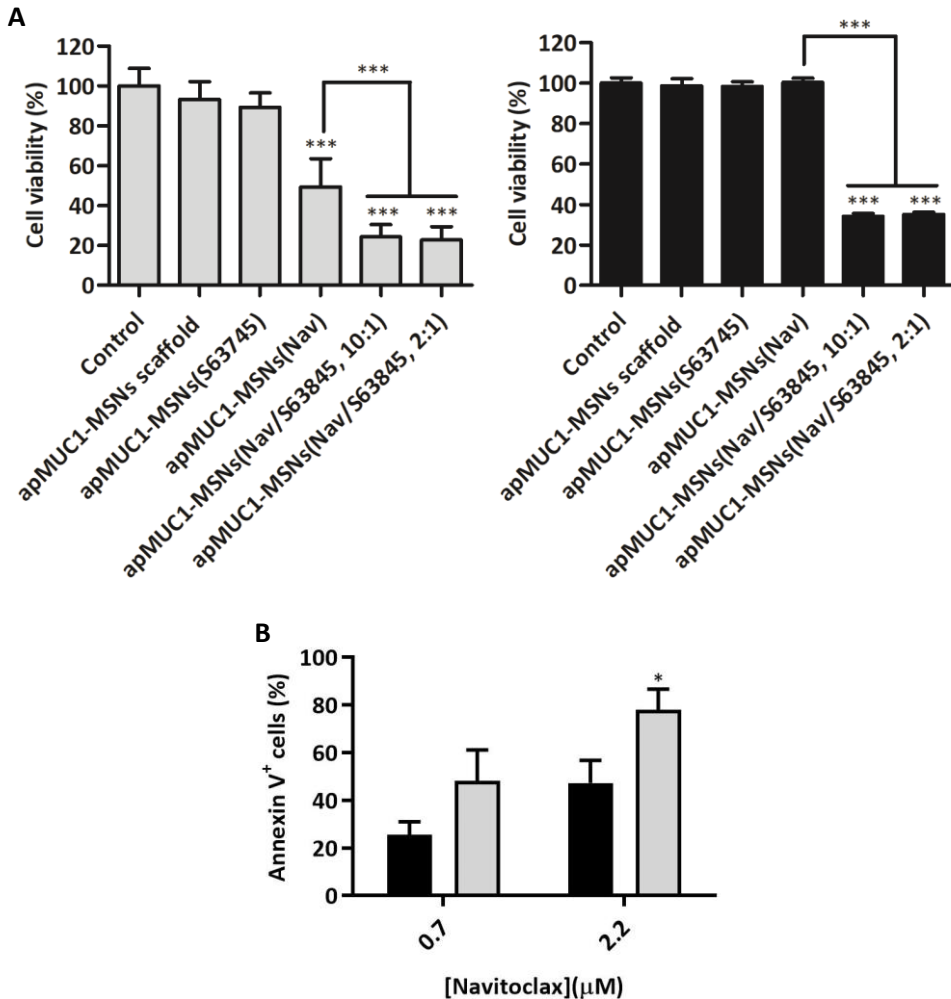


Figure 4. The therapeutic effect of apMUC1-MSNs(Nav/S63845) in TNBC cell lines and thrombocytopenia reduction in human platelets. A) Cell viability analysis by WST-1 assay in MDA-MB-231 (left) and MDA-MB-231-R (right) incubated with apMUC1-gated MSNs at 25 $\mu\text{g}/\text{ml}$ for 72 h. Data represent means \pm SEM (n=3). Statistical significance was determined by one-way ANOVA and Tukey post-test (* $p < 0.05$, *** $p < 0.001$). **B)** Thrombocytopenia induced by navitoclax in platelets. Human blood complete extract was treated with free navitoclax (grey bar) and encapsulated navitoclax in apMUC1-MSNs(Nav) (black bar). Platelet apoptosis was measured by annexin V assay assessed by flow cytometry (n = 4). Statistical significance was determined by two-way ANOVA (* $p < 0.05$).

3.4 Conclusions.

In summary, we report herein a multifunctional nanodevice capable of overcoming navitoclax resistance in TNBC by the co-delivery of navitoclax and the Mcl-1 inhibitor S63845. Nanoparticles consist of MSNs loaded with navitoclax, S63845, or a combination of both drugs, functionalised with APTES and capped with the apMUC1-targeting aptamer. Nanoparticles loaded with rhodamine B are also prepared. The nanodevice loaded with rhodamine (i.e., **apMUC1-MSNs(RhB)**) remains capped in a buffer solution, yet the payload is delivered on-command upon apMUC1 hydrolysis by DNase I. Flow cytometry and confocal microscopy studies carried out in TNBC cells revealed that nanoparticles **apMUC1-MSNs(RhB)** are preferentially internalised in TNBC cells when compared with nanoparticles capped with a random aptamer. Furthermore, the nanoparticles loaded with both drugs (i.e., **apMUC1-MSNs(Nav/S63845)**) can overcome navitoclax resistance in TNBC cell lines, which overexpress Mcl-1 anti-apoptotic protein as a resistance mechanism. Besides, navitoclax encapsulation in MSNs demonstrates to effectively protect platelets from apoptosis. This promising result suggested that the encapsulation of navitoclax can widen its clinical application, whose usage has been limited because of the induction of thrombocytopenia in patients. Moreover, we demonstrate that targeted-delivery of navitoclax and S63845 using apMUC1-gated mesoporous silica nanoparticles is an attractive strategy for specific drug release in TNBC cells by taking the advantage of the active targeting of the engineered MSNs, while increasing the treatment efficacy and reducing drug side effects. These results point MSNs as versatile platforms for the simultaneous controlled delivery of multiple chemotherapeutic agents as a synergistic treatment to overcome drug resistance in tumours, which still is an uncover need within the biomedical field.^{[40-}

43]

3.5 Experimental section.

3.5.1 Synthesis of the mesoporous silica nanodevices.

In a typical synthesis procedure,^[44] CTAB (1.00 g, 2.74 mmol) was dissolved in 480 mL of deionized water before adding a solution of NaOH (3.5 mL, 2.00 M). The temperature was adjusted at 80 °C and then TEOS (5.00 mL, $2.57 \cdot 10^{-2}$ mol) was added dropwise to the surfactant solution. The final solution was stirred for 2 h to give a white precipitate. The solid was isolated by centrifugation-washing cycles of 20 min at 9,500 rpm in deionized water until pH 7 was reached. The material was dried at 60 °C and the final solid was calcined (Mufla Furnace) at 550 °C in an oxidant atmosphere to remove the template phase, obtaining the mesoporous scaffold (MSNs).

3.5.2 Synthesis of APTES-MSNs(RhB).

The pores of the calcined MSNs were loaded with rhodamine B. For this purpose, MSNs (300 mg) were suspended in an acetonitrile solution containing rhodamine B (57.5 mg, 0.4 mmol/g solid) and stirred for 48 h. Then, an excess of (3- aminopropyl) triethoxysilane (APTES, 0.59 μ L, 2.5 mmol) was added to the mixture and stirred for 5.5 h at room temperature. Finally, the solid was isolated by centrifugation and dried at 37 °C to yield a pink solid.

3.5.3 Synthesis of apMUC1-MSNs(RhB).

The MUC1-targeting aptamer (apMUC1) (5'-GCA GTT GAT CCT TTG GAT ACC CTG G-3') was electrostatically adsorbed onto the external surface of **APTES- MSNs(RhB)**. In this respect, **APTES-MSNs(RhB)** (1 mg) were suspended in PBS and mixed with apMUC1 (150 μ L, 100 μ M). The mixture was stirred at 37 °C for

30 min and then nanoparticles were centrifuged and washed with PBS to get the final solid **apMUC1-MSNs(RhB)**. **APTES-MSNs(RhB)** were also coated with a MUC1 non-targeting aptamer (apRandom) (5'-AAG CAC TTT CAG TGG GGA GGA GGG TTG ATA GGT TAA GAG-3'), that was employed as a negative control in the targeting study, obtaining the nanoparticles referred to as **apRandom-MSNs(RhB)**.

3.5.4 Synthesis of drug-loaded apMUC1-gated MSNs.

We aimed to achieve navitoclax resistance overcoming in a TNBC cell model using navitoclax and the Mcl-1 inhibitor S63845 combination of drugs encapsulated in MSNs. For this purpose, calcined MSNs (20 mg) were mixed with 15 mg (0.015 mmol) of navitoclax (**apMUC1-MSNs(Nav)**) and 13 mg (0.015 mmol) of S63845 (**apMUC1-MSNs(S63845)**), obtaining single drug-loaded nanoparticles as non-toxicity controls in the navitoclax resistant cell line. In addition, MSNs were mixed with a combination of navitoclax and the Mcl-1 inhibitor S63845: 20 mg of MSNs were mixed with 14 mg (0.015 mmol) of navitoclax plus 1.2 mg S63845 (0.0015 mmol) of S63845 to obtain **apMUC1-MSNs(Nav/S63845, 10:1)**, and also with 10.3 mg (0.015 mmol) of navitoclax plus 4.4 mg (0.005 mmol) of S63845 to obtain **apMUC1-MSNs(Nav/S63845, 2:1)**. Mixtures were suspended in dichloromethane and stirred for 48 h at room temperature in an argon atmosphere to achieve maximum loading in the pores of the MCM-41 scaffolding. Afterward, 39 μ L (0.16 mmol) of APTES were added to the solution and the suspension was stirred for 5.5 h. Then, solids were isolated by vacuum filtration and dried overnight under vacuum flux. Finally, the MUC1-targeting aptamer (apMUC1) (5'-GCA GTT GAT CCT TTG GAT ACC CTG G-3') was electrostatically adsorbed onto the external surface of **APTES-MSNs(RhB)**. To do that, **APTES-MSNs** (2 mg) were suspended in PBS and mixed with apMUC1 (300 μ L, 100 μ M). The mixture was stirred at 37 °C for 30 min and then nanoparticles were centrifuged and washed with PBS, giving the

set of nanoparticles used to overcome navitoclax resistance in TNBC cells (Table S1).

3.5.5 Standard characterisation procedures of the prepared materials.

Powder X-ray diffraction (PXRD), transmission electron microscopy (TEM), TEM-EDX, N₂ adsorption-desorption isotherms, Fourier-transform infrared spectroscopy (FTIR), and nuclear magnetic resonance (NMR) were employed for materials characterisation. PDRX measurements were taken on Seifert 3000TT diffractometer using CuK α radiation. TEM images were acquired under Philips CM-10 that worked at 100 kV. TEM-EDX imaging was carried out using a JEOL JEM-2100 LaB6 electron microscope working at 200 kV accelerating voltage and equipped with an Oxford Instruments INCA x-sight (Si(Li) detector) and a Zeiss SESAM microscope (200 kV) equipped with an energy dispersive X-ray (EDX) spectroscopy system from ThermoFisher. The N₂ adsorption-desorption isotherms were recorded in a Micromeritics TriStar II Plus automated analyser. FTIR measurements were taken by Bruker Tensor 27 spectrometer. ¹H and ¹³C NMR spectra were recorded on a Bruker FT-NMR Avance 400 (Ettlingen, Germany) spectrometer at 300 K, using TMS as an internal standard. ζ potential was determined from the particle mobility values by applying the Smoluchwski model in a Malvern Zetasizer ZS instrument. The DLS studies to determine particle size were also conducted at in a Malvern Zetasizer Nano ZS instrument. ζ potential and DLS studies were conducted at 25 °C and in triplicate. Fluorescence measured was recorded by a JASCO FP-8500 spectrophotometer. Cell viability measurements were taken in a Wallac 1420 workstation. Confocal microscopy imaging was performed with a Leica TCS SP8 HyVolution II (Leica Microsystems Heidelberg GmbH) inverted laser scanning confocal microscope. Confocal image analysis was carried out with ImageJ software. Flow cytometry experiments were performed with a CytoFLEX S

cytometer equipped with 4 lasers and 13 fluorescence detectors (Beckman-Coulter, USA) and data analysis with CytExpert Software.

3.5.6 Cargo delivery studies.

To check the proper working of the capping aptamer, **apMUC1-MSNs(RhB)** were suspended in buffer solution (20 mM Tris-HCl, 37.5 mM MgCl₂, pH 7.5) or buffer solution plus DNase I (1 mg/mL). In a typical experiment, 1 mg of **apMUC1-MSNs(RhB)** was suspended in 1 mL of buffer solution or 1 mL of buffer solution containing DNase I and stirred at 37 °C for 60 min. At certain times aliquots were taken and centrifuged to remove the solid. Rhodamine B delivery was determined by measuring its fluorescence at 572 nm ($\lambda_{\text{ex}} = 555 \text{ nm}$).

3.5.7 Cell culture conditions.

Triple-negative breast cancer cells (MDA-MB-231) were purchased from ATCC and grown in Dulbecco's Modified Eagle Medium (DMEM)-high glucose supplemented with 10% foetal bovine serum (FBS). Cells were incubated at 37 °C in a 5% CO₂ atmosphere and 95% air. For navitoclax resistance induction, MDA-MB-231 cells were incubated with navitoclax for two months in 100mm cell culture dishes. DMEM medium containing navitoclax was weekly replaced. Finally, MDA-MB-231 resistant to navitoclax (MDA-MB-231-R) were obtained.

3.5.8 Protein expression characterisation by western blot.

Mcl-1 and MUC1 expression in the TNBC cell lines were studied by western blot. For this purpose, MDA-MB-231 and MDA-MB-231-R cell lines were grown to confluence. For Mcl-1 expression characterisation whole-cell extracts were obtained by scraping the cell monolayer using buffer lysis composed of 25 mM

Tris- HCl, pH 7.4, 1 mM EDTA, 1 mM EGTA, and 1% SDS, plus protease and phosphatase inhibitors. Lysates were resolved by western blot (12% SDS-PAGE). For MUC1 expression characterisation, cells were trypsinised and washed with PBS. Then cells were incubated with RIPA buffer, composed by 10 mM Tris-HCl (pH 8.0), 1 mM EDTA, 1% Triton X-100, 0.1% sodium deoxycholate, 0.1% SDS, 140 mM NaCl and 1 mM PMSF, for 30 min at 4°C under shaking. Lysates were separated by western blot (6% SDS-PAGE). After the western blot gel run, proteins were electrophoretically transferred to nitrocellulose membranes and blocked with non- fat milk 5%. Then, membranes were washed with 0.1% Tween/TBS and incubated overnight with primary antibodies: anti-Mcl-1 (#4572, Cell Signalling) and anti-MUC1 (VU4H5) (#4538, Cell Signalling). α -tubulin was used as reference control: anti-tubulin (ab6160, Abcam). Membranes were washed and incubated with horseradish peroxidase-conjugated secondary antibodies for chemiluminescence detection in Amersham Imager 600 equipment.

3.5.9 Cytotoxicity cell studies with apMUC1-MSNs.

The biocompatibility of **apMUC1-MSNs** was studied in MDA-MB-231 and MDA- MB-231-R cell lines. The cytotoxic effect was evaluated by WST-1 assay. TNBC cell lines were seed on 96-well plates at 10,000 cells/well one day before treatment. Then, cells were treated with different concentrations of **apMUC1-MSNs** (0, 25, 50, 100, and 200 $\mu\text{g}/\text{mL}$) for 72 h. After that incubation time with the nanoparticles, WST-1 was added to each well, and absorbance was measured at 450 nm at Wallac 1420 workstation.

3.5.10 Navitoclax resistance overcoming TNBC cells.

The proper navitoclax sensitizing activity of the nanoparticles was evaluated in MDA-MB-231-R cells. TNBC cells were seeded on 96-well plates at 10,000 cells/well and incubated with **apMUC1-MSNs(Nav)**, **apMUC1-MSNs(S63845)**, **apMUC1-MSNs(Nav/S63845, 10:1)** and **apMUC1-MSNs(Nav/S63845, 2:1)** at 25 µg/mL for 72 h. MDA-MB-231 cell line was also treated with the set of the prepared nanoparticles at the same conditions. Cell viability was assessed by WST-1 assay; 10 µL/well of WST-1 were added and incubated for an hour. Then absorbance was measured at 450 nm.

3.5.11 Targeted cellular uptake studies.

The targeting properties of the prepared nanodevices were studied in MDA-MB-231 and MDA-MB-231-R cell lines. For this aim, MSNs loaded with rhodamine B and capped with a non-targeting MUC1 random aptamer (**apRandom-MSNs(RhB)**) were prepared as a control to follow the selective targeting of **apMUC1-MSNs(RhB)**. Firstly, cellular uptake was studied by flow cytometry in TNBC cells. For this purpose, MDA-MB-231 and MDA-MB-231-R cells were seeded on 6-well plates at 300,000 cells/well one day before treatment. Cells were incubated with **apMUC1-MSNs(RhB)** and **apRandom-MSNs(RhB)** at 25 µg/mL for 30 min and washed with PBS to remove the non-internalised nanoparticles. Finally, the cells were incubated for a total time of 1 h in the presence of the nanodevices. Then, the cells were trypsinized and collected for rhodamine B quantification by flow cytometry. The single-cell fluorescence measurements were performed in CytoFLEX S (Beckman-Coulter, USA) equipped with 4 lasers and 13 fluorescence detectors and analysed in the CytoFLEX software. Additionally, nanoparticle internalisation was followed by confocal microscopy. The cells were

seeded on glass coverslips in 6-well plates at 800,000 cells/well and incubated 24 h at 37 °C. Cells were treated with **apMUC1-MSNs(RhB)** and **apRandom-MSNs(RhB)** (25 µg/mL) for 30 min. Then cells were washed with PBS and fresh media was added until complete 3 h of incubation with the nanoparticles. Finally, cell nuclei were stained with Hoechst 33342 (2 µg/mL) and fluorescence intensity was monitored through a Leica TCS SP8 confocal microscope.

3.5.12 Platelets protection assay.

Navitoclax's main side effect is the induction of thrombocytopenia in patients when treated in clinical phases. To demonstrate that navitoclax encapsulation in the nanodevices protects platelets against apoptosis, human complete blood extract was incubated with **apMUC1-MSNs(Nav)** and with equivalent dosages of the free navitoclax for 4 h. **apMUC1-MSNs** was added, with equivalent dosages of **apMUC1-MSNs(Nav)**, to discard the toxicity of the MSNs scaffold. Platelets were stained with the pan-platelet antibody CD41/phycoerythrin (#MHCD4104, Invitrogen) and apoptosis level was determined by annexin V/FITC labelling (ANXVF- 200T, Immunostep). Platelet apoptosis was determined in a CytoFLEX S flow cytometer (Beckman-Coulter, USA).

ACKNOWLEDGMENTS. Gema Vivo-Llorca thanks the Generalitat Valenciana for her fellowship ACIF/2017/072. Vicente Candela-Noguera thanks the Spanish Government for his fellowship FPU15/02753. We would like to thank Servier for the workart used in the figures of this manuscript (Servier Medical Art <https://smart.servier.com/>). We thank the Spanish Government (project RTI2018-100910-B-C41 (MCUI/AEI/FEDER, UE); SAF2017-84689-R-B (MCUI/AEI/FEDER, UE)) and the Generalitat Valenciana (project PROMETEO/2018/024 and PROMETEO/2019/065) for support.

3.6 References.




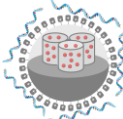

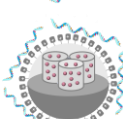


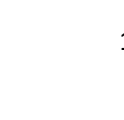
- [1] F. Bray, J. Ferlay, I. Soerjomataram, R. L. Siegel, L. A. Torre, A. Jemal, *CA Cancer J. Clin.* **2018**, *68*, 394–424.
- [2] Globocan, *Glob. Scan 2018* **2018**, *947*, 2018.
- [3] G. Turashvili, E. D. Lightbody, K. Tyryshkin, S. K. SenGupta, B. E. Elliott, Y. Madarnas, A. Ghaffari, A. Day, C. J. B. Nicol, *FASEB J. Off. Publ. Fed. Am. Soc. Exp. Biol.* **2018**, fj201800120R.
- [4] J. Collignon, L. Lousberg, H. Schroeder, G. Jerusalem, *Breast cancer (Dove Med. Press.* **2016**, *8*, 93–107.
- [5] X. Dai, T. Li, Z. Bai, Y. Yang, X. Liu, J. Zhan, B. Shi, *Am. J. Cancer Res.* **2015**, *5*, 2929–2943.
- [6] H. A. Wahba, H. A. El-Hadaad, *Cancer Biol. Med.* **2015**, *12*, 106–116.
- [7] H. Li, L. Liu, H. Chang, Z. Zou, D. Xing, *Cell Death Dis.* **2018**, *9*, 137.
- [8] X. Dai, L. Xiang, T. Li, Z. Bai, *J. Cancer* **2016**, *7*, 1281–1294.
- [9] J. T. Opferman, *FEBS J.* **2016**, *283*, 2661–2675.
- [10] H. Kalkavan, D. R. Green, *Cell Death Differ.* **2018**, *25*, 46–55.
- [11] M. C. Wei, W. X. Zong, E. H. Cheng, T. Lindsten, V. Panoutsakopoulou, A. J. Ross, K. A. Roth, G. R. MacGregor, C. B. Thompson, S. J. Korsmeyer, *Science* **2001**, *292*, 727–730.
- [12] B. Wang, Z. Ni, X. Dai, L. Qin, X. Li, L. Xu, J. Lian, F. He, *Mol. Cancer* **2014**, *13*, 98.
- [13] J. Belmar, S. W. Fesik, *Pharmacol. Ther.* **2015**, *145*, 76–84.
- [14] National Cancer Institute, *Clinical Trials Using Navitoclax*, **n.d.**
- [15] A. Kaefer, J. Yang, P. Noertersheuser, S. Mensing, R. Humerickhouse, W. Awni, H. Xiong, *Cancer Chemother. Pharmacol.* **2014**, *74*, 593–602.
- [16] K. Louault, T. L. Bonneaud, C. Séveno, P. Gomez-Bougie, F. Nguyen, F. Gautier, N. Bourgeois, D. Lousouarn, O. Kerdraon, S. Barillé-Nion, E. Al, P. Jézéquel, M. Campone, M. Amiot, P. P. Juin, F. Souazé, *Oncogene* **2019**, *38*, 3261–3273.
- [17] K. J. Campbell, S. Dhayade, N. Ferrari, A. H. Sims, E. Johnson, S. M. Mason, A. Dickson, K. M. Ryan, G. Kalna, J. Edwards, S. G. W. Tait, K. Blyth, *Cell Death Dis.* **2018**, *9*, DOI 10.1038/s41419-017-0035-2.
- [18] A. Kotschy, Z. Szlavik, J. Murray, J. Davidson, A. L. Maragno, G. Le Toumelin-Braizat, M. Chanrion, G. L. Kelly, J.-N. Gong, D. M. Moujalled, A. Bruno, M. Csekei, A. Paczal, Z. B. Szabo, S. Sipos, G. Radics, A. Proszenyak, B. Balint, L. Ondi, G. Blasko, A. Robertson, A. Surgenor, P. Dokurno, I. Chen, N. Matassova, J. Smith, C. Pedder, C. Graham, A. Studeny, G. Lysiak-Auvity, A.-M. Girard, F. Gravé, D. Segal, C. D. Riffkin, G. Pomilio, L. C. A. Galbraith, B. J. Aubrey, M. S. Brennan, M. J. Herold, C. Chang, G. Guasconi, N. Cauquil, F.

- Melchiorre, N. Guigal-Stephan, B. Lockhart, F. Colland, J. A. Hickman, A. W. Roberts, D. C. S. Huang, A. H. Wei, A. Strasser, G. Lessene, O. Geneste, *Nature* **2016**, *538*, 477–482.
- [19] D. Merino, J. R. Whittle, F. Vaillant, A. Serrano, J. N. Gong, G. Giner, A. L. Maragno, M. Chanrion, E. Schneider, B. Pal, X. Li, G. Dewson, J. Gräsel, K. Liu, N. Lalaoui, D. Segal, M. J. Herold, D. C. S. Huang, G. K. Smyth, O. Geneste, G. Lessene, J. E. Visvader, G. J. Lindeman, *Sci. Transl. Med.* **2017**, *9*, eaam7049.
- [20] Z. Li, S. He, A. T. Look, *Leukemia* **2019**, *33*, 262–266.
- [21] W. Alshaer, H. Hillaireau, J. Vergnaud, S. Mura, C. Deloménie, F. Sauvage, S. Ismail, E. Fattal, *J. Control. Release* **2018**, *271*, 98–106.
- [22] X. Xie, F. Li, H. Zhang, Y. Lu, S. Lian, H. Lin, Y. Gao, L. Jia, *Eur. J. Pharm. Sci.* **2016**, *83*, 28–35.
- [23] Y. Shen, M. Li, T. Liu, J. Liu, Y. Xie, J. Zhang, S. Xu, H. Liu, *Int. J. Nanomedicine* **2019**, *14*, 4029–4044.
- [24] Y. Yang, W. Zhao, W. Tan, Z. Lai, D. Fang, L. Jiang, C. Zuo, N. Yang, Y. Lai, *Nanoscale Res. Lett.* **2019**, *14*, 390.
- [25] M. S. Nabavinia, A. Gholoobi, F. Charbgoon, M. Nabavinia, M. Ramezani, K. Abnous, *Med. Res. Rev.* **2017**, *37*, 1518–1539.
- [26] M. Y. Hanafi-Bojd, S. A. Moosavian Kalat, S. M. Taghdisi, L. Ansari, K. Abnous, B. Malaekheh-Nikouei, *Drug Dev. Ind. Pharm.* **2018**, *44*, 13–18.
- [27] L. Pascual, C. Cerqueira-Coutinho, A. García-Fernández, B. de Luis, E. S. Bernardes, M. S. Albernaz, S. Missailidis, R. Martínez-Máñez, R. Santos-Oliveira, M. Orzaez, F. Sancenón, *Nanomedicine Nanotechnology, Biol. Med.* **2017**, *13*, 2495–2505.
- [28] J. G. Kelly, P. L. Martin-Hirsch, F. L. Martin, *Anal. Chem.* **2009**, *81*, 5314–5319.
- [29] M. Banyay, M. Sarkar, A. Gräslund, *Biophys. Chem.* **2003**, *104*, 477–488.
- [30] R. Wang, L. Yang, S. Li, D. Ye, L. Yang, Q. Liu, Z. Zhao, Q. Cai, J. Tan, X. Li, *Med. Sci. Monit.* **2018**, *24*, 412–420.
- [31] M. D. Walsh, S. M. Luckie, M. C. Cummings, T. M. Antalis, M. A. McGuckin, *Breast Cancer Res. Treat.* **1999**, *58*, 255–266.
- [32] W. H. Wilson, O. A. O. Connor, M. S. Czuczman, S. Lacasce, J. F. Gerecitano, J. P. Leonard, A. Tulpule, K. Dunleavy, H. Xiong, D. Ph, Y. Chiu, D. Ph, Y. Cui, D. Ph, S. H. Enschede, R. A. Humerickhouse, *Lancet Oncol.* **2010**, *11*, 1149–1159.
- [33] L. Gandhi, D. R. Camidge, M. R. De Oliveira, P. Bonomi, D. Gandara, D. Khaira, C. L. Hann, E. M. McKeegan, E. Litvinovich, P. M. Hemken, C. Dive, S. H. Enschede, C. Nolan, Y. L. Chiu, T. Busman, H. Xiong, A. P. Krivoshik, R. Humerickhouse, G. I. Shapiro, C. M. Rudin, *J. Clin. Oncol.* **2011**, *29*, 909–916.
- [34] C. Tse, A. R. Shoemaker, J. Adickes, M. G. Anderson, J. Chen, S. Jin, E. F. Johnson, K. C. Marsh, M. J. Mitten, P. Nimmer, L. Roberts, S. K. Tahir, Y. Xiao,

- X. Yang, H. Zhang, S. Fesik, S. H. Rosenberg, S. W. Elmore, *Cancer Res.* **2008**, *68*, 3421–3428.
- [35] M. A. Debrincat, I. Pleines, M. Lebois, R. M. Lane, M. L. Holmes, J. Corbin, C. J. Vandenberg, W. S. Alexander, A. P. Ng, A. Strasser, *Cell Death Dis.* **2015**, *6*, 1–8.
- [36] S. M. Schoenwaelder, K. E. Jarman, E. E. Gardiner, M. Hua, J. Qiao, M. J. White, E. C. Josefsson, I. Alwis, A. Ono, A. Willcox, R. K. Andrews, K. D. Mason, H. H. Salem, D. C. S. Huang, B. T. Kile, A. W. Roberts, S. P. Jackson, *Blood* **2011**, *118*, 1663–1674.
- [37] D. Muñoz-Espín, M. Rovira, I. Galiana, C. Giménez, B. Lozano-Torres, M. Paez-Ribes, S. Llanos, S. Chaib, M. Muñoz-Martín, A. C. Uceró, G. Garaulet, F. Mulero, S. G. Dann, T. VanArsdale, D. J. Shields, A. Bernardos, J. R. Murguía, R. Martínez-Máñez, M. Serrano, *EMBO Mol. Med.* **2018**, *10*.
- [38] L. Zhang, Y. Chen, Z. Li, L. Li, P. Saint-Cricq, C. Li, J. Lin, C. Wang, Z. Su, J. I. Zink, *Angew. Chemie - Int. Ed.* **2016**, *55*, 2118–2121.
- [39] D. Schmid, G. E. Jarvis, F. Fay, D. M. Small, M. K. Greene, J. Majkut, S. Spence, K. M. McLaughlin, K. D. McCloskey, P. G. Johnston, A. Kissenpfennig, D. B. Longley, C. J. Scott, *Cell Death Dis.* **2014**, *5*, e1454.
- [40] M. Janicka, J. Gubernator, *Expert Opin. Drug Deliv.* **2017**, *14*, 1059–1075.
- [41] K. H. Chun, J. H. Park, S. Fan, *Predicting and Overcoming Chemotherapeutic Resistance in Breast Cancer*, **2017**.
- [42] X. Wang, H. Zhang, X. Chen, *Cancer Drug Resist.* **2019**, *2*, 141–160.
- [43] P. T. Yin, T. Pongkulapa, H. Y. Cho, J. Han, N. J. Pasquale, H. Rabie, J. H. Kim, J. W. Choi, K. B. Lee, *ACS Appl. Mater. Interfaces* **2018**, *10*, 26954–26963.
- [44] Q. Cai, Z. S. Luo, W. Q. Pang, Y. W. Fan, X. H. Chen, F. Z. Cui, *Chem. Mater.* **2001**, *13*, 258–263.

3.7 Supporting information.

Table S1. Nanoparticles nomenclature and composition.

Nanoparticle nomenclature	Gate	Cargo	Support	Scheme
MSNs			MSNs	
APTES- MSNs			MSNs	
apMUC1-MSNs	apMUC1		MSNs	
apMUC1-MSNs(RhB)	apMUC1	RhB	MSNs	
apRandom-MSNs(RhB)	apRandom	RhB	MSNs	
apMUC1-MSNs(Nav)	apMUC1	Navitoclax	MSNs	
apMUC1-MSNs(S63845)	apMUC1	S63845	MSNs	
apMUC1-MSNs(Nav/S63845, 10:1)	apMUC1	Navitoclax/ S63845	MSNs	
apMUC1-MSNs(Nav/S63845, 2:1)	apMUC1	Navitoclax/ S63845	MSNs	

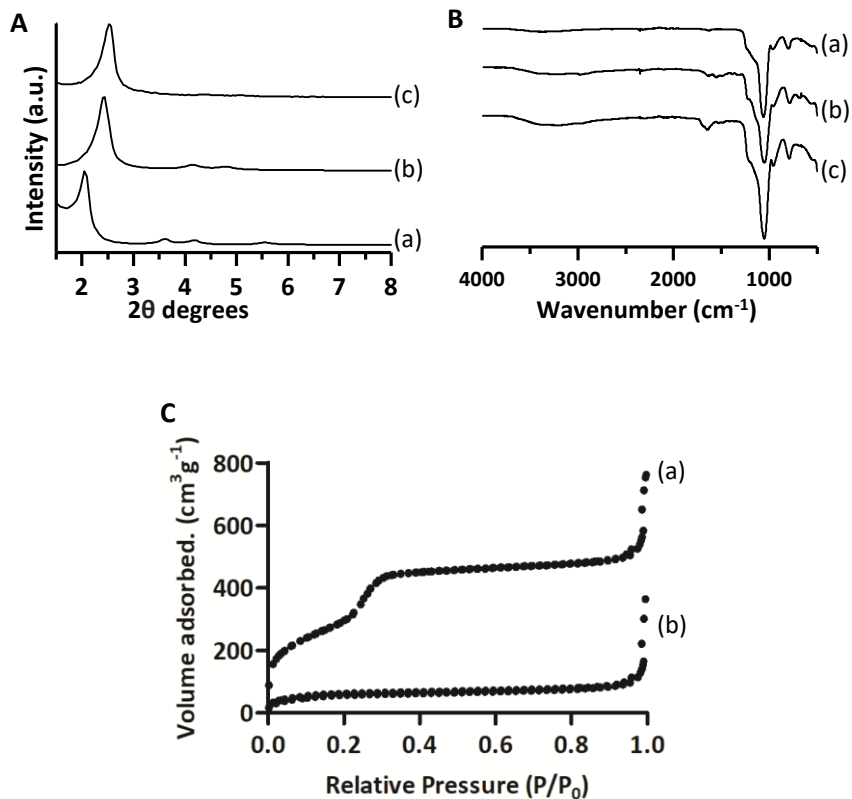


Figure S1. apMUC1-MSNs standard characterisation. A) Powder X-ray diffraction patterns of (a) MSNs as made, (b) calcined MSNs and (c) **APTES-MSNs(RhB)**. The characteristic (100) diffraction peak was observed indicating the preservation of mesoporous structure after the functionalisation processes. **B)** FTIR spectra of (a) MSNs, (b) **APTES-MSNs** and (c) **apMUC1-MSNs**. **C)** N₂ adsorption-desorption isotherms for (a) calcined MSNs and (b) **APTES-MSNs(RhB)**.

Table S2. Hydrodynamic size and ζ potential of the nanoparticles at different synthesis steps.

Nanoparticle	Cargo	Hydrodynamic size (nm) \pm SD	ζ potential (mV) \pm SD
Calcined MSNs		173.0 \pm 1.3	-27.30 \pm 1.5
APTES-MSNs	Empty	197.4 \pm 2.2	22.10 \pm 1.4
	Navitoclax	205.9 \pm 0.4	25.5 \pm 1.3
	S63845	230.1 \pm 11.2	36.00 \pm 0.6
	Navitoclax/S63845 (2:1)	196.5 \pm 2.7	33.6 \pm 1.0
	Navitoclax/S63845 (10:1)	223.2 \pm 8.9	36.4 \pm 1.9
apMUC1-MSNs	Empty	574.0 \pm 14.6	-17.50 \pm 0.2
	Navitoclax	481.7 \pm 13.8	-9.77 \pm 1.2
	S63845	577.2 \pm 19.8	-15.9 \pm 1.1
	Navitoclax/S63845 (10:1)	447.1 \pm 11.6	10.3 \pm 1.0
	Navitoclax/S63845 (2:1)	576.8 \pm 19.3	-15.6 \pm 0.3

Table S3. Content of drugs, APTES, and molecular gate apMUC1 in the different synthesized nanoparticles. Data represent the mean of the data measured by thermogravimetric studies, elemental analyses, and ^1H MNR.

Nanoparticle	Navitoclax	S63845	APTES	apMUC1
	($\mu\text{mol g}^{-1}$ solid)	($\mu\text{mol g}^{-1}$ solid)	($\mu\text{mol g}^{-1}$ solid)	($\mu\text{mol g}^{-1}$ solid)
apMUC1-MSNs	--	--	2722.7 \pm 84.1	8.7 \pm 0.7
apMUC1-MSNs(Nav)	97.5 \pm 7.2	--	2261,9 \pm 111.2	9.1 \pm 1.1
apMUC1-MSNs(S63845)	--	102.0 \pm 48.0	2768.0 \pm 142.1	6.1 \pm 1.9
apMUC1- MSNs(Nav/s63845,10:1)	106.9 \pm 11.9	11.9 \pm 2.8	2879.9 \pm 146.8	4.9 \pm 3.1
apMUC1- MSNs(Nav/S63845,2:1)	60.3 \pm 8.0	31.9 \pm 3.7	2307.7 \pm 156.0	11.0 \pm 3.0

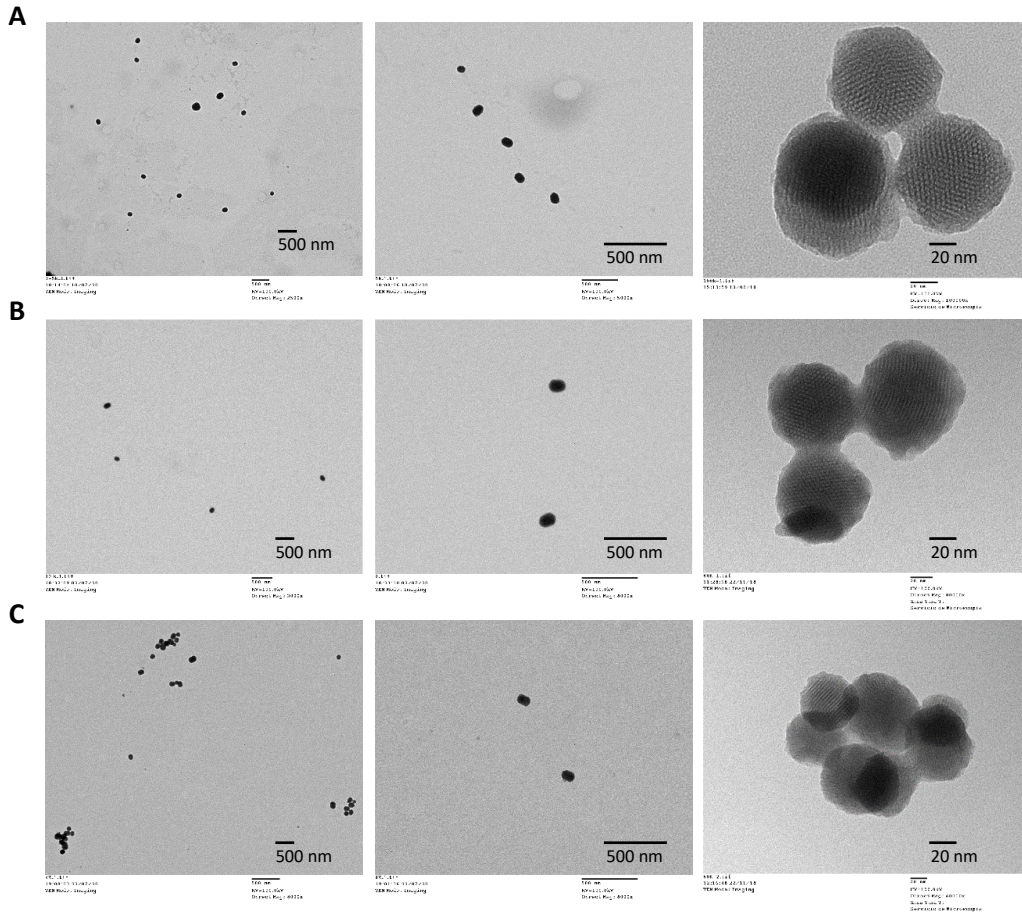


Figure S2. Representative TEM images of apMUC1-MSNs at different synthesis steps. A) calcined MSNs, B) APTES-MSNs and C) apMUC1-MSNs.

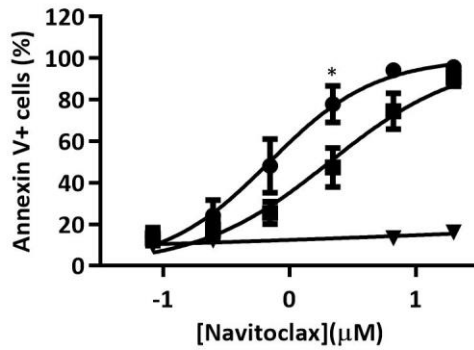


Figure S3. apMUC1-MSNs(Nav) for platelets protection against apoptosis. Navitoclax dose-response curve in platelets. Human blood complete extract was treated with free navitoclax (●), encapsulated navitoclax in apMUC1-MSNs(Nav) (■) and apMUC1-MSNs (▼). Platelet apoptosis was measured by annexin V assay assessed by flow cytometry (n = 4). Statistically significance was determined by two-way ANOVA (* p < 0.05).

**Chapter 4 | CRISPR/Cas9 machinery and
model drug co-delivery as one-shot
treatment strategy**

Nanodevices for the efficient co-delivery of CRISPR/Cas9 editing machinery and an entrapped cargo

Alba García-Fernández,^{[a],[c],[d]} Gema Vivo-Llorca,^{[a],[b],[d]} Mónica Sancho,^{[d],[e]}
Alicia García Jareño,^{[d],[e]} José Ramón Murguía,^{[a],[c],[d]} Ramón Martínez-
Máñez,^{[a],[b],[c],[d]}* Mar Orzáez^{[d],[e]}* and Félix Sancenón^{[a],[b],[c],[d]}

[a] Instituto Interuniversitario de Investigación de Reconocimiento Molecular y Desarrollo Tecnológico (IDM), Universitat Politècnica de València, Universitat de València. Spain.

[b] Departamento de Química, Universitat Politècnica de València, Camí de Vera s/n, 46022, València, Spain.

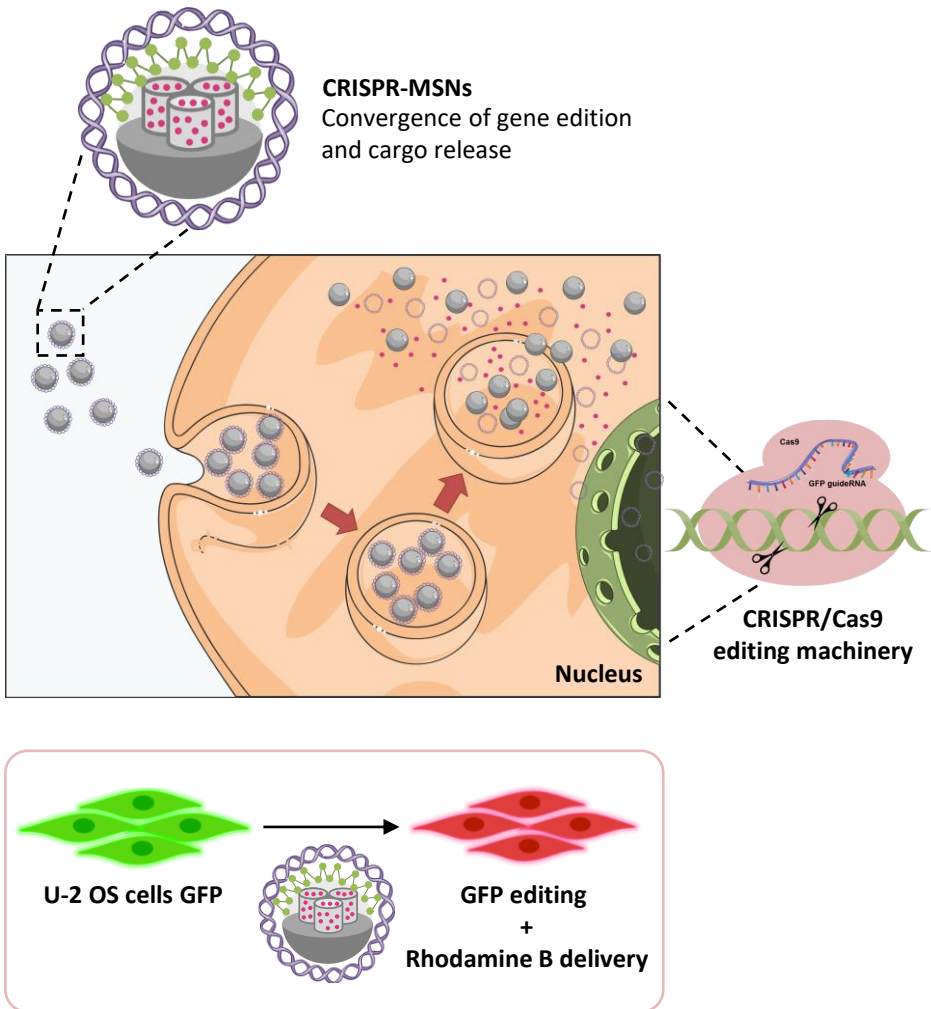
[c] CIBER de Bioingeniería, Biomateriales y Nanomedicina (CIBER-BBN) Spain.

[d] Unidad Mixta UPV-CIPF de Investigación en Mecanismos de Enfermedades y Nanomedicina, València, Universitat Politècnica de València, Centro de Investigación Príncipe Felipe, València, Spain.

[e] Centro de Investigación Príncipe Felipe, Laboratorio de Péptidos y Proteínas, Carrer d'Eduardo Primo Yúfera, 3, 46012 València, Spain.

Submitted

▪ **Graphical abstract.**



4.1 Abstract.

The emergence of CRISPR genome editing technology is opening the way to a new era in the treatment of genetic diseases. Regarding the safety limitations of viral delivery systems, recent research has focused on developing new non-viral vectors for effective and safe CRISPR release. In this work, we report a pioneering nanodevice capable of simultaneously delivering CRISPR/Cas9 gene-editing machinery and releasing an entrapped cargo. The nanodevice displays an enhanced endosomal escape promoted by protonated PEI groups. The system is based on MSNs loaded with rhodamine B (as a model drug), functionalised with PEI and finally capped with the CRISPR Cas9 vector (to edit the GFP gene). The gene-editing potential of nanoparticles is verified by knocking down the gene expression of the green fluorescent protein by ca. 45% in U-2 OS-GFP cells. The co-delivery of rhodamine B as a result of pore opening is also verified. Taken together, our results show the potential of preparing advanced nanodevices for disease treatment by co-delivering drugs and gene editing machinery for possible applications, such as restoring sensitivity in drug-resistant malignancies and simultaneously delivering the drug.

4.2 Introduction.

The genomic era has evidenced that many diseases are caused by genetic defects that can be theoretically repaired. However, only recently has the genetic engineering field advanced enough to provide efficient genomic repairing technology. The discovery in bacteria and archaea of rudimentary immune systems formed by RNA-directed DNA endonucleases, such as Cas9, encoded in clustered regularly interspaced short palindromic repeats (CRISPR) recently led to the development of the CRISPR/Cas9 technology, which represents a major advance in

the genetic engineering field.^[1-4] This genome-editing system is formed by two main components; the non-specific CRISPR-associated endonuclease (Cas9) and guide RNA (gRNA). gRNA directs the Cas9 endonuclease to produce targeted double-stranded breaks in chromosomes that can be repaired by either non-homologous end joining or by homologous recombination.^[5] Despite the huge potential of the CRISPR technology in basic research and potential therapeutics for genome regulation, the efficient delivery of CRISPR/Cas9 systems to cells remains challenging.^[6,7]

Both physical methods and viral vectors have been adopted in the delivery of the Cas9-based gene-editing platform. However, viral vectors are generally concerned with safety issues due, for instance, to immunogenicity complications or limited loading capacities; whereas most physical methods (e.g., electroporation, microinjection, osmocytosis, mechanical cell deformation, and hydrodynamic injection) are applicable only for *in vitro* delivery and their use in *in vivo* protocols is difficult.^[8-10] These limitations have empowered the need to study CRISPR/Cas9 delivery using nanoparticles.^[11,12] Lipid nanoparticles,^[13] ribonucleoprotein nanoparticles,^[14,15] DNA nanoclews,^[16] polymeric nanoparticles,^[17,18] gold nanoparticles,^[19,20] and metal-organic frameworks^[21] have been successfully used to deliver the Cas9-based gene-editing system.

From another point of view, MSNs can be excellent potential nanoplatforms to deliver CRISPR/Cas9 gene-editing machinery and an entrapped payload at the same time.^[22-24] Accordingly, here we report one of the very first examples in the literature of a MSNs capable of simultaneously delivering the CRISPR/Cas9 technology and an entrapped cargo.^[25] To accomplish this aim, we prepare pH-responsive MSNs loaded with RhB (as a model drug), capped with PEI and a CRISPR/Cas9 plasmid targeting the GFP coding gene (as a model reporter gene).

4.3 Results and Discussion.

4.3.1 Assembly and characterisation of CRISPR-MSNs.

MSNs were prepared using CTAB as a template and TEOS as a hydrolytic inorganic precursor. Calcination of the mesostructured phase resulted in the starting porous scaffold. The pores of nanoparticles were loaded with RhB (as a model drug cargo) and then capped with a polyethyleneimine (PEI) layer (**PEI- RhB- MSNs**) via electrostatic interactions between the negatively charged external surface of nanoparticles and the positively charged PEI polymer. The PEI cationic polymeric layer was used as both (i) a suitable positive layer to attach the negatively charged CRISPR/Cas9 vector and (ii) to enable nanoparticles for endosomal escape, needed for enhanced plasmid delivery to the cytosol. Finally, the CRISPR/Cas9 vector (editing the GFP38 gene position) was adsorbed onto **PEI- RhB-MSNs** to give final nanoparticles ^{GFP38}**CRISPR-RhB-MSNs** (Figure 1). The CRISPR/Cas9 vector included both single guide RNA (sgRNA) and endonuclease Cas9 in one autonomously replicable plasmid (Figure S1).

The prepared nanoparticles were characterised using powder X-ray diffraction (PXRD), N₂ adsorption-desorption isotherms, Fourier-transform infrared spectroscopy (FTIR), transmission electron microscopy (TEM), dynamic light scattering (DLS), ζ potential, and elemental analyses. In the powder X-ray patterns of MSNs as made, calcined MSNs, and PEI-MSNs, the characteristic (100) diffraction peak was observed. This indicates the preservation of the mesoporous structure after the functionalisation processes (Figure S2A). The FTIR spectrum of **PEI- RhB- MSNs** showed the symmetric and asymmetric stretching bands of amine moieties from PEI within the 3100-2900 cm⁻¹ range, which indicates the PEI-coating of nanoparticles (Figure S2B). The N₂ adsorption-desorption curve of MSNs

corresponded to a type IV isotherm, which is typical of mesoporous materials, whereas the curve for **PEI-RhB-MSNs** was typical of mesoporous silica-filled pores (Figure S2C). Moreover, a remarkable reduction in the specific surface and pore volume, compared with MSNs, was observed (Figures S2D).

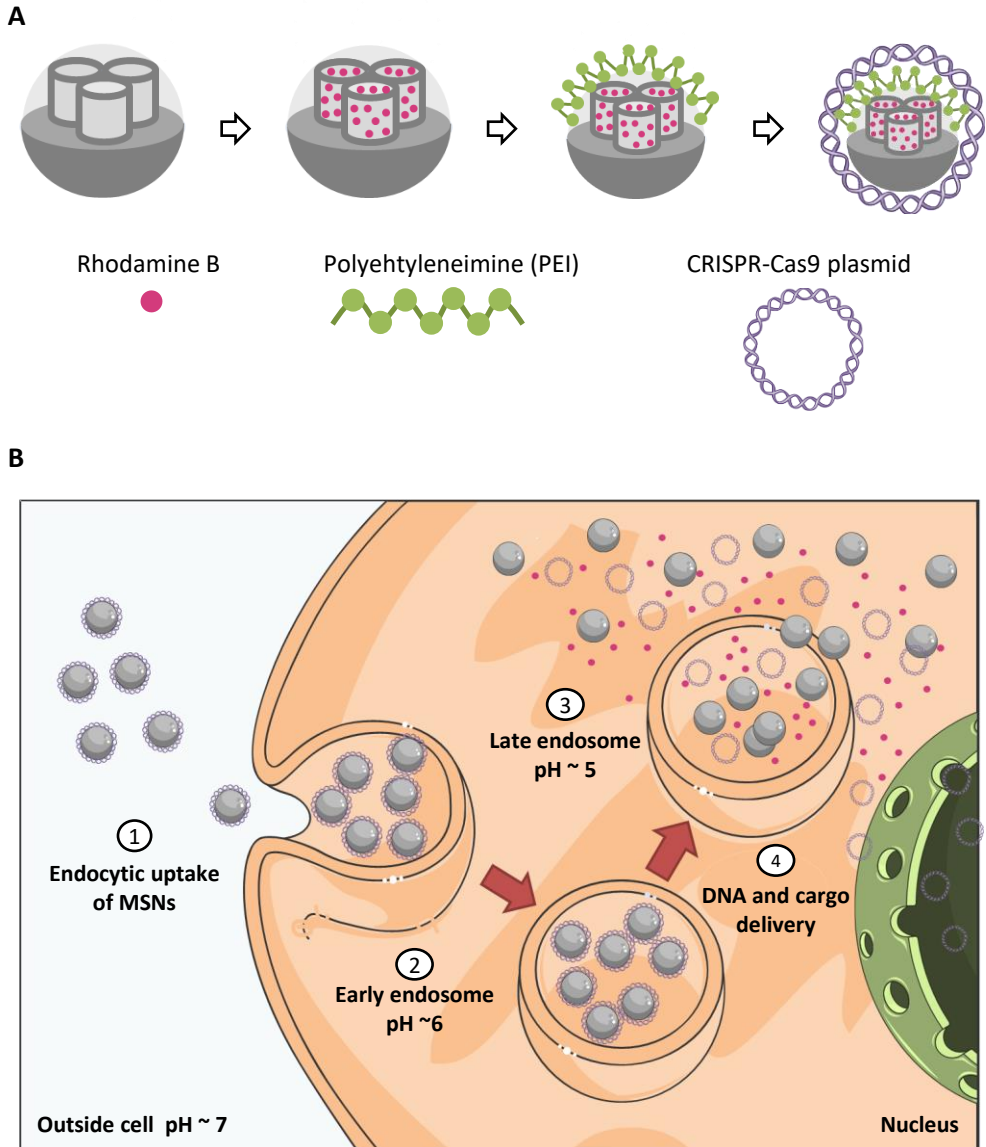


Figure 1. Scheme of CRISPR-RhB-MSNs. **A)** Scheme of mesoporous silica nanoparticles (MSNs) loaded with rhodamine B (RhB), functionalised with polyethyleneimine (PEI) polymer, and capped with the CRISPR/Cas9 plasmid. **B)** Scheme of CRISPR and dye cell delivery by **CRISPR-RhB-MSNs**. Figure 1B was produced using a template from the Server Medical Art platform.

Taking into account thermogravimetric and elemental analyses, the organic content of **GFP38-CRISPR- RhB-MSNs** was determined and came to 0.04 g/g SiO₂ of RhB, 0.2 g/g SiO₂ of PEI, and 25 µg/mg SiO₂ of plasmid (**Figure S2E**). The TEM images of calcined MSNs and **PEI-RhB-MSNs** showed mesoporous spherical nanoparticles whose average size was ca. 100 nm, which is suitable for intracellular delivery (**Figure 2A**).

After characterizing the starting material, different DNA/**PEI-RhB-MSNs** (w/w) ratios were tested to assess the nucleic acid binding capacity of the nanoparticle. For this purpose, the CRISPR/Cas9-free plasmid was incubated with **PEI-RhB-MSNs** and the obtained nanoparticles were subjected to an electrophoretic mobility shift assay. An optimal 1:25 DNA/PEI-RhB-MSNs ratio was established to obtain the final nanodevice (**Figure 2B**). The average size of the prepared nanoparticles was also studied by DLS. The hydrodynamic diameters increased from 91 ± 9 to 122 ± 16 and 145 ± 21 nm for calcined MSNs, **PEI-RhB-MSNs**, and **GFP38-CRISPR-RhB-MSNs**, respectively (**Figure 2C**). The ζ potential measurements showed that the negatively charged calcined MSNs -24 ± 1 mV became positively charged upon RhB loading and addition of PEI $+7.48 \pm 0.5$ mV. Moreover, plasmid adsorption turned back the ζ potential to negative values -11.53 ± 2 mV, which indicates the incorporation of the vector into the final **GFP38-CRISPR-RhB-MSNs** nanodevice (**Figure 2D**).

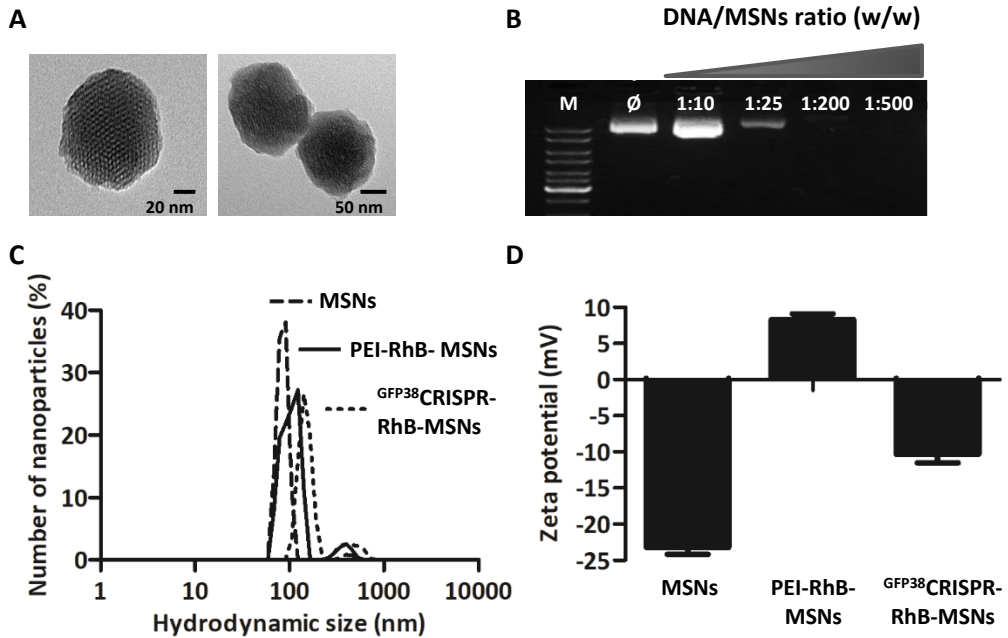


Figure 2. Characterisation of CRISPR-MSNs. **A)** The TEM images of calcined MSNs (left) and PEI- RhB- MSNs (right). **B)** Gel shift mobility assay of GFP^{38} CRISPR-RhB-MSN generated at different DNA/PEI-MSNs ratios. M: MW marker and ϕ : naked DNA plasmid (GFP^{38} CRISPR/Cas9-free plasmid) as control. **C)** Hydrodynamic size of MSNs, PEI- MSNs, and GFP^{38} CRISPR-RhB-MSNs. **D)** ζ potential of MSNs, PEI-RhB-MSNs, and GFP^{38} CRISPR-RhB- MSNs.

4.3.2 Controlled release, biocompatibility, and internalisation studies.

The pH-responsive cargo release from GFP^{38} CRISPR-RhB-MSNs was tested in simulated plasma at pH 7 or by mimicking endosomal conditions at pH 5.0. Uncapping and subsequent delivery were determined by the fluorescence emission measurement at 585 nm ($\lambda_{ex} = 525$ nm) of RhB released at the scheduled times (Figure 3A). At pH 7, cargo delivery was poor and only around 10% of RhB was released after 90 min, whereas a marked cargo delivery was found at an acidic pH 5. Maximum delivery was observed at pH 5 within 1 h. Cargo release was attributed

to the partial protonation of PEI coating, which induced its disassembly with the CRISPR/Cas9 vector and results in pore opening.

The stability of the CRISPR/Cas9 vector in nanoparticles at a physiological pH 7 was also studied. In a typical experiment, **GFP³⁸CRISPR-RhB-MSNs** and free **GFP³⁸CRISPR/Cas9** DNA plasmid were incubated at 37 °C for 10 min with the DNase I enzyme. Then the DNA bound to the nanoparticles was released using heparin and analysed by agarose electrophoresis. As seen in [Figure 3B](#), the **GFP³⁸CRISPR/Cas9**-free plasmid treated with DNase I had completely degraded ([Figure 3B](#), lane 3), whereas the CRISPR/Cas9 vector in nanoparticles was protected from DNase I digestion under conditions in which the free plasmid was unstable ([Figure 3B](#), lane 5). In lane 4 the proper disassembly of the CRISPR/Cas9 vector from MSNs is observed upon heparin addition. The digestion of the DNA disassembled from **GFP³⁸CRISPR-RhB-MSNs** was observed after heparin and DNase I treatment ([Figure 3B](#), lane 6). Therefore, DNA protection on MSNs was confirmed.

The biocompatibility of **GFP³⁸CRISPR-RhB-MSNs** was tested at different concentrations in U-2 OS-GFP cells by the WST-1 assay ([Figure S3A](#)). The results showed that **GFP³⁸CRISPR-RhB-MSNs** were well-tolerated at concentrations of 25 µg/mL after 24 or 48 h of incubation. However, cell viability lowered to 70% when higher concentrations of nanoparticles were used (50 and 100 µg/mL). We also analysed the cellular uptake efficiency of nanoparticles. For this purpose, similar nanoparticles are covalently labelled with RhB and capped with PEI and **GFP³⁸CRISPR- Cas9** (i.e., **GFP³⁸CRISPR-RhB*-MSNs**) were prepared and cellular uptake was assessed by flow cytometry ([Figure S3B](#)). The kinetic studies indicated that in 15 min, 90% of the cellular population incorporated **GFP³⁸CRISPR-RhB*-MSNs**.

To demonstrate the endosomal escape of nanoparticles, U-2 OS cells were treated with ^{GFP38}CRISPR-RhB*-MSNs in the presence of an endosomal marker (Figure 3C, left panel). Fluorescence confocal microscopy analysis showed no overlapping signals between the endosomal marker (green) and nanoparticles (red) after 1 h of transfection (Figure 3C, left panel). The same behaviour was observed when cells were incubated with nanoparticles (red) and a lysosome marker (green)(Figure 3D, right panel), which indicates the effective endosomal escape of nanoparticles. Confocal microscopy analysis of the internalisation of nanoparticles in the presence of the endocytic inhibitor dynasore^[26] showed significantly reduced cellular uptake, which thus confirms endocytosis to be the internalisation mechanism (Figures 3D).

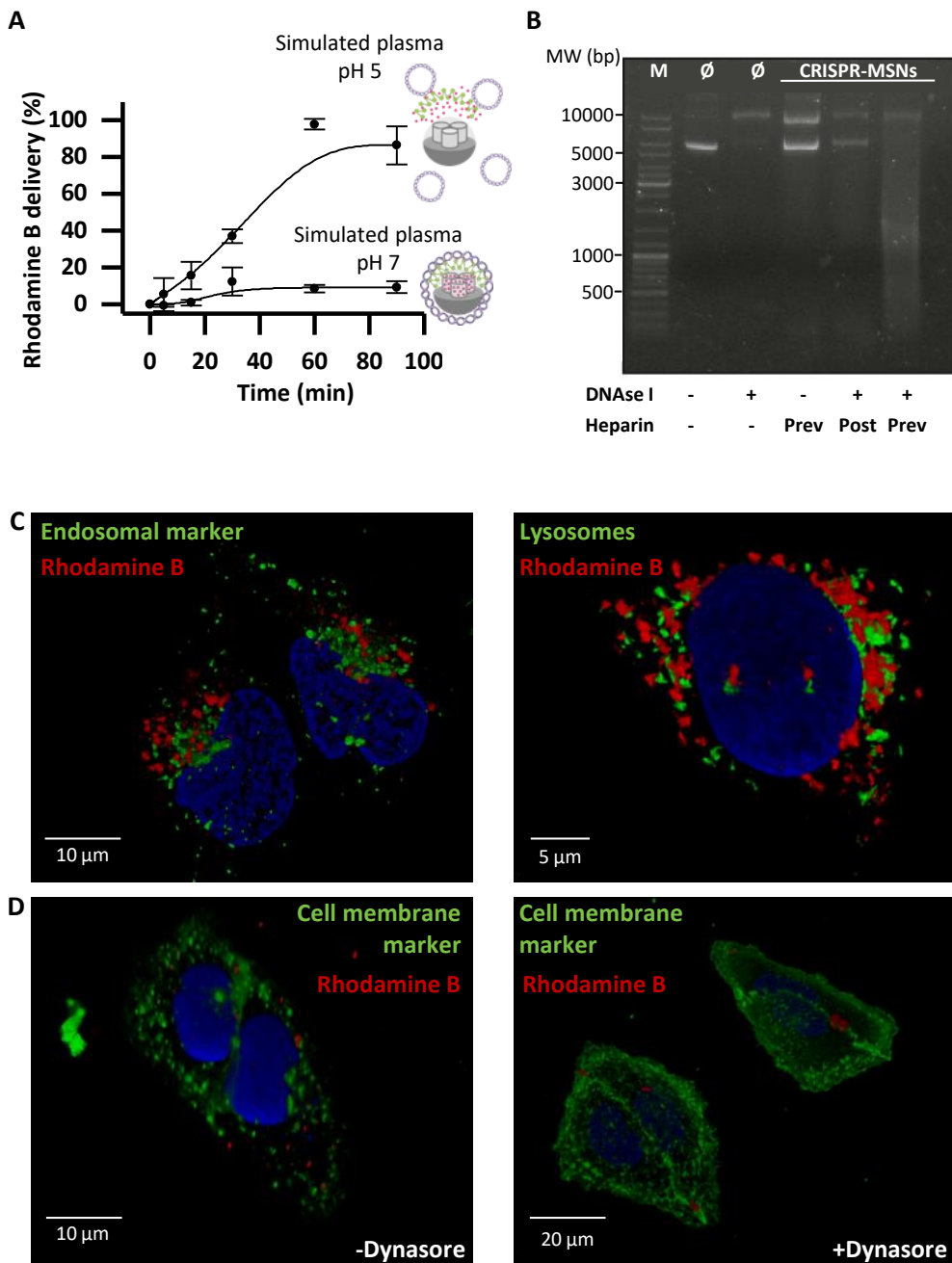


Figure 3. Internalisation and delivery characterisation of CRISPR-MSNs. A) Delivery profile of ^{GFP38}CRISPR-RhB-MSNs in the presence of simulated plasma at pH 7 or 5. **B)** Stability

studies of ^{GFP38}CRISPR-MSN in the presence of DNase I. Lane 1: MW marker (M). Lane 2: the naked ^{GFP38}CRISPR plasmid (ϕ). Lane 3: ^{GFP38}CRISPR treated with DNase I. Lane 4: ^{GFP38}CRISPR- R_hB-MSNs treated with heparin (Prev) to disassemble the MSNs-DNA complex. Lane 5: ^{GFP38}CRISPR-R_hB-MSNs complex treated with DNase I and then with heparin (post). Lane 6: ^{GFP38}CRISPR-R_hB-MSNs previously disassembled with heparin (prev) and finally treated with DNase I. **C**) Cellular internalisation of ^{GFP38}CRISPR-R_hB*-MSNs (red) in U-2 OS cells in the presence of endosomal marker (green) after 30 min of incubation (left panel) and lysosomal marker (green) after 1 h of incubation (right panel). **D**) ^{GFP38}CRISPR- R_hB*- MSNs (red) in the U-2 OS cells treated with cell membrane marker (green) in the absence (left panel) and presence (right panel) of the endocytosis inhibitor dynasore after 1h of incubation.

4.3.3 Gene editing of GFP and cargo delivery cellular studies.

To assess the efficiency of gene editing by nanoparticles, we used sgRNA to target the coding region of green fluorescent protein (GFP) in U-2 OS-GFP cells. GFP gene editing could produce a loss of GFP gene expression and diminished cellular green fluorescence. Studies were first carried out with the nanoparticles that contained the CRISPR/Cas9 gene-editing machinery, but with no cargo (^{GFP38}CRISPR- MSNs) to demonstrate the efficiency of gene knockdown by mesoporous nanoparticles. Confocal microscopy analysis of U-2 OS-GFP cells treated with ^{GFP38}CRISPR-MSNs revealed a remarkable decrease in green fluorescence intensity (Figure 4A and 4B). A decrease of GFP expression was also confirmed by western blot analysis (Figure 4C). Similar nanoparticles containing a random plasmid were also prepared (^{random}CRISPR-MSNs) and tested. No changes in either fluorescence or GFP expression were observed when cells were treated with ^{random}CRISPR-MSNs (Figure 4). Other sgRNAs targeting other GFP gene positions were also cloned, and the corresponding nanoparticles ^{GFP149}CRISPR- MSNs, and ^{GFP178}CRISPR-MSNs were prepared and tested in U-2 OS-

GFP cells. By targeting these other GFP gene positions, green fluorescence intensity also diminished (Figures S4).

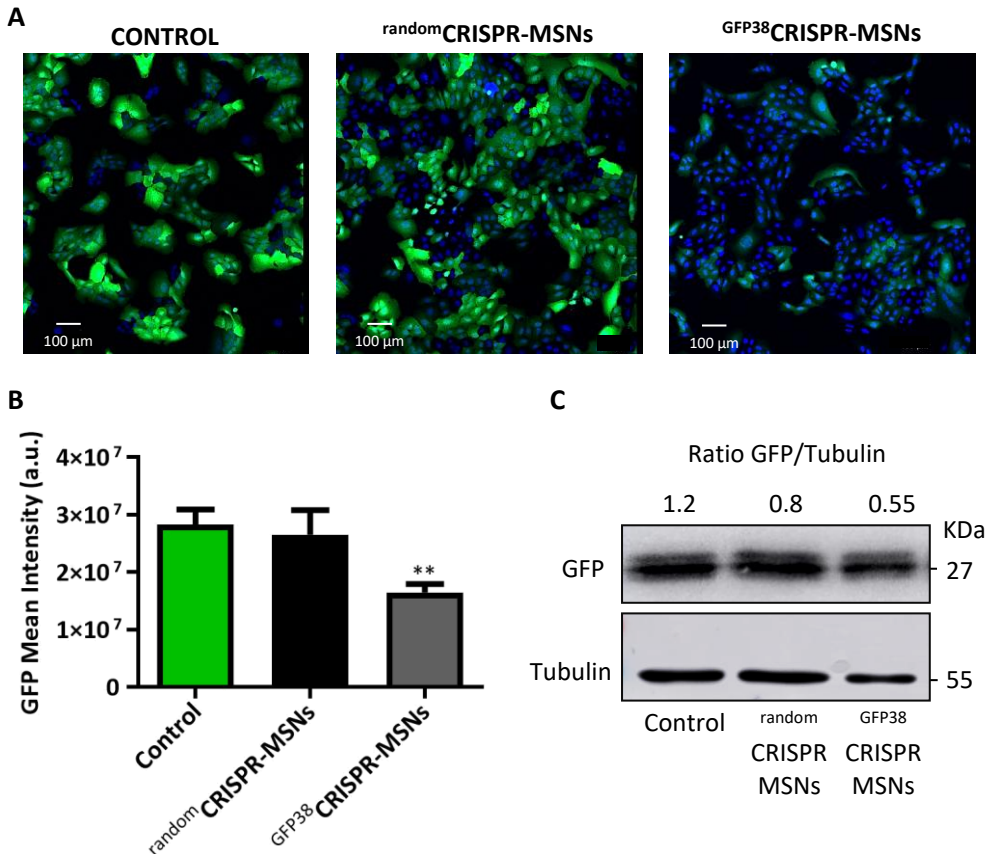


Figure 4. GFP³⁸CRISPR-MSNs for gene editing in U-2 OS-GFP cells. **A)** Confocal microscopy images of genome editing by the CRISPR/Cas9 system delivered by MSNs as carriers. Edition efficiency is judged by loss of GFP expression monitored as loss of green fluorescence intensity in the population. GFP cells are shown in green and blue marks the nuclei with Hoechst 4332. **B)** GFP fluorescence quantification by the analysis of the confocal images. Data represent the mean \pm SEM of at least three independent experiments. Statistical significance was determined by one-way ANOVA and Dunnet post-test (** $p < 0.025$). **C)** Quantification of GFP expression in cell lysates of GFP³⁸CRISPR-MSNs editing studies analysed by western blot.

Having demonstrated the use of ^{GFP38}**CRISPR-MSNs** to deliver the CRISPR/Cas9 editing machinery, we aimed to confirm that particles could simultaneously deliver the plasmid and an entrapped cargo to cells. For this study, the nanoparticles ^{GFP38}**CRISPR-RhB-MSNs** containing the CRISPR/Cas9 vector and RhB (as a model drug) were tested in U-2 OS-GFP cells. As a control, similar nanoparticles containing a random plasmid and loaded with RhB were also prepared (^{random}**CRISPR- RhB- MSNs**) and tested. Confocal microscopy analysis showed that in the U-2 OS-GFP cells treated with ^{GFP38}**CRISPR-RhB-MSNs**, GFP-associated fluorescence and GFP expression levels lowered, while no changes were observed in the cells treated with ^{random}**CRISPR-RhB-MSNs** (Figure 5A and 5B). In all cases, nanoparticles (both ^{GFP38}**CRISPR-RhB-MSNs** and ^{random}**CRISPR-RhB-MSNs**) delivered the cargo (i.e., RhB) to cells, as assessed by the increased red fluorescence observed in the confocal images (Figure 5A and 5C). Similar results were obtained with ^{GFP149}**CRISPR- RhB-MSNs** and ^{GFP178}**CRISPR-RhB-MSNs** nanoparticles targeting other GFP gene positions (Figure S5).

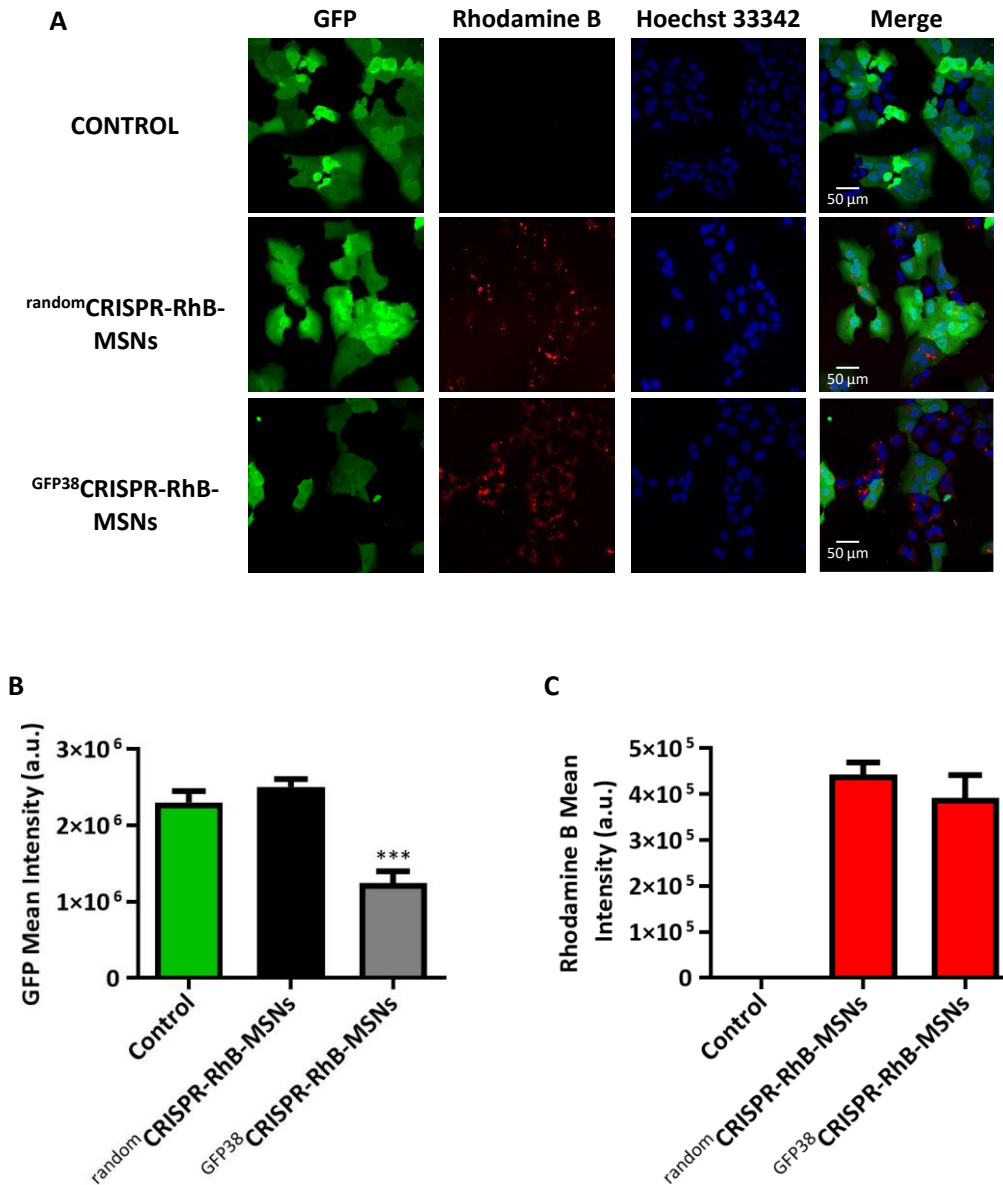


Figure 5. ^{GFP38}CRISPR-RhB-MSNs gene editing and cargo co-delivery to U-2 OS-GFP cells. **A)** Confocal microscopy images of genome editing and cargo delivery from CRISPR-RhB-MSNs. Edition efficiency is judged by loss of GFP expression monitored as loss of green fluorescence intensity in the population and delivery efficiency by the fluorescence intensity of rhodamine (red). Nuclei are blue stained with Hoechst 4332. **B)** GFP fluorescence

quantification by the analysis of confocal images. Statistical significance was determined by one-way ANOVA and Dunnett post-test (***) $p < 0.001$). **C)** Quantification of the RhB fluorescence intensity delivered from nanoparticles by the analysis of confocal images. Data represent the mean \pm SEM of at least three independent experiments.

4.4 Conclusions.

In summary, we report a nanosystem capable of efficiently co-delivering CRISPR/Cas9 editing machinery and a cargo in cells. Nanoparticles consisted of MSNs loaded with RhB (as model cargo) and capped with PEI and the CRISPR/Cas9 vector (^{GFP38}CRISPR-RhB-MSNs). The nanodevice remained capped at a neutral physiological pH, whereas both the capping ensemble and cargo were delivered at an acidic pH. The CRISPR/Cas9 vector in nanoparticles was protected from DNase I digestion under conditions in which the free plasmid was unstable. Confocal microscopy studies carried out with U-2 OS cells revealed that the nanodevice escapes from endosomes and reached the cytosol. We evaluated the capability of **CRISPR-RhB-MSNs** to edit the GFP gene in a U-2 OS-GFP cell line. The nanoparticles showed remarkable GFP editing and simultaneous cargo delivery. Confocal microscopy analysis showed that in the U-2 OS-GFP cells treated with ^{GFP38}CRISPR- RhB-MSNs, GFP expression levels lowered as a result of CRISPR/Cas9 editing machinery delivery. Furthermore, the nanodevice was also able to deliver the RhB payload, as evidenced by the increased red fluorescence observed by confocal microscopy. To our knowledge, these data represent one of the very first examples in the literature of MSNs capable of co-delivering the CRISPR/Cas9 system and a cargo. While few investigations led to the development of MSNs as delivery systems of CRISPR/Cas9 machinery as a single therapeutic agent,^[27-29] only one recent paper did manage to perform a dual therapy based on genome editing and drug co-delivery.^[25] The convergence of gene editing and cargo release in the same

cell with a unique nanoparticle provides enormous potential for designing more advanced and complex CRISPR editing systems for new applications. The dual therapeutic approach could implement one-shot treatments to simultaneously edit genes and release drugs. For example, targeting the CRISPR/Cas9 editing machinery to genes of therapeutic interest (such as drug resistance genes expressed in tumours) combined with drug delivery might allow to sensitise refractory patients, and thus improve the therapeutic outcome.

4.5 Materials and methods.

4.5.1 Materials.

All the chemicals were purchased from Sigma-Aldrich, unless otherwise specified, and were used as received. DNA oligonucleotides, CellLight Early Endosomes-GFP, and LysoTracker Green DND-26 were purchased from ThermoFisher, CRISPR plasmid pX330-U6-Chimeric_BB-CBh-hSpCas9 was obtained from Addgene. Branched polyethyleneimine (PEI) (M.W. 10,000) was obtained from Polysciences. GFP antibody was acquired from Santa Cruz Biotechnology (GFP (B-2): sc-9996). U-2 OS-GFP cells were a gift from Susana Llanos from the Centro Nacional de Investigaciones Oncológicas (CNIO, Spain).

4.5.2 General methods.

Powder X-ray diffraction (PXRD), transmission electron microscopy (TEM), N₂ adsorption-desorption isotherms, fluorescence spectrophotometry, Fourier-transform infrared spectroscopy (FTIR), thermogravimetric and elemental analyses were employed for materials characterisation. PXRD measurements were taken on a Seifert 3000TT diffractometer using CuK_α radiation. TEM images were acquired under a JEOL TEM-1010 electron microscope that worked at 100 kV. The N₂

adsorption-desorption isotherms were recorded in a Micromeritics TriStar II Plus automated analyser. To determine the ζ potential of the bare and functionalised nanoparticles, Zetasizer Nano ZS equipment (Malvern Instruments, Malvern, UK) was used. Samples were dispersed in distilled water at a concentration of 1 mg/mL. The ζ potential was calculated from the particle mobility values by applying the Smoluchowski model. The average of five recordings was reported as the ζ potential. Measurements were taken at 25 °C. The DLS studies to determine particle size were also conducted at 25 °C in a Malvern Zetasizer Nano ZS instrument. All the measurements were taken in triplicate on previously sonicated highly dilute water dispersions. Fluorescence measurements were taken in a JASCO FP-8500 spectrophotometer. FTIR measurements were recorded by a Bruker Tensor 27 spectrometer. The thermogravimetric analyses were carried out in TGA/SDTA 851e Mettler Toledo equipment in an oxidant atmosphere (air, 80 mL/min) with a heating programme that consisted of a heating ramp of 10 °C per min from 393 K to 1273 K, and an isothermal heating step at this temperature for 30 min. Elemental analysis was run in a CE Instrument EA-1110 CHN elemental analyser. Cell viability measurements were taken with a Wallac 1420 workstation. Confocal microscopy imaging was performed with a Leica TCS SP8 HyVolution II (Leica Microsystems Heidelberg GmbH) inverted laser scanning confocal microscope.

4.5.3 Synthesis of mesoporous silica nanoparticles (MSNs).

CTAB (1.00 g, 2.74 mmol) was dissolved in 480 mL of deionized H₂O before adding a solution of NaOH (3.5 mL, 2.00 M). The solution temperature was adjusted to 80 °C and then TEOS (5.00 mL, 2.57×10^{-2} mol) was added dropwise to the surfactant solution at maximum stirring. The mixture was stirred for 2 h to give a white precipitate. The solid was isolated by centrifugation and washed with deionized H₂O until a neutral pH was reached. Finally, the solid was dried at 60 °C.

To prepare the final porous material, MSNs were calcined at 550 °C in an oxidant atmosphere to remove the template phase.

4.5.4 Synthesis of PEI-MSNs.

25 mg of PEI were dissolved in 1 mL of ethanol and sonicated for 5 min. Then PEI solution was added to 50 mg of MSNs suspended in 4 mL of EtOH. The suspension was stirred for 3 h at room temperature. The solid was isolated by centrifugation and washed. Finally, the solid was dried and **PEI-MSNs** were obtained.

4.5.5 Synthesis of CRISPR-MSNs.

In order to obtain the **CRISPR-MSNs** complexes to transfect cells, a suspension of **PEI-MSNs** nanoparticles (25 µg/mL) was mixed with 1 µg/mL of the CRISPR/Cas9 vector in Opti-MEM and was incubated for 30 min. The mixture was prepared using vectors ^{GFP38}CRISPR/Cas9, ^{GFP149}CRISPR/Cas9, ^{GFP178}CRISPR/Cas9, and ^{random}CRISPR/Cas9 to yield solids ^{GFP38}**CRISPR-MSNs**, ^{GFP149}**CRISPR-MSNs**, ^{GFP178}**CRISPR-MSNs**, and ^{random}**CRISPR-MSNs**, respectively.

4.5.6 Synthesis of PEI-RhB-MSNs.

50 mg of calcined MCM-41 nanoparticles and 28 mg (0.16 mmol) of rhodamine B were suspended in 10 mL of ethanol. The mixture was stirred for 24 h at room temperature to achieve maximum loading in the pores of the MSNs scaffolding. Afterward, the solid was isolated by centrifugation and 25 mg of PEI suspension in ethanol was added. The suspension was stirred for 3 h. Finally, the pink solid was isolated and washed with ethanol, and dried at 37 °C.

4.5.7 Synthesis of CRISPR-RhB-MSNs.

In order to obtain the **CRISPR-RhB-MSNs** complexes, 1 $\mu\text{g}/\text{mL}$ of DNA was incubated for 30 min with **PEI-RhB-MSNs** in Opti-MEM (25 $\mu\text{g}/\text{mL}$) at room temperature. The mixture was prepared using vectors $\text{GFP}^{38}\text{CRISPR}/\text{Cas9}$, $\text{GFP}^{149}\text{CRISPR}/\text{Cas9}$, $\text{GFP}^{178}\text{CRISPR}/\text{Cas9}$, and $\text{random}\text{CRISPR}/\text{Cas9}$ to yield solids $\text{GFP}^{38}\text{CRISPR-RhB-MSNs}$, $\text{GFP}^{149}\text{CRISPR-RhB-MSNs}$, $\text{GFP}^{178}\text{CRISPR-RhB-MSNs}$, and $\text{random}\text{CRISPR-RhB-MSNs}$, respectively.

4.5.8 Synthesis of CRISPR-RhB*-MSNs.

To graft rhodamine B onto mesoporous silica nanoparticles, 2 mg of rhodamine B isothiocyanate (RBIT) were reacted with 20 μL of (3-aminopropyl)triethoxysilane (APTES) in 2 mL of anhydrous ethanol. The mixture was stirred in the dark overnight at room temperature. Then 10 mg of MCM-41 nanoparticles were dispersed in 5 mL of anhydrous ethanol and 40 μL of RBIT/APTES mixture were added. The suspension was left in the dark for 5.5 h at room temperature. Nanoparticles were washed and dried to yield **RhB*-MSNs**. In order to obtain **PEI-RhB*-MSNs**, 10 mg of **RhB*-MSNs** were stirred with 5 mL of ethanol, and 5 mg of PEI were added. The mixture was incubated for 3 h at room temperature. The solid was washed and dried to yield **PEI-RhB*-MSNs**. Finally, to obtain **CRISPR-RhB*-MSNs**, 1 $\mu\text{g}/\text{mL}$ of the CRISPR/Cas9 vector was added to 25 $\mu\text{g}/\text{mL}$ of the prepared solid in Opti-MEM and was incubated for 30 min.

4.5.9 Preparation of the CRISPR/Cas9 vector.

The oligonucleotides encoding sgRNA were designed based on the genomic sequence to edit, following the recommendations of the bibliography;^[5] length of 20 nucleotides complementary to 20 nucleotides of the GFP sequence followed for

a PAM: 5'-(N20)-NGG-3'. Firstly, plasmid pX330-U6-Chimeric_BB-CBh-hSpCas9 was digested by the Bpil enzyme (BbsI) and ligated with the annealed oligonucleotides following standard procedures. Finally, the presence of the insert of GFP gRNA was corroborated by sequencing.

4.5.10 Assembly and characterisation of CRISPR-RhB-MSNs.

To assess the efficacy of DNA binding to MSNs, agarose gel electrophoresis of the naked plasmid and **CRISPR-RhB-MSNs** complexes was performed. For this purpose, the purified plasmid and **PEI-RhB-MSNs** at various molar ratios (1:10, 1:25, 1:200, 1:500) were mixed in Opti-MEM and incubated at 37 °C for 30 min. Then nanoparticles were centrifuged, and supernatants were loaded in agarose gel.

4.5.11 CRISPR-RhB-MSNs delivery studies.

In order to test the proper opening mechanism of **CRISPR-RhB-MSNs**, 1 mg of solid was suspended in 1 mL of simulated plasma at pH 7.0 or in 1 mL of simulated plasma at pH 5.0.^[30] Suspensions were stirred at 37°C. At scheduled times (0, 15, 30, 60, and 90 min) an aliquot was obtained from each suspension and centrifuged to eliminate the solid. Rhodamine B delivery was followed by measuring fluorescence emission at 585 nm ($\lambda_{ex} = 525$ nm).

4.5.12 Stability studies of the CRISPR/Cas9 vector in MSNs complexes.

^{GFP38}**CRISPR-RhB-MSNs** and free ^{GFP38}CRISPR/Cas9 DNA were incubated at 37 °C for 10 min with DNase I enzyme (0.5 ng/mL). Moreover, the DNA bound to nanoparticles was released using heparin (7.5 mg/mL) in the absence of DNase I and analysed by agarose electrophoresis to confirm correct DNA disassociation. In addition, heparin was previously added to disassemble the DNA from

^{GFP38}CRISPR- RhB- MSNs, and DNase I was added to corroborate the protection of the vector on MSNs.

4.5.13 Toxicity studies with CRISPR-RhB-MSNs.

U-2 OS-GFP cells were seeded on a 24-well plate at 50,000 cells/well and treated with different concentrations of ^{GFP38}CRISPR-RhB-MSNs (0, 25, 50, and 100 µg/ml). Cells were incubated for 24 h and 48 h, and viability was determined by adding cell proliferation reagent WST-1 for 1 h. Finally, cell viability was measured at 450 nm in the Wallac Workstation.

4.5.14 Cellular uptake studies with CRISPR-RhB*-MSNs.

U-2 OS cells were seeded on glass coverslips in 6-well assays plates at 500,000 cells/well and incubated at 37 °C. To perform the studies, similar PEI-MSNs were synthesized but contained rhodamine B covalently anchored to the silica surface through a thiourea bond (^{GFP38}CRISPR-RhB*-MSNs). In this case, to demonstrate the endosomal escape, 1 µg/mL of the CRISPR/Cas9 vector was added to a suspension (25 µg/mL) of the prepared solid in Opti-MEM and was incubated for 30 min. Cells were treated and incubated with the early endosomal marker (in green) for 30 min, and in the presence of a green lysotracker for 1 h. Additionally, to demonstrate endocytic cellular uptake, the cells were treated with ^{GFP38}CRISPR-RhB*-MSNs at 25 µg/mL and incubated for 1 h in the absence or presence of the endocytic inhibitor (Dynasore, 100µM). Before visualisation cell membrane marker (wheat germ agglutinin marker) was added to the cell culture. Coverslips were washed with PBS and DNA marker Hoechst 33342 was added. Slides were visualised under a confocal microscope Leica TCS SP8 HyVolution II. On the other hand, ^{GFP38}CRISPR- RhB*- MSNs uptake was analysed by flow cytometry in U-2 OS cells.

For this purpose, U-2 OS cells were seeded on a 6 well-plate at 250,000 cells/well and treated with 25 µg/mL of ^{GFP38}CRISPR-RhB*-MSNs for 15, 30, 60 and 120 min. Cells were washed with PBS to remove the non-internalised nanoparticles and collected for rhodamine B quantification by flow-cytometry. The single-cell fluorescence measurements were performed in CytoFLEX S (Beckman-Coulter, USA) equipped with 4 lasers and 13 fluorescence detectors and analysed in the CytoFLEX software.

4.5.15 Gene editing of GFP in U-2 OS-GFP cells with CRISPR-MSNs.

The gene-editing ability of the prepared solid was analysed. Cells were cultured in 6-well plates at 500,000 cells/well 1 day before transfection. Then the medium was replaced with DMEM supplemented with 5% FBS. The CRISPR complexes were prepared by mixing 1 µg/mL of DNA with 25 µg/mL of PEI-MSNs in Opti-MEM medium for 30 min. Cells were incubated with the prepared complexes for 4 h. Afterward, the media were replaced, and cells were incubated for 48 h. Finally, the cells were washed several times with PBS and DNA marker Hoechst 33342 was added. Slides were visualized under a confocal microscope Leica TCS SP8 HyVolution II. The quantification of GFP-associated fluorescence intensity for the different treatments was performed by analysing the confocal images with the Image J software. Moreover, the expression of the GFP levels in the U-2 OS-GFP cells was confirmed by western blot analysis. To determine the amount of GFP, whole-cell extracts were obtained by lysing cells in a buffer that contained 25 mM Tris-HCl, pH 7.4, 1 mM EDTA, 1 mM EGTA, and 1% SDS, plus protease and phosphatase inhibitors. Lysates were resolved by SDS-PAGE, transferred to nitrocellulose membranes, blocked with 5% non-fat milk, washed with 0.1% Tween/PBS, and incubated overnight with a specific primary antibody against GFP (sc-9996, Santa Cruz Biotechnology). α -Tubulin (ab6160, Abcam) was detected in

cell lysates as the reference control. Membranes were washed and probed with the appropriate secondary antibody conjugated with horseradish peroxidase for enhanced chemiluminescence detection.

4.5.16 Gene editing of GFP in U-2 OS-GFP cells with CRISPR-RhB-MSNs.

We also determined the editing properties of **CRISPR-RhB-MSNs**. Cells were cultured in 6-well plates at 500,000 cells/well 1 day before transfection. Next, the medium was replaced for DMEM supplemented with 5% FBS. The CRISPR complexes were prepared by mixing 1 $\mu\text{g}/\text{mL}$ of DNA with 25 $\mu\text{g}/\text{mL}$ of **PEI-RhB-MSNs** in Opti-MEM medium for 30 min. In the following step, the cells were incubated with the prepared complexes for 4 h before replacing the media. After that, cells were grown for 48 h. Ultimately, cells were washed several times with PBS and DNA marker Hoechst 33342 was added. Slides were visualized under a confocal microscope Leica TCS SP8 HyVolution II. The quantification of the GFP-associated fluorescence intensity and rhodamine B-associated fluorescence intensity for the different treatments was performed by analysing the confocal images with the Image J software.

4.6 References.

- [1] F. J. M. Mojica, L. Montoliu, *Trends Microbiol.* **2016**, *24*, 811–820.
- [2] F. J. Mojica, C. Ferrer, G. Juez, F. Rodríguez-Valera, *Mol. Microbiol.* **1995**, *17*, 85–93.
- [3] J. A. Doudna, E. Charpentier, *Science (80-.)*. **2014**, *346*, 1258096–1258096.
- [4] M. Newman, F. M. Ausubel, *Curr. Protoc. Mol. Biol.* **2016**, *115*, 31.4.1-31.4.6.
- [5] F. A. Ran, P. D. Hsu, J. Wright, V. Agarwala, D. A. Scott, F. Zhang, *Nat. Protoc.* **2013**, *8*, 2281–2308.
- [6] P. D. Hsu, E. S. Lander, F. Zhang, *Cell* **2014**, *157*, 1262–1278.
- [7] H. X. Wang, M. Li, C. M. Lee, S. Chakraborty, H. W. Kim, G. Bao, K. W. Leong, *Chem. Rev.* **2017**, *117*, 9874–9906.
- [8] S. Hindriksen, A. J. Bramer, M. A. Truong, M. J. M. Vromans, J. B. Post, I. Verlaan-Klink, H. J. Snippert, S. M. A. Lens, M. A. Hadders, *PLoS One* **2017**, *12*, e0179514.
- [9] Z.-Y. He, K. Men, Z. Qin, Y. Yang, T. Xu, Y.-Q. Wei, *Sci. China. Life Sci.* **2017**, *60*, 458–467.
- [10] C. Liu, L. Zhang, H. Liu, K. Cheng, *J. Control. Release* **2017**, *266*, 17–26.
- [11] S. Aghamiri, S. Talaei, A. A. Ghavidel, F. Zandsalimi, S. Masoumi, N. H. Hafshejani, V. Jajarmi, *J. Drug Deliv. Sci. Technol.* **2020**, *56*, 101533.
- [12] F. Chen, M. Alphonse, Q. Liu, *WIREs Nanomedicine and Nanobiotechnology* **2020**, *12*, e1609.
- [13] M. Wang, J. A. Zuris, F. Meng, H. Rees, S. Sun, P. Deng, Y. Han, X. Gao, D. Pouli, Q. Wu, I. Georgakoudi, D. R. Liu, Q. Xu, *Proc. Natl. Acad. Sci. U. S. A.* **2016**, *113*, 2868–2873.
- [14] R. Mout, M. Ray, G. Yesilbag Tonga, Y.-W. Lee, T. Tay, K. Sasaki, V. M. Rotello, *ACS Nano* **2017**, *11*, 2452–2458.
- [15] J. S. Ha, J. S. Lee, J. Jeong, H. Kim, J. Byun, S. A. Kim, H. J. Lee, H. S. Chung, J. B. Lee, D.-R. Ahn, *J. Control. Release* **2017**, *250*, 27–35.
- [16] W. Sun, W. Ji, J. M. Hall, Q. Hu, C. Wang, C. L. Beisel, Z. Gu, *Angew. Chemie Int. Ed.* **2015**, *54*, 12029–12033.
- [17] M. Yan, J. Wen, M. Liang, Y. Lu, M. Kamata, I. S. Y. Chen, *PLoS One* **2015**, *10*, e0127986.
- [18] Y.-L. Luo, C.-F. Xu, H.-J. Li, Z.-T. Cao, J. Liu, J.-L. Wang, X.-J. Du, X.-Z. Yang, Z. Gu, J. Wang, *ACS Nano* **2018**, *12*, 994–1005.
- [19] P. Wang, L. Zhang, W. Zheng, L. Cong, Z. Guo, Y. Xie, L. Wang, R. Tang, Q. Feng, Y. Hamada, K. Gonda, Z. Hu, X. Wu, X. Jiang, *Angew. Chemie - Int. Ed.* **2018**, *57*, 1491–1496.
- [20] R. Mout, V. M. Rotello, *Bio-protocol* **2017**, *7*, DOI 10.21769/BioProtoc.2586.
- [21] S. K. Alsaiani, S. Patil, M. Alyami, K. O. Alamoudi, F. A. Aleisa, J. S. Merzaban,

- M. Li, N. M. Khashab, *J. Am. Chem. Soc.* **2018**, *140*, 143–146.
- [22] F. Torney, B. G. Trewyn, V. S.-Y. Lin, K. Wang, *Nat. Nanotechnol.* **2007**, *2*, 295–300.
- [23] T. Xia, M. Kovochich, M. Liong, H. Meng, S. Kabehie, S. George, J. I. Zink, A. E. Nel, *ACS Nano* **2009**, *3*, 3273–3286.
- [24] M. Kar, N. Tiwari, M. Tiwari, M. Lahiri, S. Sen Gupta, *Part. Part. Syst. Charact.* **2013**, *30*, 166–179.
- [25] B.-C. Zhang, B.-Y. Luo, J.-J. Zou, P.-Y. Wu, J.-L. Jiang, J.-Q. Le, R.-R. Zhao, L. Chen, J.-W. Shao, *ACS Appl. Mater. Interfaces* **2020**, *12*, 57362–57372.
- [26] E. Macia, M. Ehrlich, R. Massol, E. Boucrot, C. Brunner, T. Kirchhausen, *Dev. Cell* **2006**, *10*, 839–850.
- [27] A. Nouredine, A. Maestas-Olguin, E. A. Saada, A. E. LaBauve, J. O. Agola, K. E. Baty, T. Howard, J. K. Sabo, C. R. S. Espinoza, J. A. Doudna, J. S. Schoeniger, K. S. Butler, O. A. Negrete, C. J. Brinker, R. E. Serda, *Acta Biomater.* **2020**, *114*, 358–368.
- [28] X. Xu, O. Koivisto, C. Liu, J. Zhou, M. Miihkinen, G. Jacquemet, D. Wang, J. M. Rosenholm, Y. Shu, H. Zhang, *Adv. Ther.* **2020**, *n/a*, 2000072.
- [29] J. Gong, H.-X. Wang, Y.-H. Lao, H. Hu, N. Vatan, J. Guo, T.-C. Ho, D. Huang, M. Li, D. Shao, K. W. Leong, *Adv. Mater.* **2020**, *32*, 2003537.
- [30] A. Oyane, H.-M. Kim, T. Furuya, T. Kokubo, T. Miyazaki, T. Nakamura, *J. Biomed. Mater. Res. A* **2003**, *65*, 188–195.

4.7 Supporting information.

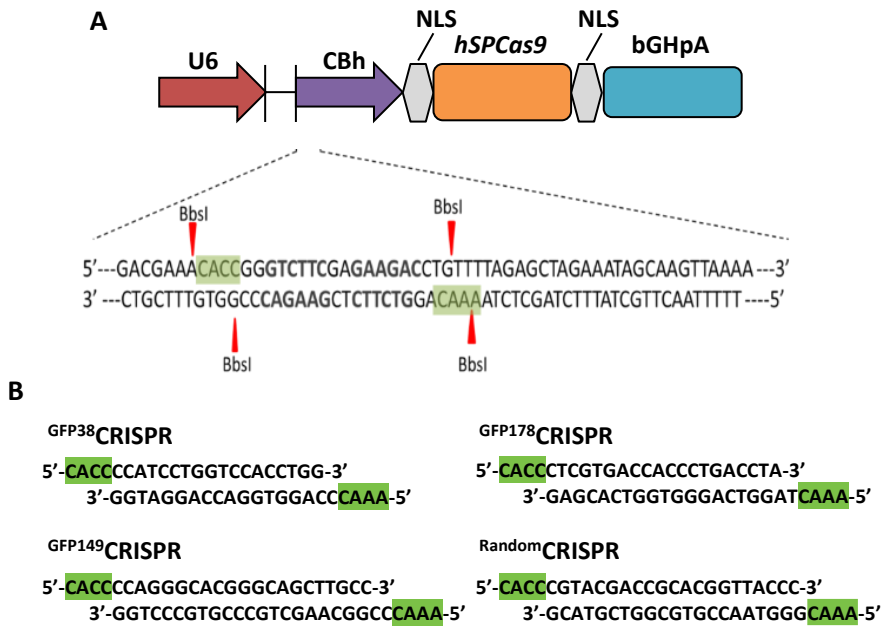








Figure S1. CRISPR vector design. **A)** Map image of pX330-U6-Chimeric_BB-CBh-hSpCas9 from Dr. Feng Zhang's lab published in Science (at the top) and the schematic representation of the guide sequence insertion site (at the bottom). This plasmid contains two expression cassettes, a human codon-optimised SpCas9 or SpCas9n, and the single guide RNA. The vector can be digested using BbsI, and a pair of annealed oligos can be cloned into the vector. **B)** Guide sequences selected to edit the expression of the GFP gene at positions 38, 149, and 178. Random sgRNA does not match with GFP, as a negative control of genome editing.

Table S1. Nanoparticles nomenclature and composition. RhB indicated that dye was loaded inside the porous network of the inorganic scaffold, whereas RhB* indicated that dye was covalently anchored onto the support.

Nanoparticles nomenclature	Vector	Gate	Cargo	Support	Scheme
MSNs				MSNs	
PEI-MSNs		PEI		MSNs	
PEI-RhB-MSNs		PEI	RhB	MSNs	
randomCRISPR-MSNs	randomCRISPR	PEI		MSNs	
GFP38CRISPR-MSNs	GFP38CRISPR	PEI		MSNs	
GFP149CRISPR-MSNs	GFP149CRISPR	PEI		MSNs	
GFP178CRISPR-MSNs	GFP178CRISPR	PEI		MSNs	
GFP38CRISPR-RhB*-MSNs	randomCRISPR	PEI	RhB*	MSNs	
randomCRISPR-RhB-MSNs	randomCRISPR	PEI	RhB	MSNs	
GFP38CRISPR-RhB-MSNs	GFP38CRISPR	PEI	RhB	MSNs	
GFP149CRISPR-RhB-MSNs	GFP149CRISPR	PEI	RhB	MSNs	
GFP178CRISPR-RhB-MSNs	GFP178CRISPR	PEI	RhB	MSNs	

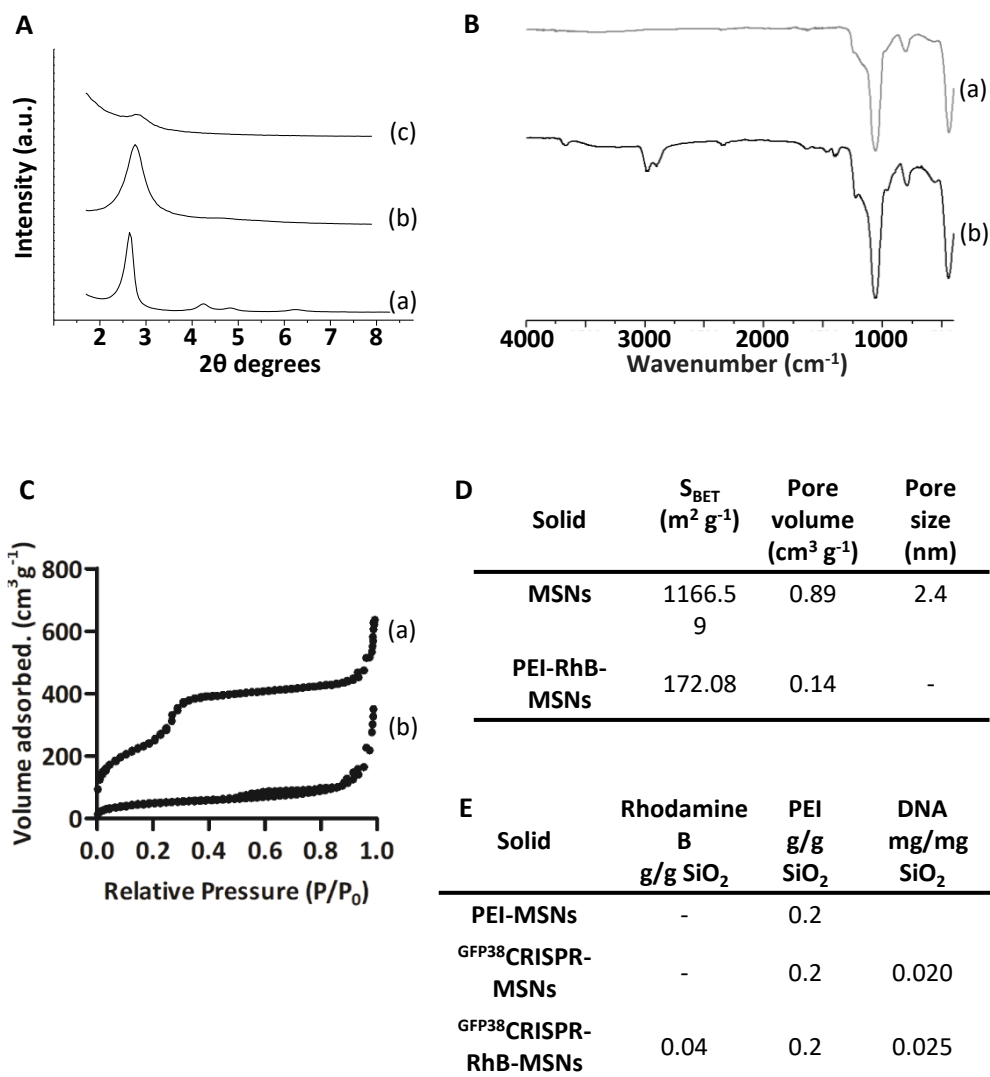


Figure S2. CRISPR-MSNs standard characterisation. **A)** Powder X-ray patterns of (a) MSNs as made, (b) calcined MSNs and (c) PEI-MSNs. The characteristic (100) diffraction peak was observed indicating the preservation of the mesoporous structure after the functionalisation processes. **B)** FTIR spectra of (a) MSNs and (b) PEI-RhB-MSNs showing the symmetric and asymmetric stretching bands of amine moieties from PEI at ca. 3100-2900 cm^{-1} interval indicating the proper PEI-coating of the nanoparticles. **C)** Nitrogen adsorption-desorption isotherm for (a) MSNs and (b) PEI-MSNs. The isotherm for the

starting MSNs corresponds to a type IV isotherm, typical of these materials. In contrast, the isotherm obtained for **PEI-MSNs** is typical of mesoporous materials with filled mesopores with a marked decrease in the external surface when compared with MSNs. **D)** BET specific surface values from the N₂ adsorption-desorption isotherm and pore volumes and pore sizes calculated applying the BJH model ($P/P_0 < 0.7$) for selected materials. **E)** Content of RhB, PEI, and plasmid from the different prepared materials.

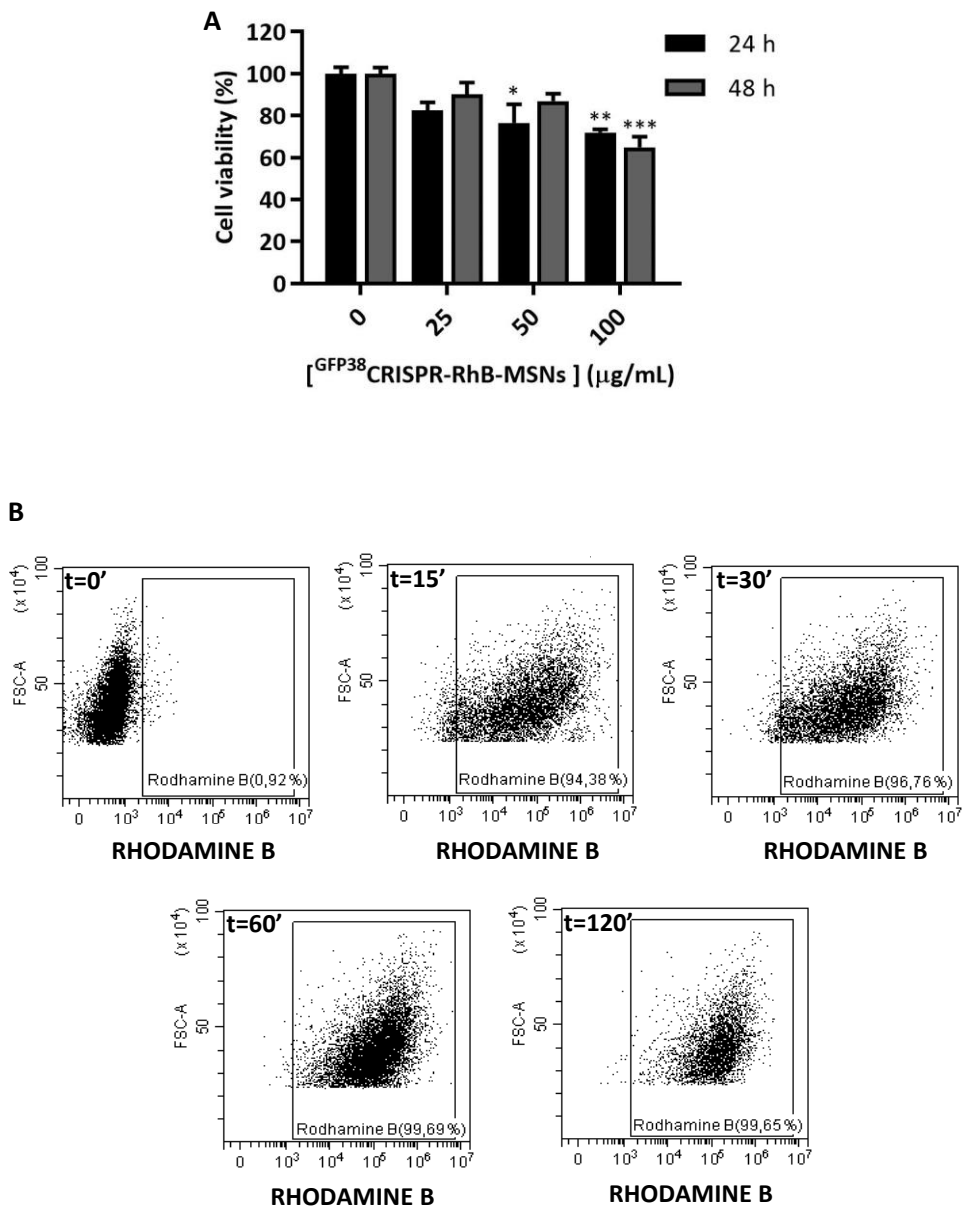


Figure S3. Cellular characterisation for CRISPR-MSNs. A) Cell viability studies by WST-1 assays at different ^{GFP³⁸}CRISPR-RhB-MSNs concentrations at 24 (black bars) and 48 h (grey bars). Data represent the mean \pm SEM of at least three independent experiments. Statistical significance was determined by one-way ANOVA and Dunnett post-test (* $p < 0.05$, ** $p <$

0.025, *** $p < 0.001$). **B)** Cellular uptake for ^{GFP38}CRISPR-RhB*-MSNs at different times (t = 0, 15, 30, 60 and 120 min) assessed by flow cytometry.

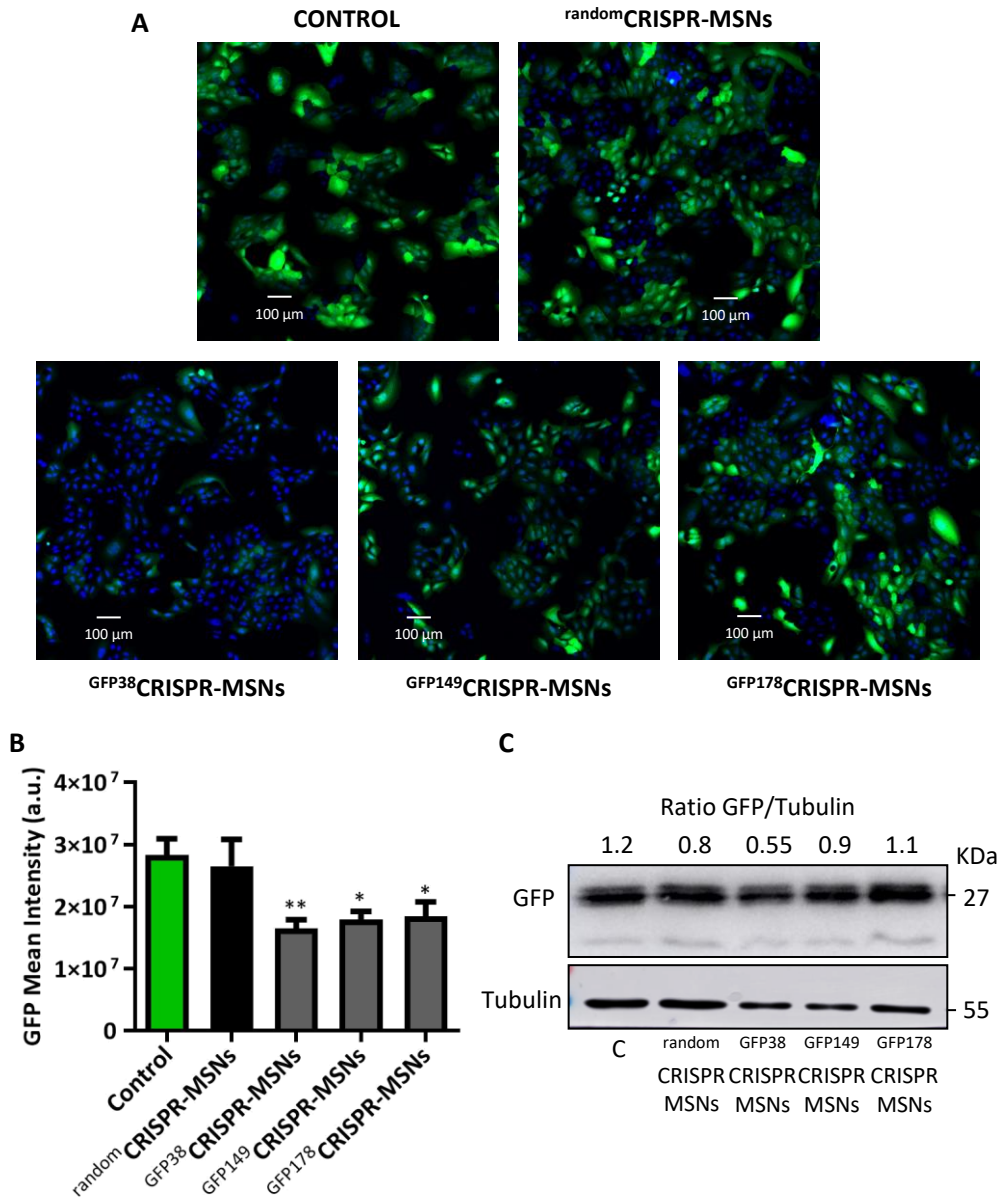


Figure S4. CRISPR-MSNs for gene editing into U-2 OS-GFP cells. A) Confocal microscopy images of genome editing by CRISPR/Cas9 system delivered by MSNs as carriers. Edition efficiency is judged by loss of GFP expression monitored as loss of green fluorescence intensity in the population. In green GFP cells and blue marked the nuclei with Hoechst 4332. **B)** GFP fluorescence quantification by confocal image analysis. Data represent the

mean \pm SEM of at least three independent experiments. Statistical significance was determined by one-way ANOVA and Dunnet post-test (* $p < 0.05$, ** $p < 0.025$). **C**) Quantification of GFP expression in cell lysates of **CRISPR-MSNs** editing studies analysed by western blot.

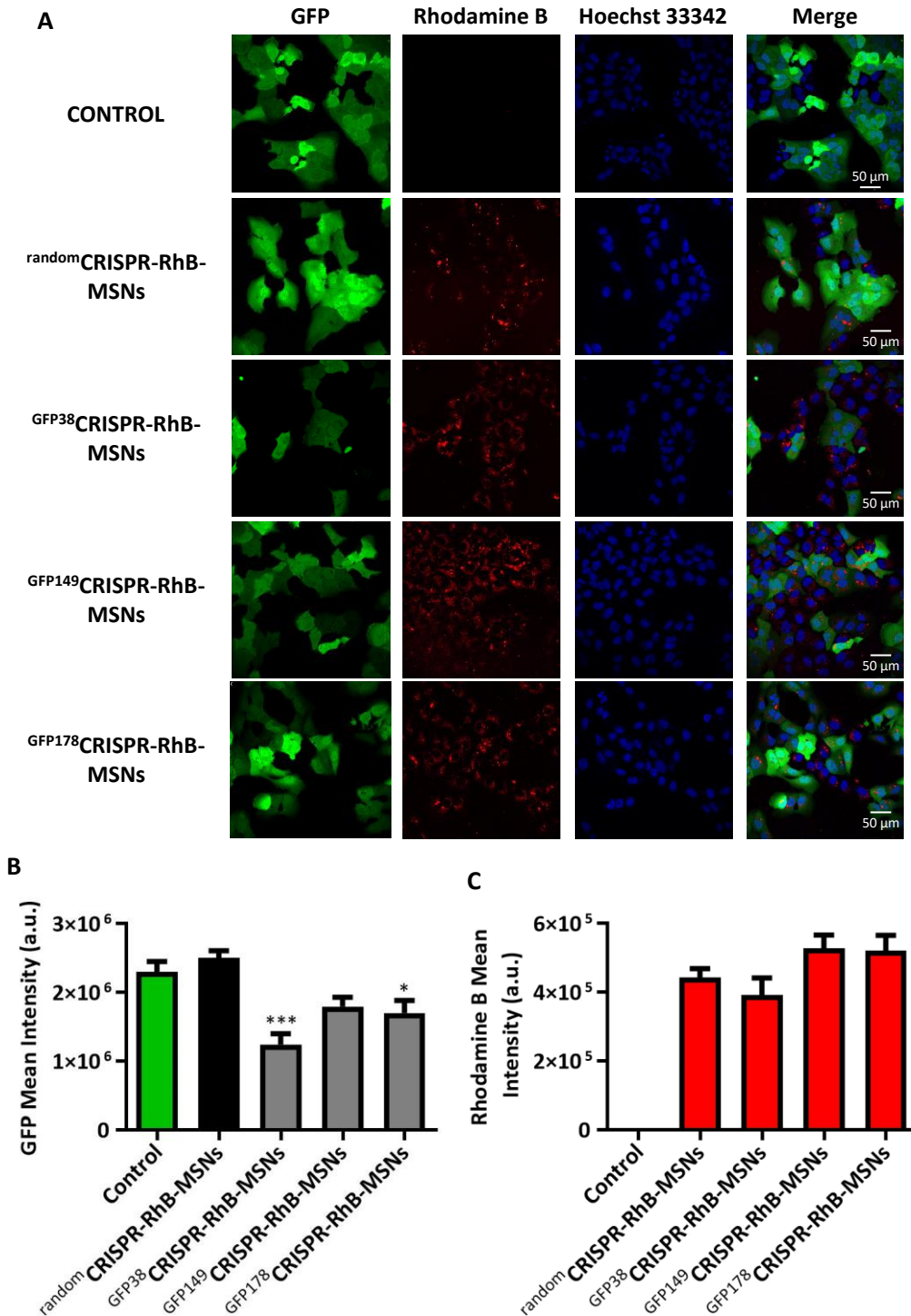


Figure S5. CRISPR-RhB-MSNs gene editing and cargo co-delivery into U-2 OS-GFP cells. A) Confocal microscopy images of genome editing and cargo delivery from **CRISPR-RhB-MSNs**. Edition efficiency is judged by loss of GFP expression monitored as loss of green fluorescence intensity in the population and the delivery efficiency by the fluorescence intensity of rhodamine B (red). The nuclei are marked in blue with Hoechst 4332. **B)** Quantification of GFP fluorescence intensity by confocal image analysis. Statistical significance was determined by one-way ANOVA and Dunnett post-test (* $p < 0.05$, *** $p < 0.001$). **C)** Quantification of rhodamine B fluorescence intensity delivered from nanoparticles by confocal image analysis. Data represent the mean \pm SEM of at least three independent experiments.

Chapter 5 | Enzyme prodrug therapy for breast cancer treatment

Horseradish peroxidase-functionalised gold nanoconjugates for breast cancer enzyme prodrug therapy

Gema Vivo-Llorca,^{[a],[b],[c]} Ángela Morella-Aucejo,^{[a],[b]} Alba García-Fernández,^{[a],[b],[c],[d]} Paula Díez,^{[a],[b],[c],[f]} Antoni Llopis-Lorente,^{[a],[b]} Ramón Martínez Mañez*^{[a],[b],[c],[d],[f]} and Mar Orzáez^{[c],[d]}

^[a] Instituto Interuniversitario de Investigación de Reconocimiento Molecular y Desarrollo Tecnológico (IDM). Universitat Politècnica de València, Universitat de València. Spain. E-mail: rmaez@qim.es

^[b] Departamento de Química, Universitat Politècnica de València, Camí de Vera s/n, 46022, València, Spain.

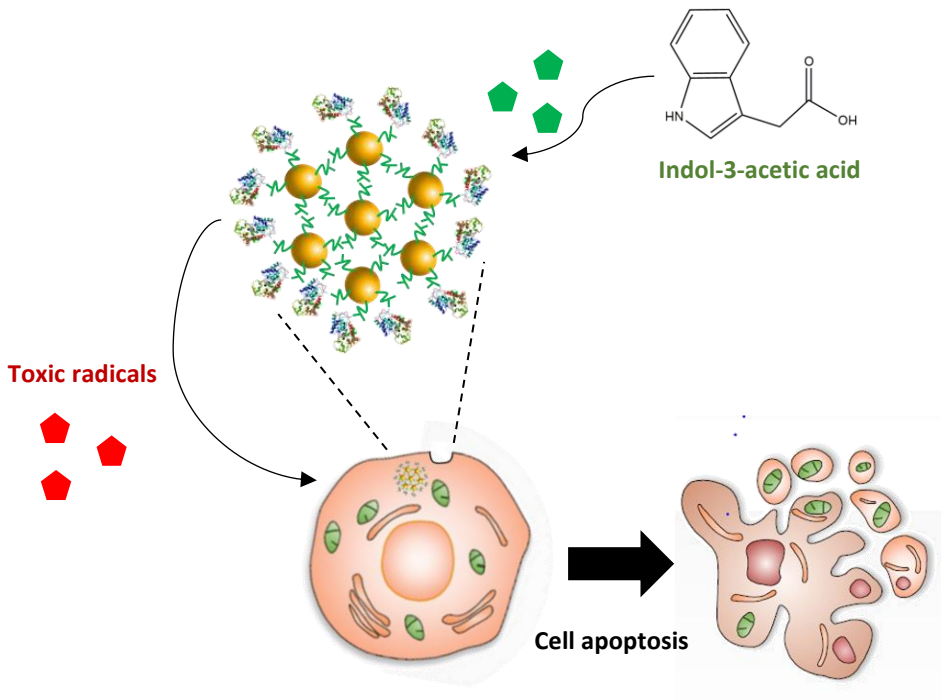
^[c] CIBER de Bioingeniería, Biomateriales y Nanomedicina (CIBER-BBN), Spain.

^[d] Unidad Mixta UPV-CIPF de Investigación de Mecanismos de Enfermedades y Nanomedicina, València, Universitat Politècnica de València, Centro de Investigación Príncipe Felipe, València, Spain.

^[e] Centro de Investigación Príncipe Felipe, Laboratorio de Péptidos y Proteínas, Carrer d'Eduardo Primo Yúfera, 3, 46012, València, Spain.

^[f] Unidad Mixta de Investigación en Nanomedicina y sensores. Universitat Politècnica de València, Instituto de Investigación Sanitaria la Fe, 46026, València, Spain.

▪ Graphical abstract.



5.1 Abstract.

Breast cancer is the first cause of death among women. Patients suffering from triple-negative breast cancer (TNBC) lack effective treatments, which represent a clinical concern due to the associated poor prognosis and high mortality. Therefore, these medical unresolved problems need to be urgently addressed. As an approach to succeed over conventional therapy limitations, we present herein a novel nanodevice based on gold nanoparticles to efficiently perform enzyme prodrug therapy (EPT) in breast cancer cells. The enzyme horseradish peroxidase (HRP) oxidises the prodrug indole-3-acetic acid (IAA) to release toxic oxidative species. In this scenario, we present a novel gold nanodevice to efficiently transport the HRP to breast cancer cells, (**HRP-AuNCs**). The nanodevice was biocompatible and properly internalised by breast cancer cell lines. Co-treatment with **HRP-AuNCs** and IAA (**HRP-AuNCs/IAA**) reduced viability below 5% in breast cancer cell lines. Interestingly, multicellular tumour spheroid-like cultures (3D cellular models) co-treated with **HRP-AuNCs/IAA** resulted in a 74% reduction of cell viability at non-toxic doses for the free formulated HRP plus IAA. Our results demonstrate that nanoformulation of HRP has a crucial role to enhance the enzyme therapeutic effect and might help to bypass the clinical limitations of current tumour enzyme therapies. These results show **HRP-AuNCs** as promising nanodevices for EPT in breast cancer.

5.2 Introduction.

As previously detailed in the introduction (see [section 1.6](#)), breast cancer is the most commonly diagnosed cancer and the leading cause of death among women worldwide, accounting for 24% of total cancer cases with 15% of related mortality.^[1,2] Currently, the main treatment strategies are surgery, radiotherapy,

chemotherapy, and hormone therapy.^[3] A significant shortcoming associated with those therapies is the lack of specificity, which leads to reduced efficacy and dose-limiting side effects (i.e., nausea, fatigue, infertility, cardiac dysfunction, etc.).^[4] In this scenario, nanoparticle-based therapies for controlled release and tumour-targeted delivery of these drugs represent an essential technology to improve treatment outcomes. The use of nanoparticles as on-command delivery systems provides many potential benefits; including increased drug solubility, decrease degradation during circulation, and targeting to the desired locations. Nanocarriers present the advantage of preferentially accumulate in solid tumours, through the EPR effect (see [section 1.5](#)). This unique phenomenon is considered the landmark of nanoparticle passive targeting, which is translated into the therapeutic improvement derived from treatment with nanomaterials.^[5-10] The ability to use nanotechnology to improve the pharmacologic profile of a drug promises to increase efficacy, while decreased unwanted side effects.^[11]

On the other hand, enzymes have been investigated as effective agents for cancer treatment.^[12,13] Particularly, enzyme prodrug therapy (EPT) emerged as a novel therapeutic approach, where enzymes catalyse the activation of non-toxic prodrugs to produce toxic drugs at targeted locations.^[14] The success of EPT leans on the specific prodrug activation in the tumour site for the efficient elimination of cancer cells, whereas sparing healthy tissues.^[15] Poor stability and potential immunogenicity are the critical limiting factors for enzyme cancer therapy.^[16-19] As a consequence, the development of efficient delivery systems to carry sufficient enzyme amount to the targeted location is greatly important.

Within this context, directed enzyme prodrug therapy (DEPT) has been developed, which mainly employs antibodies^[18-23] and viruses^[24-27] as enzyme vehicles. However, these approaches do not completely accomplish therapeutic

needs, as their clinical application is mainly hindered by the potential immunogenicity and risk of mutation.^[16,18,19,28,29] One of the possible approaches to overcome the limitations of conventional DEPT is to use abiotic nanoparticles as delivery systems. Several studies have focused on conjugating therapeutic enzymes on different nanomaterials, such as liposomes^[30,31], polymers,^[32–34] dendrimers,^[35] iron oxide nanoparticles,^[36,37] and silica nanoparticles.^[38–40] Among inorganic nanomaterials, gold nanoparticles (AuNPs) present unique chemical, physical and biological properties that make them ideal scaffolds to be exploited for biomedical applications (further detailed in [section 1.4](#)). AuNPs are of special interest as enzyme nanocarriers. Enzyme conjugation with AuNPs has demonstrated to increase the enzyme stability,^[41–45] as well as the enzyme affinity for the substrate,^[46–48] and the sensitivity when gold nanosystems are used for sensing applications.^[49–51] As a consequence, enzyme nanoformulation in gold nanoparticles is presented as a plausible solution for the handicap of poor stability associated with enzyme therapy, which could improve enzyme release and therapeutic effect in the tumour.

Despite their numerous advantages, AuNPs remain to be fully exploited in the EPT field, where only a few studies have been reported.^[52,53] We aimed to widen the gold-based nanomaterials applications by developing AuNPs conjugates (AuNCs) as enzyme nanocarriers to perform EPT in breast cancer tumour cells. We chose the enzyme-prodrug system consisting of the enzyme horseradish peroxidase (HRP) and the prodrug indole-3-acetic acid (IAA). Horseradish peroxidase (HRP; EC 1.11.1.7) is a redox glycoenzyme with an accessible ferroporphyrin group at the active site, which is naturally found in horseradish roots.^[54] From a biomedical point of view, HRP presents numerous highlightable features (namely, biocompatibility, high stability at 37 °C, high catalytic activity at

neutral pH, and the possibility of conjugation to nanoparticles and antibodies).^[52–57] In recent years, HRP has gained remarkable attention in cancer research, since in combination with IAA, it has demonstrated antitumour activity *in vitro*^[60–63] and *in vivo*.^[64,65] Indole-3-acetic acid is a naturally occurring plant growth phytohormone^[66] that can be used as a non-toxic prodrug because it is well-tolerated by humans.^[67,68] Horseradish peroxidase catalyses the oxidation of IAA to release free radicals (i.e., 3-methylene-2-oxindole) and reactive oxygen species (ROS) (i.e., O_2^- , and H_2O_2), which induce oxidative stress and cell death by activating apoptotic pathways.^[69–77]

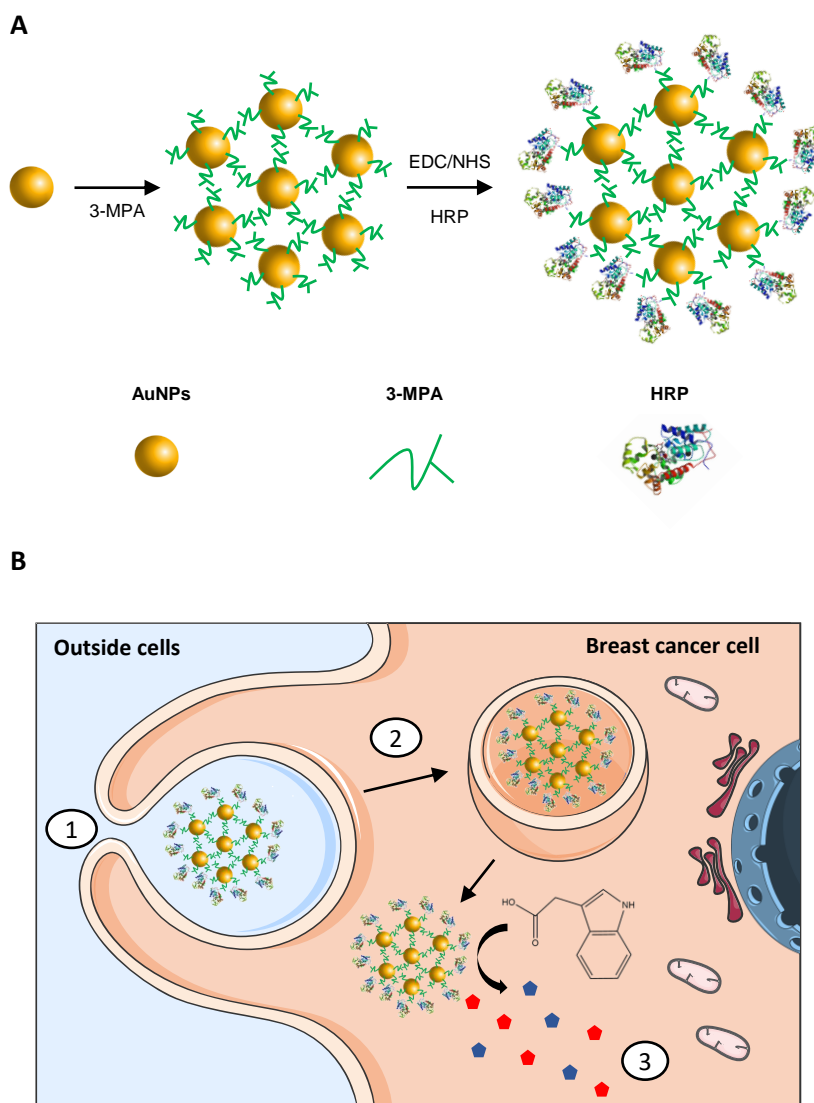
In this scenario, few studies have been reported using nanoparticles as HRP carriers for cancer treatment,^[34,38–40] yet none of them employ AuNPs. Based on the above, we report herein the first gold nanodevice for EPT through HRP/IAA enzyme prodrug system. We focused our attention on the preparation and evaluation of the therapeutic effect of the novel nanodevice **HRP-AuNCs** in breast cancer models.

5.3 Results and Discussion.

5.3.1 Synthesis and characterisation of HRP-AuNCs.

In order to prepare the nanodevice, we first synthesised AuNPs by reduction of Au^{III} with sodium citrate, according to the Turkevich–Frens method.^[78,79] The resulting AuNPs were functionalised with 3-mercaptopropionic acid (3-MPA) to obtain the nanoconjugates termed as **(3-MPA)-AuNCs**. The carboxylic group of **(3-MPA)-AuNCs** was activated by EDC/NHS reaction and then it reacted with amino groups in the HRP enzyme. This resulted in the final gold nanoconjugate decorated with covalently attached HRP through amide bonds (**HRP-AuNCs**) ([Scheme 1A](#) and [Table S1](#)). The prepared nanoparticles were expected to be internalised by breast

cancer cells and produce free radical species upon treatment with the prodrug IAA. Free radicals are known to induce apoptotic cell death by regulating intracellular signal transduction pathways (Scheme 1B).^[74–77]



Scheme 1. Scheme of HRP-AuNCs. A) Scheme of gold nanoparticles (AuNPs) functionalised with 3-MPA. The carboxylic group in the gold nanoconjugates (**3-MPA**)-AuNCs was activated by EDC/NHS reaction. After, HRP was grafted on the nanoconjugates surface through amide

bond formation between the carboxylic group of the 3-MPA and the amine residues of the enzyme. **B)** Scheme of the mechanism of action of **HRP-AuNCs**. **HRP-AuNCs** are internalised by endocytosis (1,2). Then, the HRP oxidises the exogenous prodrug IAA leading to the production of IAA-derived free radicals and ROS (3), which induce tumour cell death by apoptosis. Figure 1B was produced using a template from the Server Medical Art platform.

The nanodevices were characterised using transmission electron microscopy coupled with energy-dispersive X-ray spectroscopy (TEM-EDX), ultraviolet-visible (UV-Vis) spectrophotometry, hydrodynamic diameter scattering (DLS), and ζ potential. TEM images of **HRP-AuNCs** showed spherical gold nanoparticles with an average size of ca. 20 nm (Figure 1A). Moreover, mapping of the final nanodevice showed the presence of Au atoms from the gold scaffold, S atoms from 3-MPA, and N from the enzyme (Figure 1B). UV-Vis measurements (Figure 1C) of AuNPs showed a single absorption band at 524 nm, characteristic of the surface plasmon resonance of spherically shaped nanospheres with ca. 20 nm of diameter. In the **HRP-AuNCs**, the 524 nm band was displaced to longer wavelengths. We also monitored the preparation process of the final nanodevices measuring the DLS and the ζ potential. The hydrodynamic diameter increased after each preparation step (Figure 1D). The starting gold colloid showed a hydrodynamic diameter of 25.7 ± 0.2 nm. The functionalisation of the AuNPs with 3-MPA to obtain **(3-MPA)-AuNCs** increased the hydrodynamic size to 222 ± 17 nm, which indicated the formation of the nanoconjugates of AuNPs. The subsequent HRP attachment yielded the **HRP-AuNCs** with a hydrodynamic diameter of 376 ± 29 nm, which confirmed the attachment of the enzyme to the nanoconjugate surface. In relation to ζ potential (Figure 1D), functionalisation with 3-MPA motives increased the ζ potential to -35 ± 4 mV compared to the starting AuNPs, which presented a surface charge of -37 ± 3 mV. Further functionalisation with HRP resulted in a ζ potential of -15 ± 2 mV,

which indicated the correct incorporation of the positively charged enzyme to the nanoconjugate surface.

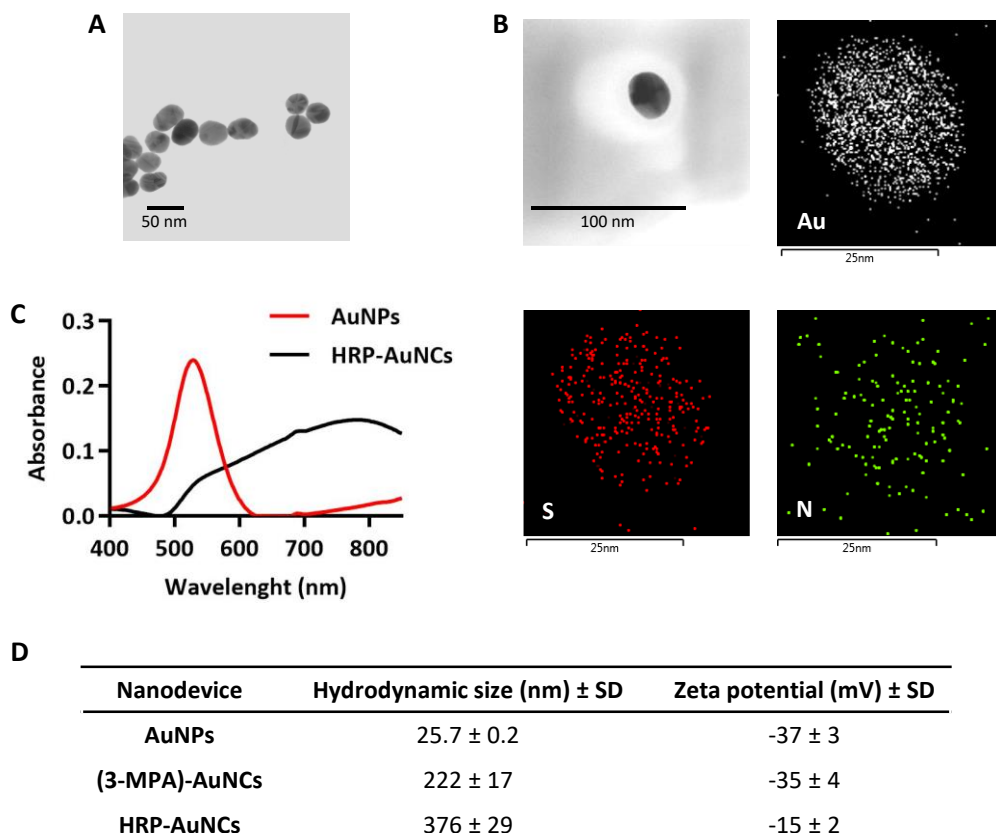


Figure 1. Characterisation of HRP-AuNCs. **A)** Representative TEM image of the final nanodevice **HRP-AuNCs**. **B)** TEM-EDX map for **HRP-AuNCs** showing the presence of Au (from the gold scaffold), S (from the 3-MPA), and N (from the HRP). **C)** UV-Vis spectra of AuNPs and **HRP-AuNCs**. **D)** Hydrodynamic size determined by dynamic light scattering and ζ potential of AuNPs, (3-MPA)-AuNCs and **HRP-AuNCs**. Data represent mean \pm SD (n = 3).

5.3.2 Activity and stability of HRP-AuNCs.

Enzyme immobilization may result in alterations of the enzyme properties.^[80] Thus, it is critical to check the enzyme activity after enzyme conjugation with the

gold scaffold. This was carried out by measuring the specific peroxidase activity of **HRP-AuNCs** following a standard activity assay based on the ABTS oxidation (see materials and methods section). One unit (U) of HRP is defined as the amount of enzyme that oxidises 1.0 μmol of ABTS per minute at pH 5.0 at 25 °C [i.e., $\text{H}_2\text{O}_2 + \text{ABTS} \rightarrow 2\text{H}_2\text{O} + \text{oxidised ABTS}$]. The free HRP activity was determined as $2.47 \cdot 10^7$ U per mg of enzyme. On the other hand, the HRP activity on **HRP-AuNCs** was determined as 0.25 U per mg of nanoparticles.

Since the recent discovery that metal nanoparticles present intrinsic enzyme- mimetic activity similar to natural peroxidases,^[81–84] increasing attention has been paid to inorganic peroxidase mimetics.^[85–87] Remarkably, gold nanoparticles have been found to have catalytic activity for H_2O_2 decomposition, meaning that gold nanomaterials might be used as new nanodevices based on their peroxidase-like activity.^[88–92] For this reason, we aimed to determine whether AuNPs presented intrinsic peroxidase activity by the ABTS oxidation assay. Nevertheless, negligible peroxidase activity was detected with AuNPs (Figure S1), which can be explained because of the lower affinity of AuNPs for H_2O_2 and ABTS compared to HRP.^[81,89] Consequently, we confirmed that the peroxidase activity of **HRP-AuNCs** can be attributed exclusively to the presence of the enzyme.

5.3.3 Biocompatibility and cellular uptake of HRP-AuNCs.

Breast cancer is a complex disease. It has been recognised as a set of diseases affecting the same anatomical structure but is characterised by great heterogeneity within patients. Molecular expression of a variety of biomarkers led to breast cancer classification into subtypes.^[93–95] Among breast cancer subtypes, we explored the EPT efficacy in luminal A and TNBC cell lines. In the first step, the biocompatibility of the nanodevice was tested in MCF-7 and MDA-MB-231 cell lines

(luminal A and TNBC cells, respectively). For this purpose, MDA-MB-231 and MCF-7 cell lines were incubated in presence of **HRP-AuNCs** at different concentrations (0-750 $\mu\text{g}/\text{mL}$). The results showed that **HRP-AuNCs** were well-tolerated by both cell lines after 48 hours of treatment (Figure 2A, 2B). Only the highest concentration of **HRP-AuNCs** (i.e., 750 $\mu\text{g}/\text{mL}$) showed certain toxicity in MDA-MB-231 cells.

We also analysed the internalisation of the nanoconjugates as a critical previous step to conduct targeted EPT. To accomplish this aim, the breast cancer cell lines were incubated with **HRP-AuNCs** for 6 h before TEM visualization. TEM results showed that the nanosystem was successfully internalised by MDA-MB-231 (Figure 2C) and MCF-7 cells (Figure 2D). **HRP-AuNCs** nanoparticles were preferentially localized in endocytosis vesicles identified as secondary lysosomes. This data match with other studies in the bibliography, which indicate that gold nanoparticles are sequestered in lysosomes after following the endocytic pathway.^[96–99]

Considering the biocompatibility and proper internalisation of **HRP-AuNCs**, we concluded that the nanodevices are suitable candidates for breast cancer treatment, and thus further evaluation of EPT effectiveness was performed.

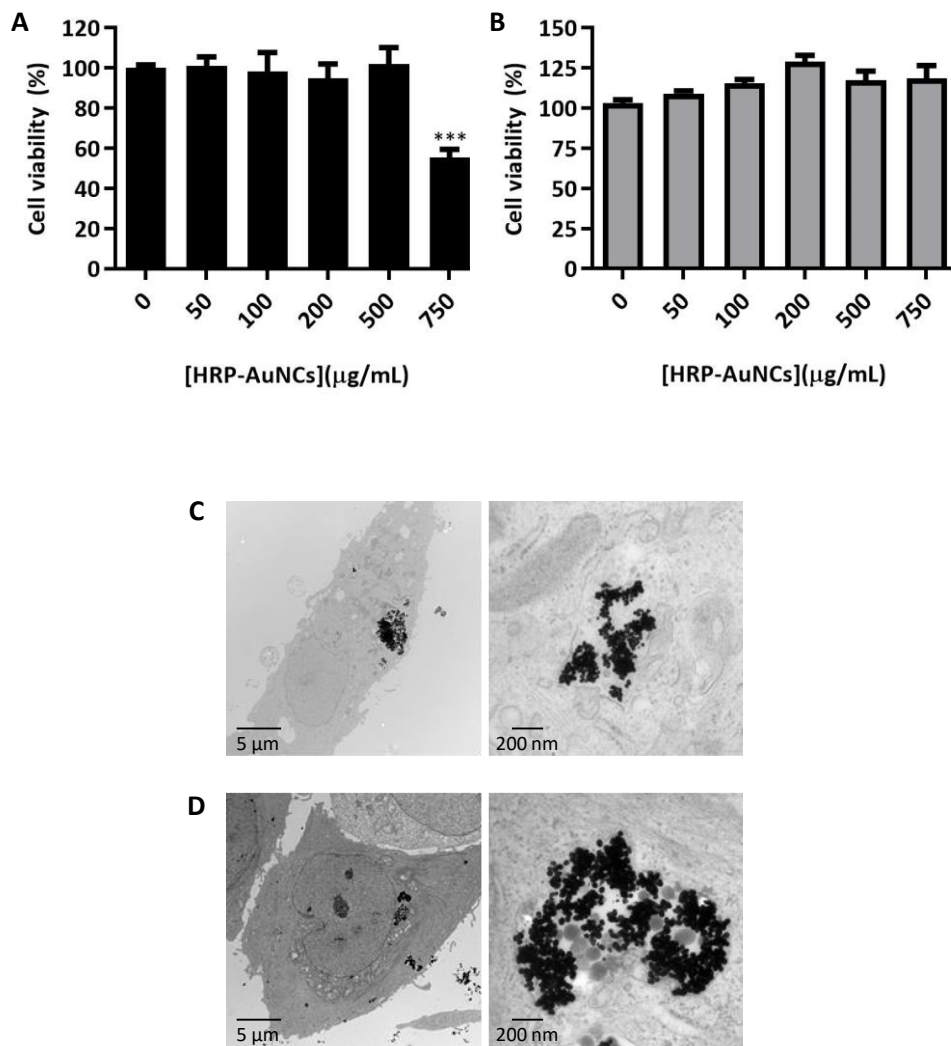


Figure 2. Biocompatibility and internalisation of HRP-AuNCs. Cytotoxicity profile of HRP- AuNCs in **A)** MDA-MB-231 and **B)** MCF-7. Cell viability was studied by WST-1 assay in presence of different nanoparticle dosages after 48 h of incubation. Data represent means \pm SEM ($n = 3$). Statistically significance was determined by one-way ANOVA and Dunnett post-test (***) $p < 0.001$). TEM images of HRP-AuNCs uptake by **C)** MDA-MB-231 and **D)** MCF-7 after 6 h of incubation with 50 $\mu\text{g/mL}$ of nanoconjugates.

5.3.4 HRP-AuNCs for EPT in breast cancer cells.

As stated above, this work aimed to use **HRP-AuNCs** in combination with IAA (**HRP-AuNCs/IAA**) to induce breast tumour cell death through an oxidative stress mechanism. The efficiency of **HRP-AuNCs/IAA** for EPT was explored in luminal A and TNBC cell lines. MDA-MB-231 and MCF-7 cells were treated with **HRP-AuNCs** (9.3×10^{-2} U/mL and 6.4×10^{-2} U/mL, respectively) in the absence or presence of 500 μ M IAA. After 48 h of incubation, cell viability was evaluated by WST-1 assay. A significant reduction in cell viability was observed with **HRP-AuNCs/IAA** treatment in MDA-MB-231 (Figure 3A) and MCF-7 (Figure 3B), whereas no cell death was detected when cells were treated with **HRP-AuNCs** or IAA alone. We also evaluated the EPT efficiency using the free HRP at equivalent enzyme activity units to that found in the nanoparticles. Remarkably, free HRP/IAA treatment did not reduce the cell viability of breast cancer cell lines. These results present HRP nanoformulation as a pivotal feature to outperform the antitumour effect of the free enzyme prodrug therapy system.

On the other hand, considering the HRP-like activity attributed to gold nanoparticles along bibliography (*vide ante*),^[88,89,100,101] we further evaluated the ability of AuNPs to perform EPT in combination with IAA (AuNPs/IAA) (Figure S2). As expected, and in concordance with ABTS oxidation assay (*vide ante*), neither AuNPs alone nor AuNPs/IAA treatments reduced the cell viability in the breast cancer cell lines.

The obtained results proved that **HRP-AuNCs** are a promising tool to conduct EPT in different breast cancer subtypes: i.e., luminal A and TNBC. Other examples are found in the bibliography using silica^[38–40] and chitosan^[34] nanoparticles loaded with HRP to induce EPT in tumour cellular models. However, this is the very first

time a gold based nanodevice is presented as an efficient mechanism to enhance the antitumoural effect induced by the HRP/IAA dual system.

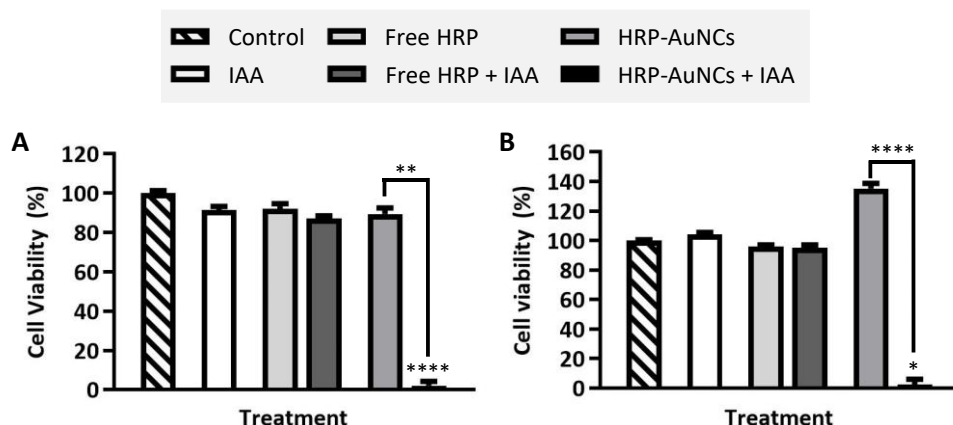


Figure 3. HRP-AuNCs for EPT in breast cancer cells. Cell viability assessment in **A)** MDA-MB-231 and **B)** MCF-7 treated with HRP-AuNCs or free HRP in the absence or presence of IAA. Cell viability was determined after 48 h of incubation by WST-1 assay. Data represent means \pm SEM (n=3). Statistically significance was determined by one-way ANOVA and Dunns post-test (* $p < 0.05$, ** $p < 0.025$, **** $p < 0.001$).

5.3.5 HRP-AuNCs for EPT in breast cancer multicellular tumour spheroid-like cultures.

Multicellular tumour spheroid cultures (MCTS) are 3D culture systems regarded as a more stringent and representative model on which to perform *in vitro* experiments. 3D cell cultures promote greater *in vivo*-like behaviour than their two-dimensional (2D) counterparts, due to recreating more of the characteristic traits of the native tumour microenvironment (such as cell-cell and cell-cellular matrix interactions, hypoxia, drug penetration, drug response, and resistance).^[102,103] Furthermore, MCTS represent a relevant physiological model as they are enriched with cancer stem cells (CSC) or show stem cell-like features. CSCs present self-renewal and differentiation capacity. Besides, they are related to the metastatic

process and the development of chemo/radiotherapy resistance.^[104,105] Therefore, MCTS would predict *in vivo* tumour response more accurately than 2D cultures, and they constitute a more precise model in which to study tumour response to novel therapeutic agents.

Consequently, we studied the ability of **HRP-AuNCs**/IAA to induce cell death in multicellular tumour spheroid-like cultures of TNBC subtype, as tumour-simulated conditions. To carry out this study, we first created MTSC from MDA-MB-231 cells using non-adhered culture plates (Figure S3). The spheroid-like cultures were incubated with **HRP-AuNCs** (0.15 U/mL) in the absence or presence of IAA at a concentration of 250 μ M for 48 h. While single treatments using **HRP-AuNCs** or IAA alone did not affect cell viability, the co-treatment using **HRP-AuNCs** and IAA induced spheroid cell death, by significantly reducing the cell viability down to 26% (Figure 4). Interestingly, free formulated HRP combined with IAA did not induce any effect on cell viability.

As far as we know, these encouraging results show for the first time a HRP equipped nanodevice as an efficient vehicle to induce EPT in MTSC cultures. The obtained favourable data evidence that **HRP-AuNCs** are successful nanodevices to enhance the antitumour activity of HRP/IAA in a complex biological system such as MCTS cultures, which recapitulates the architecture and microenvironment of a living tumour. Importantly, the ability to induce cell death in a 3D TNBC cancer model identifies **HRP-AuNCs** as promising nanodevices regarding triple-negative tumour management, which currently lacks targeted and effective treatments.

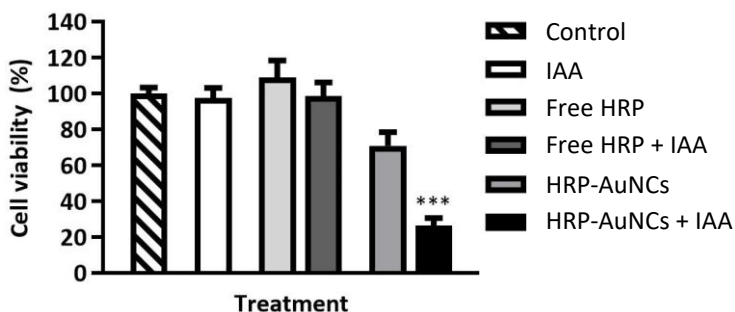


Figure 4. HRP-AuNCs for EPT in triple-negative breast cancer MCTS. Cell viability assessment in MCTS formed by MDA-MB-231 cells incubated with **HRP-AuNCs** or free HRP in the absence or presence of IAA. Cell viability was determined after 48 h of incubation by WST-1 assay. Data represent means \pm SEM (n=3). Significant differences were compared to control according to one-way ANOVA and Dunns post-test (***) $p < 0.001$.

5.4 Conclusions.

In summary, we report here the design, preparation, characterisation, and evaluation of a nanodevice based on gold nanoparticles decorated with the enzyme horseradish peroxidase (**HRP-AuNCs**) to perform EPT in breast cancer cells. Gold conjugates were synthesized using gold nanoparticles as starting materials, which were first functionalised with 3-mercaptopropionic acid to yield **(3-MPA)-AuNCs**. **(3-MPA)-AuNCs** were then equipped with HRP (**HRP-AuNCs**). The proper formation and enzyme activity of the nanodevice were determined by TEM-EDX, UV-Vis spectrophotometry, DLS, ζ potential, and peroxidase activity assay. Biocompatibility experiments demonstrated that **HRP-AuNCs** were well-tolerated by breast cancer cell lines (i.e., luminal A and TN subtypes). Moreover, TEM visualisation of both breast cancer cell subtypes treated with **HRP-AuNCs** revealed that nanoparticles were successfully internalised and located in secondary lysosomes. Furthermore, the co-treatment with **HRP-AuNCs** and IAA efficiently triggered cell death induced by oxidative stress. However, treatment with the free

formulated enzyme at equivalent catalytic activity did not alter cell survival. Remarkably, we also demonstrated that **HRP-AuNCs** combined with IAA led to cell viability reduction in triple-negative breast cancer MCTS, while free HRP/IAA did not affect the cell culture integrity.

AuNPs represent a feasible scaffold for the development of novel nanodevices with advanced applications, as they possess several advantages including well-established, fast, and relative low-cost synthesis, easy stabilization by surface coating, and biocompatibility (see [section 1.4](#) and [section 1.5](#)). In accordance with our results, previous studies with silica nanoparticles showed the ability of encapsulated HRP to transform IAA into free radicals to perform prodrug tumour therapy in colon^[38] and cervix cancer.^[39,40] Horseradish peroxidase has also been nanoformulated using polymeric chitosan nanoparticles to induce cell death in a breast cancer cellular model.^[34] Differential studies would shed light on the most appropriate nanoformulation in terms of reproducibility of synthesis, enzyme stability and activity, *in vivo* biodistribution, safety, and antitumour efficacy, etc. Currently, antibodies^[18,19,23,106] and viruses^[25-27,107] as enzyme vehicles are the most advanced in clinical trials. However, these approaches do not completely accomplish the therapeutic needs. As a consequence, the development of novel abiotic enzyme nanocarriers are a promising alternative to advance enzyme prodrug therapy toward application in patients. Gold-based nanomaterials have not been approved for clinical use, but several clinical trials in early phases (ClinicalTrials.gov Identifier: NCT03020017, NCT01270139, NCT02837094, and NCT04081714) are studying their application for the treatment of cancer and other ailments. Further investigations would promote the incorporation of gold nanoparticles in cancer treatment, where enzyme prodrug therapy represent an

encouraging strategy to increase the specificity and efficiency of conventional tumour therapies.

5.5 Experimental section.

5.5.1 Synthesis of gold nanoparticles (AuNPs).

Gold nanoparticles were synthesized based on the Turkevich-Frens method.^[78,79] Briefly, 100 mL of 0.34 mM HAuCl₄·3H₂O solution was brought to 100 °C under stirring and refluxing. Then, 1.5 mL of a 1% sodium citrate solution was added to synthesize 20 nm gold nanoparticles. The initially faint yellow colour turns to blue-black and finally red wine in 10 min. After this, the colloidal suspension was let to cool at room temperature.

5.5.2 Synthesis of HRP-functionalised gold nanoconjugates (HRP- AuNCs).

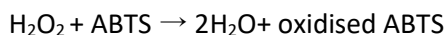
20 mL of the 20 nm colloidal suspension of AuNPs were mixed with 20 µL of 3- mercaptopropionic acid (3-MPA) and stirred for 1 h. The red wine solution turns to a blue-black colour due to aggregation. After 1 h, the solid **(3-MPA)-AuNPs** was isolated by centrifugation at 9,500 rpm for 20 min. Then, the nanoparticles were washed with ethanol by centrifugation-washing cycles of 5 min at 12,500 rpm and resuspended in PBS (pH 7.4). In the next step, the **(3-MPA)-AuNPs** were reacted with 1 mg of N-(3-dimethylaminopropyl)-N'-ethylcarbodiimide (EDC) and 1 mg of N- hydroxysuccinimide (NHS) under stirring for 30 min. Finally, 2 mg of HRP type-VI were added to the mixture and stirred overnight at 4 °C. The final **HRP-AuNCs** were isolated by centrifugation-washing cycles of 5 min at 12,500 rpm in PBS buffer.

5.5.3 Standard characterisation procedures of HRP-AuNCs.

Transmission electron microscopy coupled with energy-dispersive X-ray spectroscopy (TEM-EDX) and ultraviolet-visible (UV-Vis) spectrophotometry, dynamic light scattering (DLS), and ζ potential were employed for the nanomaterial characterisation. TEM-EDX imaging was carried out using a JEOL JEM-2100 LaB6 electron microscope working at 200 kV accelerating voltage and equipped with an Oxford Instruments INCA x-sight (Si(Li) detector) and a Zeiss SESAM microscope (200 kV) equipped with an energy dispersive X-ray (EDX) spectroscopy system from ThermoFisher. UV-visible spectra were recorded with a JASCO V-650. The DLS studies determined particle size and were conducted at 25 °C in a Malvern Zetasizer Nano ZS instrument. The ζ potential was calculated from the particle mobility values by applying the Smoluchowski model and was also measured at 25 °C in a Malvern Zetasizer Nano ZS instrument. DLS and ζ potential measurements were taken in triplicate on nanoparticle dispersions at 1 mg/mL diluted in deionised water.

5.5.4 HRP activity assay.

The method we used to determine HRP activity was based on the enzyme oxidation of 2,2'-Azino-bis(3-ethylbenzothiazoline-6-sulfonic acid) diammonium salt (ABTS) according to Sigma Aldrich instructions.^[108,109] HRP catalyses a redox reaction with ABTS and H₂O₂ as substrates. The ABTS is oxidised to produce the ABTS cation radical, which can be measured as a colour change at 405 nm. The H₂O₂ is reduced to yield H₂O.



In order to measure the activity of the free HRP and **HRP-AuNCs** a reaction mixture was prepared as follows: 966.7 μL of 9.1 mM of ABTS (8.7 mM), 33.3 μL of 0.3% (w/w) of H_2O_2 (0.01% w/w), and 10 μL of 1 mg/mL of **HRP-AuNCs** (0.01 mg/mL) or 16.6 μL of 1×10^{-8} mg/mL free HRP (1.66×10^{-10} mg/mL). The peroxidase-like activity of the starting AuNPs was also evaluated at the same conditions of **HRP-AuNCs** (0.01 mg/mL). The ABTS solution was prepared in 100 mM phosphate buffer (pH 5) and the free HRP was dissolved in 40 mM phosphate buffer (pH 6.8). The absorbance was monitored at 405 nm as a function of time for 2 min.

Peroxidase oxidase activity of free HRP was estimated by applying the equation:

$$\frac{\text{Enzyme units}}{\text{mg}} = \frac{(\Delta - \Delta_{\text{Blank}}) \times V_T \times F_D}{\epsilon_{\text{ABTS}} \times L \times V_{\text{HRP}}}$$

The peroxidase activity of **HRP-AuNCs** and AuNPs required slightly variations in the equation:

$$\frac{\text{Enzyme units}}{\text{mg}} = \frac{(\Delta - \Delta_{\text{Blank}}) \times V_T}{\epsilon_{\text{ABTS}} \times L \times V_{\text{HRP-AuNCs}}}$$

Where, Δ is the slope of the graph (min^{-1}), Δ_{Blank} is the slope of the graph for the blank (min^{-1}), V_T is the total volume in the cuvette, F_D is the dilution factor of enzyme, ϵ_{ABTS} is the molar extinction of oxidised $\text{ABTS}^{\cdot-}$ at 405 nm ($36.8 \text{ mM}^{-1} \text{ cm}^{-1}$), L is the optical path in the cuvette (1 cm), V_{HRP} is the volume of enzyme added (mL) and $V_{\text{HRP-AuNCs}}$ is the volume of nanoconjugates added (mL).

5.5.5 Cell culture conditions.

Triple-negative breast cancer cells (MDA-MB-231) were purchased from ATCC. Hormone receptor-positive MCF-7 was kindly provided by Maria Jesus Vicent research group from the Centro de Investigación Príncipe Felipe. Cells were grown in Dulbecco's Modified Eagle Medium (DMEM)-high glucose supplemented with 10% foetal bovine serum (FBS) and incubated at 37 °C in a 5% CO₂ atmosphere and 95% air. Cells were periodically detached with trypsin-EDTA (0.25% w/w), diluted, and incubated with fresh culture media.

5.5.6 Biocompatibility studies with HRP-AuNCs.

The biocompatibility of **HRP-AuNCs** was assessed in MDA-MB-231 and MCF-7. The cytotoxic effect was evaluated by WST-1 assay. MDA-MB-231 (10,000 cells/well) and MCF-7 (7,500 cells/well) were seeded on 96-well plates overnight. The cells were treated with **HRP-AuNCs** at different concentrations (0, 100, 200, 500 and 750 µg/mL) for 48 h. After that incubation time, WST-1 (10 µL/well) was added and incubated for 1 h. The absorbance was recorded at 450 nm at Wallac 1420 workstation.

5.5.7 Cellular uptake studies.

The cellular internalisation of **HRP-AuNCs** was studied in MDA-MB-231 and MCF-7 by TEM. MDA-MB-231 (50,000 cells/well) and MCF-7 (35,000 cells/well) were seeded on 8-well chamber slide (ThermoFisher Scientific 177445) the day before treatment. The cells were treated with **HRP-AuNCs** at 50 µg/mL. After 6 h of incubation with the nanoconjugates, the cells were carefully washed with PBS and incubated with 3% glutaraldehyde prepared in PBS at 37 °C for 10 min. Then, the glutaraldehyde was replaced with fresh 3% glutaraldehyde, and cells were

incubated for 2 h at room temperature. Finally, the cells were washed 5 times with PBS and kept at 4 °C for further TEM visualisation. The fixed cell samples were further processed in the TEM service of the Centro de Investigación Príncipe Felipe and finally, the images were acquired using a microscope FEI Tecnai Spirit G2 operating at 80 kV with a digital camera (Soft Image System, Morada).

5.5.8 HRP-AuNCs for EPT in breast cancer cells.

Enzyme prodrug therapy carried out by the starting AuNPs, **HRP-AuNP**, and free HRP was evaluated in MDA-MB-231 (10,000 cells/well) and MCF-7 (7,500 cells/well) cell lines. The cells were seeded on 96-well plates one day before treatment. The cytotoxic effect of EPT was assessed after treatment with AuNPs, **HRP-AuNCs**, or free HRP in the absence or presence of IAA at a concentration of 500 µM for 48 h. AuNPs were used at different concentrations (200, 300 and 400 µg/mL). **HRP-AuNCs** and free HRP were used at the enzyme activity of 9.3×10^{-2} U/mL for MDA-MB-231 treatment and 6.4×10^{-2} U/mL for MCF-7 treatment. Untreated cells and single-agent treatment, i.e., AuNPs, **HRP-AuNCs**, free HRP, or IAA alone, were used as controls. After 48 h of incubation, WST-1 (10 µL/well) was added and incubated for 1 h. The absorbance was recorded at 450 nm at Wallac 1420 workstation.

5.5.9 HRP-AuNCs for EPT in triple-negative breast cancer MCTS.

Multicellular tumours spheroids-like cultures were prepared according to the literature with slight modifications.^[110,111] Briefly, 1.5% of agarose was added to PBS and autoclaved. Next, 50 µL/well of hot (80-90 °C) solution were added to a 96-well plate (flat bottom) under sterile conditions. After agarose solidification, a concave non-adherent bottom was obtained. The MDA-MB-231 cells grown as a monolayer

were detached with trypsin to generate a single-cell suspension. Then, cells were seeded at 5,000 cells/well in a final volume of 200 μL /well and centrifuged at 1,000 rpm for 10 min. Matrigel thawed at 4 $^{\circ}\text{C}$ overnight was added at a final concentration of 2.5% with ice-cold pipette tips to each well. The plates were incubated under standard cell culture conditions (37 $^{\circ}\text{C}$, 5% CO_2 , in a humidified incubator) for 3 days. Afterward, the spheroid-like culture was treated with the **HRP-AuNCs** (0.15 U/mL) in the absence or presence of IAA at a concentration of 250 μM . Untreated and single-agent treated cells (i.e., **HRP-AuNCs**, free HRP, or IAA alone) were employed as controls. After 48 h of incubation, the cell viability was determined by WST-1 assay. WST-1 reagent (20 μL /well) was added to each well and incubated for 4 h. Finally, the absorbance was measured at 450 in a Wallace 1420 workstation.

5.6 References.

- [1] Globocan, *Glob. Scan 2018* **2018**, 849, 2018.
- [2] Globocan, *Glob. Scan 2018* **2018**, 947, 2018.
- [3] F. Cardoso, S. Kyriakides, S. Ohno, F. Penault-Llorca, P. Poortmans, I. T. Rubio, S. Zackrisson, E. Senkus, *Ann. Oncol.* **2019**, 30, 1194–1220.
- [4] A. H. Partridge, H. J. Burstein, E. P. Winer, *J. Natl. Cancer Inst. Monogr.* **2001**, 334, 135–142.
- [5] G. F. Paciotti, L. Myer, D. Weinreich, D. Goia, N. Pavel, R. E. McLaughlin, L. Tamarkin, *Drug Deliv. J. Deliv. Target. Ther. Agents* **2004**, 11, 169–183.
- [6] J. F. Hainfeld, H. M. Smilowitz, M. J. O’connor, F. A. Dilmanian, D. N. Slatkin, *Nanomedicine* **2013**, 8, 1601–1609.
- [7] C. H. Wang, C. J. Liu, C. C. Chien, H. T. Chen, T. E. Hua, W. H. Leng, H. H. Chen, I. M. Kempson, Y. Hwu, M. Hsiao, T. C. Lai, J. L. Wang, C. S. Yang, H. M. Lin, Y. J. Chen, G. Margaritondo, *Mater. Chem. Phys.* **2011**, 126, 352–356.
- [8] M. M. Sheno, I. Iltis, J. Choi, N. A. Koonce, G. J. Metzger, R. J. Griffin, J. C. Bischof, *Mol. Pharm.* **2013**, 10, 1683–1694.
- [9] S. Sarkar, S. Konar, P. N. Prasad, S. Rajput, B. N. P. Kumar, R. R. Rao, A. Pathak, P. B. Fisher, M. Mandal, *Langmuir* **2017**, 33, 7649–7659.
- [10] M. Ghorbani, H. Hamishehkar, *Int. J. Pharm.* **2017**, 520, 126–138.
- [11] P. Tran, S.-E. Lee, D.-H. Kim, Y.-C. Pyo, J.-S. Park, *J. Pharm. Investig.* **2020**, 50, 261–270.
- [12] C. M. Ensor, F. W. Holtsberg, J. S. Bomalaski, M. A. Clark, *Cancer Res.* **2002**, 62, 5443–5450.
- [13] V. I. Avramis, S. Sencer, A. P. Periclou, H. Sather, B. C. Bostrom, L. J. Cohen, A. G. Ettinger, L. J. Ettinger, J. Franklin, P. S. Gaynon, J. M. Hilden, B. Lange, F. Majlessipour, P. Mathew, M. Needle, J. Neglia, G. Reaman, J. S. Holcenberg, L. Stork, *Blood* **2002**, 99, 1986–1994.
- [14] N. Schellmann, P. M. Deckert, D. Bachran, H. Fuchs, C. Bachran, *Mini Rev. Med. Chem.* **2010**, 10, 887–904.
- [15] G. Xu, H. L. Mcleod, *Clin. Cancer Res.* **2001**, 7, 3314–3324.
- [16] S. K. Sharma, K. D. Bagshawe, R. G. Melton, R. F. Sherwood, *Cell Biophys.* **1992**, 21, 109–120.
- [17] A. D. AlQahtani, L. Al-mansoori, S. S. Bashraheel, F. B. Rashidi, A. Al-Yafei, P. Elsinga, A. Domling, S. K. Goda, *Eur. J. Pharm. Sci.* **2019**, 127, 79–91.
- [18] R. J. Francis, S. K. Sharma, C. Springer, A. J. Green, L. D. Hope-Stone, L. Sena, J. Martin, K. L. Adamson, A. Robbins, L. Gumbrell, D. O’Malley, E. Tsiompanou, H. Shahbakhti, S. Webley, D. Hochhauser, A. J. Hilson, D. Blakey, R. H. J. Begent, *Br. J. Cancer* **2002**, 87, 600–607.
- [19] M. P. Napier, S. K. Sharma, C. J. Springer, K. D. Bagshawe, A. J. Green, J.

- Martin, S. M. Stribbling, N. Cushen, D. O'Malley, R. H. J. Begent, *Clin. Cancer Res.* **2000**, *6*, 765–772.
- [20] K. D. Bagshawe, C. J. Springer, F. Searle, P. Antoniow, S. K. Sharma, R. G. Melton, R. F. Sherwood, *Br. J. Cancer* **1988**, *58*, 700–703.
- [21] P. D. Senter, M. G. Saulnier, G. J. Schreiber, D. L. Hirschberg, J. P. Brown, I. Hellström, K. E. Hellström, *Proc. Natl. Acad. Sci. U. S. A.* **1988**, *85*, 4842–4846.
- [22] P. D. Senter, G. J. Schreiber, D. L. Hirschberg, S. A. Ashe, K. E. Hellström, I. Hellström, *Cancer Res.* **1989**, *49*, 5789–5792.
- [23] A. Mayer, R. J. Francis, S. K. Sharma, B. Tolner, C. J. Springer, J. Martin, G. M. Boxer, J. Bell, A. J. Green, J. A. Hartley, C. Cruickshank, J. Wren, K. A. Chester, R. H. J. Begent, *Clin. Cancer Res.* **2006**, *12*, 6509 LP – 6516.
- [24] T. Nishiyama, Y. Kawamura, K. Kawamoto, H. Matsumura, N. Yamamoto, T. Ito, A. Ohyama, T. Katsuragi, T. Sakai, *Cancer Res.* **1985**, *45*, 1753–1761.
- [25] T. F. Cloughesy, J. Landolfi, D. J. Hogan, S. Bloomfield, B. Carter, C. C. Chen, J. B. Elder, S. N. Kalkanis, S. Kesari, A. Lai, I. Y. Lee, L. M. Liau, T. Mikkelsen, P. L. Nghiemphu, D. Piccioni, T. Walbert, A. Chu, A. Das, O. R. Diago, D. Gammon, H. E. Gruber, M. Hanna, D. J. Jolly, N. Kasahara, D. McCarthy, L. Mitchell, D. Ostertag, J. M. Robbins, M. Rodriguez-Aguirre, M. A. Vogelbaum, *Sci. Transl. Med.* **2016**, *8*, 1–23.
- [26] B. Sangro, G. Mazzolini, M. Ruiz, J. Ruiz, J. Quiroga, I. Herrero, C. Qian, A. Benito, J. Larrache, C. Olagüe, J. Boan, I. Peñuelas, B. Sádaba, J. Prieto, *Cancer Gene Ther.* **2010**, *17*, 837–843.
- [27] N. Ji, D. Weng, C. Liu, Z. Gu, S. Chen, Y. Guo, Z. Fan, X. Wang, J. Chen, Y. Zhao, J. Zhou, J. Wang, D. Ma, N. Li, *Oncotarget* **2016**, *7*, 4369–4378.
- [28] L. A. Martin, R. Vile, N. R. Lemoine, K. Sikora, H. S. Pandha, *Lancet* **1997**, *3*, 1793–1794.
- [29] I. Niculescu-Duvaz, R. Spooner, R. Marais, C. J. Springer, *Bioconjug. Chem.* **1998**, *9*, 4–22.
- [30] G. Huysmans, A. Ranquin, L. Wyns, J. Steyaert, P. Van Gelder, *J. Control. Release* **2005**, *102*, 171–179.
- [31] R. Chandrawati, M. T. J. Olesen, T. C. C. Marini, G. Bisra, A. G. Guex, M. G. de Oliveira, A. N. Zelikin, M. M. Stevens, *Adv. Healthc. Mater.* **2017**, *6*, 1700385.
- [32] R. Satchi-Fainaro, H. Hailu, J. W. Davies, C. Summerford, R. Duncan, *Bioconjug. Chem.* **2003**, *14*, 797–804.
- [33] T. Nishimura, Y. Sasaki, K. Akiyoshi, *Adv. Mater.* **2017**, *29*, 1702406.
- [34] X. Cao, C. Chen, H. Yu, P. Wang, *Biotechnol. Lett.* **2015**, *37*, 81–88.
- [35] A. Gopin, S. Ebner, B. Attali, D. Shabat, *Bioconjug. Chem.* **2006**, *17*, 1432–1440.
- [36] N. Gupta, C. Gupta, S. Sharma, B. Rathi, R. K. Sharma, H. B. Bohidar, *RSC Adv.*

- 2016**, *6*, 111099–111108.
- [37] J. Zhou, J. Hou, J. Rao, C. Zhou, Y. Liu, W. Gao, *Int. J. Nanomedicine* **2020**, *15*, 4639–4657.
- [38] B. Y. Hung, Y. Kuthati, R. K. Kankala, S. Kankala, J. P. Deng, C. L. Liu, C. H. Lee, *Nanomaterials* **2015**, *5*, 2169–2191.
- [39] Y.-R. Chiu, W.-J. Ho, J.-S. Chao, C.-J. Yuan, *J. Nanoparticle Res.* **2012**, *14*, 829.
- [40] F.-P. Chang, Y. Hung, J.-H. Chang, C.-H. Lin, C.-Y. Mou, *ACS Appl. Mater. Interfaces* **2014**, *6*, 6883–6890.
- [41] D. Li, Q. He, Y. Cui, L. Duan, J. Li, *Biochem. Biophys. Res. Commun.* **2007**, *355*, 488–493.
- [42] S. Shikha, K. G. Thakur, M. S. Bhattacharyya, *RSC Adv.* **2017**, *7*, 42845–42855.
- [43] I. Venditti, C. Palocci, L. Chronopoulou, I. Fratoddi, L. Fontana, M. Diociaiuti, M. V. Russo, *Colloids Surfaces B Biointerfaces* **2015**, *131*, 93–101.
- [44] R. Villalonga, R. Cao, A. Fragoso, A. E. Damiao, P. D. Ortiz, J. Caballero, *J. Mol. Catal. B Enzym.* **2005**, *35*, 79–85.
- [45] M. Y. Icimoto, A. M. Brito, M. P. Ramos, V. Oliveira, I. L. Nantes-Cardoso, *Catalysts* **2020**, *10*, 78.
- [46] C.-S. Wu, C.-T. Wu, Y.-S. Yang, F.-H. Ko, *Chem. Commun.* **2008**, 5327–5329.
- [47] P. Pandey, S. P. Singh, S. K. Arya, V. Gupta, M. Datta, S. Singh, B. D. Malhotra, *Langmuir* **2007**, *23*, 3333–3337.
- [48] D. Lan, B. Li, Z. Zhang, *Biosens. Bioelectron.* **2008**, *24*, 934–938.
- [49] M. Liu, C. Jia, Y. Huang, X. Lou, S. Yao, Q. Jin, J. Zhao, J. Xiang, *Analyst* **2010**, *135*, 327–331.
- [50] Y. Duan, W. Wu, Q. Zhao, S. Liu, H. Liu, M. Huang, T. Wang, M. Liang, Z. Wang, *Int. J. Environ. Res. Public Health* **2020**, *17*, 4427.
- [51] W.-J. Kim, H. Y. Cho, B. Jeong, S. Byun, J. Huh, Y. J. Kim, *Sensors (Basel)*. **2017**, *18*, 55.
- [52] V. V. Gwenin, C. D. Gwenin, M. Kalaji, *Langmuir* **2011**, *27*, 14300–14307.
- [53] S. D. Anderson, R. J. Hobbs, V. V. Gwenin, P. Ball, L. A. Bennie, J. A. Coulter, C. D. Gwenin, *J. Funct. Biomater.* **2019**, *10*, 45.
- [54] N. C. Veitch, *Phytochemistry* **2004**, *65*, 249–259.
- [55] P. Wardman, *Curr. Pharm. Des.* **2002**, *8*, 1363–1374.
- [56] M. Ad, H. Lemos, J. C. Oliveira, J. A. Saraiva, M. A. L. Escola, S. De Biotechnologia, U. Cato, *LWT - Food Sci. Technol.* **2000**, *33*, 362–368.
- [57] K. Chattopadhyay, S. Mazumdar, *Biochemistry* **2000**, *39*, 263–270.
- [58] H. Li, L. Chen, Y. Shi, B. Yuan, Y. Ma, H. Wei, G. Zhao, *Chem. - An Asian J.* **2017**, *12*, 176–180.
- [59] L. F. F. Dalmazzo, B. A. Santana-Lemos, R. H. Jácomo, A. B. Garcia, E. M. Rego, L. M. da Fonseca, R. P. Falcão, *Leuk. Res.* **2011**, *35*, 657–662.
- [60] O. Greco, L. K. Folkes, P. Wardman, G. M. Tozer, G. U. Dachs, *Cancer Gene*


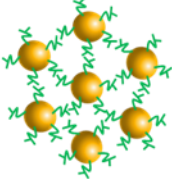
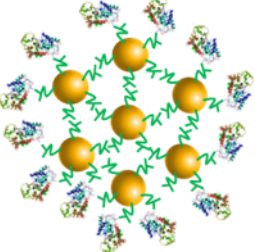
- Ther.* **2000**, *7*, 1414–1420.
- [61] G. Bonifert, L. Folkes, C. Gmeiner, G. Dachs, O. Spadiut, *Cancer Med.* **2016**, *5*, 1194–1203.
- [62] J. Tupper, O. Greco, G. M. Tozer, G. U. Dachs, *Cancer Gene Ther.* **2004**, *11*, 508–513.
- [63] L. Folkes, L. Candeias, P. Wardman, *Int. J. Radiat. Oncol.* **1998**, *42*, 917–920.
- [64] M. Dai, J. Liu, D. E. Chen, Y. Rao, Z. J. Tang, W. Z. Ho, C. Y. Dong, *Cancer Gene Ther.* **2012**, *19*, 77–83.
- [65] J. Tupper, M. R. Stratford, S. Hill, G. M. Tozer, G. U. Dachs, *Cancer Gene Ther.* **2010**, *17*, 420–428.
- [66] M. J. Bennett, A. Marchant, S. T. May, R. Swarup, *Philos. Trans. R. Soc. B Biol. Sci.* **1998**, *353*, 1511–1515.
- [67] I.-A. M. and D. Diengott, *Proc. Soc. Exp. Biol. Med.* **1956**, *93*, 109–110.
- [68] K. Ryšánek, V. Vitek, *Experientia* **1959**, *15*, 217–218.
- [69] L. K. Folkes, M. F. Dennis, M. R. L. Stratford, L. P. Candeias, P. Wardman, *Biochem. Pharmacol.* **1999**, *57*, 375–382.
- [70] M. P. De Melo, T. C. P. Curi, C. K. Miyasaka, A. C. Palanch, R. Curi, *Gen. Pharmacol.* **1998**, *31*, 573–578.
- [71] L. P. Candeias, L. K. Folkes, M. Porssa, J. Parrick, P. Wardman, *Free Radic. Res.* **1995**, *23*, 403–418.
- [72] T. Kawano, N. Kawano, H. Hosoya, F. Lapeyrie, *Biochem. Biophys. Res. Commun.* **2001**, *288*, 546–551.
- [73] C. Huang, L. Y. Liu, T. S. Song, L. Ni, L. Yang, X. Y. Hu, J. S. Hu, L. P. Song, Y. Luo, L. S. Si, *World J. Gastroenterol.* **2005**, *11*, 4519–4523.
- [74] D.-S. Kim, S.-E. Jeon, Y.-M. Jeong, S.-Y. Kim, S.-B. Kwon, K.-C. Park, *FEBS Lett.* **2006**, *580*, 1439–1446.
- [75] D. S. Kim, S. E. Jeon, K. C. Park, *Cell. Signal.* **2004**, *16*, 81–88.
- [76] D.-S. Kim, S.-Y. Kim, Y.-M. Jeong, S.-E. Jeon, M.-K. Kim, S.-B. Kwon, K.-C. Park, *Biol. & Pharm. Bull.* **2006**, *29*, 1625–1629.
- [77] Y. M. Jeong, M. H. Oh, S. Y. Kim, H. Li, H. Y. Yun, K. J. Baek, N. S. Kwon, W. Y. Kim, D. S. Kim, *Pharmazie* **2010**, *65*, 122–126.
- [78] J. Turkevich, P. C. Stevenson, J. Hillier, *Discuss. Faraday Soc.* **1951**, *11*, 55–75.
- [79] G. Frens, *Nat. Phys. Sci.* **1973**, *241*, 20–22.
- [80] R. C. Rodrigues, C. Ortiz, Á. Berenguer-Murcia, R. Torres, R. Fernández-Lafuente, *Chem. Soc. Rev.* **2013**, *42*, 6290–6307.
- [81] L. Gao, J. Zhuang, L. Nie, J. Zhang, Y. Zhang, N. Gu, T. Wang, J. Feng, D. Yang, S. Perrett, X. Yan, *Nat. Nanotechnol.* **2007**, *2*, 577–583.
- [82] N. Wang, L. Zhu, D. Wang, M. Wang, Z. Lin, H. Tang, *Ultrason. Sonochem.* **2010**, *17*, 526–533.

- [83] F. F. Peng, Y. Zhang, N. Gu, *Chinese Chem. Lett.* **2008**, *19*, 730–733.
- [84] S. Liu, F. Lu, R. Xing, J.-J. Zhu, *Chem. – A Eur. J.* **2011**, *17*, 620–625.
- [85] S. Gao, H. Lin, H. Zhang, H. Yao, Y. Chen, J. Shi, *Adv. Sci.* **2019**, *6*, 1801733.
- [86] J. Kim, H. R. Cho, H. Jeon, D. Kim, C. Song, N. Lee, S. H. Choi, T. Hyeon, *J. Am. Chem. Soc.* **2017**, *139*, 10992–10995.
- [87] L. Gao, Y. Liu, D. Kim, Y. Li, G. Hwang, P. C. Naha, D. P. Cormode, H. Koo, *Biomaterials* **2016**, *101*, 272–284.
- [88] S. Wang, W. Chen, A.-L. Liu, L. Hong, H.-H. Deng, X.-H. Lin, *Chemphyschem* **2012**, *13*, 1199–1204.
- [89] D. Lou, Y. Tian, Y. Zhang, J. Yin, T. Yang, C. He, M. Ma, W. Yu, N. Gu, *J. Nanosci. Nanotechnol.* **2018**, *18*, 951–958.
- [90] Y. Tao, E. Ju, J. Ren, X. Qu, *Adv. Mater.* **2015**, *27*, 1097–1104.
- [91] L. Gao, M. Liu, G. Ma, Y. Wang, L. Zhao, Q. Yuan, F. Gao, R. Liu, J. Zhai, Z. Chai, Y. Zhao, X. Gao, *ACS Nano* **2015**, *9*, 10979–10990.
- [92] T. K. Sharma, R. Ramanathan, P. Weerathunge, M. Mohammadtaheri, H. K. Daima, R. Shukla, V. Bansal, *Chem. Commun.* **2014**, *50*, 15856–15859.
- [93] C. Vallejos, H. Gómez, W. Cruz, J. Pinto, R. Dyer, R. Velarde, J. Suazo, S. Neciosup, M. León, M. De La Cruz, C. Vigil, *Clin. Breast Cancer* **2010**, *10*, 294–300.
- [94] C. M. Perou, T. Sørile, M. B. Eisen, M. Van De Rijn, S. S. Jeffrey, C. A. Rens, J. R. Pollack, D. T. Ross, H. Johnsen, L. A. Akslen, Ø. Fluge, A. Pergammenschikov, C. Williams, S. X. Zhu, P. E. Lønning, A. L. Børresen-Dale, P. O. Brown, D. Botstein, *Nature* **2000**, *406*, 747–752.
- [95] J. S. Reis-Filho, L. Pusztai, *Lancet* **2011**, *378*, 1812–1823.
- [96] A. Balfourier, N. Luciani, G. Wang, G. Lelong, O. Ersen, A. Khelifa, D. Alloyeau, F. Gazeau, F. Carn, *Proc. Natl. Acad. Sci. U. S. A.* **2020**, *117*, 103–113.
- [97] M. Liu, Q. Li, L. Liang, J. Li, K. Wang, J. Li, M. Lv, N. Chen, H. Song, J. Lee, J. Shi, L. Wang, R. Lal, C. Fan, *Nat. Commun.* **2017**, *8*, 15646.
- [98] K. Qiu, Y. Du, J. Liu, J.-L. Guan, H. Chao, J. Diao, *Theranostics* **2020**, *10*, 6072–6081.
- [99] X. Ma, Y. Wu, S. Jin, Y. Tian, X. Zhang, Y. Zhao, L. Yu, X.-J. Liang, *ACS Nano* **2011**, *5*, 8629–8639.
- [100] W. He, Y.-T. Zhou, W. G. Wamer, X. Hu, X. Wu, Z. Zheng, M. D. Boudreau, J.-J. Yin, *Biomaterials* **2013**, *34*, 765–773.
- [101] C.-P. Liu, K.-C. Chen, C.-F. Su, P.-Y. Yu, P.-W. Lee, *Catalysts* **2019**, *9*, 517.
- [102] H. Lu, M. H. Stenzel, *Small* **2018**, *14*, 1702858.
- [103] D. Lv, Z. Hu, L. Lu, H. Lu, X. Xu, *Oncol Lett* **2017**, *14*, 6999–7010.
- [104] T. Ishiguro, H. Ohata, A. Sato, K. Yamawaki, T. Enomoto, K. Okamoto, *Cancer Sci.* **2017**, *108*, 283–289.
- [105] T. Herheliuk, O. Perepelytsina, A. Ugnivenko, L. Ostapchenko, M. Sydorenko,

- Stem cell Investig.* **2019**, *6*, 21.
- [106] K. D. Bagshawe, S. K. Sharma, C. J. Springer, P. Antoniwi, J. A. Boden, G. T. Rogers, P. J. Burke, R. G. Melton, R. F. Sherwood, *Dis. Markers* **1991**, *9*, 233–238.
- [107] G. Palù, A. Cavaggioni, P. Calvi, E. Franchin, M. Pizzato, R. Boschetto, C. Parolin, M. Chilosi, S. Ferrini, A. Zanusso, F. Colombo, *Gene Ther.* **1999**, *6*, 330–337.
- [108] J. Keesey, in *Biochem. Inf.*, Boehringer Mannheim Biochemicals, Indianapolis, IN, **1987**, p. 58.
- [109] J. Pütter, R. Becker, in *Methods Enzym. Anal. 3rd Ed., Vol III* (Ed.: H.-Ui. Bergmeyer), Verlag Chemie, Deerfield Beach, FL, **1974**, pp. 286–293.
- [110] J. Friedrich, C. Seidel, R. Ebner, L. A. Kunz-Schughart, *Nat. Protoc.* **2009**, *4*, 309–324.
- [111] A. Ivascu, M. Kubbies, *J. Biomol. Screen.* **2006**, *11*, 922–932.

5.7 Supporting information.

Table S1. Nanoparticle nomenclature and composition.

Nanoparticle nomenclature	Surface functionalisation	Scheme
AuNPs		
(3-MPA)-AuNCs	3-MPA	
HRP-AuNCs	3-MPA and HRP	

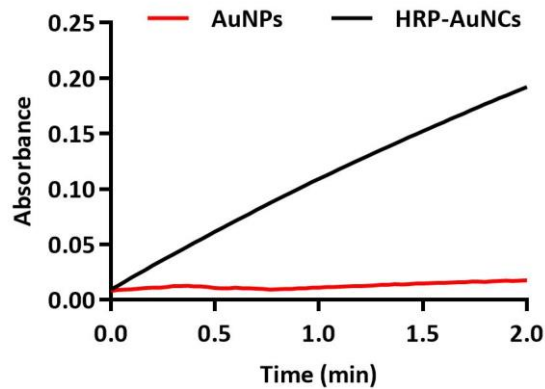


Figure S1. AuNPs and HRP-AuNCs enzyme activity. ABTS oxidation kinetic by AuNPs (red) and HRP-AuNCs (black) measured for 2 min at 405 nm.

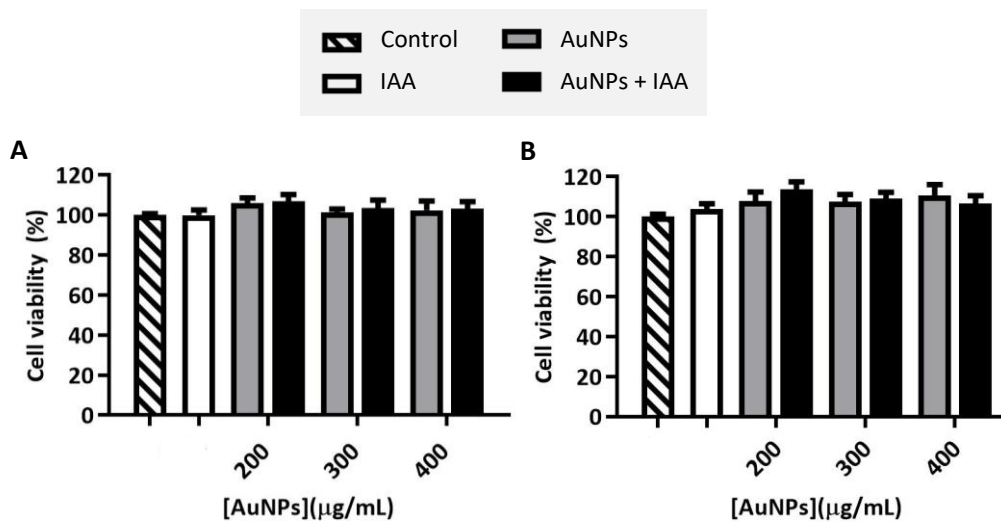


Figure S2. AuNPs for EPT in breast cancer cells. Cell viability analysis in **A)** MDA-MB-231 and **B)** MCF-7 incubated with AuNPs in the absence or presence of IAA. Cell viability was determined after 48 h of incubation by WST-1 assay. Data represent means \pm SEM (n=3). Statistically significance was determined by one-way ANOVA and Dunns post-test.

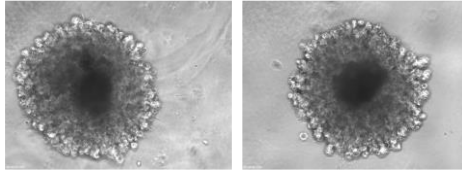


Figure S3. 3-day-old MDA-MB-231 multicellular tumour spheroid-like cultures. The structures present apoptotic/necrotic areas in the center. The images were taken under an optical microscope.

Chapter 6 | Conclusions and future perspectives

Nanotechnology is an exciting and ever-growing area, which is gaining particular interest as an alternative to conventional treatments; especially, in pathologies that require controlled and targeted drug administration.

One of the pathologies most benefited from nanomedicine has been cancer, which is a leading cause of death in developed countries. Despite advances forward to more sophisticated therapies, treatments are still mainly based on conventional therapies, regardless of their well-known secondary effects. In this scenario, nanotechnology constitutes a powerful strategy to overcome many of the limitations of such therapies. The capability of nanomedicines to specifically release drugs in the diseased site has risen as a promising mechanism to increase the therapeutic effect, while diminishing side-effects.

In the last years, the development of biomolecule-functionalised nanomaterials has remarkably increased in the biomedical field. In this context, the present Ph.D. thesis has aimed to contribute to this field by developing new nanodevices with biomedical applications, particularly for breast cancer treatment. For this purpose, three different nanomaterials have been prepared. Two of them are based on stimuli-responsive gated mesoporous silica materials and the third one is based on gold nanoparticles as enzyme carriers.

Responding to the first objective of this thesis, in the third chapter, a nanocarrier consisting of aptamer-gated mesoporous silica nanoparticles were prepared. The nanodevice was loaded with navitoclax and the Mcl-1 inhibitor S63845. The nanodevice was functionalised with an aptamer cap that targets the MUC1 surface protein, which is overexpressed in breast tumour cells. The proper gating mechanism of the aptamer was confirmed; the cargo was only released in the presence of DNase I, which can degrade the molecular gate. The biocompatibility

of the designed nanosystem was proved in the triple-negative cell line MDA-MB-231, and the navitoclax-resistant counterpart cell line MDA-MB-231-R. Additionally, it was demonstrated the preferential accumulation of the nanodevices in the targeted cells. The nanoparticles showed a great therapeutic effect in terms of navitoclax resistance overcoming in the triple-negative breast cancer cell model. As far as we know, this is the first time that the co-delivery of navitoclax and S63845 using mesoporous silica nanoparticles has been described as a drug resistance overcoming mechanism. Furthermore, the encapsulation of navitoclax in the mesoporous scaffold effectively reduced thrombocytopenia in human blood samples. This result proves that the encapsulation of drugs with a narrow therapeutic index could represent a step forward in their clinical application due to the reduction of the side effects. In light of the promising results, we concluded that the designed aptamer gated-mesoporous silica nanoparticles are a useful tool to overcome navitoclax resistance in breast cancer. The conceptual idea of drug co-delivery opens the opportunity to develop multifunctional systems loaded with different drug combinations aimed to solve drug resistance problems according to the patient's needs.

Attending to the second objective of this work, pH-responsive mesoporous silica nanoparticles able to simultaneously deliver the CRISPR/Cas9 editing machinery and an entrapped cargo has been reported. The nanoparticles were loaded with rhodamine B (as a model drug) and capped with PEI and a CRISPR/Cas9 plasmid. The CRISPR/Cas9 plasmids were designed for the genome editing of the GFP gene (as a model gene). The proper working of the capping ensemble was tested; the cargo was only released in acidic simulated plasma, due to molecular gate disruption upon polyethyleneimine 'proton sponge' effect. Enhanced stability of the CRISPR/Cas9 vector coating the nanoparticles was also confirmed under

conditions in which the free plasmid was unstable. The prepared nanoparticles were biocompatible and well-tolerated by the osteosarcoma cells employed as a cancer cell line model. The nanoparticle internalisation by the endocytosis was shown. Moreover, the nanoparticles displayed successful endosomal escape boosted by the protonated PEI. Importantly, the nanoparticles effectively performed simultaneous GFP editing and cargo delivery into the cells. From a broad perspective, this double-hit strategy could be used to develop a variety of nanodevices by selecting target genes with therapeutic interest, such as drug resistance genes, and drugs to which cancer cells commonly develop resistance. Future perspective includes the development of novel MSNs for the controlled delivery of CRISPR/Cas9 plasmid targeted to *Mcl-1*. The nanosystem would be loaded with navitoclax. In this case, we also aim to overcome navitoclax resistance in triple-negative breast cancer, yet through a genome-editing strategy. *Mcl-1* editing would disrupt the Mcl-1-mediated resistance. Therefore, the delivered navitoclax in edited cells could effectively induce apoptosis.

The last objective of this thesis was accomplished in the fifth chapter. In this case, enzyme-functionalised gold nanoconjugates are presented. The gold nanoparticles were decorated with the enzyme HRP to perform EPT. The prepared nanodevice takes advantage of the HRP capacity to transform the prodrug IAA into toxic radical species able to induce apoptosis in tumour cells. The proper enzyme activity of the conjugated enzyme was confirmed. Moreover, the biocompatibility and efficient internalisation of the nanodevice were corroborated in the breast cancer cellular models under study (i.e., luminal A and TNBC cells). We demonstrated that the therapeutic effect of the nanoformulated-HRP is enhanced compared with the free enzyme in breast cancer cells and multicellular tumour spheroids. To our knowledge, this is the first example of gold nanoparticles used as

enzyme carriers to perform EPT in breast cancer cells and spheroids. The ability to accomplish effective EPT in MCTS highlights the great potential of the designed nanodevice. The obtained results indicate that enzyme nanoformulation constitutes a promising opportunity to improve tumour enzyme therapy performance. What is more, HRP-coated gold nanoconjugates could be an effective alternative candidate for breast cancer therapy.

A general conclusion that can be extracted from this Ph.D. thesis is that the functionalisation of nanoparticles with biomolecules of biological interest can be used for the development of new nanodevices to manage breast cancer disease. Moreover, the smart loading, as well as the incorporation of targeting agents and specific enzymes to inorganic nanosystems, allows performing superior functions to those found in free formulations. The use of selected biomolecules as functional components provides gated-nanomaterials with on-command controlled release behaviour with the possibility of specifically targeting a diseased area.

It is worthy to highlight that, despite the complex nanodevices described in the literature, nanotechnology is still in the initial stages of biomedical applications, and further investigations are required before nanoparticles are fully implanted into clinical routine. Future efforts should be focused on overcoming some drawbacks, such as the long-term effects of nanoparticles persisting the living organisms. Nevertheless, with no doubt new advances in the field of nanotechnology will assist future medicine towards more precise treatments; especially, the smart functionalised nanodevices able to outperform conventional therapies. We hope that the results achieved in this Ph.D. thesis help pushing nanotechnology closer to clinical practice, by inspiring future investigations to develop new smart nanodevices for their application in breast cancer or any other biomedical unresolved need.

